Evaluating and Developing Methods for Non-Destructive Monitoring of Biomass and Nitrogen in Wheat and Rice Using Hyperspectral Remote Sensing

Inaugural-Dissertation

zur

Erlangung des Doktorgrades

der Mathematisch-Naturwissenschaftlichen Fakultät

der Universität zu Köln

vorgelegt von

Martin Leon Gnyp

aus Oppeln

2014

Berichterstatter:	Prof. Dr. Georg Bareth
	Prof. Dr. Karl Schneider
Tag der mündlichen Prüfung:	14.04.2014

Abstract

Aboveground plant biomass and plant nitrogen are two important parameters for plant growth monitoring, which have a decisive influence on the final yield. Mismanagement of fertilizer or pesticide inputs leads to poor plant growth, environmental pollution, and accordingly, yield loss. Biomass development is driven by nutrient supply, temperature, and phenology. Crop biomass reaches its highest weight at the harvest time. In contrast, plant nitrogen is dependent from fertilizer inputs to the soil and from biomass. Destructive measurement of both parameters is time-consuming and labor-intensive. Remote sensing offers remotely non-direct observation methods from outer space, air space, or close-range in the field by sensors. This dissertation focuses on non-destructive monitoring of plant biomass (the primary parameter) and plant nitrogen (the secondary parameter) using hyperspectral data from non-imaging field spectrometers and the imaging EO-1 Hyperion satellite.

The study was conducted on two field crops: winter wheat of two growing seasons of the Huimin test site in the North China Plain; and rice of three growing seasons of the Jiansanjiang test site in the Sanjiang Plain of China. Study fields were set up in different spatial scales, from small experimental scale to large farmers' scale. Extensive field measurements were carried out, including both destructive measuring and non-destructive hyperspectral remote sensing of biomass and plant nitrogen. Besides, two years' Hyperion images were acquired at the Huimin test site. Four different approaches were used to develop the estimation models, which include: vegetation indices (VIs), band combinations, Optimum Multiple Narrow Band Reflectance (OMNBR) and stepwise Multiple Linear Regression (MLR), and derivatives of reflectance. Based on these four approaches, models were constructed, compared, and improved step by step. Additionally, a multiscale approach and a new VI, named GnyLi, were developed. Since experimental and farmers' fields were differently managed, several calibration and validation methods were tested and the field datasets were pooled.

All tested approaches and band selections were greatly influenced by single growth stages. The broad band VIs saturated for both crops at the booting stage at the latest and were greatly outperformed by the narrow band VIs with optimized band combinations. Model applications from experimental to farmers' scale using the narrow bands measured by field spectrometers mostly failed due to the effects of different management practices and crop cultivars at both spatial scales. In contrast, the multiscale approach was successfully applied in winter wheat monitoring to transfer data and knowledge from field spectrometer measurements from the experimental scale to the farmers' field scale and the scale that is covered by the Hyperion imagery. The GnyLi and the Normalized Ratio Index (NRI) based on the optimized band combinations performed the best in the up-scaling process in the winter wheat study. In the rice study, MLR or OMNBR models based on 4–6 narrow bands better explained biomass variability compared to VIs based on broad bands and optimized band combinations. The models were more robust when data from different scales were pooled and then randomly divided into calibration and validation datasets. Additional model improvements were obtained using derivatives of reflectance.

This dissertation evaluates different hyperspectral remote sensing approaches for non-destructive biomass and plant nitrogen monitoring, with the main focus on biomass estimation. The results and comparisons of different approaches revealed their potentials and limits. Development of new VIs, such as GnyLi, is advantageous due to the saturation problem of broad band VIs. However, the developed VIs need to be tested and improved for different crops and sites. Detection of optimized band combinations facilitates the development of new VIs, which are site-specific and crop-specific. MLR-based models may better explain the biomass variability; nevertheless, with more bands, they are prone to the issues of over-fitting and collinearity. Hence, no more than six bands were recommended to select from the hyperspectral data. Derivatives of reflectance were beneficial at the early growing season of rice when the canopy was strongly influenced by background signals from soil and water. However, their benefits were reduced when more bands were used.

Zusammenfassung

Oberirdische Pflanzenbiomasse und Pflanzenstickstoff sind zwei wichtige Parameter für das Monitoring von Pflanzenwachstum, die einen entscheidenden Einfluss auf den Ertrag haben. Mißmanagement von Stickstoffdüngung und Pestizideinsatz führen zu schlechtem Pflanzenwachstum, Umweltverschmutzung, und entsprechendem Ertragsverlust. Die Entwicklung von Biomasse wird von Nährstoffversorgung, Temperatur, und Phänologie gesteuert. Die Biomasse von Feldfrüchten erreicht ihr höchstes Gewicht zur Erntezeit. Demgegenüber ist Pflanzenstickstoff von der Düngerzufuhr in den Boden und von der Biomasse abhängig. Die destruktive Messung von beiden Parametern ist zeitaufwendig und arbeitsintensiv. Die Fernerkundung bietet indirekte Beobachtungsmethoden durch Sensoren aus dem Weltraum, Luftraum, und dem Nahbereich im Feld. Diese Dissertation legt den Schwerpunkt auf nicht-destruktives Monitoring primär von Pflanzenbiomasse und sekundär von Pflanzenstickstoff unter Verwendung hyperspektraler Daten von nichtbildgebenden Feldspektrometern und dem bildgebenden EO-1 Hyperion Satelliten.

Die Studie wurde an zwei Feldfrüchten durchgeführt: während der Wachstumsperioden von Winterweizen in zwei Jahren auf dem Versuchsgelände in Huimin in der nordchinesischen Tiefebene und während der Wachstumsperioden von Reis in drei Jahren auf dem Versuchsgelände in Jiansanjiang in der Sanjiang Ebene von China. Die Versuchsfelder wurden in unterschiedlichen Skalen angelegt, von der kleinen Versuchsfeldskala bis zu großen Farmskala. Umfangreiche Feldmessungen wurden durchgeführt, welche destruktives als auch nicht-destruktives, hyperspektrales Erfassen von Biomasse und Pflanzenstickstoff einbezogen haben. Zusätzlich wurden Hyperionaufnahmen von zwei Jahren für das Versuchsgelände in Huimin berücksichtigt. Vier unterschiedliche Methoden wurden für die Schätzmodelle genutzt: Vegetationsindizes (VIs), Bandkombinationen, Optimierte Multiple Narrow Band Reflexion (OMNBR), schrittweise Multiple Lineare Regression (MLR) und Reflexionsableitungen. Basierend auf diesen vier Methoden wurden Modelle entwickelt, verglichen und schrittweise verbessert. Zusätzlich wurden eine Multiskala-Methode und ein neuer VI namens GnyLi entwickelt. Da die Versuchs- und Farmfelder unterschiedlich bewirtschaftet wurden, wurden einige Kalibrierungs- und Validierungsmethoden getestet und die Felddatensätze zusammengefaßt.

Alle getesteten Methoden und Bandselektionen wurden im hohen Maß durch einzelne Entwicklungsstadien beeinflußt. Für beide Feldfrüchte waren die Breitband VIs spätestens zum Stadium des Ährenschwellens gesättigt und wurden durch Schmalband VIs mit optimierten Bandkombinationen deutlich übertroffen. Modellübertragungen von der Versuchs- zur Farmskala unter Verwendung von Schmalband VIs gemessen durch Feldspektrometer waren meistens nicht erfolgreich, bedingt durch unterschiedlichen Bewirtschaftungsverfahren und Feldfruchtsorten in beiden räumlichen Skalen. Im Gegensatz dazu, wurde die Multiskala-Methode erfolgreich auf das Monitoring von Winterweizen angewendet, welche die Transferierbarkeit von Daten und Erkenntnissen der Feldspektrometermessungen von der Versuchsskala auf die Farmskala und die Skala der Hyperionaufnahme, ermöglicht. Der GnyLi und der auf optimierten Bandkombinationen

basierende Normalisierte Ratio Index (NRI) erzielten die besten Ergebnisse beim Hochskalierungsprozess in der Winterweizenstudie. In der Reisstudie erklärten MLR oder OMNBR Modelle, die auf 4–6 schmalen Bändern basieren, die Biomassenvariabilität besser als VIs, die auf breiten Bändern und optimierten Bandkombinationen basieren. Die Modelle waren robuster, wenn Daten von unterschiedlichen Skalen zusammengefasst und dann zufällig in Kalibrierungs- und Validierungsdatensätze geteilt wurden. Zusätzliche Modellverbesserungen wurden durch Reflexionsableitungen erreicht.

Diese Dissertation bewertet unterschiedliche hyperspektrale Erfassungsmethoden für nicht-destruktives Monitoring von Biomasse und Pflanzenstickstoff mit dem Hauptfokus auf die Abschätzung von Biomasse. Die Ergebnisse und Vergleiche der unterschiedlichen Verfahren zeigen ihre Potentiale und Grenzen auf. Die Entwicklung von neuen VIs, wie z. B. des GnyLi, ist von Vorteil, bedingt durch das Sättigungsproblem von Breitband VIs. Allerdings müssen die entwickelten VIs für verschiedene Feldfrüchte und Standorte getestet und verbessert werden. Die Detektion von optimierten Bandkombinationen ermöglicht die Entwicklung von neuen Bandkombinationen, die standort- und feldfruchtspezifisch sind. MLR-basierte Modelle können besser die Variabilität von Biomasse erklären. Dennoch tendieren sie mit mehr Bändern zu Problemen, wie zum Beispiel Überanpassung und Kollinearität. Deshalb werden nicht mehr als sechs Bänder zur Auswahl von hyperspektralen Daten empfohlen. Die Reflexionsableitungen waren vorteilhaft im frühen Entwicklungsstadium von Reis, wenn der Bestand stark durch Hintergrundsignale vom Boden und Wasser beeinflußt war. Jedoch wurde deren Nutzen gemindert, wenn mehr Bänder verwendet wurden.

Acknowledgements

The present thesis was prepared during the phase of two projects "Regional N-management in Huimin County, Shandong Province, China" and "Microwave imaging to derive upland rice characteristics in Jiansanjiang, Heilongjiang Province, China", funded by the International Bureau (IB) and the Federal Ministry of Education and Research (BMBF). I gratefully acknowledge the financial support from the projects. Both projects were conducted in cooperation with our colleagues from the China Agricultural University (CAU) in Beijing.

I wish to express my gratitude to my supervisor, Prof. Dr. Georg Bareth, for introducing me to this research field, for the opportunity to work in his research group, and for his guidance and invaluable suggestions for improving this work.

I sincerely thank Prof. Dr. Karl Schneider for consenting to act as the second examiner and also Prof. Dr. Bülent Tezkan for chairing the examination committee.

I am indebted to my Chinese supervisors, Prof. Dr. Xinping Chen, Ass. Prof. Fei Li, and especially Ass. Prof. Dr. Yuxin Miao from CAU, for their guidance and support during the field campaigns in Huimin and Jiansanjiang. I greatly appreciated their knowledge and their fruitful thoughts. In particular, I am grateful for Ass. Prof. Yuxin Miao for his valuable comments and his efforts of acting as the corresponding author for my fifth manuscript (chapter 7).

Thanks also go to many student helpers from our group and also from CAU for their cooperation and assistance during the field campaigns. Many thanks also to the farmers for their hospitality and consent to carry out our measurements in their fields.

Many thanks to Prof. Fei Yuan from the Minnesota State University for her comfort and encouragement during my thesis writing and especially her readiness to help me whenever needed.

I thank to my colleagues in our group for their friendly conversations and collaborations, particularly to Wolfgang, Kang, Dirk, Helge, Juliane, and Simon.

My wholehearted thanks to my parents Theresa and Leon for their constant loving care of me and for their assurance of their support at all times, and also to my brother Michael.

Table of contents

1. Introduction

1.1 Preface and introduction of the topic

For thousands of years, food security has played and still plays a critical role for humans in every country and society. Food security denotes having physical and economic access to sufficient, safe, and nutritious foods (FAO, 2013). Food security is associated with healthy life, prosperous society, and finally, with a flourishing economy. Food access guarantees for peace and social stability, which is a major concern at a national scale (CHEN et al., 2011). Conversely, food insecurity may result in famines caused by wars or natural disasters, which have haunted states and societies in their histories, exterminating or forcing people to emigrate. At present, food insecurity remains an issue in less developed countries (BUDDE et al., 2010). FAO (2013) estimated that 1 billion of the worldwide population was affected by food insecurity in 1990–92 and 0.842 billion was affected in 2011–2013. Most affected countries are primarily in the Southern hemisphere, including South Asia, Sub-Saharan Africa, and East Asia (FAO, 2013). In contrast to developing countries, highly developed countries are able to maintain food security because of agricultural mechanization, although less people are employed in the agricultural sector. In the case of China, food security has emerged as a key national task since the great famine in the 1950s (NYBERG, 1998). Food self-sufficiency is a central goal of China's agricultural policy (HUANG, 1998; MIAO et al., 2011). However, maintaining global food security is challenging due to the increasing world population.

The world population is expected to increase rapidly over the next decades. The UN (2012) estimated the world population will reach to 9.5 billion people by 2050, an additional population gain of 2.3 billion. Approximately 60% of the 7.2 billion total population live in Asia. The most populated countries include China, with 1.361 billion people, and India, with 1.236 billion people. China and India together have one third of the world's population. China has 19% of the world's population; however, China has only 8% of the arable land (HOERING, 2010; FAOSTAT, 2011). China's agricultural land is exceptionally small relative to its population (LELE et al., 1998) and is mainly in the eastern, northeast, and south regions (Fig. 1.1). These regions have the highest cropland density and simultaneously the highest population density (CAI et al., 2013; YOU et al., 2013). In particular, the study areas of this dissertation, the North China Plain and Sanjiang Plain, are two of the main agricultural zones in China (Fig. 1.1).

In these agricultural zones, rural-urban migration and planned urbanization have led to higher food demand from the growing cities (CAI et al., 2013), which, therefore, have put pressure on local agriculture close to metropolitan areas to increase productivity. The rural areas may only satisfy the increased demand for food security by increasing the yield. In addition, Chinese cities and major agricultural firms have begun to acquire agricultural products and arable land from overseas with some financial and political encouragement from the government called "going out" (HOERING, 2010; LANG and MIAO, 2013). These cities and firms have leased arable land not only in neighboring states but also in Africa for extending rice production and in Australia for sheep farming. The largest deal was

made with Russia, where the largest cereal producer of China has established a long-term lease agreement for 430,000 ha of arable land near the northeast border of Heilongjiang Province (HOERING, 2010). Using that strategy, China is attempting to satisfy its resource demands and to avoid increasing import rates.

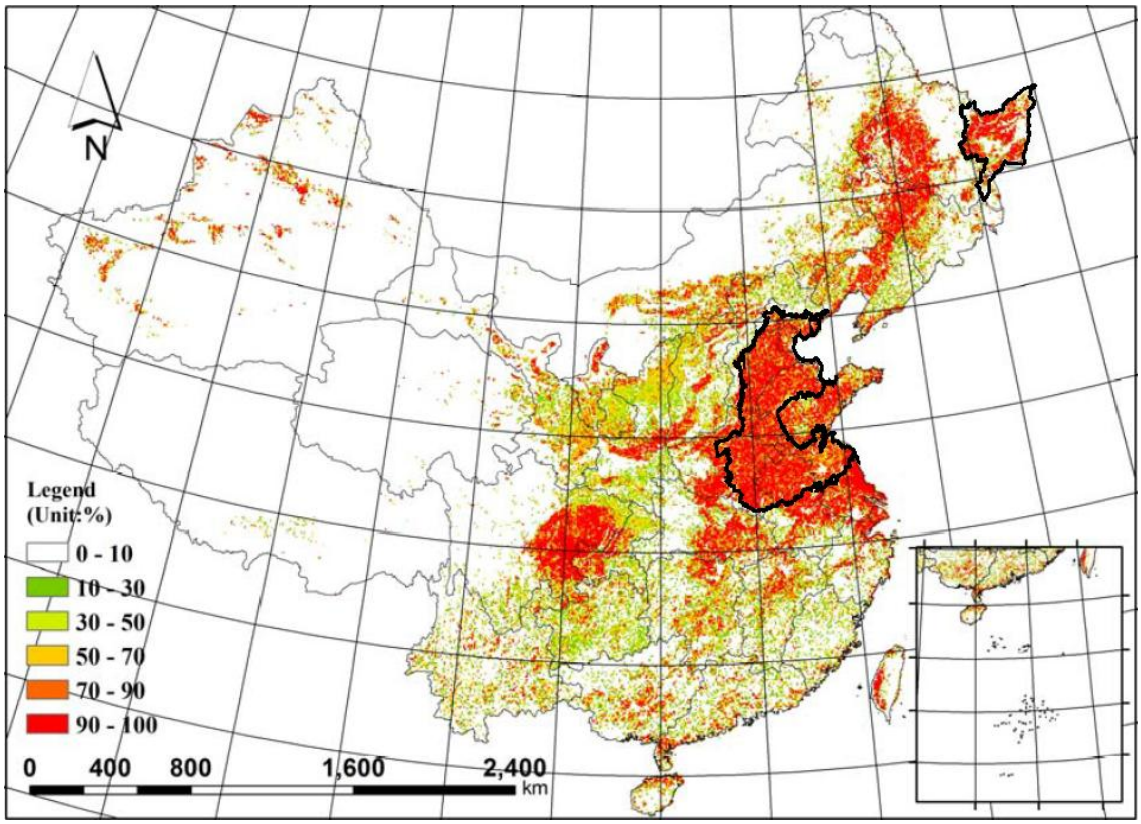

Fig. 1.1 Cropland density in China with the two main agricultural zones "North China Plain" in the east and "Sanjiang Plain" in the northeast (modified from YOU et al., 2013; ISG, 1991; ERIM, 1999).

A massive increase in agricultural productivity associated with the Green Revolution has facilitated feeding a fast growing world population. In China, agricultural productivity rose 8% yearly in the 1980s, 1990s, and 2000s (SUN and KUNG, 1998; ZHANG et al., 2012a) and the population increased 1.5% yearly in the 1980s and 1990s but 0.6% in the 2000s (UN, 2012). The revolution, which was associated with mechanization in agriculture and intensive fertilizer application, pushed people to move to the cities. This process has been completed in the highly developed countries but not in developing countries that have high fertility rates (UN, 2012), high migration pressure from rural area to the cities, and often unfavorable climate conditions. With limited agricultural land, developing countries have to follow the Green Revolution as well to feed their growing population by providing sufficient food on the market.

Agronomic products are traded on bourses and are dependent on supply and demand in the market. Since the 2007–2008 food crises, food prices have doubled, and recently, these prices have remained at a high level (FAOSTAT, 2012). These high prices have resulted in protests in developing

countries and in the tendency for food scandals (HOERING, 2010). Fig. 1.2 shows the importance of China in the market. Maize, rice, and wheat compose two-thirds of the human food consumption of plant-based foods. China is the largest agricultural market, producing 22% (510 Mio. t) of maize, rice, and wheat on 8% of the global arable land (FAOSTAT, 2011); however, China's large population (19% of world population) consumes most of this production. In contrast to that, China produced 30% of the global fertilizer but consumed 32% of that fertilizer for only 8% of the global arable land in 2011 (Fig. 1.2).

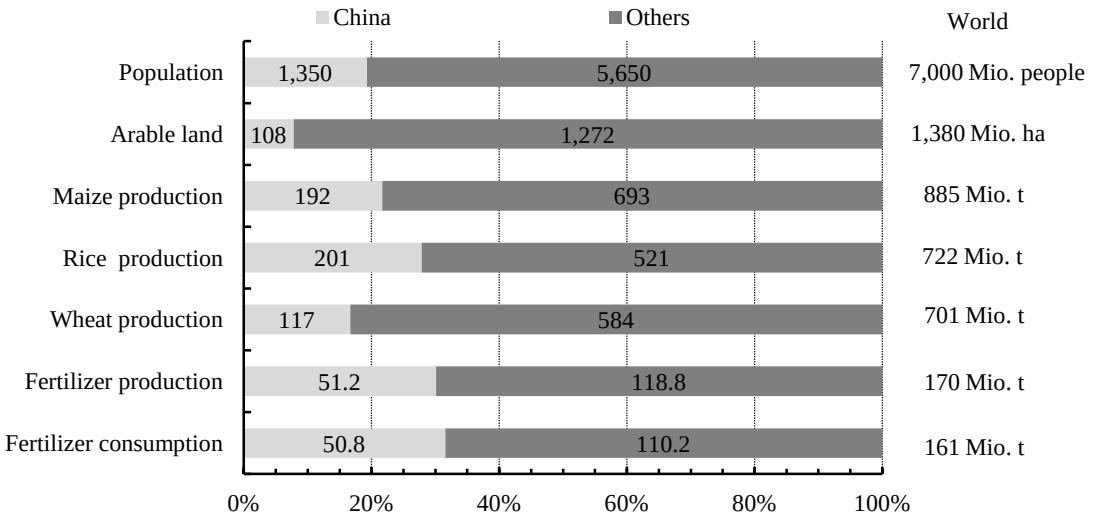

Fig. 1.2 China's absolute and relative share of world's inputs and outputs in 2011 - The population, arable land, main crops, and fertilizer data were from FAOSTAT (2011).

In addition to food security and to the pressure of a growing population, crops have become a lucrative target for energy production in the world market, particularly in developed economies (CHEN et al., 2011). Since 2007, China has financially supported its national climate change program to reduce greenhouse gases (HOERING, 2010). Recently, using renewable energy resources has become an important issue in many countries. Agricultural biofuel and biomass energy have become key words. Many countries are searching for independence of their feedstocks from petroleum by investigating renewable resources, given the increased prices of petroleum feedstocks. Expanding energy crops means less arable land for food production, which will result in a lower food supply and higher food prices in the world market. This issue has been hotly debated in the media.

Crops are renewable resources that produce much biomass. Cereal, such as wheat and rice, accumulate approximately 50–70% of their biomass in grains and 30–50% in straws at harvest. Straw serves as animal food or as renewable energy from the remaining biomass. Straw may be pressed into biomass pellets, which has an approximate energy value of 4.44 kWh/kg compared with 11.86 kWh/kg of fuel oil (TFZ, 2013). Recently, pellet heating has become approximately 50% cheaper per energy equivalent than oil heating. Using biomass pellets is a more efficient way for protecting resources, as long these pellets do not compete against food security.

Increasing agricultural production and productivity may be attained by new cultivars or better management. Therefore, this dissertation investigates the principles for a better management. To improve the management of farm inputs, precise agriculture was introduced in the middle of the 1980's (MULLA, 2013). Precision agriculture involves better management of farm inputs, such as fertilizers, herbicides, seeds, by performing the right management at the right time and place (BONGIOVANNI and LOWENBERG-DEBOER, 2004; NELLIS et al., 2009; MULLA, 2013). Its technologies combine sensors, information systems, enhanced machinery, and informed management to detect spatial and temporal within-field variability (ZHANG et al., 2002; GEBBERS and ADAMCHUK, 2010; YAO et al., 2011). Hence, precision agriculture makes use of Global Positioning System (GPS) and a Geographic Information System (GIS) obtaining a precise position of mismanaged locations or zones within the field. Thus, precision agriculture optimizes production outputs by minimizing inputs, e.g., fertilizer (SEELAN et al., 2003; SCHELLBERG et al., 2008) and improves the sustainability of food supply by decision-making (YAO et al., 2011). In contrast, destructive measurements of crop growth/parameters for decision making in agriculture at field, regional, national, or global scales are extremely cost and labor intensive. Timely, precise and comprehensive information on crop production and methods for different spatial scales are required (DUVEILLER et al., 2012).

An important method to monitor crop growth and crop vitality for forecasting, modeling, and simulating yield, biomass, stress and/or nutrient status of crops at diffeent spatial scales is remote sensing (PINTER et al., 2003; NELLIS et al., 2009; YAO et al., 2011). Remote sensing plays a strong role in the agriculture and its remotely provided information are urgently required for decision making (ATZBERGER, 2013). Remote sensing is a non-destructive, cost-effective, and non-contact technique for the indirect monitoring of plant growth quantities (ATZBERGER, 2013; WILSON et al., 2014). Remote sensing remotely collects the information about a phenomenon or object (LILLESAND et al., 2008) by active or passive aquisition systems. Particularly, remote sensing applications in agriculture are based on the interactions of the electromagnetic radiation with the crop canopy, which contains information about the plant and plant-surranding materials, such as soils or even water. Remote sensing sensors are carried by satellites, aircrafts, unmanned aerial vehicles, tractors, or people in the field offering different spatial resolution, imaging and non-imaging spectral data (MULLA, 2013). Depanding on the collected number of spectral bands and spectral resolution, remote sensing is classified in multispectral (few broad bands) and hyperspectral (many narrow bands) acquisition systems.

Hyperspectral remote sensing provides a particularly powerful tool for diagnosis and plant monitoring (HANSEN and SCHJOERRING, 2003; JONES and VAUGHAN, 2010). Hyperspectral sensors/spectrometers, such as satellite imaging sensors (e.g., EnMap, Hyperion, or PRISMA), airborne imaging sensors (e.g., AISA EAGLE, CASI, or HyMap), and non-imaging hand-held sensors (e.g., FieldSpec 3 from ASD, HandySpec from tec5), remotely sense many continuous narrow bands and provide a high spectral resolution (THENKABAIL et al., 2011). The last mentioned sensors, such as

hand-held sensors, represent proximal remote sensing or close-range field spectrometers and, currently, offer the highest number of narrow spectral bands (> 2000 bands) in hyperspectral remote sensing. Proximal sensors are the most common remote sensing devices for a precise site-specific management in precision agriculture (JONES and VAUGHAN, 2010). This combined technology offers the real-time monitoring of plant nutrients and plant vitality. Therefore, hyperspectral remote sensing opens a wide field for detailed quantitative analyses of plant characteristics compared with multispectral sensors (KUMAR et al., 2006; MIGDALL et al., 2009; THENKABAIL et al., 2011). These detailed quantitative analyses involve the evaluation of spectral reflectance signatures caused, e.g. by phenology-driven changes in the biophysical and biochemical process in the plants and nutrient inputs, such as of fertilizer.

For the linkage of hyperspectral sensed data/reflectance with plant biophysical and biochemical characteristics, diverse methods and approaches are known, such as vegetation indices, optimized combination of narrow bands, and optimum multiple narrow band reflectance based on stepwise multiple linear regression (THENKABAIL et al., 2000; 2011; XAVIER et al., 2006), or derivatives of reflectance (DEMETRIADES-SHAH et al., 1990). Hyperspectral remote sensing has been widely used in agricultural applications, such as biomass monitoring using non-imaging field spectrometers (CASANOVA et al., 1998; SERRANO et al., 2000; YANG and CHEN, 2004; ROYO and VILLEGAS, 2011; JIN et al., 2013; FU et al., 2014), or imaging spectrometers (HABOUDANE et al., 2004; MUTANGA and SKIDMORE, 2004; PSOMAS et al., 2011; JARMER, 2013; MARIOTTO et al., 2013), and plant nitrogen monitoring using non-imaging field spectrometers (OSBORNE et al., 2002; YI et al., 2007; STROPPIANA et al., 2009; RYU et al., 2011; MIPHOKASAP et al., 2012; LI et al., 2014) or imaging spectrometers (TIAN et al., 2011; VIGNEAU et al., 2011; INOUE et al., 2012).

Particularly, in this dissertation, hyperspectral remote sensing data from hand-held field spectrometers and from the EO-1 satellite-carried Hyperion spectrometer are important for non-destructive monitoring of plant vitality or plant nutrient status, e.g. of biomass and plant nitrogen in wheat and rice. In combination with ground-based information about plant characteristics, hyperspectral remote sensing enables to better assess potential impacts to the food supply, and hence, to the food security.

1.2 Problem statement

Food security issues for a growing population, such as China, may be addressed by increasing the input of the international market or by increasing crop yields. The Green Revolution offers not only opportunities but also challenges and problems. China is extremely vulnerable to water shortage, drought, and flooding, which can lead to crop failure. To ensure food security, China is paying a high price for its environment and peoples' health (HOERING, 2010). Many environmental problems occur, such as groundwater contamination and soil degradation due to over-fertilization and nitrate leaching.

Mineral fertilizer input, such as nitrogen, may significantly increase the yield; however, nitrogen is a major pollutant. Nitrogen application is relatively ineffective because many crops only absorb 30–75% of nitrogen from the soil (TIVY, 1993), which often leads to suboptimal management practices (CUI et al., 2013) and to low nitrogen use efficiency (RAUN et al., 2002). However, Chinese farmers often apply much fertilizer at a high environmental cost to prevent low yields (CUI et al., 2010). In the past, the Chinese government supported farmers by subsidizing nitrogen fertilizer production. Hence, both fertilizer input and production increased. Generally, higher fertilizer application increases the yield and farmers' income (GAO et al., 2006). In particular, the more developed eastern coastal provinces have demanded a two-fold higher fertilizer application than the economically backward central and western regions (GAO et al., 2006).

The overuse of nitrogen fertilizer means an oversupply of nitrogen to soil, ground water, and to the atmosphere. Plant disease and pest infestation may occur and reduce the potential yield. The mineral is dissolved in water and is finally leached into groundwater. In the 1960s and 1970s, high nitrate concentrations were observed in rivers and ground water in developed countries (TIVY, 1993). ZHANG et al. (1996) reported that more than half of the 69 locations in the North China Plain exceeded high or critical nitrate rates in drinking water. High fertilizer applications are highly related to high nitrate content in groundwater. Soils may be strongly acidified by nitrification, and their quality for agricultural use may be reduced (BÜNEMANN et al., 2006). Furthermore, the contaminated groundwater affects animal and human health.

Contaminated water can cause childhood and animal diseases. People often consume polluted nutrients without knowing their impacts. Because humans are at the top of food chain, humans pay a heavy price for this pollution. Nitrogen absorption in blood can result in typical symptoms, such as blue baby syndrome, hemoglobin in blood, and decreased functioning of the thyroid gland (SELF and WASKOM, 2013). Babies and children are more sensitive to the health effect of nitrate than adults are. Protecting children's health has become a high priority for the Chinese government since the last food scandals (HOERING, 2010). Regular nitrate tests are required to test the drinking water. Proper management of nitrogen sources may minimize the contamination of drinking water. Negative impacts of health have often been ignored, whereas nutrition and other benefits of agriculture have not always been optimized (MCDERMOTT and GRACE, 2011).

These negative impacts on health and on the environment threaten human food security and cause socioeconomic problems. A sustainable land use of arable land meets increasing food access, which involves favorable conditions for the environment, economy, and society (LIU et al., 2013). Precise crop management is essential for sustainable development and for environmental protection. Effective nitrogen fertilizer management tactics are required to ensure a fertilizer supply with minimum losses to the environment (CHEN et al., 2010). Knowledge regarding crop phenology, weather influence, dynamic soil, and nutrients are important parameters for timely and precise farming.

In order to support decision-making, precision farming requires the precise monitoring of plant growth and fertilizer input (GEBBERS and ADAMCHUK, 2010). Therefore, precision agriculture makes use of diverse remote sensing technologies (satellite, airborne, ground-based). Remote sensing technologies, such as based on imaging data, have their disadvantages due to atmospheric conditions and to inadequate repeat intervals (LILLESAND et al., 2008). Those intervals represent revisit times of two or three weeks, in worst case, between two successive overpasses of a study area and, additionally, have the disadvantage of fixed-time image acquisition (JONES and VAUGHAN, 2010; MUÑOZ-HUERTA et al., 2013). Moreover, multispectral satellite sensors have less bands, and thus, acquire less information than hyperspectral ones (SCHAEPMAN, 2009; ORTENBERG, 2011). In contrast, hyperspectral proximal sensors, such as spectrometers, measure the observed plant canopy with a high amount of data and high spectral resolution (NELLIS et al., 2009; THENKABAIL et al., 2011), are more flexible and transportable, are more independent of atmospheric corrections (JONES and VAUGHAN, 2010), and have an acquisition window of several hours (MILTON et al., 2009).

1.3 Outline and aims

This dissertation arose within the framework of two Sino-German projects entitled, "Regional N-management in Huimin County, Shandong Province, China (2006–2007)" and "Microwave imaging to derive upland rice characteristics in Jiansanjiang, Heilongjiang Province, China (2007–2009)", which were funded by the International Bureau (IB) and the Federal Ministry of Education and Research (BMBF). Both projects involved the multidisciplinarity of the Institute of Geography at the University of Cologne and of the College of Resources and Environmental Science at the China Agricultural University (CAU) of Beijing in physical geography, geoinformation, remote sensing, agriculture, precision agriculture, and plant nutrition. The study sites - Huimin County and Jiansanjiang - are located in the North China Plain and the Sanjiang Plain, respectively. Huimin was selected because of an existing experimental station and because of cooperation between Prof. Dr. Bareth, Prof. Dr. Fusuo Zhang, and Prof. Dr. Xinping Chen from CAU since 1999. The collaboration in Jiansanjiang started in 2007, managed by Ass. Prof. Dr. Yuxin Miao, who established another experimental station (Jiansanjiang) for CAU in 2011. The projects aimed to benefit from the multidisciplinary Sino-German cooperations. The main purpose of these projects was to monitor the growth of agricultural parameters, such as biomass and plant nitrogen, using hyperspectral non-imaging and imaging data. In addition, the microwave image data mentioned in the title of the second project were acquired during the field campaigns but were not studied in this dissertation. In fact, microwave data were acquired at both study sites and were used in Wolfgang Koppe's dissertation. This dissertation aims at answering the following research aims:

- How may biomass and plant nitrogen be non-destructively determined by hyperspectral remote sensing?

- Which non-destructive method is the most promising for the monitoring of biomass or plant nitrogen by hyperspectral remote sensing?
- Are the diverse methods transferrable to other fields or sites?
- Which role does phenology play in the diverse non-destructive estimation methods derived from hyperspectral remote sensing data?
- Does hyperspectral remote sensing explain the higher variability in biomass or plant nitrogen when the diverse methods are improved stepwise?

To address the main research aims, four different approaches were evaluated: vegetation indices (VIs), best band combinations, optimum multiple narrow band reflectance (OMNBR), stepwise multiple linear regression (MLR), and derivatives of reflectance. Extensive destructive measurements of biomass and plant nitrogen and non-destructive hyperspectral measurements were conducted following diverse growth stages at the two selected study sites from 2006–2009. The samples and hyperspectral measurements (Humin test site) were synchronized with the satellite overpass of EO-1 Hyperion. Diverse VIs and best band combinations were investigated for winter wheat at the Huimin test site, and their performance for biomass and plant nitrogen estimations was compared (chapters 3–4). Additionally, multiscale biomass models based on different VIs, which were derived from field hyperspectral measurements, were developed and tested with Hyperion imageries (chapter 5). Because the rice canopy at the Jiansanjiang test site has different influences on its reflectance patterns, additional MLR models were applied to compare the aforementioned methods (chapters 6–7). To address corresponding issues caused by the soil and water background noise in paddies, the methods were further improved by involving more time-intensive pre-processing analyses, such as smoothing and derivatives of reflectance (chapter 7). VIs, band combinations, and OMNBR models were developed, tested, and compared.

In addition, different calibration and validation methods were tested to investigate whether the estimation may be improved: calibration with experimental data and validation with farmers' data (chapter 3–6) and a pooled dataset of experimental and farmers' data, with random division in calibration and validation subsets (chapter 7).

This dissertation is organized into nine chapters. This introduction (chapter 1) is followed by a basic chapter (chapter 2), with the basics of agronomy and the phenology of winter wheat and rice (chapter 2.1), the definitions of biomass and plant nitrogen (chapter 2.1.3), an overview of the basics of remote sensing and proximal remote sensing of vegetation (chapter 2.2), and a geographic overview of the study areas and of the ground truth in the test sites. Then, chapters 3–7 follow with the five research papers corresponding to the briefly summarized research focuses and results:

Chapter 3 (LI et al., 2008): The broad bands of the Quickbird satellite sensor were simulated using hyperspectral field data. Spectral indices were calculated to estimate biomass and plant nitrogen

in winter wheat at different growth stages based on experimental data. The results were validated using farmers' field data. The simulated bands were used to determine the N status at a large observational scale in the next step with the best performing index, RVI.

Chapter 4 (KOPPE et al., 2010): The broad band vegetation indices from EO-1 ALI imagery, and the narrow band vegetation indices and best band combinations from EO-1 Hyperion imagery were calculated for farmers' fields across the winter wheat growing season to estimate the biomass, plant height, and N status at a large scale. The best band combinations for the Normalized Ratio Index (NRI) provided best estimates of biomass and plant nitrogen.

Chapter 5 (GNYP et al., 2014b): A multiscale approach regarding the experimental and farmers' fields was performed to upscale stepwise regression models. The models were based on hyperspectral indices derived from field hyperspectral data for estimating winter wheat biomass across the entire growing season. Finally, the approach was transferred to a larger scale using EO-1 Hyperion data. As shown in chapter 5, the proposed NRI and a newly developed index (GnyLi) have the highest accuracies.

Chapter 6 (GNYP et al., 2013): The best band combinations based on SR and NRI equations and multiple linear regression (MLR) models were derived from field hyperspectral data and were fitted on multiyear experimental data at different growth stages of rice. The established multiyear models were tested at a large scale using data collected from farmers' fields. The best band combinations and MLR bands for biomass estimation were identified.

Chapter 7 (GNYP et al., 2014a): The experimental and farmers' field data were randomly divided into a calibration and validation dataset for each growth stage of rice. Spectral data were smoothed, and derivatives of reflectance were calculated to establish regression models based on the best band combination and optimum multiple narrow band reflectance (OMNBR) for biomass estimation. GreenSeeker broad bands were simulated. The derivatives, along with the raw hyperspectral data, were used for regression models. The OMNBR model, which was coupled with the derivative spectra, slightly improved models' accuracy.

Chapter 8 contains a discussion of the following main topics: four different non-destructive methods for the estimation of biomass and plant nitrogen by remote sensing, uncertainties by model up-scaling, the importance of single growth stages and growing season, the effect of sample size and diverse calibration/validation methods, potential errors and disadvantages in statistics and hyperspectral data collection, and unexplained biomass and plant nitrogen by hyperspectral reflectance.

Chapter 9 summarizes the main conclusions and provides an overview of future challenges and outlooks.

2. Basics

2.1 Agronomy of winter wheat and rice and their geographical extent

Maize, rice, and winter wheat are the main crops in both China and in the world. The production of rice and winter wheat amounted to 722 and 701 Mio. t in 2011 (Fig. 1.2), respectively (FAOSTAT, 2011), which correspondently ranked the 2nd and 3rd place in the world production after maize. Wheat is cultivated around the globe where agriculture is possible, whereas rice grows mostly in Asia. China is the main producer of both crops. Winter wheat mainly grows in Central and East China, whereas rice dominates the agricultural area in South China. Wheat represents the basic cereal to make flour for the Chinese steamed bread, named mantao, in North China, and rice is the main food in South China. Winter wheat and rice are basic elements for many staple foods and alcoholic products. In addition, the biomass of shoots serves as animal feed and biofuel. Concerning photosynthesis, wheat and rice belong to C3 plants. As such, these crops thrive in cool environments (ACEVEDO et al., 2002). Temperature, water, and nitrogen mainly regulate the growth of both crops.

2.1.1 Winter wheat

Winter wheat is a cereal grain with a long cultivation history having its origins in Fertile Crescent. Wheat belongs to the family of sweet grasses (Poaceae), subfamily of Pooideae and tribe of Triticeae. Mutations reproduced specific and replicable species of wheat, and breeders bred diverse cultivars for each region and country. The major cultivated species is *Triticum aestivum* (*T. aestivum*), which is also known as bread wheat. Additional cultivated species are *Triticum spelta* (*T. spelta*) and *Triticum durum*. Wheat grows as winter or summer cereal. Their differences are in the sowing time and in the growth duration. Winter cereal is sown in autumn, requires a vernalization in winter season, and its main growth is in late autumn and from spring to summer. Summer cereal is sown in spring, is not resistant to cold climate, and grows until autumn. Winter wheat is valued as a cold crop for temperate climates (FRANKE, 1997). Its root system is more extensive than that of summer wheat because of the extra time available for growth (BOWDEN et al., 2007).

2.1.1.1 Global producing areas of winter wheat

Wheat or winter wheat mainly grows in the northern hemisphere (Fig. 2.1). The largest producer is the European Union (EU), followed by China and India (FAOSTAT, 2012). Climate conditions in the EU enable its cultivation in most of the countries. The geographic extent of wheat covers from 23.5 °N (Tropic Cancer) to 60°N in the northern hemisphere, including India and China. In particular, the Indian union territories located south of the Himalayas and the North China Plain in China are the main producers in Asia (Fig. 2.1). In the southern hemisphere, wheat is cultivated from 23.5°S to 40°S (Tropic of Capricorn), including the western, southern, and eastern Australian coasts and Argentina. According to FAOSTAT (2011, 2012), China, India, and Australia are the only countries in the top 15 ranking, which significantly increased their annual production and total yield, whereas

Germany and Russia reduced their production in favor of other crops. The rapid development of Asia and Australia has led to high food staples demand driven by rising population in those continents. The world's most productive farms with the highest yield for wheat in 2012 were in Netherlands and Belgium, with 8.9 t/ha (FAOSTAT, 2012).

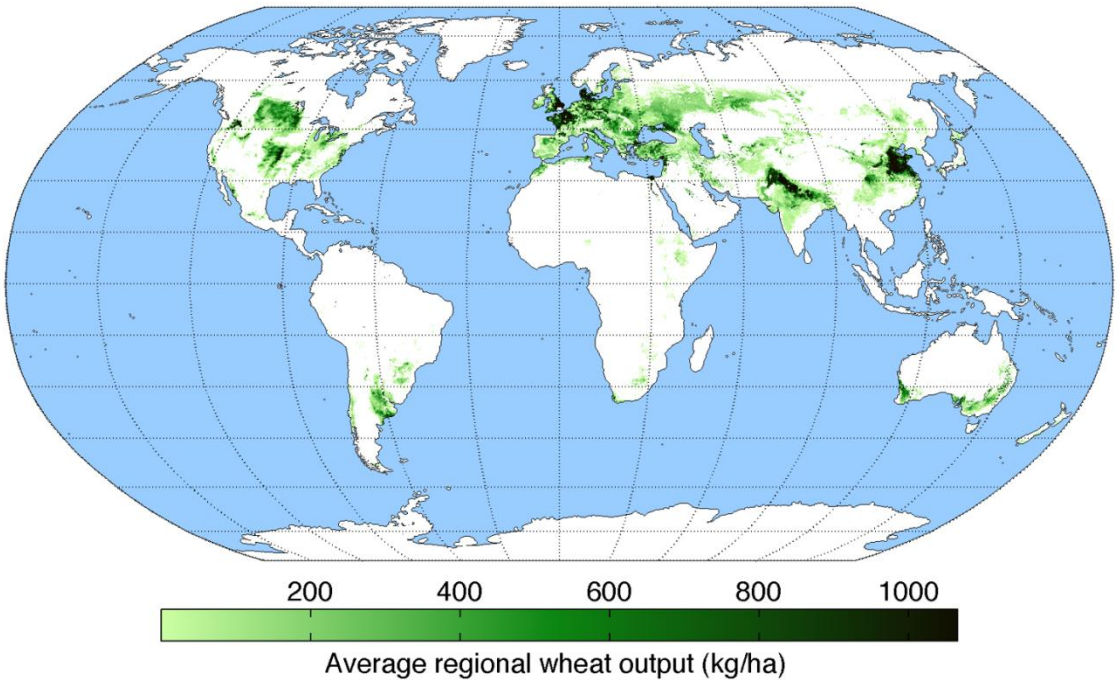

Fig. 2.1 Geographical extent of wheat production in the 2000. The map was compiled by the University of Minnesota Institute on the Environment based on provided data by MONFREDA et al. (2008). Map source: http://en.wikipedia.org/wiki/Wheat. 2014-01-22.

2.1.1.2 Phenology of winter wheat

The phenology of winter wheat can be described in three main phases or cycles (BOWDEN et al., 2008). Each cycle breaks down into primary and secondary growth stages (Fig. 2.2). The first cycle represents the vegetative cycle, which contains the principle stages of germination, leaf development, and tillering. The first cycle stands for growth of roots, leaves, and tillers. Tillers are connected to the mother plant by internodes in the root system and represent daughter plants having their own main culm with several leaves. The vegetative cycle is interrupted by vernalization in winter, without plant growth (Fig. 2.2). Plants normally reach the leaf development stage before vernalization begins. The second growth cycle is called the reproductive cycle. The principle growth stages of this cycle are stem elongation, booting, heading, and flowering. Plants initiate developing heads, the spikelet, and the flag leaf before heading initiates. Senescence occurs after heading above the middle of the ear and proceeds upwards and downwards (ZADOCKS et al., 1974). Moisture stress, temperature, flowering time, nitrogen, and herbicides influence reproductive development (BOWDEN et al., 2008). In the third growth cycle, which is called grain development or reproductive post-heading, grains develop from flowering to physiological maturity. Carbohydrates and protein are

deposited in the grain as the grain grows and ripens (BOWDEN et al., 2008). Simultaneously, the water content decreases. The primary growth stages are fruit development, ripening, and maturity. Growth conditions during that cycle affect the grain quality. According to the BBCH scale of MEIER (2001), the first cycle corresponds to BBCH code 00 to 29, the second cycle to BBCH code 30 to 65, and the third to BBCH code 66 to 99. Alternatively, the Feekes scale may be used, which was introduced by ZADOCKS et al. (1974).

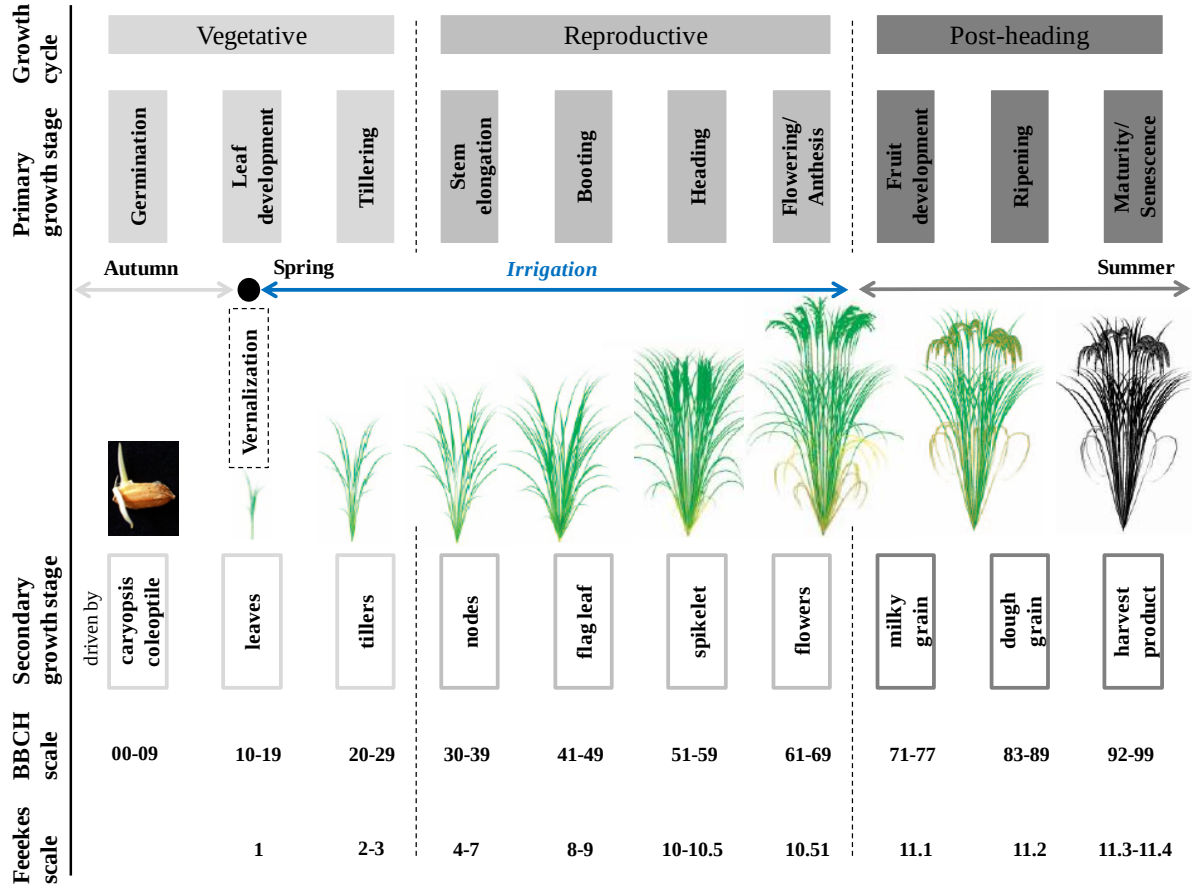

Fig. 2.2 Winter wheat phenology (own illustration; plant pictures modified from WATANABE et al., 2005). Winter wheat in the North China Plain requires irrigation.

2.1.1.3 Growth requirements and cultivation practice for winter wheat

Winter wheat has high demands on climate, soil, and site selection. The preferred climate has a cool winter, warm summer, and intensive insolation. As a winter cereal, winter wheat requires a vernalization of at least six to nine weeks, with a temperature from 0–5°C (DIE LANDWIRTSCHAFT, 2006). Winter wheat has a low optimal temperature of approximately 0°C (WANG and ENGEL, 1998). Vernalization is important for the growth and development during the stem elongation and ear emergence at the heading stage. The plants are frost-resistant until -22°C (FRANKE, 1997). Hence, the crop benefits from temperate climates. Winter wheat requires heavy, nutrient soils, particularly loamy or black soils with high water availability (FRANKE, 1997). Winter wheat develops rich deep root systems up to 1 m and is less sensitive to drainage (TIVY, 1993). The most important soil layer is the

first 0–30 cm layer, which corresponds to half of the water absorption (DEMIRCAN, 1995). A pH value of 6 to 8 is common. Most suitable site locations for wheat cultivation are flat plains, such as the North China Plain or the United States (U.S.) Great Plains (INGRAM, 2005). The common cultivation practice is a seed drill with row spacing of 10–13 cm. A drill machine precisely sows the seedlings with a density of 320–380 seed corns per m² and 2–3 cm deep into the soil. The previous crop has significant importance to yield losses of winter wheat. The best previous crops are beet, rape, or maize (DIE LANDWIRTSCHAFT, 2006).

2.1.2 Rice

Similar to wheat, rice is a cereal grain; however, its earliest archaeological evidence originates from East and Central China. Rice belongs to the Poaceae family, genus *Oryza*, and is classified in different species, which divide the Oryza into subgroups that categorize the *Oryza* into regional geographical extensions, e.g., *Oryza sativa*, also known as Asian rice in Asia, *Oryza nivara* in Southeast Asia, or *Oryza glaberrima* in Africa. In addition, rice is classified into classes of rice land according to topography, water regime and flooding regime (MOORMANN and BREEMEN, 1978). The major categories are irrigated, rainfed lowland, deep water, upland, and tidal wetlands. As for wheat, thousands of cultivars exist that are specific for diverse regions and countries. Rice growth is dependent on climatic conditions and on the geographical location in summer and winter as a single, double, or triple crop in many Asian countries. Rice cultivars are categorized into two main groups - tropical and temperate (VAN NIEL and MCVICAR, 2004). The growth cycle for temperate cultivars is approximately 140–150 days, and the growth cycle for tropical cultivars is 30 days shorter.

2.1.2.1 Global producing areas of rice

Rice is a dominant crop in Southeast Asia, China, and Japan. The main producers, China, India and Indonesia, produce half of the world's total rice (Fig. 2.3). The geographic extent of rice is from 47°N to 35°S. Rice cultivation is dependent on the cultural background and on the water regime. It is apparent that rice plays an important role in Southeast and East Asian cuisine and culture. In addition, high annual precipitations benefit rice cultivation. The average precipitation in these regions amounts to 1,000–2,000 mm. In China, the main production area is the Middle and Lower Chang Jiang agricultural region, south of the North China Plain (Fig. 2.3). Rice cultivation in Northeast China receives a lower precipitation of 480–1,080 mm (LIANG et al., 2011). Not including Asian countries, Brazil, USA, Egypt, and Nigeria are in the top 20 ranked producers (FAOSTAT, 2012). Rice cultivation is unusual in EU due to its temperate climate conditions and culture. The exception is South Europe, including France, Spain, and Italy. The most famous European rice area is in the Po Valley in Italy. The world's most productive farms with the highest rice yield are in Australia, with 10.8 t/ha (FAOSTAT, 2012).

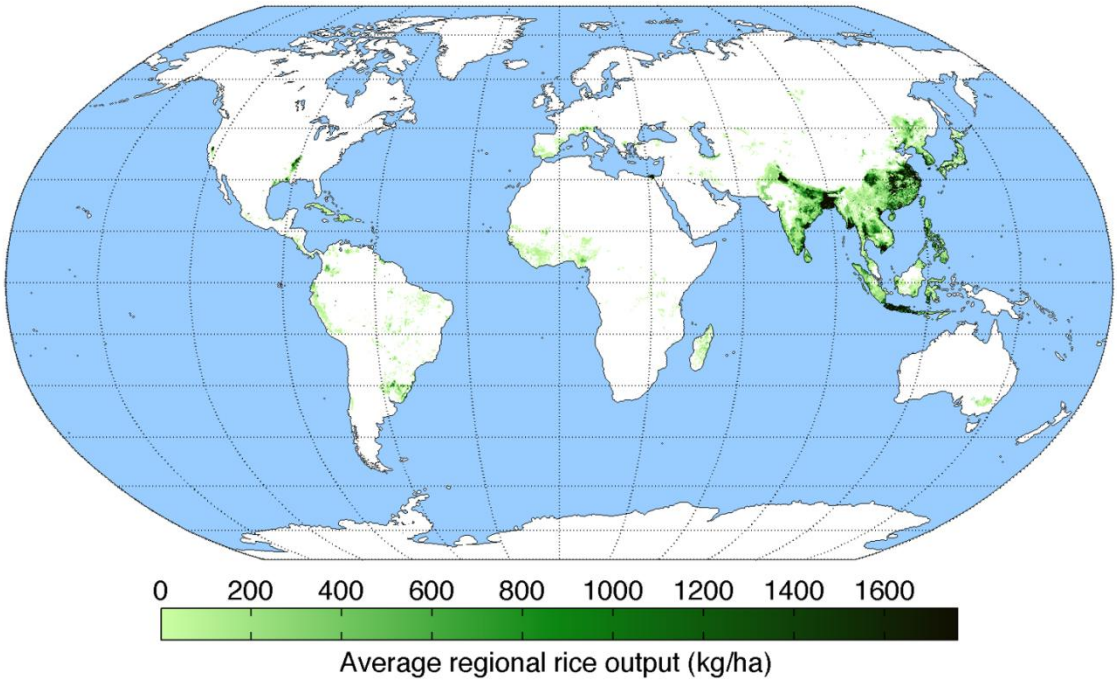

Fig. 2.3 Geographical extent of rice production in 2000 . The map was compiled by the University of Minnesota Institute on the Environment based on provided data by MONFREDA et al. (2008). Map source: http://en.wikipedia.org/wiki/Wheat. 2014-01-22.

2.1.2.2 Phenology of rice

The phenology of rice generally conforms to that of wheat, with the main difference in its transplantation (Fig. 2.4). Asian temperate rice is mostly transplanted, which often induces a stoppage of development followed by recovery (ZADOCKS et al., 1974). Rice plant growth is composed of three main growth cycles. The vegetative cycle is defined by germination, initiation of tillering and active tillering. Asian temperate rice often germinates in rice nurseries, grows in greenhouses until leaf development, and is transplanted to fields after the frost period. The growth cycle in the field is characterized by tillering and ends when the maximum tiller (main culm or daughter plant) number is reached. The number of tillers is an important parameter because each tiller develops a panicle, which represents a yield component (YOSHIDA, 1981). Transplanted rice has higher tiller density (10–30 tillers per hill) than direct-seeded rice (2–5 tillers per hill). The reproductive cycle starts at the panicle initiation stage (stem elongation), followed by booting, heading, and ends with flowering. This cycle is characterized by increasing plant height, declining tiller number, and ear emergence. Flowering proceeds from the top of the panicle downwards (ZADOCKS et al., 1974). The third growth cycle is responsible for grain filling. This cycle extends from flowering to maturity and is known as the reproductive post-heading cycle (CASANOVA et al., 1998) or the ripening cycle (YOSHIDA, 1981). This cycle is subdivided in fruit development, ripening, and maturity stages (YOSHIDA, 1981). This cycle initiates the senescence of plant leaves and shoots, whereas the weight of grains increases. The first two cycles are important for nitrogen fertilization, which is applied in the flooded paddies. In contrast,

the paddies are not flooded beginning with the third cycle (Fig. 2.4). Phenological stages of rice may also be described using BBCH codes or Feekes scale.

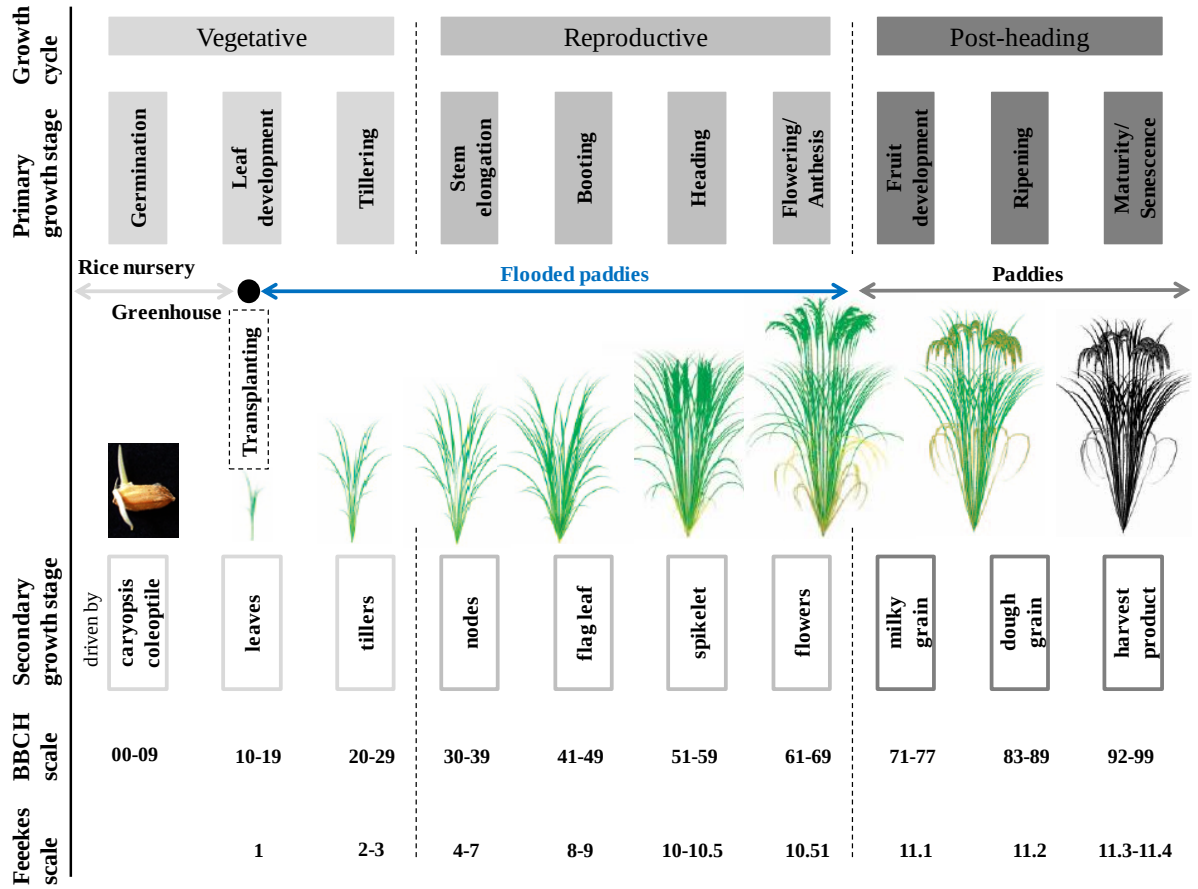

Fig. 2.4 Rice phenology (own illustration; plant pictures modified from WATANABE et al., 2005).

2.1.2.2 Growth requirements and cultivation practice for rice

Rice production depends on climate, water management, and site selection. Rice grows under tropical and temperate conditions. Rice in temperate zones requires a minimum temperature of 13°C for growth and is not frost-resistant (YOSHIDA, 1981). Its critical temperatures are 7°C (lowest) and 45°C (highest), depending on different growth stages. Depending on the climate, one (temperate with 140–150 growth cycle days) to three (tropical with 110–120 growth cycle days) rice crops can grow per year. Rice grows in all type of soils, except for extremely sandy ones (MOORMANN and VAN BREEMEN, 1978). Deep tillage or mulching has positive effects on biomass development and yield (KATO et al., 2007). Soils with a pH value of 6–7 are the best for rice cultivation; however, a pH value of 4 to 8 is also unproblematic (MOORMANN and VAN BREEMEN, 1978). Rice is extremely sensitive to the water regime and to water stress (FUKAI and COOPER, 1995). In particular, the water temperature and water depth determine growth and development. At the early stages, water temperature affects yield by affecting the panicle number, whereas at the later stages, air temperature controls the yield parameters (YOSHIDA, 1981). Increasing the water depth is an efficient method for protecting rice

plant against low temperatures. Rice cultivation requires 200 mm water monthly (MOORMANN and VAN BREEMEN, 1978; YOSHIDA, 1981). Hence, the site location is dependent on the water regime and on water availability. Temperate rice grows mostly in paddy fields, which represent flooded parcels of arable land with a water depth of approximately 5–15 cm. The seedlings are sown in rice nurseries and grown in greenhouses before transplanting to fields after the frost period. Thus, four to five pre-germinated rice seedlings (120–150 seedlings per m^2) are planted on one hill (28 hills per m^2) with a hill spacing of 12 cm and with a row distance of approximately 35 cm. At this stage, the seedlings usually have four leaves and radial root systems, which later extend to 60 cm deep (TIVY, 1993). The irrigation is stopped one month before harvest.

2.1.3 Biomass and plant nitrogen

Agronomic parameters represent specific information regarding the biophysical or biochemical process in a plant. Regular measurements during the phenological cycles of crops, particularly during critical growth stages, are important for monitoring plant growth and precise fertilization. Some of these measurements may be non-destructively measured using remote sensing technology. In this chapter, only the relevant parameters for this dissertation, such as biomass, plant nitrogen, and their destructive methods of measurements, will be defined and introduced in the context of agriculture, particularly for winter wheat and rice. Destructive measurements are required to develop methods for monitoring biomass and plant nitrogen.

2.1.3.1 Biomass

Biomass, which is also called fresh matter, dry matter, or phytomass, is a biological material produced by living organisms, mostly plants. Photosynthesis is the ultimate source for biomass production (BEADLE and LONG, 1985). In the process of photosynthesis, plants absorb solar illumination and transform carbon dioxide (CO_2) and water (H_2O) in carbohydrates (CH_2O) and oxygen (O_2) (KUMAR et al., 2006). Plants grow and develop different plant organs below and above the soil surface during their growth cycle. In the cases of winter wheat and rice, which represent the family of sweet grasses, there is underground root biomass and aboveground biomass, which consists of leaves, stems, nodes, tillers, and heads with panicles, spikelet, and grains. Generally, the dry total aboveground biomass is of particular interest. The dry mass exponentially increases at the vegetative growth cycle, rises slowly during the reproductive cycle, and reaches up to 20 t/ha at harvest time. Fresh biomass samples must be cleaned from soil or other particles and roots must be cut from the aboveground biomass. Because fresh matter contains water, the fresh matter must be dried to determine the dry matter. The drying process requires dry boxes. Waste agricultural biomass in the form of dried plant materials may be used as fuel, an energy source, animal food, or organic fertilizer.

The following chapters only refer to the dry total aboveground biomass of all organs, such as leaves, stems, and heads.

2.1.3.2 Plant nitrogen

Plant nitrogen refers to the nitrogen concentration (% of dry matter) in the plant. For their survival, plants require nutrients, which are absorbed in liquid form by plant roots from the soil and accumulate in different plant organs. Nitrogen is one of the mineral nutrients and is dissolved in water. Nitrogen is one of the chemical elements, in addition to other mineral nutrients (e.g., phosphorus, potassium, calcium, sulfur, or magnesium) and non-mineral nutrients (carbon, oxygen), that controls plant growth and health. The plant nitrogen concentration is measured on a dry matter weight basis in quantities from 0.2–4.0%, whereas the range from 1.8–3.6% of dry mass indicates nitrogen sufficiency in grass grains (BARKER and BRYSON, 2007). Its concentration is differentially distributed in the plant organs, with the highest concentration in leaves. For the process of plant nitrogen determination, the aboveground biomass has to be dried, milled, and then analyzed in the laboratory. There are two methods to analyze their concentrations. One method is digestion using inorganic acids, known as Kjeldahl-N (MUÑOZ-HUERTA et al., 2013), and the other is the elementary analysis method, which uses gases and is performed using a C/N/P or C/N Analyzer. The Kjeldahl digestion method was used to estimate plant nitrogen in both studies. Plant nutrition plays an important role in calculating the nitrogen nutrition index (NNI). That index is the ratio of the actual measured N content of the crop and the critical N content, which indicates the minimum N content required for the maximum biomass production of the canopy (MISTELE and SCHMIDTHALTER, 2008).

2.2 Remote sensing and proximal remote sensing of vegetation

Remote sensing and proximal sensing of vegetation bring together a wide range of disciplines, including physics, mathematics, computing, environmental science, and biology (JONES and VAUGHAN, 2010). The use of remote sensing for agricultural applications is one of the main fields of remote sensing (CLEVERS, 1999; ATZBERGER, 2013). Remote sensing and proximal sensing differ in their available scale: large scale (region) compared with close range (field) scale. Both sciences are important in precision agriculture by providing the opportunity of precise plant monitoring. This chapter primarily refers to the remote monitoring of biomass and plant nitrogen. The principles of remote sensing, their basic physics, and some selected non-destructive monitoring methods will be introduced.

2.2.1 Principles of remote sensing

Remote sensing indirectly detects information regarding the electromagnetic radiation (EMR) from earth's surface without making contact with the object. LILLESAND et al. (2008) described remote sensing as follows: "Remote sensing is the science and the art of obtaining information about an object, area, or phenomenon through the analysis of data acquired by a device that is not in contact with the object area, or phenomenon under investigation". One particular advantage of remote sensing is that remote sensing is a non-contact and non-destructive method (JONES and VAUGHAN, 2010).

Remote sensing has two acquisition systems, active and passive. Active systems emit EMR by themselves and scan the reflected radiation of measured objects from the target. Because an active system is not used in this dissertation, only passive systems will be explained in detail. Passive systems detect the reflected EMR from objects or their emitted EMR and transform the radiation into digital information. Solar radiation is the most common source of passive systems. Thus, a passive system is strongly dependent on solar radiation and on acquisition time. In addition, remote sensing classifies the acquisition systems into two systems based on their spectral resolution: multispectral sensing and hyperspectral remote sensing.

2.2.2 Multispectral remote sensing

Multispectral remote sensing systems operate with multiple (usually 2–16) broad spectral (>10 nm) bands (Fig. 2.5). Multispectral information is widely known as broadband data with limited spectral analyses (THENKABAIL et al., 2011). Most multispectral sensors have four bands in the visible (blue, green, red) and near infrared (NIR) domains. Airborne and satellite multispectral remote sensing data can compose true color images. Multispectral remote sensing is not the focus of this disseration; however, the multispectral sensor EO-1 ALI (NASA, Washington, D.C., USA) and the simulated multispectral Quickbird (DigitalGlobe, Longmont, Colorado, USA) and GreenSeeker (Trimble Navigation Limited, Sunnyvale, California, USA) bands derived from field hyperspectral data were included in three of the published journal papers (chapters 3, 4, 7).

2.2.3 Hyperspectral remote sensing

Compared with multispectral remote sensing, hyperspectral systems acquire information across the electromagnetic spectrum (Fig. 2.5). The continuous collected information represents many narrow spectral bands (usually > 200) with high spectral resolution (< 10 nm). The term hyperspectral is often used for spectroscopy and spectrometry and usually denotes the presence of many spectral bands (SCHAEPMAN, 2009). Hyperspectral data are superior to traditional broadband analyses in spectral information (THENKABAIL et. al., 2011). Hyperspectral remote sensing uses imaging or non-imaging spectrometers. Recently, hyperspectral sensors have been mounted on satellite, airborne, or unmanned aerial vehicle (UAV) platforms. Hyperspectral data are useful for meaningful spectral libraries (LAUDIEN et al., 2006; CHAUHAN and MOHAN, 2013; THENKABAIL et al., 2013). Spectral libraries are attractive for identifying surface materials without new required field campaigns (CHEN and CAMPAGNA, 2009). Vegetation indices are commonly used for the quantification of different surface materials. Because hyperspectral remote sensing produce much data, band selection is important for extracting the information of interest (BAJWA and KULKARNI, 2011). An example of a hyperspectral satellite sensor is EO-1 Hyperion, with 220 bands. The airborne hyperspectral sensor AVIRIS has 220 bands. Full range spectrometers (350–2500 nm) provide 2,151 narrow bands representing high dimensionality and multicollinearity.

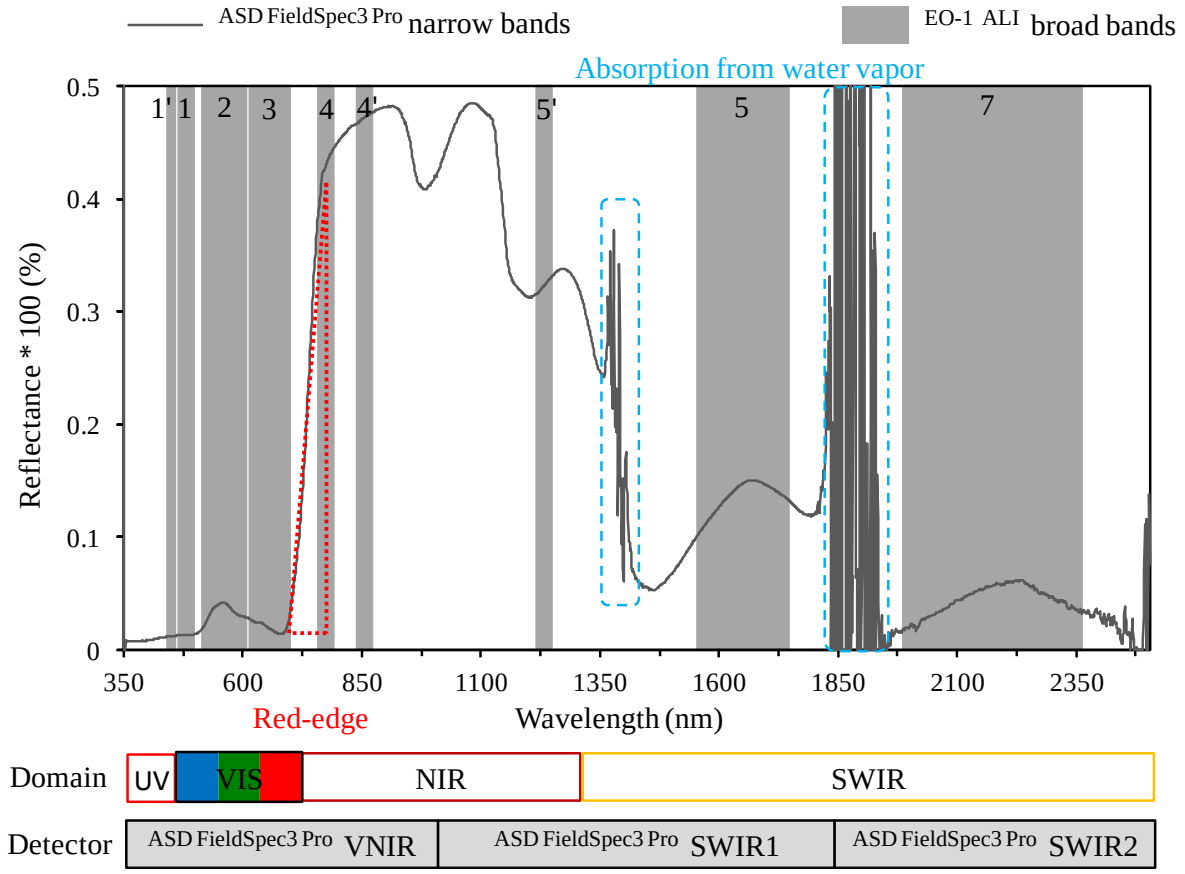

Fig. 2.5 The narrow bands from ASD FieldSpec3 Pro and the broad bands from EO-1 ALI (own illustration). Domains follow the definition by KUMAR et al. (2006).

2.2.4 Proximal sensing

Proximal sensing, or close-range sensing, is the imaging or non-imaging acquisition of objects from a close range that have a high resolution at a small scale. Proximal sensors are able to capture spectra of individual leaves, plant organs, and canopies, which remains impossible for satellite or airborne sensors. Typical examples of proximal sensing systems are non-imaging active systems, such as CropCircle (Holland Scientific Inc., Lincoln, Nebraska, USA) and GreenSeeker, and non-imaging passive system spectrometers. Simple hand-held sensors mounted on fixed platforms (e.g., tractors) or hand-held sensors carried in the field are sufficient for small scale, infrequent monitoring or for calibration purposes (JONES and VAUGHAN, 2010). These sensors are widely used for the calibration of airborne and satellite sensors (MILTON et al., 2009; ROZENSTEIN et al., 2014). The scale and acquisition area are dependent on acquisition height (distance between the sensor and the canopy) and field of view. Depending on the number of bands, proximal sensors may acquire multispectral or hyperspectral information. Field spectrometers represent hyperspectral proximal sensors that collect a half (350–1000 nm) or full (350–2500 nm) range of the electromagnetic spectrum with a sensor-canopy distance of several centimeters to several meters. Due to that close sensor-canopy distance, atmospheric corrections, which are needed for imaging airborne or satellite systems, are not required for field spectrometers (JONES and VAUGHAN, 2010).

In addition, new sensors, such as Cubert (Cubert GmbH, Ulm, Germany), provide imaging and non-imaging information regarding the canopy and open new opportunities in plant monitoring from close-range to far-range on hand-held UAV platforms.

2.2.5 Basic physics of spectrometry and reflectance

Spectrometry is a technology for measuring the power of optical radiation in narrow contiguous wavelength intervals (SCHAEPMAN, 2009). Proximal sensors, such as spectrometers, represent optical instruments of spectroscopy to measure the electromagnetic radiation (EMR) (KUMAR et al., 2006). The EMR consists of time-varying electric and magnetic fields that travel in the form of a wave at the speed of light (JONES and VAUGHAN, 2010). It is a form of radiant energy and is characterized by the frequency (Hz) or wavelengths (nm). Frequency is inversely proportional to wavelength according to Eq. (2.1):

$$\lambda = c/f \quad \text{or} \quad \lambda f = c \qquad \text{(Eq. 2.1)}$$

where λ, c, and f were wavelength, constant speed of electromagnetic waves, and frequency

Electromagnetic waves carry energy at a given wavelength given by Eq. 2.2:

$$E_\lambda = h f = h c/\lambda \qquad \text{(Eq. 2.2)}$$

where h, f, and λ were Planck's constant ($6.63\ 10^{-34}$ J s), frequency, and wavelength

Spectrometry is based on solar or artificial radiation that interacts in absorption, transmittance, or reflectance with surfaces or objects. Different objects have different spectral characteristics. Solar radiation varies during the day, reaching the highest intensity at noon, and depends on many other factors, including latitude, incident angle, daytime, or atmospheric conditions, such as cloud coverage. Surface roughness, differences in optical properties and biochemical contents also affect the reflectance (KUMAR et al., 2006; JONES and VAUGHAN, 2010). Calibration measurements are mandatory for minimizing these potential errors. Most spectrometers acquire spectral reflectance, which displays the ratio between reflected and total radiation. The basic physics of reflectance are dependent on acquisition parameters, such as geometry, site, time, and wavelength. KUMAR et al. (2006) utilized a function of those four parameters to describe the reflectance change when one of those variables was slightly changed. The reflectance intensity and its interaction with surfaces or objects are different at various wavelengths (VAN DER MEER, 2006) and will be discussed in the next chapter.

2.2.6 Spectral reflectance of plants and the influence of phenology

As mentioned in chapter 2.1.3, plants use solar illumination for photosynthesis. The ratio of the reflected portion by the plants to the total incident solar radiation can be called the spectral reflectance of plants, which is dependent on plant structure, other tissues, biochemical components, and on the distribution and arrangement of plants in the space (JONES and VAUGHAN, 2010). Plants reflect a continuous spectrum of solar radiation. In particular, the visible (VIS), red edge (RE), near-infrared (NIR), and shortwave-infrared (SWIR) reflectance are important, and their domains are variously defined in the literature. This section uses spectral domains defined by KUMAR et al. (2006):

1. Visible light (VIS) in the spectral range of 400–700 nm
2. Red-edge (RE) in the spectral region of 690–720 nm
3. Near-infrared region (NIR) in the spectral range of 700–1300 nm
4. Shortwave-infrared region (SWIR) in the spectral range of 1300–2500 nm

Remote sensing uses plant properties of reflectance and absorption for monitoring agronomic parameters, such as biomass and plant nitrogen, in the aforementioned four spectral domains. These domains reveal different interactions of the radiation in the plants controlled by biochemical contents. The first domain, the VIS, is characterized by low reflectance and transmittance due to strong absorptions by chlorophylls and by carotenes (KUMAR et al., 2006). The red-edge represents the shift from the VIS to the NIR domain, which is characterized by a rapid reflectance increase in plants from 690 nm to 720 nm. GUYOT and BARET (1988) applied a simple linear model using different wavelengths to that noticeable slope. At the first point (approximately 690 nm), the absolute minimum was observed and in the second point (approximately 720 nm), a significant inflection point was detected in the reflectance. One characteristic of a healthy plant is a dramatic spectral increase in that domain (LILLESAND et al., 2008). Plants reach the highest reflectance and transmittance in the NIR domain (VAN LEEUWEN, 2009). Plant reflectance in this domain primarily results from the internal cell structure and is highly variable between diverse crops (LILLESAND et al., 2008). In the SWIR domain, the reflectance is much lower than in the NIR domain. Strong water absorption and minor absorption features of other biochemical contents dominate the reflectance (KUMAR et al., 2006). The main water absorption bands are centered at wavelengths of approximately 1400, 1900, and 2500 nm. Lignin, cellulose, starch, and protein contents in plants are associated with the biochemical absorption features, which are masked by the water content in leaves (KUMAR et al., 2006).

Plant spectral reflectance is strongly influenced by growth stages when different organs develop and by changes in the biochemical contents. In addition, leaf angles, leaf arrangement, shaded leaves, and crop row orientation caused significant reflectance changes (JOHANNSEN and DAUGHTRY, 2009). During the vegetative growth cycle, leaves and their biochemical components control the reflectance. Leaves and stems, and heads equally influence the reflectance characteristics during the reproductive growth cycle. During the post-heading or grain filling growth cycle, chlorophylls degrade faster than carotenes and are not important for the reflectance. Carotenes and xanthophylls now

become the dominant chemicals in leaves (KUMAR et al., 2006). Leaves lose their green color at the heading stage and appear yellow because the dominant chemicals absorb blue light and reflect green and red light (KUMAR et al., 2006). With progressing plant senescence, brown pigments appear, and the reflectance decreases. The growth stage, nutrient availability, water status, and disease affect the spectral properties of plant canopies and are important for management decisions based on the correct growth stage (JOHANNSEN and DAUGHTRY, 2009; PIMSTEIN et al., 2009). Agricultural production follows strong seasonal patterns related to the biological growth cycle (ATZBERGER, 2013).

Diverse plants and crops reveal different reflectance intensity in the maximal reflectance. The maximal reflectance of plants is approximately 80% before the heading stage is reached. Winter wheat plants reach higher reflectance caused by their broader leaves compared with rice plants. In addition, diverse cultivars have a strong impact on reflectance. In the case of rice crops, water surrounding the plant influences field reflectance (MARTIN and HEILMANN, 1986; VAN NIEL and MCVICAR, 2004; KUENZER and KNAUER, 2013).

2.2.7 Remote sensing methods for the non-destructive monitoring of biomass and nitrogen

This chapter only refers to non-destructive monitoring methods of biomass and nitrogen based on hyperspectral data. As mentioned in 2.2.3, hyperspectral data processing and analysis are more complex, with advantages and disadvantages. Allowing band selection and optimization is advantageous; however, additional processing is required to remove the redundant information from hundreds of bands. Four different methods will be introduced for hyperspectral data analysis: vegetation indices, optimized best two band combinations, optimum multiple narrow band reflectance, and derivatives of reflectance. These analysis methods are used and are discussed stepwise in the five papers (chapters 3–7).

2.2.7.1 Published vegetation indices (VIs)

Vegetation indices (VIs) are usually used to study vegetation cover, which indicates the amount of green vegetation present in a view, whereas spectral indices are related to the parameter of interest, e.g., water content or growth stages (JONES and VAUGHAN, 2010). There are hundreds of diverse vegetation and spectral indices using two, three or four bands. These indices are new variables calculated by mathematical equations based on combinations of at least two or more spectral bands. VIs are developed to detect different biochemical properties or plant diseases associated with plant vitality. Depending on the remote sensing data and on the mathematical function, VIs are categorized in broad or multispectral, narrow or hyperspectral, combined, normalized, or simple ratio indices. In addition, ROBERTS et al. (2011) classified the VIs based on the interest in the estimating structure (LAI, green biomass, fraction), biochemicals (pigments, anthocyanins, carotenoids, lignin), or physiology (light use efficiency, stress). The widely known VIs are the Simple Ratio (SR) and the

Normalized Difference Vegetation Index (NDVI). They are developed in the 1960s and 1970s based on discrete red and NIR bands.

VIs are crop-, cultivar-, site-, and sensor-specific. The transfer from fixed bands often failed in a multiyear approach (from one year to another year), although one cultivar is used for the same crop and at the same site. Temporal variations in temperature and insolation strongly influence plant growth development, and thus, the interannual differences in spectral reflectance exist. SR and NDVI are commonly used and optimized by selecting the best band combinations.

2.2.7.2 Optimized best two band combinations

To overcome the problem of fixed bands, THENKABAIL et al. (2000) introduced a band combination method, which systematically identifies the most effective narrow wavelengths for predicting biophysical quantities of each crop. Band combinations reduce the data dimension by reducing the number of bands without sacrificing significant information (THENKABAIL et al., 2011). The method requires a calculation of lambda (λ_1) by lambda (λ_2) plots to identify redundant and unique bands, which involves all possible narrow bands. Redundant bands are perfectly correlated with each other, and thus, only one of the two bands may be sufficiently used with an agronomic parameter and another narrow band (THENKABAIL et al., 2011). A correlation matrix or contour plot denotes the correlation of each two narrow bands with an agronomic parameter. Hence, the best band combination represents the highest correlated narrow band pair of all possible matrices.

Because the matrices increase dramatically with the number of available bands, an automated calculation is of high value. In this manner, higher correlations to agronomic parameters of interest are detected than by published vegetation indices (VIs). The method may be applied on all VIs that use at least two or more spectral bands. Most common combinations use two bands by optimizing the SR and NDVI. The required time for calculating the combinations increases when using more than two bands and a simple visualization of more than three dimensions is problematic.

Furthermore, this method avoids the well-known saturation effect of VIs. NDVI saturates at LAI of 2.5–3, which usually occurs at the vegetative growth cycle. Band combinations enable more accurate estimations of biomass or plant nitrogen at growth stages of interest and across the growth season.

2.2.7.3 Optimum multiple narrow band reflectance (OMNBR) and stepwise multiple linear regression (SMLR)

Compared with band combinations, the optimum multiple narrow band reflectance (OMNBR) method requires at least two available bands and has no limit to band number. THENKABAIL et al. (2000) suggested this method for crop biomass estimation. The OMNBR is based on stepwise multiple linear regression (MLR). Since the last view years, OMNBR has also been known as the hyperspectral multiple-band model (HMBM) and follows the same computation (THENKABAIL et al., 2011). Bands

with highest correlations with the predicted agronomic parameter are added stepwise to the regression equation. The equation fitting is stopped when the best regression model predictability is achieved.

A critical problem of OMNBR is the over-fitting and collinearity problem. Over-fitting occurs when an added band does not significantly improve the previous model accuracy. Collinearity occurs when redundant bands, which are highly correlated with each other, are used as the predictors. Particularly for abundance of data from hyperspectral sensors, many bands cause the collinearity problem. A test of the collinearity diagnostics notes the multicollinearity problem by indicating how many bands can be smoothly used. Most OMNBR models use six or less bands to avoid the over-fitting issue.

2.2.7.4 Derivatives of reflectance

At the tillering and stem elongation stages, background signals have a mixed effect on canopy reflectance, particularly when there is low canopy density. The reflectance responds to the objects in the field of view, such as plants, soil, and water. The latter ones, soil and water reflectance, represent background signals that reduce the reflectance signal of the plant. The effect of background signals may be reduced by lowering the senor-canopy distance or reflectance measurements on a leaf scale (ALVARO et al., 2007). In addition, derivatives of reflectance reduce background signals from soil or water. The advantage of derivatives of reflectance is their ability to locate and to characterize subtle spectral details (LILLESAND et al., 2008), to improve the signal-to-ratio-noise ratio (OWEN, 1995), as well as to eliminate background signals and to resolve overlapping spectral features (DEMITRIADES-SHAH et al., 1990). Derivatives of reflectance are extremely sensitive to noises (TSAI and PHILPOT, 1998). Their calculation requires a spectral smoothing in advance. The most common smoothing method is the Savitsky-Golay procedure (SAVITSKY and GOLAY, 1964). The first and second derivatives of reflectance are widely applied in reflectance processing and are used to improve the above-mentioned methods. The second derivative of reflectance has the additional advantage that this derivative is relatively insensitive to variations in illumination (TSAI and PHILPOT, 1998).

2.3 Study areas and ground truth in the test sites

The two study areas – the North China Plain with the Huimin test site and the Sanjiang Plain with the Jiansanjiang test site – fundamentally differ in their geographical extents, agricultural history, and ecosystems. The first study area, the North China Plain, is in the "heart" of China, which is characterized by high population density and which forms the origin of Chinese civilization. The optimized small-scale farming and limited agricultural land leave no space for another land use, except for winter wheat and summer maize cropping systems. In contrast, the more northern located Sanjiang Plain has a short agricultural background characterized by several land use changes in its history. The low populated plain is known for large-scale farming, such as granary in Northeast China, and for its northernmost high-quality rice production.

2.3.1 North China Plain (NCP)

The North China Plain (NCP), also named the Huang-Huai-Hai Plain, is in East China and extends over Henan, Hebei, and Shandong, and partly over Anhui and Jiangsu provinces, as well as the municipalities of Beijing and Tianjin (Fig. 2.6). Due to the diverse definitions of the plain, the definition and calculated area based on the GIS analysis by BARETH (2003) have been adopted for this dissertation. The NCP is bordered by the Yanshan Mountains in the North, the Bo Hai Sea and the hills of Shandong in the East, the Yangtze Plain in the South, and the Taihang Shan Mountains and the edge of Shanxi plateau in the West (Fig. 2.6). The plain is the largest alluvial floodplain of East China, which evolved from the deposits of the Huang He River (also called Yellow River). The Huang He River enters the NCP toward the Loess Plateau, flows from southwest to northeast, and enters the Bo Hai Sea north of the hills of Shandong. The NCP covers an area of 328,000 km², ranging from 113°E to 120°E and from 32°N to 41°N. The maximal north-south extension is approximately 900 km, and the maximal west-east extension is approximately 700 km. The plain region is less than 50 m above sea level. The southern part of the NCP, named the Central Plain (Chinese: Zhongyuan), formed the origin of Chinese civilization. The first dynasty in China, named the Xia Dynasty (2,100–1,600 BC), originated here. The entire NCP has been settled since the Spring and Autumn period (722–481 BC) of Chinese history (MÜLLER, 1997).

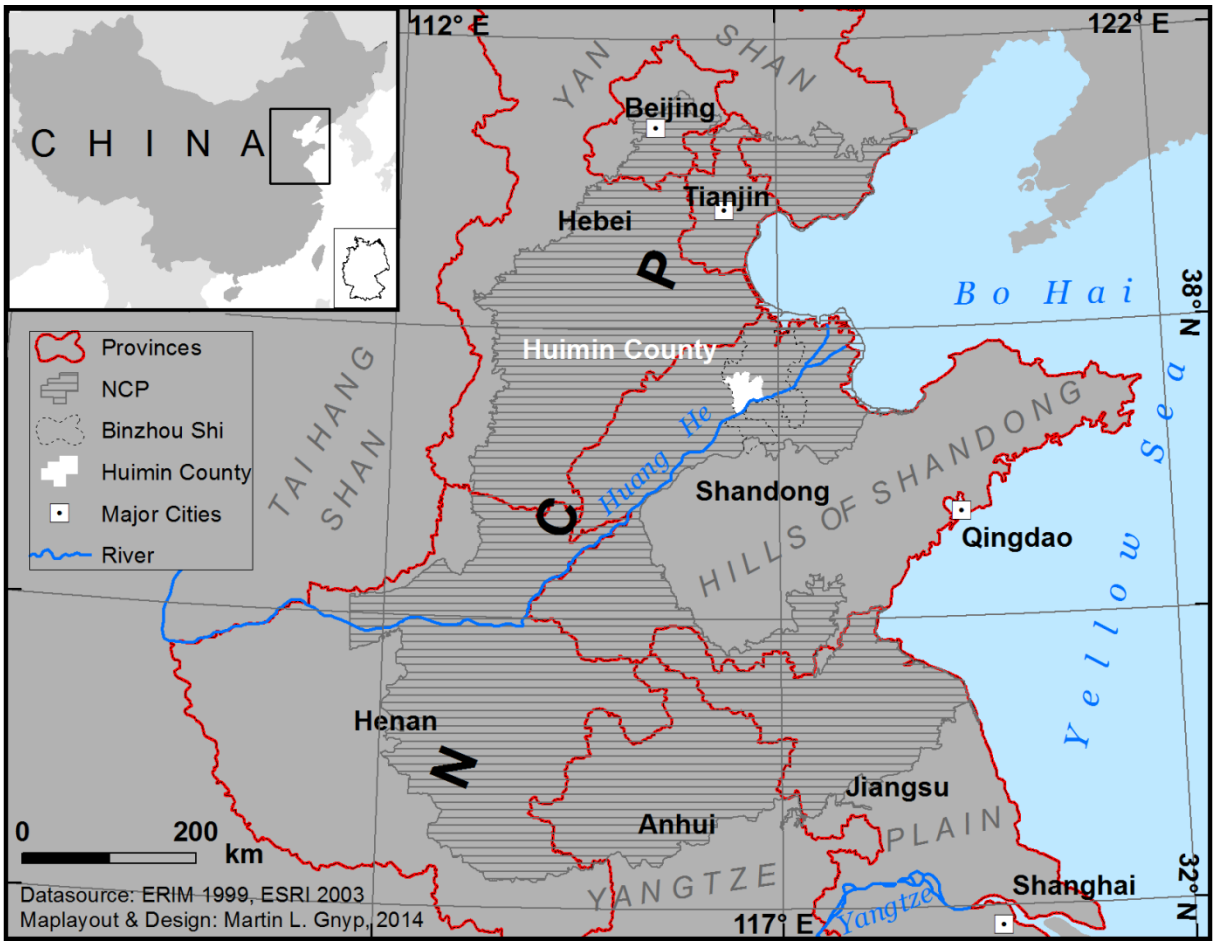

Fig. 2.6 Geographical locations of the North China Plain (NCP) and the Huimin test site.

2.3.1.1 Climatic conditions in the NCP

The climate of the NCP is influenced by the Siberian Anticyclone and by the East Asian Monsoon. Winter is cold and dry and is dominated by the Siberian Anticyclone. Conversely, summer is hot and humid and is characterized by high precipitation, which comes with the air masses from the south and southeast during the monsoon season. Fig. 2.7 exemplary shows the monsoon-driven summer precipitation at the Huimin test site in the NCP. The monsoon reaches the southern NCP approximately on June 30 and reaches the northern NCP approximately on July 20 (MÜLLER, 1997). Summer precipitation decreases from the south (approximately 900 mm) to the north (approximately 600 mm) of the plain. Following the Köppen climate classification, the northern and eastern regions of the plain are classified as Dwa climates, the central region is classified as the BSk climate, and the southern region is classified as the Cwa climate.

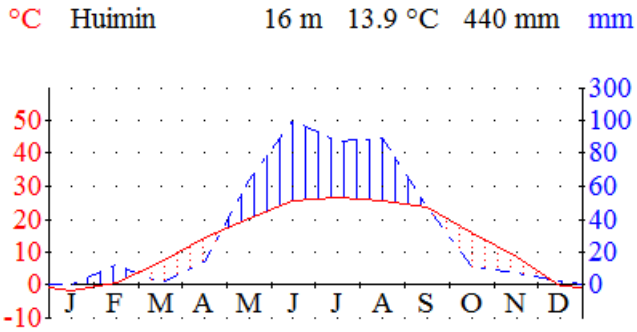

Fig. 2.7 Climograph of Huimin (2005–2007) based on data from the meteorological station of Huimin (37°28'N, 132°30'E). Th graph was plotted in Klima 0.9.

However, the climate has extremely high interannual variations in temperature and precipitations (see Table 2.1). The observations from the meteorological station of Huimin show insufficient precipitation compared with the high temperature in spring. Hence, winter wheat has to be irrigated as required.

Table 2.1 Climate conditions in Huimin (2005–2007) based on data from the meteorological station of Huimin (37°28'N, 132°30'E).

Huimin	Precipitation (mm)			Temperature (°C)		
	2005	2006	2007	2005	2006	2007
January	0.0	0.9	0.5	-2.6	-1.3	-1.9
February	13.3	10.6	12.0	-2.6	0.2	4.5
March	1.3	0.0	0.7	5.6	8.1	6.9
April	16.3	10.6	13.5	15.9	13.6	14.0
May	37.0	92.7	63.4	20.2	20.4	21.6
June	73.8	100.1	140.1	26.4	26.1	25.2
July	105.3	114.8	39.4	27.4	26.4	26.2
August	120.5	99.5	45.4	25.4	25.9	25.3
September	96.0	11.7	36.9	26.4	23.9	21.4
October	10.5	0.3	*23.0	14.9	17.8	*16
November	3.5	17.4	*0.0	8.6	8.1	*9
December	1.8	0.5	*5.0	-2.3	-0.5	*1
Sum/Mean	479.3	459.1	379.7	13.6	14.1	14.1

* Data from meteorological station of Jinan

2.3.1.2 Soils of the NCP

Soils of the NCP are influenced by three factors: basic materials, river flow changes in the Huang He river basin, and anthropogenically influenced agricultural landscape. The basic materials are loess and alluvial loess. As a dominant river of the plain, the Huang He transported sediments from the Loess Plateau and accumulated these sediments in the NCP over several thousands of years until the present (DU et al., 1990). The Huang He changed its river flow and adapted its present course in 1897 north of the hills of Shandong (LEUNG, 1996). Because the plain is extremely flat and only has a weak depression, the plain has weak drainage. The influence of sea water results in soil salination (LIU and HSEUNG, 1990). The irrigation practice also has an impact (ACEVEDO et al., 2002). In addition, anthropogenic influence has left an agricultural landscape without any forest in the last 2,500 years. Consequently, LIU and HSEUNG (1990) characterized the soil of the alluvial floodplain as fluvo-aquic or salinized fluvo-aquic soils. DU et al. (1990) described the fluvo-aquic soil in the NCP as yellow fluvo-aquic soil. The content of soil organic matter in the soils amounts to 0.5–1.0% and reaches higher percentages of 1.0–1.5% in the areas close to the Bo Hai Sea (INSTITUTE OF SOIL SCIENCE, 1986). The pH value is extremely high (7.5–8.5) and homogenous across the NCP.

2.3.1.3 Agricultural ecosystems of the NCP

The NCP has been solely used as agricultural land for several centuries. The NCP belongs to the oldest agricultural landscape, except for the Fertile Crescent. For over 4,000 years, Chinese farmers have managed to produce modest crop yields and to develop different strategies of crop rotations (MIAO et al., 2011). The main crops are winter wheat, summer maize, rarer millet, soybean, and cotton. Maize was not planted in the 1970s but has become important in recent decades (MÜLLER, 1997). Recently, a summer maize and winter wheat intercropping has become a common crop rotation in the NCP. The climate allows two cropping per year. Because the spring is extremely dry due to the climate conditions, winter wheat has to be irrigated as required, whereas summer maize receives sufficient precipitation during the summer monsoon (Fig. 2.7 and Table 2.1). Average water consumption is approximately 450 mm for wheat and 360 mm for maize (LIU et al., 2001). Consequently, a water deficit exists with a maximum of 300 mm in the northern part of the NCP and decreases to the southern part because the annual precipitation amounts to 600 nm in the northern and 900 mm in the southern regions. Apart from the mentioned main crops, specialty crops (e.g., vegetable or tomato) occupy a central position. The specialty crops are planted in greenhouses, which are constructed from loess loam. The agriculture of the NCP is known for small-scale farming with fields smaller than 1.5 ha per farmer. The NCP produces approximately 30% of China's food (FANG et al., 2010).

2.3.1.4 Huimin test site and experimental design

The Huimin test site (37.3°N, 117.4°E) is located at the lower reaches of the Huang He River, approximately 100 km west of the Bo Hai Sea in the North China Plain (Fig. 2.6). The test site is representative of the NCP and was selected because of the existing long-term field experiments by the China Agricultural University and because of the opportunity to collect ground truth data from selected fields. Two field campaigns were performed during the growth seasons of winter wheat in 2005/2006 and 2006/2007. Winter wheat was sown in October 2005 and in October 2006. The experimental design included fields of diverse sizes: small experimental fields (level 1), large experimental fields (level 2), small farmers' fields (level 3), and large farmers' fields (level 4).

Level 1 was composed of small experimental fields and had a split-plot design with four replications. The main plots consisted of six nitrogen (N) fertilizer treatments: control without N application (0 kg Na ha^{-1}), 40% of the optimum N rate (Opt), 70% of Opt, 100% of Opt, 130% of Opt, and conventional N rate fertilizer application of 369 kg N ha^{-1} (Con). The optimum N rate (Opt) was determined based on the soil N_{min} method and amounted to 133 and 155 kg N ha^{-1} in 2005/2006 and 2006/2007, respectively (LI et al., 2010). The existence of two cultivars, Kenong9204 and Lumai23, virtually doubled the plots to 48 plots. Each plot size was 4.5 m by 7 m in 2005/2006 and 4 m by 9 m in 2006/2007. Level 2 included larger experimental fields with 20 plots and a size of 10 m by 15 m per plot. The experiment used the cultivar Weimai8 and had 5 N rates (0, 25, 50, 75, and 100 kg N ha^{-1}) and four replicates. During topdressing, each plot was divided into two equal parts (7.5 m by 10 m). One part received N topdressing and the other half did not.

The small farmers' fields (level 3) were closely located next to the experimental fields. In 2005/2006 and in 2006/2007, 16 and 14 farmers' fields were randomly selected, respectively. Each farmer's field was divided into four plots: Control without N (0 kg N ha^{-1}), Opt based on soil N_{min} before sowing, nitrogen fertilization optimization algorithm (NFOA) based on the fertilizer application during shooting stage, and conventional N rate (Con) with 133 or 155 kg N ha^{-1} similar to level 1. The plot size was 150 m^2 for the Control plots, 75 m^2 for the Opt and NFOA plots, and variable size (800-1,200 m^2) for the Con plots. In addition to those fields, another 69 farmers' fields (42 fields in 2005/2006 and 27 in 2006/2007) were selected in four different villages (Shizhang, Xili, Xujia, and Dongjie), which represented level 4. The four villages were closely located next to each other with a distance of less than 4 km. The farmers used different cultivars, Jimai20, Jimai21, Weimai8, Lumai23, Zimai12, and Lumai8. The farmers managed their fields according to their usual practice without any formal treatments.

2.3.1.5 Field measurements at the Huimin test site

Spectral reflectance and agronomic parameter measurements were collected between the tillering and ripening stages of winter wheat in 2006 and 2007 (March to May of each year). High resolution, non-imaging spectrometers from ASD (Analytical Spectral Devices, Inc., Boulder, CO,

USA) acquired the spectral reflectance above the winter wheat canopy. A Handheld FieldSpec Pro (spectral range of 325 to 1,075 nm) was used in 2006, and a QualitySpec Pro (spectral range of 350 to 1,800 nm) was used in 2007.

The Handheld FieldSpec (Unit 1298) is equipped with one detector covering the visible (VIS) and near infrared (NIR) domains, with 512 element silicon photo-diodes. This detector has a spectral resolution of 3.5 nm at 700 nm but captures the samplings in a 1.6 nm interval. The collected spectra were subdivided into 1 nm band width using an interpolation method of the ASD spectrometer. The QualitySpec (Unit 5038) has two detectors, one in the VNIR (350–1000 nm), which is equipped with 512 element silicon photo-diodes array, and another one in the SWIR1 (1001–1800 nm), with TE-cooled InGaAS photo-diodes. The device is configured for collecting spectra in a spectral resolution of 3 nm at 700 nm and 10 nm at 1400 nm, with a sampling interval of 1.4 nm in the VNIR and 2.4 nm in the SWIR1. The Handheld FieldSpec provides 751 hyperspectral bands, and the QualitySpec has 1,451 hyperspectral bands. The Handheld FieldSpec has a built-in fiber optic, whereas the QualitySpec uses an external 1.5 m long fiber optic cable that is equipped with 19 silica glass fibers to detect the VNIR spectra and 19 fibers for the SWIR1.

Both devices used a 25° default field of view and were fixed on an orthogonal construction at a height of 1 m above the canopy. The devices are passive systems depending on solar or artificial illumination and require a calibration by a barium sulphate ($BaSO_4$) white reference panel and a dark current measure (ASD TECHNICAL GUIDE, 1999). In the field, the measurements were taken by solar illumination under mostly cloudless conditions from 10 a.m. to 2 p.m. Local Mean Time (solar noon at 12 a.m. in June) to keep the illumination geometry as equal as possible. The calibrations were repeated in regular intervals (10–15 minutes) to respond to changes in solar illumination or in diffuse skylight. The spectrometers were operated with RS3 or Indico Pro software from ASD, where the sample counts were set to twenty for a white reference and to ten for each scanning position. Those settings are recommended for outdoor measurements taking a multiple spectra with the spectrum averaging set to reduce low-frequency effects (FIELDSPEC USER MANUAL, 2007). In addition to the technical settings, the number of the scan positions per plot differed between the two years for the experimental and farmers' fields (e.g., LI et al., 2008; LI et al., 2010; GNYP et al., 2014b). There were 3-6 scan positions per plot in 2006 and 6 scan positions in 2007.

After taking spectral reflectance, several agronomic parameters, such as biomass, plant nitrogen concentration of collected biomass, N uptake, and nitrate content, were destructively collected, whereas plant height and chlorophyll content (SPAD) were non-destructively measured. The aboveground biomass was sampled through randomly cutting an area of 100 cm by 30 cm at the early growth stage, 50 cm by 50 cm at later stages, and 30 cm by 30 cm before the harvest. The high biomass amount at the beginning was necessary to have sufficient dry matter for determining the plant nitrogen concentration in the laboratory. Fresh biomass samples were weighed and oven dried at 70°C to a constant weight to determine the dry matter. Finally, the biomass values were scaled to kg/m² or

to t/ha for each sample date. The dried biomass was milled, and the plant nitrogen concentration was determined using the Kjedahl-N method (LI et al., 2008). N uptake was derived by multiplying the whole plant N concentration and the dry biomass. Nitrate content, plant height, and chlorophyll are only relevant to the first two published papers of LI et al. (2008) and KOPPE et al. (2010), and therefore, their explanations are omitted in this chapter.

In addition to the field ground truth data, hyperspectral satellite images from EO-1 ALI and Hyperion were simultaneously acquired when the ground truth data were collected in 2006 and in 2007. The specifications and pre-processing of the satellite data for this field campaigns were discussed in detail by KOPPE et al. (2010), KOPPE et al. (2012), and GNYP et al. (2014b).

2.3.2 Sanjiang Plain (SJP)

The Sanjiang Plain (SJP) is located in northeastern China, Heilongjiang Province, and is a part of the Northeast China Plain (also known as the Manchurian Plain, covering approximately 350,000 m²). The SJP is bordered by Siberia and the Heilong River in the north and by the Wusuli River in the east (Fig. 2.8). The SJP is situated at the lower reaches of the Songhua River and is 450 km west of the Pacific Ocean. The plain is an alluvium floodplain of the following three (San=Chinese for three) rivers: Heilong, Songhua, and Wusuli (jiang=Chinese for river). Songhua and Wusuli flow into the Heilong River near Tongjiang and Khabarovsk, respectively (Fig. 2.8).

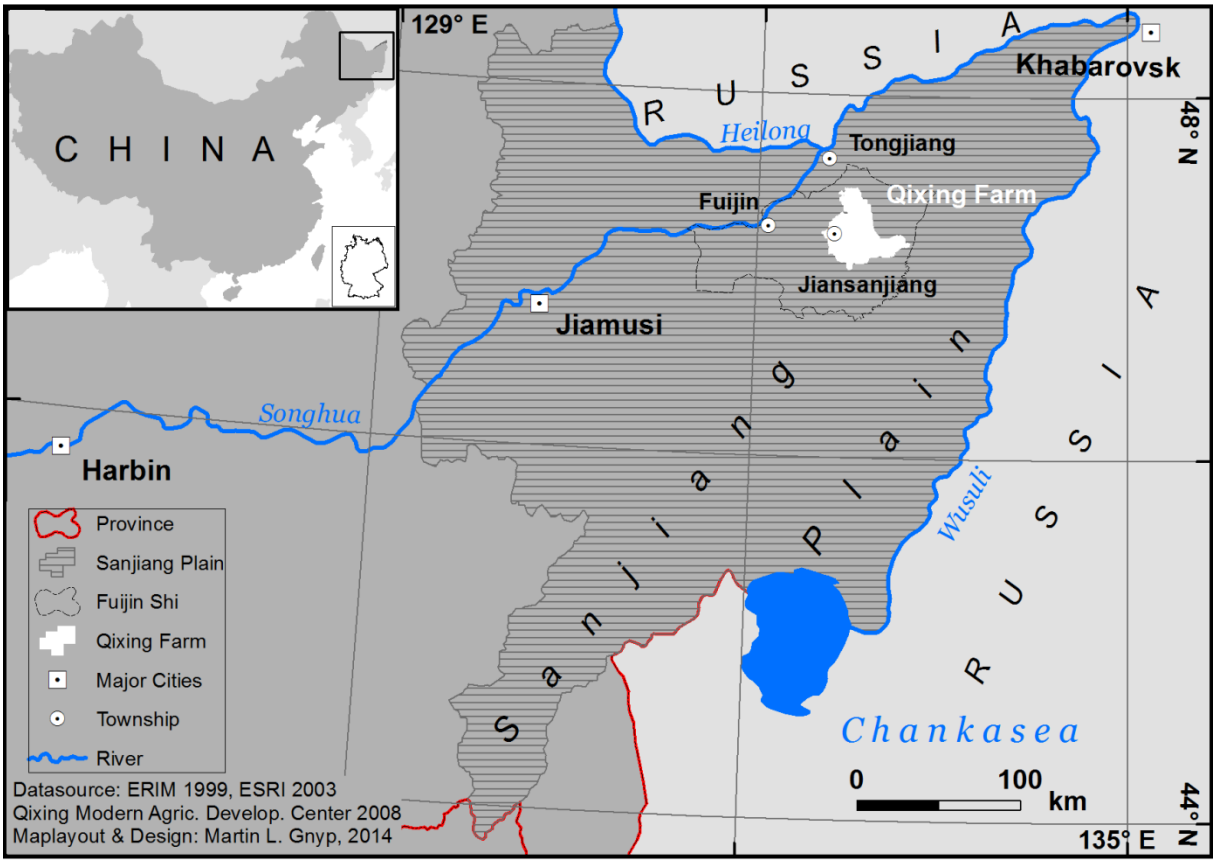

Fig. 2.8 Geographical locations of the Sanjiang Plain (SJP) and the Jiansanjiang test site.

The SJP covers an area of 108,900 km², which extends from 129° E to 135° E and from 44°N to 48°N. The maximal north-south extension is approximately 500 km, and the maximal west-east extension is approximately 350 km. The main part (~60%) is plain (50–70 m above sea level), whereas the remaining part is hilly and mountainous (WANG and YANG, 2001), with elevations reaching up to 1,000 m. The SJP is historically known as part of Manchuria and was opened to Han Chinese migration after the Treaty of Peking in 1860 (MEYERS CHINA ATLAS, 2010), when the recent frontier between China and Russia was established. This region is nicknamed the "Great Northern Granary" (GAO and LIU, 2011).

2.3.2.1 Climatic conditions in the SJP

The climate of the JSP is influenced by the Siberian Anticyclone and by the East Asian Monsoon. Hence, the winter is cold and dry. The summer is warm-temperate, humid and characterized by high precipitation, which is caused by the air masses from the south and southeast during the monsoon season. Compared with the North China Plain, the monsoon precipitation occurs two weeks (ca. July 15) later to the more northern-located SJP (MÜLLER, 1997). The annual precipitation is 550 nm per year (WANG and YANG, 2001) and corresponds to the amount in the northern part of the North China Plain. Approximately 70% of the precipitation occurs from June through September (Fig. 2.9 and Table 2.2). Following the Köppen climate classification, the area along the lower reaches of the Songhua River is classified as Dwa climate, whereas the northeastern and southern parts, which are mountainous, are classified as Dwb climate.

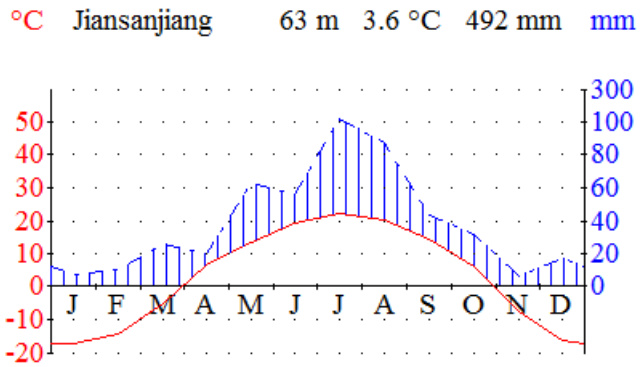

Fig. 2.9 Climograph of Jiansanjiang (2007–2009) based on data from the meteorological station of Jiansanjiang (47°17'N, 132°38'E). Th graph was plotted in Klima 0.9.

The boreal climate, Dwc, is approximately 300 km next to the Dwb climate zone of the SJP. As shown in the climograph of Jiansanjiang, the continental climate and the high variability in the monsoon intensity lead to extremely high interannual temperature differences (Table 2.2).

Table 2.2 Climate conditions in Jiansanjiang (2007–2009) based on data from the meteorological station of Jiansanjiang (47°17'N, 132°38'E).

	Precipitation (mm)			Temperature (°C)			Insolation (hours)		
Month	2007	2008	2009	2007	2008	2009	2007	2008	2009
January	4.3	0.0	16.6	-12.6	-20.3	-18.9	189	194	127
February	22.5	1.9	6.1	-12.2	-13.6	-16.7	179	223	161
March	34.1	30.1	13.2	-7.4	0.5	-7.6	218	174	228
April	7.8	33.0	17.9	5.4	8.4	6.4	283	181	278
May	61.0	90.0	37.6	12.9	12.0	15.7	203	183	235
June	78.7	18.0	71.1	20.7	21.0	17.5	292	274	131
July	55.9	112.0	204.4	22.1	23.2	20.6	344	221	162
August	123.0	31.0	107.9	21.4	20.4	20.4	283	235	201
September	35.0	46.0	51.3	15.2	14.3	13.9	177	228	223
October	54.9	33.2	6.9	5.4	6.1	6	199	187	186
November	0.0	12.0	6.2	-5.8	-7.5	-9.3	175	151	137
December	13.9	4.2	33.5	-13.6	-15.0	-20.5	157	125	135
Sum/Mean	491.1	411.4	572.7	4.3	4.1	2.3	2698	2376	2204

2.3.2.2 Soils of the SJP

The soils of the Sanjiang Plain are more heterogeneous compared with those soils of the NCP because of different geomorphology forms, such as alluvial plain, meander belts, depressions, rivers and lacustrine terraces, high floodplains, and low floodplains (LIU et al., 2013). In addition, the process of land use changes still continues. Soil types, such as meadow soil, lessive, swamp soil, Albic black soil, and black soil, compose more than 95% of the area (WANG et al., 2006). Meadow soils can raise one crop per year, and the agricultural utilization of these soils develops rather rapidly (ZENG and CHENG, 1990). Meadow and swamp soil mainly occur along the Songhua River. Albic and black soils are formed on the terrace in the lower reaches of the Heilong, Songhua, and Wusuli Rivers (ZENG et al., 1990). The remaining less than 5% are classified as dark brown forest soils, particularly in the mountainous southern region (SONG and XU, 1990) and partly paddy soils in southeastern region of the SJP (GONG and XU, 1990). However, the fast changes in cultivation patterns over the last three decades has resulted in variations in soil properties of the SJP (QUYANG et al., 2013) and may not present the actual soil type. Most likely, the current percentage of paddy soils is higher. The INSTITUTE OF SOIL SCIENCE (1986) mapped the soils of the SJP. The results showed a high content of organic matter, with 4–10%, and >10% for the swamp soils. The pH value ranges from 5–7.5 depending on the present soil.

2.3.2.3 Agricultural ecosystems of the SJP

The Sanjiang Plain has a short agricultural history with the original natural landscape of forest and marshes. Forests covered 68% of the Heilongjiang Province in 1896, and have largely been deforested since then (GAO and LIU, 2012). The SJP is characterized by land use changes since the migration of the Han Chinese until the present. Deforestation was caused by a demand for timber and by population-driven land reclamation for agriculture. Supported by the Chinese government with development programs that began in the early 1950s, which strongly encouraged the settlement and

reclamation of wetland, the natural landscape has changed, and the area has quickly developed into an important agricultural area in China (ZHOU and LIU, 2005). In 2005, the agricultural area was 55% of the total area, with 30% forest, 7% marshland, 3% grass, and 4% for the others, compared with 7% for agricultural area and 49% for marshland in 1949 (ZHOU and LIU, 2005). The area produces large quantities of high quality beans and rice in China (ZHANG et al., 2010). In addition to those main crops, maize and wheat are cultivated. Only one crop per year is cultivated due to the temperate climate conditions (see Table 2.2 and Fig. 2.9). In the last two decades, rice has become the major crop in the SJP. Climate warming, which has resulted in temperature increasing by 1°C from 1970–2009 (CHEN et al., 2012), has made possible a northward and eastward expansion of rice cultivation following the 2°C isoline (GAO and LIU, 2011). Rice cultivation requires an annual mean temperature of higher than 1°C (LIU et al., 2005). The primary rice producing areas are located along the Songhua, Wusuli, and Naoli Rivers. Due to agricultural modernization, the agricultural area of the SJP has been reorganized into 50 farm units at a large scale (LIU et al., 2013), where each farmer manages approximately 15–30 ha land.

2.3.2.4 Jiansanjiang test site and experimental design

The Jiansanjiang test site belongs to the Qixing farm (47.2°N, 132.8°E), which is approximately 60 km south of the Songhua's river outfall into the Heilong River, in the northeastern corner of the Sanjiang Plain, which is bordered by Russia in the north and in the east (Fig. 2.8). Similar to the Huimin test site, the China Agricultural University of Beijing established an experiment station at this site for the purpose of large scale remote sensing research. Three field campaigns were performed from 2007 through 2009.

Experimental fields were set up at two sites (Keyansuo and Qixing experimental stations), and nine farmers' fields were selected. At the two experimental sites, a randomized plot design, with at least three replications and five N rates, was used. In 2007, a randomized complete block design, with four replications and seven N rate treatments, was used (0, 60, 75, 90, 105, 120, and 150 kg N ha^{-1}). Two experimental fields were set up at the Keyansuo station, and two fields were set up at the Qixing station at the peripheral of the Jiansanjiang Township. Each experimental field had 28 plots, with a size of 5 m by 8 m per plot. In total, 112 plots were used in these four fields. In 2008 and 2009, one experiment was set up at each experimental station. A randomized split plot design was used, with four replications of five N rates (0, 35, 70, 105, and 140 kg N ha^{-1}). The plot size was 10 m by 10 m in 2008 and 2.5 m by 12 m (Qixing site) and 6 m by 10 m (Keyansuo site) in 2009 for the main plots. In contrast to 2007, the 2008 and 2009 experimental designs had subplots or the main plots were split into two equal subplots during topdressing. Details regarding N fertilizer application before transplanting and during the growth season (topdressing) for all experimental fields were described in GNYP et al. (2014a). All experimental fields used one cultivar, Kongyu131. The fields were managed and were fertilized by the students of the China Agricultural University of Beijing.

In addition to experimental fields, nine farmers' fields were selected: 5 farmers' fields in 2007, 2 farmers' fields in 2008, and 2 farmers' fields in 2009. The 2008 farmers' fields were at the peripheral of the Jiansanjiang Township, close to the experimental fields, and the other selected fields were in the villages Qixing 35 and Qixing 69 at the Qixing farm. The farmers managed the fields on their own and transplanted diverse cultivars to the paddies in 2007; however, Kongyu131 was generally transplanted in 2008 and 2009. The fields, whose sizes ranged from 12–27 ha, represented the common practice of large scale farming in northeastern China. Each field consisted of several plots with different sizes (400–8,000 m^2).

2.3.2.5 Field measurements at the Jiansanjiang test site

Similar to the Huimin test site, diverse agronomic data were collected after the spectral reflectance measurements at the Jiansanjiang test site. The whole field campaigns lasted five months for each year, from the leaf development to the harvest stages of paddy rice from 2007–2009. In particular, the measurements from the tillering to heading (June to August of each year) are of importance for the following chapters. The spectral reflectance was measured by two ASD (Analytical Spectral Devices, Inc., Boulder, CO, USA) spectrometers.

A QualitySpec Pro (spectral range of 350 to 1800 nm) was used in all fields in 2007 and in the experimental fields of 2009, whereas a FieldSpec3 Pro (spectral range of 350 to 2500 nm) was used in all fields in 2008 and in all farmers' fields in 2009. The detailed information regarding the QualitySpec (Unit 5038) instrument can be founded in chapter 2.3.1.5. The FieldSpec3 Pro (Unit 16183) is a full-range spectrometer with 2,151 narrow hyperspectral bands. This device has identical spectral resolutions, sampling interval, and wavelength accuracies as the QualitySpec. The two devices differ in the numbers of detectors, fibers, and in the extended spectral range of the SWIR1 (1001–1830 nm). The FieldSpec Pro has one additional detector to capture the SWIR2 (1831 – 2500 nm). This device is equipped with identical photo-diodes and operates with an external 1.5 m long fiber optic cable. That cable has 19 additional silica glass fibers to detect the SWIR2 and 57 fibers in total.

The field of view and calibration conditions are identical to that of the QualitySpec Pro. Spectral measurements were obtained under mostly cloudless conditions from 9 a.m. to 1 p.m. Local Mean Time. (solar noon at 11 a.m. in June). The measurements were obtained at a height of approximately 0.3 m at early stages and at 1 m nadir above the rice canopy at later stages. The lower height between the sensor and canopy was selected due to the expected background signals from flooded water and from soil of the paddies at the tillering and stem elongation stages. Settings for the sample counts (RS3 or Indico Pro software) were identical to those settings of spectral measurements in the Huimin test site: twenty counts for a white reference and ten counts of dark current scan. Within one plot, five to six scanning positions were selected at representative positions in each plot. These positions were randomly selected by selecting an average tiller number per plot.

In this section, only the important agronomic metrics, such as tillers and aboveground biomass, are explained. Differing from that of winter wheat, the biomass positions for the experimental plots were systematically selected. At the beginning of the campaign, twenty representative hills (clusters of rice plants) in a row were selected per plot (an average of 28 hills/m²). In a pre-campaign, the tillers of all twenty hills were counted and were averaged per plot. That averaged tiller number (±1 tiller) was used to find three to five hills with identical tiller numbers per plot beyond the measured row. These positions were marked and selected for spectral measurements in the experimental fields, and then, the biomass was sampled. In the farmers' fields, three to five representative hills were randomly selected beyond the marked position of the spectral measurements. At the later stages (booting to heading), less than five hills were selected, with at least three hills per plot. The sampled hills were rinsed with water, and the roots were clipped. Then, the samples were oven dried at 105°C for 30 minutes to stop the biophysical process and to prevent mold growth. Finally, the samples were dried at 70°C until reaching a constant weight.

3. Estimating N status of winter wheat using a handheld spectrometer in the North China Plain

F. LI[a, b], M.L. GNYP[c], L. JIA[a, d], Y. MIAO[a], Z. YU[a], W. KOPPE[c], G. BARETH[c], X. CHEN[a, *], F. ZHANG[a]

received: 27 July 2007, received in revised from: 1 November 2007, accepted: 1 November 2007
published in 2008: Field Crops Research 106, 77-85. DOI: 10.1016/j.fcr.2007.11.001
Original accepted manuscript is used and embedded in dissertation format.

a. College of Resources & Environmental Sciences, China Agricultural University, 100094, Beijing, China
b. College of Ecology & Environmental Science, Inner Mongolia Agricultural University, 010019, Hohhot, China
c. Institute of Geography, University of Cologne, 50923, Köln, Germany
d. Institute of Agriculture Resource & Environment, Hebei Academy of Agricultural and Forestry Sciences, 050051, Shijiazhuang, China

*Corresponding author, Tel.: +86 10 62733454; fax: +86 10 62731016.
Email: chenxp@cau.edu.cn (X. P. Chen)

Abstract

Excessive nitrogen (N) fertilizer application is very common in the North China Plain. Diagnosis of in-season N status in crops is critical for precision N management in this area. Remote sensing, as a timely and nondestructive tool, could be an alternative to traditional plant testing for diagnosing crop N status. The objectives of this study were to determine which vegetation indices could be used to estimate N status in winter wheat (*Triticum aestivum L.*) under high N input conditions, develop models to predict winter wheat N uptake using spectral vegetation indices and validate the models with data from farmers' fields. An N rate experiment and a variety-N experiment were conducted in Huimin, Shandong Province from 2005/2006 to 2006/2007 to develop the models. Positive linear relationships between simple ratio vegetation indices (red vegetation index, RVI and green vegetation index, GVI) and N uptake were observed independent of growth stages and varieties (R^2, 0.48–0.74). In contrast, the relationships between normalized difference vegetation indices (NDVI and GNDVI), red and green normalized difference vegetation index (RGNDI), and red and green ratio vegetation index (RGVI) were exponentially related to N uptake (R^2, 0.43–0.79). Subsequently, 69 farmers' fields in four different villages were selected as datasets to validate the developed models. The results indicated that the prediction using RVI had the highest coefficient of determination (R^2, 0.60), the lowest root mean square error (RMSE, 39.7 kg N ha^{-1}) and relative error (RE, 30.5%) across different years, varieties and growth stages. We conclude that RVI can be used to estimate nitrogen status for winter wheat in over-fertilized farmers' fields before heading.

Abbreviations: NDVI, Red normalized difference vegetation index; GNDVI, Green normalized difference vegetation index; RGNDI, Red and green normalized difference vegetation index; RVI, Red ratio vegetation index; GVI, Green ratio vegetation index; RGVI, Red and green ratio vegetation index; Opt, optimum N rate; Con, conventional N rate; RMSE, Root mean square error; RE, Relative error

Keywords: Vegetation indices; N uptake; Over-fertilization; Field spectrometer

3.1 Introduction

Nitrogen (N) is the most limiting factor for growing crops and is also the most concerned nutrient element for maintaining a friendly environment in the North China Plain. Its instantaneous and accurate estimation in crops is a key to precision N management. Traditional soil and plant testing methods have obtained great success for lowering N rates without reducing crop yields in the North China Plain (LIU et al., 2003a; CHEN et al., 2004, 2006); however, these methods are time-consuming, labor-intensive. Remote sensing, as a fast and non-destructive method to estimate certain plant parameters, has been applied more and more to determine crop N status during the growing season (FILELLA et al., 1995; HANSEN and SCHJOERRING, 2003; BRONSON et al., 2003; GISLUM et al., 2004; CLAY et al., 2006; ZHANG et al., 2006). The spectral parameters determination of crop canopies provide instantaneously an opportunity for applying N fertilizer in-season (RAUN et al., 2002; JIA et al., 2004).

For wheat, whole-plant N concentration and uptake level are important indicators for assessing plant N status. The direct method of predicting N status using remote sensing is a linear approach by combining spectral reflectance from two or more characteristic wavebands. However, the linear combination of many spectral bands may result in "over fitting" if inadequate methods were used (THENKABAIL et al., 2000). Additionally, the important reflectance wavelengths for predicting N concentration change with sampling date due to differences in ground cover and growth stage (OSBORNE et al., 2002). Compared with direct spectral reflectance, spectral vegetation indices may be more reliable in predicting plant N status. The NDVI is the most widely used vegetation index but it became less sensitive when the biochemical and biophysical variables of crops reached high values. The studies of FLOWERS et al. (2003) indicated that wheat N uptake over 100 kg N ha^{-1}at GS-30 saturated NDVI values. GITELSON et al. (1996) indicated that green NDVI (GNDVI) was more sensitive than NDVI under these conditions. However, MOGES et al. (2004) suggested that predicting forage crop N uptake using NDVI was more robust than using GNDVI. In addition, NDVI provided a wider range in values, so differences could be more easily differentiated. XUE et al. (2004) reported that a robust model between GVI and rice leaf N accumulation was established independent of growth stages. A limited number of studies have been published using RVI to predict whole-plant N concentration and plant N uptake (REYNIERS et al., 2006). However, most of these studies were

conducted under controlled experimental conditions few studies have been performed on real farmer's fields under high N fertilizer input and different cultural conditions.

Therefore, the objectives of this study were to: 1) determine which spectral vegetation indices could be used to determine N status in winter wheat under high N input conditions of North China Plain; 2) develop models to predict plant N uptake with spectral vegetation indices; and 3) evaluate the models using the datasets from 69 farmers' fields.

3.2 Materials and methods

3.2.1 Site descriptions

The study site at Huimin County is located on the north shore of the lower reaches of the Yellow River in the northeast of Shandong province on the North China plain at 37°6' – 37°36' N, 117°16' – 117°49' E. This area is characterized by a typical warm-temperature subhumid continental monsoon climate. The average temperature is 12.3 °C with 182 frost-free days each year. Annual average precipitation is 578 mm (over a recent 30-year period), of which 61–84% occurs between June and August (JU et al., 2006). Less rainfall occurred in wheat growth season. Hence farmers in this area irrigated their wheat by canal irrigation from the Yellow River. Fig. 3.1 shows the total rainfall and mean temperature per month in the years of 2005/2006 and 2006/2007. The temperature was very similar in these two years. The precipitation in the wheat season of study from October 2005/2006 to June 2006/2007 was 230.7 and 248.2 mm, respectively. The main crops in this area are wheat, maize (*Zea mays L.*) and cotton (*Gossypium hirsutum L.*), and winter wheat-summer maize rotation is the main cropping system which accounts for 66% of the total cultivated area. The average grain yield of winter wheat is 5,175 kg ha^{-1} in Shandong province in recent 10 years (1997–2006).

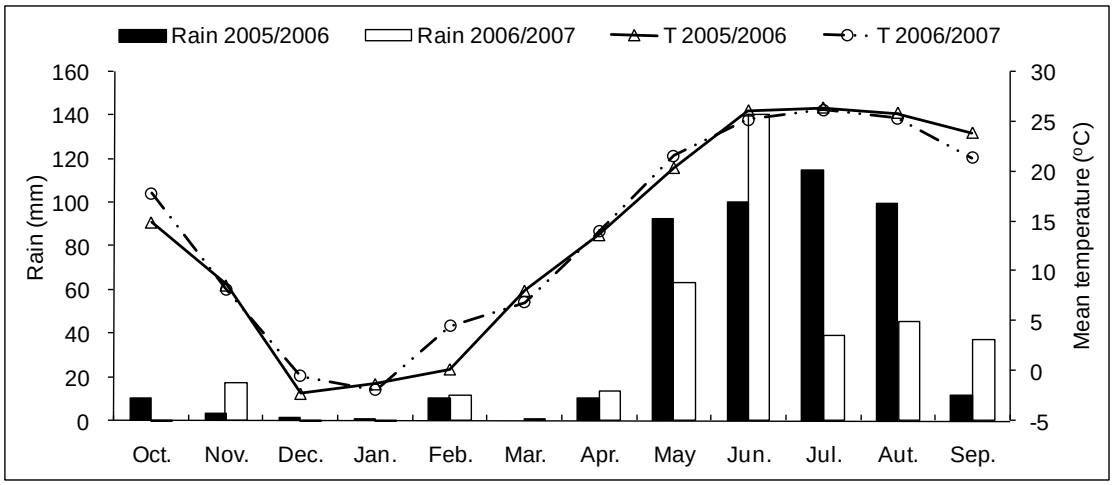

Fig. 3.1 Total rainfall (mm) and mean temperature (T, °C) per month in the years 2005/2006 and 2006/2007 in Huimin County.

3.2.2 Description of the experiments

3.2.2.1 Experiment 1: Nitrogen rate experiment

This field experiment was conducted in 2005/2006 and 2006/2007 at Xizhangliu Village of Huimin County, Shandong province. This area is representative of soil and crop management in the North China Plain. The soil at the experimental field was fine-loamy with a total N content of 0.79 g kg^{-1}, Olsen P of 14.2 mg kg^{-1}, exchangeable K of 201.5 mg kg^{-1} and organic matter content of 13.8 g kg^{-1} in the 0–30 cm layer. A local winter wheat cultivar, Weimai8 was planted on Oct 12th 2005 and Oct 4th 2006. Nitrogen fertilizer as urea was applied at five rates (0, 25, 50, 75, 100 kg N ha^{-1}) before planting. At Feekes growth stage 6 (LARGE, 1954), each plot was divided into two parts: one received and one did not receive N topdressing. The topdressing N rate was determined based on an improved N_{min} method (CHEN et al., 2006). All experiment plots received 120 kg P_2O_5 ha^{-1} as triple super-phosphate and 90 kg k_2O ha^{-1} as potassium sulfate pre-plant. The plot area was 15 m by 10 m with four replications.

3.2.2.2 Experiment 2: Variety-N experiment

This experiment was carried out at the same site as experiment 1. Field soil in the 0–30 cm layer contained 0.90 g kg^{-1} total N, 18.8 mg kg^{-1} Olsen P, 194.4 mg kg^{-1} exchangeable K and 14.5 g kg^{-1} organic matter in 2005/2006. The experiment was conducted in a different field at the same site in 2006/2007 to avoid any residue fertilizer effect from the previous year. The soil was a fine loam with 1.08 g kg^{-1} total N, 20.3 mg kg^{-1} Olsen P, 154.4 mg kg^{-1} exchangeable K and 14.1 g kg^{-1} organic matter in the 0–30 cm layer.

A split-plot design with four replications was used in this study. The main plot consisted of six N treatments: control (no N was applied), 40% of optimum N rate (Opt), 70% of Opt, Opt, 130% of Opt and conventional N rate fertilization (Con), and the subplot consisted of two winter wheat cultivars: Kenong9204 (new cultivar) and Lumai23 (local cultivar). Leaf shapes and colors of these two cultivars varied greatly. Kenong9204 had shallow leaf color and relatively thin, narrow and erect leaf. Lumai23 had deeper leaf color.

The Opt was based on plant N demands and soil N supply for two growing periods (sowing to shooting, shooting to harvest). Soil mineral N (N_{min}) was tested in the effective rooting depth at different growth periods. The Opt for the two growing periods was determined with the formula: Opt = target soil N supply – soil N_{min} (see CHEN et al., 2006 for more details). The conventional N treatment represents local farmer's practice, with 103 kg N ha^{-1} being applied before sowing and 266 kg N ha^{-1} at shooting stage as top-dressed fertilizer. All plots received 120 kg P_2O_5 ha^{-1} as triple super-phosphate and 90 kg K_2O ha^{-1} as potassium sulfate pre-plant. The plot area was 4.5 m by 7 m in 2005/2006 and 4 m by 9 m in 2006/2007, respectively.

3.2.2.3 Experiment 3: Farmer's fields

Huimin County is a representative area in the North China Plain. The cultural conditions in that local area, especially N fertilization and planting date, are different among farmers and villages.

69 farmers' fields (42 fields in 2005/2006 and 27 in 2006/2007) were selected in four different villages (Shizhang, Xili, Xujia and Dongjie village all in Huimin County) to validate the developed models. Wheat was sowed from Sept. 17 to Oct. 28 in 2005, and from Sept. 16 to Oct. 3 in 2006. The varieties were Jimai21, Jimai20, Weimai8, Lumai23, Zimai12 and Lumai8. All the fields were managed by the farmers according to their common practices. A summary of the soil chemical properties and conditions of the 69 fields is given in Table 3.1.

Table 3.1 Average soil chemical properties of field in four different villages.

Village	Chemical properties	Mean	Min.	Max.	S.D.
Shizhang	Total N (g/kg)	0.74	0.60	0.86	0.09
	Olsen-P (mg/kg)	27.3	14.8	48.1	13.1
	Exchangeable-K (mg/kg)	96.0	78.6	110.4	9.5
	Organic matter (g/kg)	11.8	9.5	14.4	1.7
Xili	Total N (g/kg)	0.89	0.72	1.03	0.08
	Olsen-P (mg/kg)	22.2	11.3	45.6	11.1
	Exchangeable-K (mg/kg)	123.4	86.6	166.1	23.3
	Organic matter (g/kg)	13.7	11.2	15.9	1.4
Xujia	Total N (g/kg)	1.00	0.79	1.32	0.11
	Olsen-P (mg/kg)	31.0	11.9	53.9	13.8
	Exchangeable-K (mg/kg)	146.6	86.2	222.0	29.4
	Organic matter (g/kg)	14.7	10.2	18.5	1.5
Dongjie	Total N (g/kg)	1.01	0.83	1.18	0.11
	Olsen-P (mg/kg)	45.4	32.9	56.6	8.0
	Exchangeable-K (mg/kg)	116.2	65.6	172.6	42.2
	Organic matter (g/kg)	15.1	11.5	17.9	2.1

S.D., Standard deviation.

3.2.3 Fields measurements and data collection

3.2.3.1 Spectral reflectance measurement

Canopy spectral reflectance was measured using the ASD Hand-held Fieldspec optical sensor (Analytical Spectral Devices, Inc., Boulder, CO) from 10 am to 2 pm under cloudless conditions. This hyperspectral device measures the visible (VIS) and near infrared (NIR) spectrum with 512 channels in the 325-1075 nm wavelength domain. The reflectance of the target is calculated with the calibration measurements of dark current and a white reference panel with known reflectance properties (ASD User's Guide 2002). The field of view of the used ASD Fieldspec is 25 degrees. Three tent-poles, which were combined with moveable joins, formed the frame of the device. The construction was designed to put the measurement equipment to the desired height above crop canopy. A mounted sprit-level guaranteed vertical nadir measurements (see LAUDIEN et al., 2006 for more details). In this study, the sensor was mounted on the tripod boom and held in a nadir orientation 1 m above the

canopy. To reduce the possible effect of sky and field conditions, spectral measurements were taken at three sites in each plot and were averaged to represent the canopy reflectance of each plot. The spectral data were collected at 10 different times for Experiment 1 and Experiment 2 and 8 times for Experiment 3 in 2006 and 6 times for all experiments in 2007.

This study was conducted with the consideration of using broad band satellite remote sensing images for determining crop N status at large scales in the future, so reflectance measurements at the canopy scale were averaged to reflectance of Quickbird satellite bandwidths: 520 to 600 nm as green (G), 630 to 690 nm as red (R) and 760 to 900 nm as near infrared (NIR) bands. Three normalized difference vegetation indices (NDVI, GNDVI and RGNDI) and three ratio vegetation indices (RVI, GVI and RGVI) were then calculated (Table 3.2).

Table 3.2 Spectral vegetation indices evaluated in this study.

Vegetation indices	Abbreviation	Formula	References
Normalized Difference Vegetation Index	NDVI	(NIR - R)/(NIR + R)	ROUSE et al. (1974)
	GNDVI	(NIR - G)/(NIR + G)	GITELSON and MERZLYAK (1998)
	RGNDI	(R-G)/(R+G)	
Ratio Vegetation Index	RVI	NIR/R	JORDAN, 1969
	GVI	NIR/G	
	RGVI	R/G	

3.2.3.2 Plant and soil measurement

Aboveground biomass was destructively sampled by randomly cutting 100 by 30 cm vegetation in each plot or farmer's field from scanned plants. All plant samples were oven dried at 70^{o}C to constant weight and then weighed, ground, and their Kjeldahl-N determined. Biomass was collected at Feekes growth stage 4, 6 and 9 for Experiments 1 and 2 and at Feekes growth stage 4, 6, 7 and 9 for Experiment 3 in 2006, and at Feekes growth stage 4, 5, 7, 9 and 10 for all experiments in 2007. At least one sample was collected in each farmer's field. The plant N uptake was determined by multiplying whole-plant N concentration and dry biomass. The nitrate concentration in the stem base of the wheat plant was tested using a reflect meter (Merck Co., Darmstadt, Germany) at shooting and heading stages. Chlorophyll meter readings using SPAD 502 (Minolta, Ramsey, NJ) were taken at mid-length of the uppermost fully expanded leaf from 30 randomly selected plants per plot each time after Fieldspec sensor data were collected.

For soil N_{min} analysis, soil samples were taken at pre-plant, at Feekes growth stage 4, 6, 9 and after harvest in 2005/2006, while at pre-plant, Feekes growth stage 6 and after harvest in 2006/2007. Five 90-cm-deep soil cores were collected from each sub-plot, separated into 0–30, 30–60, and 60–90cm layers. Fresh soil samples were sieved, extracted with 0.01 mol l^{-1} $CaCl_2$ solution and NH_4^+–N and NO_3^-–N were analyzed by using the Continuous Flow Analysis (TRAACS 2000, BRAN and LUEBBE, Germany).

3.2.4 Statistical analysis

The correlations between agronomic parameters and spectral reflectance and vegetation indices were analyzed using SAS software (SAS Inst., 1990). Data collected from Experiment 1 and 2 were mainly used for developing the regression models, and data collected from the farmer's fields (Experiment 3) were subsequently used to validate the regression models under different cultural conditions. Generally, the performance of the model was estimated by comparing the differences in coefficient of determination (R^2), root meat square error (RMSE), and relative error (RE, %) in prediction. The higher the R^2 and the lower the RMSE and RE, the higher the precision and accuracy of model to predict plant N uptake. The RMSE and RE were calculated using Eq. (3.1) and Eq. (3.2), respectively:

$$\text{RMSE} = \sqrt{\frac{1}{n}\sum_{i=1}^{n}\left(y_i-\hat{y}_i\right)^2} \qquad \text{(Eq. 3.1)}$$

$$\text{RE}(\%) = \frac{100}{\bar{y}}\sqrt{\frac{1}{n}\sum_{i=1}^{n}\left(y_i-\hat{y}_i\right)^2} \qquad \text{(Eq. 3.2)}$$

where y_i, $\hat{y}_i$ and $\bar{y}$ were measured, predicated values and mean of the measured values of crop variables, respectively, and n was the number of samples.

3.3 Results

3.3.1 Variation of agronomic variables

The agronomic parameters varied greatly across different growing stages, N treatments and winter wheat varieties, especially for biomass and N uptake (Table 3.3). The standard deviation of aboveground biomass and N uptake were larger than those of other agronomic parameters. This result indicated that aboveground biomass and N uptake would be easier to be estimated by remote sensing than other parameters. Plant total N concentration was highest at Feekes growth stage 4–5 and then decreased as plant developed to Feekes growth stage 9–10, which resulted from the dilution effect as discussed by JUSTES et al. (1994).

Table 3.3 Descriptive statistics of winter wheat aboveground biomass, plant total N concentration, N uptake, nitrate concentration of basal stem, SPAD readings, and soil mineral N (Nmin) before Feekes growth stage 9 for experiment 1 and 2 in 2006 and 2007.

	Experiment 1 (Mean±S.D.)			Experiment 2 (Mean±S.D.)		
	Feekes	Feekes	Feekes	Feekes	Feekes	Feekes
Aboveground Biomass (kg/ha)	1255±79	3139±14	5277±16	1380±69	2856±17	6078±1542
N uptake (kg/ha)	49±33	100±45	115±43	55±28	94±63	144±54
Whole-plant N concentration	38.7±2.5	32.0±3.3	21.5±2.4	40.2±2.5	32.0±3.5	23.0±4.1
SPAD readings	52.3±3.3	47.8±2.3	49.7±1.8	49.7±2.4	47.4±2.3	51.3±2.0
Nitrate concentration of basal stem	ND	1699±34	2889±96	ND	1711±34	2980±946
N_{min} (kg/ha)	114±46	87±37	67±51	120±35	158±26	108±89

S.D., standard deviation; ND, no data.

3.3.2 Relationships between spectral indices and agronomic variables

The correlation coefficients between spectral vegetation indices (NDVI, GNDVI, RGNDI, RVI, GVI and RGVI) and agronomic parameters are shown in Table 3.4. Better relationships were observed between spectral vegetation indices and plant N uptake, aboveground biomass and SPAD readings at Feekes growth stages 4–7 than those at Feekes growth stages 9–10. Similar to the findings of FLOWERS et al. (2003), biomass seemed to influence the relationships between whole-plant N concentration and spectral reflectance. The relationship was stronger at higher biomass values.

Plant N uptake was calculated as the product of crop N concentration and aboveground biomass. It correlated more strongly with spectral vegetation indices than the other four agronomic parameters (SPAD readings, plant N content, nitrate content and N_{min}) at all measured growth stages. However, the correlation coefficients of the measured soil mineral N with the spectral vegetation indices were generally not significant, suggesting that it would be difficult to use remote sensing data to estimate soil available N conditions.

Table 3.4 Correlation coefficients (R^2) for relationship between spectral vegetation indices (NDVI, GNDVI, RGNDI, RVI, GVI, RGVI) and agronomic parameters in 2006 and 2007.

Spectral indices	SPAD reading	Nitrate content of basal stem (mg/l)	Aboveground biomass (kg/ha)	Plant N concentration (g/kg)	Plant N uptake (kg/ha)	N_{min} (kg/ha)
Feekes growth stage 4–5 (n=204)						
NDVI	0.46**	–	0.83***	-0.12	0.80***	-0.18
GNDVI	0.47**	–	0.84***	-0.13	0.81***	-0.17
RGNDI	-0.44**	–	-0.78***	0.05	-0.76***	0.16
GVI	0.48**	–	0.81***	-0.05	0.79***	-0.12
RVI	0.50**	–	0.85***	-0.09	0.83***	-0.13
RGVI	-0.44**	–	-0.79***	0.06	-0.77***	0.17
Feekes growth stage 6–7 (n=156)						
NDVI	-0.29**	0.04	0.83***	0.12	0.79***	0.05
GNDVI	-0.29**	0.07	0.85***	0.08	0.81***	0.24*
RGNDI	0.38**	0.02	-0.86***	-0.14	-0.82***	0.28*
GVI	-0.39**	0.03	0.89***	0.07	0.86***	0.04
RVI	-0.36**	0.05	0.89***	0.06	0.86***	0.21
RGVI	0.36**	0.03	-0.84***	-0.15	-0.81***	0.29*
Feekes growth stage 9–10 (n=176)						
NDVI	-0.05	0.48**	0.68***	0.51**	0.67***	-0.06
GNDVI	-0.01	0.48**	0.70***	0.54**	0.69***	0.03
RGNDI	0.12	-0.44**	-0.64***	-0.49**	-0.64***	0.23*
GVI	-0.09	0.50**	0.67***	0.57**	0.69***	-0.07
RVI	-0.06	0.50**	0.67***	0.56**	0.69***	0.04
RGVI	0.12	-0.44**	-0.63***	-0.48**	-0.63***	0.23*
All stages (n=536)						
NDVI	0.08	0.10	0.70***	-0.42**	0.74***	-0.17*
GNDVI	0.09	0.09	0.72***	-0.40**	0.77***	-0.14*
RGNDI	0.07	0.03	-0.73***	0.42**	-0.79***	0.26**
GVI	-0.10	-0.12	0.77***	-0.36**	0.84***	-0.17*
RVI	-0.01	-0.06	0.78***	-0.38**	0.84***	-0.13*
RGVI	0.04	0.00	-0.72***	0.43**	-0.77***	0.25**

* Significant at the 0.05 probability level.
** Significant at the 0.01probability level.
*** Significant at the 0.001probability level.

Across all three growing stages, spectral vegetation indices were not significantly correlated with SPAD meter readings. The correlation coefficients between spectral vegetation indices and plant N uptake were all higher than other agronomic parameters (Table 3.4), indicating that plant N uptake was more suitable to be estimated using remote sensing vegetation indices at different growth stages before heading. Plant N uptake is an important indicator for assessing the plant N status. BAETHGEN and ALLEY (1989) reported that the sufficient level of N uptake for winter wheat was 95 kg N ha^{-1} at growth stage 30. Based on this information, a logical next step will be to establish a model using spectral vegetation indices to predict plant N uptake for in-season precision N management purposes.

3.3.3 Establishment of the regression model between spectral VI and plant N uptake

The coefficients of determination (R^2) for models in three growth stages and two varieties were computed and listed for six spectral indices (Table 3.5). More variability in plant N uptake could be explained at early growth stages (Feekes 4–7) than late growth stage (Feekes 9–10), while differences between the two varieties were relatively small. Across years, varieties and growth stages, GNDVI could explain 77% of plant N uptake variability, which is more than any other vegetation indices (Table 3.5).

Figure 3.2 shows relationships between spectral vegetation indices (NDVI, GNDVI, RGNDI, RVI, GVI and RGVI) and plant N uptake across growth stages, varieties and years. The exponential relationships between NDVI and GNDVI with plant N uptake (Fig. 2a, b, R^2=0.74, 0.77, respectively) is in agreement with the findings of MOGES et al (2004) and LUKINA et al. (2001). Both NDVI and GNDVI values were saturated at values of 0.8-0.9. Saturation phenomenon occurs commonly in relationships of normalized difference vegetation indices and agronomic parameters. In contrast to NDVI, GNDVI, RGNDI and RGVI, RVI and GVI were linearly related to plant N uptake (Fig. 3.2c and d).

Table 3.5 Coefficient of determination (R^2) for relationships between spectral indices and plant N uptake as affected by different growth stages and varieties.

Spectral indices	Growth stages			Varieties		All[a]
	Feekes 4–5 (n=204)	Feekes 6–7 (n=156)	Feekes9–10 (n=176)	Kenong9204 (n=168)	Lumai23 (n=168)	(n=536)
NDVI	0.72**	0.76**	0.51**	0.78**	0.62**	0.74**
GNDVI	0.74**	0.76**	0.55**	0.79**	0.66**	0.77**
RGNDI	0.61**	0.77**	0.44**	0.73**	0.73**	0.72**
RVI	0.65**	0.74**	0.49**	0.71**	0.70**	0.72**
GVI	0.69**	0.74**	0.48**	0.74**	0.70**	0.71**
RGVI	0.63**	0.76**	0.43**	0.76**	0.70**	0.72**

n, number of samples for model establishment.
[a] data from experiment 1 and 2 in 2006 and 2007.
** Significant at the 0.01 probability level.

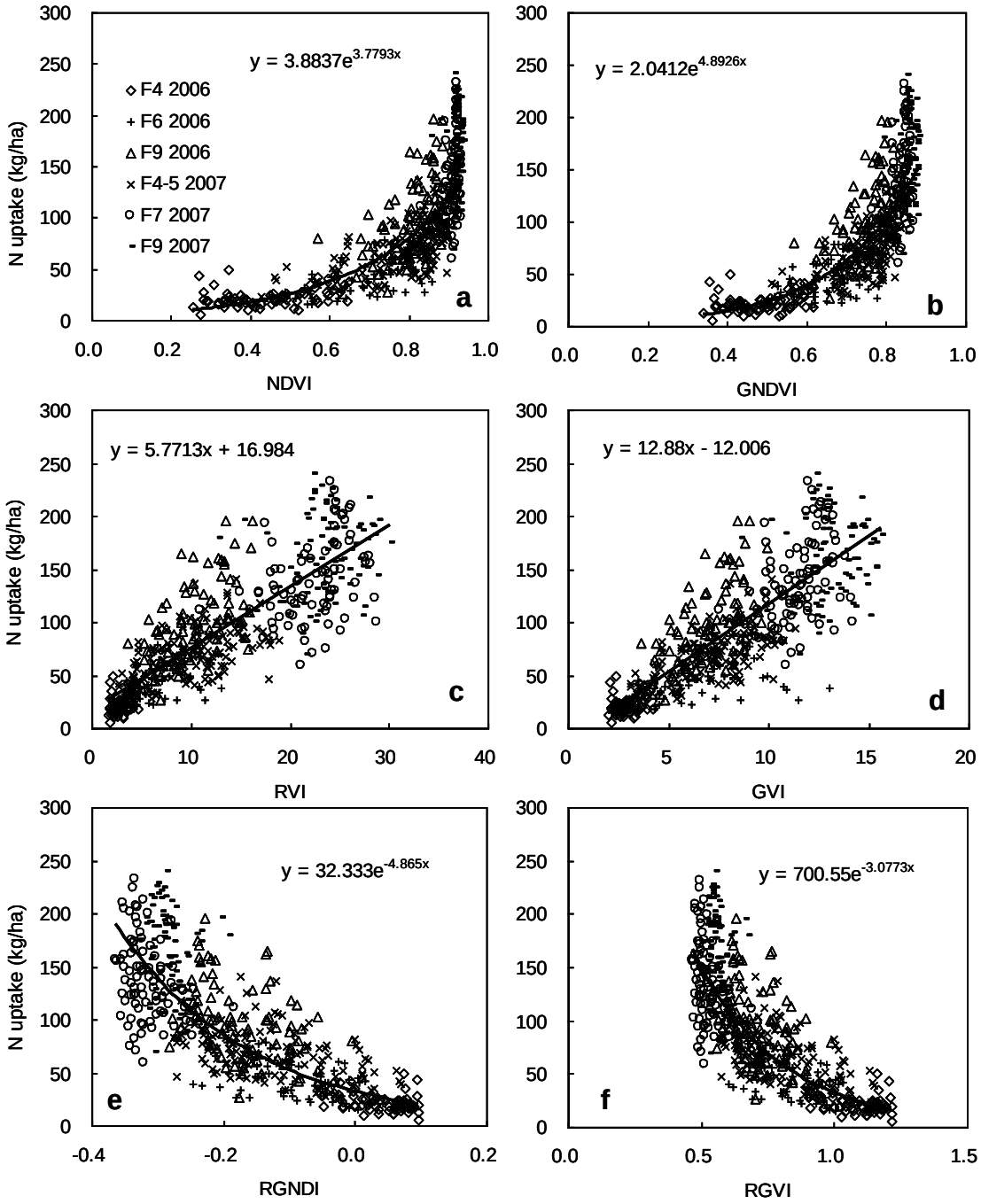

Fig. 3.2 Relationships between normalized difference vegetation indices (NDVI, a; GNDVI, b; RGNDI, e), simple ratio vegetation indices (RVI, c; GVI, d; RGVI, f) and plant N uptake across years, experiments, treatments and growth stages. (F4, 5, 6, 7, 9: Feekes growth stage 4, 5, 6, 7 and 9).

3.3.4 Validation of the established model with data from the farmers' fields (Experiment 3)

Basic statistics of N fertilization and plant N uptake at four growth stages in the farmer's fields are shown in Table 3.6. Pre-plant N rates varied from 0 to 230 kg N ha^{-1}, with the coefficient of variation (CV, %) being 46.1%. The average pre-plant N application rates varied from 78 to 121 kg N ha^{-1} in different villages (data not shown). An average of 261 kg N ha^{-1} was applied as topdressing across different farmer's field, which is much higher than crop needs (CHEN et al., 2006). The

measured aboveground plant N uptake, especially at Feekes growth stage 4–5, was strongly influenced by the different nitrogen fertilization and planting date at the four sampling stages. The high variation of plant N uptake in the farmer's fields made the dataset suitable for validating the developed models.

The validation results of models for different growth stages and varieties are presented in Table 3.7. Across growth stages and varieties, the RVI model had the lowest RMSE (39.7 kg N ha^{-1}) and RE (30.5%) and the highest R^2 (0.60) as compared with other five spectral indices models.

Table 3.6 Descriptive statistics of N rate and plant N uptake at different growth stages across 69 farmers' fields in 2006 and 2007.

	Mean kg N ha^{-1}	Min.	Max.	CV (%)
N rate				
Pre-plant N	106	0	230	46.1
Topdressing N	261	16	382	24.3
Total	367	58	535	24.3
Plant N Uptake				
Growth stages				
Feekes 4–5	75	15	139	50.6
Feekes 6–7	130	44	227	33.3
Feekes 9–10	182	100	247	21.3
All	129	15	247	44.3

CV, coefficient of variation.

3.4 Discussion

The relationships between spectral vegetation indices and whole-plant N concentration were greatly affected by growth stages. This is probably due to differences in aboveground biomass. Similar to the findings of FLOWERS et al. (2003), the relationships between whole-plant N concentration and spectral indices were relatively stronger at higher biomass sites. In contrast, the relationships between spectral vegetation indices and plant N uptake were consistently strong, without being significantly affected by growth stages and years. Thus, a model between spectral VI and N uptake was established for all data from Experiment 1 and Experiment 2 including all sampling stages and two years (Fig. 3.2). Consistent with the studies of STONE et al. (1996) and LUKINA et al. (2001), the NDVI was exponentially related to the plant N uptake regardless of years, growth stages and varieties. A difference was that our relationship extended to Feekes growth stage 10 (before heading), when growth parameters reached maximum, whereas their relationship was at initial growing stage from Feekes growth stage 4 to 6 (before shooting). However, similar to the relationships between NDVI and other plant properties (SERRANO et al., 2000; YANG et al., 2004), at the upper end of NDVI and GNDVI, the indices did not have significant differences because of the saturation of the reflectance factors. Small changes in NDVI and GNDVI values may result in large changes in plant N uptake (Fig. 3.2a and b). THENKABAIL et al. (2000) reported that the sensitivity of NDVI was improved using the portions of green and red spectrum. This was confirmed by results of this study (Fig. 3.2e).

XUE et al. (2004) found that leaf N accumulation in rice had a strong linear correlation with GVI. In this study, we found a linear relationship between RVI and plant N uptake of winter wheat, which accounted for 72% of plant N uptake variation (Fig. 3.2c). RVI seemed to be a better spectral index to assess N status by predicting plant N uptake for winter wheat before heading stage.

Before a model can be applied in practice, it should be validated using data not used to develop the model. Models with high R^2 values may not necessarily have better prediction performance. In previous studies modeling the relationships of spectral indices with leaf area index, leaf dry weight, leaf N concentration, leaf N accumulation and yield for rice, wheat or corn (XUE et al., 2004; CHANG et al., 2005; ELWADIE et al., 2005; FERRIO et al., 2005; NGUYEN et al., 2006), the validation datasets were always from self-designed controlled fields. An important difference in this study is that the validation dataset was obtained from different "real" farmers' fields under different environmental and management conditions (years, fields, varieties, planting date, growth stages, and N applications, etc.). The results indicated that the performance of NDVI, GNDVI, GVI and RGVI in predicting plant N uptake was affected by different growth stages and varieties, while the performance of RVI was relatively more consistent (Table 3.7). Therefore, the results of this study demonstrated the feasibility of predicting winter wheat N uptake using RVI before heading stage.

Table 3.7 Validation results for models (Table 3.5) established using spectral vegetation indices with data from 69 farmers' fields (Experiment 3) in 2006 and 2007.

Spectral indices	Validation indicators	Growth stages			Varieties		All (n=392)
		Feekes 4–5 (n=148)	Feekes 6–7 (n=145)	Feekes 9–10 (n=99)	All[a] (n=392)	All (n=392)	
NDVI	R^2	0.71	0.36	0.29	0.58	0.59	0.58
	RMSE (kg/ha)	40.9	39.7	53.8	50.4	48.6	48.3
	RE (%)	44.7	30.6	28.5	38.7	37.3	37.1
GNDVI	R^2	0.73	0.34	0.28	0.58	0.58	0.58
	RMSE (kg/ha)	37.9	37.9	51.8	45.8	42.2	43.3
	RE (%)	41.5	29.2	27.5	35.2	32.4	33.2
RGNDI	R^2	0.72	0.33	0.25	0.63	0.62	0.63
	RMSE (kg/ha)	37.3	57.6	49.7	44.1	46.0	44.4
	RE (%)	40.8	44.4	26.3	33.9	35.3	34.1
RVI	R^2	0.72	0.35	0.30	0.60	0.60	0.60
	RMSE (kg/ha)	31.5	39.3	46.6	39.4	44.5	39.7
	RE (%)	34.5	30.3	24.7	30.3	34.2	30.5
GVI	R^2	0.73	0.32	0.29	0.58	0.58	0.58
	RMSE (kg/ha)	31.2	43.8	47.8	40.7	49.1	40.9
	RE (%)	34.1	33.8	25.3	31.3	37.7	31.4
RGVI	R^2	0.72	0.32	0.25	0.62	0.62	0.62
	RMSE (kg/ha)	38.8	47.8	52.2	44.8	47.8	46.3
	RE (%)	42.5	36.8	27.6	34.4	36.7	35.6

n, Number of samples for model validation.
[a] All data from experiment 3 in 2006 and 2007.

Perhaps the most encouraging finding in this study is the successful validation of the developed model using datasets from 69 farmers' fields in different villages for two years under different cultural conditions. The validated model may be used to guide farmers to apply suitable rates of N fertilizers. To ensure high yields, most farmers apply much more N fertilizers than crop needs in the North China Plain. The studies of JU et al. (2006) showed that annual N fertilizer inputs reached 553 kg N ha^{-1} and annual N surpluses were 354 kg N ha^{-1} on average in winter wheat and summer maize rotation system in this area. Our demonstration experiments on 37 farmers' fields of four villages in 2005 and 2006 found that the optimal N rate was 110 kg N ha^{-1} on average, whereas farmers generally applied 381 kg N ha^{-1}. The average soil residual N reached 241 kg N ha^{-1} in farmers' fields (data not shown), which was much higher than the baseline standard of 100 kg N ha^{-1} for environmental safety in Europe (SCHLEEF et al., 1994). High soil residual N can easily result in high nitrate leaching losses (CHEN et al., 2005; FANG et al., 2006; LI et al., 2007). Therefore, using remote sensing to determine optimal N rates directly or indirectly should be a priority for future studies in this area, which may result in significant economic and environmental benefits due to decreased N rates and environment pollution.

Acknowledgements

This research was financially supported by the Natural Science Foundation of China (Project number: 30571080), the Program for Changjiang Scholars and Innovative Research Team in University (IRT 0511), International Bureau of the BMBF, Germany and the GIS & RS Group of the University of Cologne.

References * (*for chapter 3)

BAETHGEN, W.E., ALLEY, M.M., 1989. Optimizing soil and fertilizer nitrogen use by intensively managed winter wheat. II. Critical levels and optimum rates of nitrogen fertilizer. Agronomy Journal, 81, 120-125.

BRONSON, K.F., CHUA, T.T., BOOKER, J.D., KEELING, J.W., LASCANO, R.J., 2003. In-season nitrogen status sensing in irrigated cotton: II. Leaf nitrogen and biomass. Soil Science Society of America Journal, 67, 1439-1448.

CHANG, K.W., SHEN, Y., JENG-CHUNG L., 2005. Predicting rice yield using canopy reflectance measured at booting stage. Agronomy Journal, 97, 872-878.

CHEN, J.Y., TANG, C.Y., SAKURA, Y., YU, J.J., FUKUSHIMA, Y., 2005. Nitrate pollution from agriculture in different hydrogeological zones of the regional groundwater flow system in the North China Plain. Hydrogeology Journal, 13, 481–492.

CHEN, X.P., ZHOU, J.C., WANG, X.R., BLACKMER, A.M., ZHANG, F.S., 2004. Optimal rates of nitrogen fertilization for a winter wheat-corn cropping system in northern china. Communication in Soil Science and Plant Analysis, 35, 583-597.

CHEN, X.P., ZHANG, F.S., RÖMHELD, V., HORLACHER, D., SCHULZ, R., BÖNING-ZILKENS, M., WANG, P., CLAUPEIN, W., 2006. Synchronizing N supply from soil and fertilizer and N demand of winter wheat by an improved N-min method. Nutrient Cycling in Agroecosystems, 74, 91-98.

CLAY, D.E., KIM, K. I., CHANG, J., CLAY, S.A., DALSTED, K., 2006. Characterizing water and nitrogen stress in corn using remote sensing. Agronomy Journal, 98, 579-587.

ELWADIE, M.E., PIERCE, F.J., QI, J., 2005. Remote sensing canopy dynamics and biophysical variables estimation of corn in Michigan. Agronomy Journal, 97, 99-105.

FANG, Q.X., YU, Q., WANG, E.L., CHEN, Y.H., ZHANG, G.L., WANG, J., 2006. Soil nitrate accumulation, leaching and crop nitrogen use as influenced by fertilization and irrigation in an intensive wheat–maize double cropping system in the North China Plain. Plant and Soil, 284, 335–350.

FERRIO, J.P., VILLEGAS, D., ZARCO, J., APARICIO, N., ARAUS, J.L., ROCO, C., 2005. Assessment durum wheat yield using visible and near-infrared reflectance spectra of canopies. Field Crops Research, 94, 126-148.

FILELLA, I., SERRANO, L., SERRA, J., PEÑUELAS, J., 1995. Estimating wheat nitrogen status with canopy reflectance indices and discriminant analysis. Crop Science, 35, 1400-1405.

FLOWERS, M., WEISZ, R., HEINIGER, R., 2003. Quantitative approaches for using color infrared photography for assessing in-season nitrogen status in winter wheat. Agronomy Journal, 95, 1189-1200.

GISLUM, R., MICKLANDER, E., NIELSEN, J.P., 2004. Qualification of nitrogen concentration in perennial ryegrass and red fescue using near-infrared reflectance spectroscopy (NIRS) and chemometrics. Field Crops Research, 88, 269-277.

GITELSON, A.A., KAUFMAN, Y.G., MERZLYAK, M.N., 1996. Use of a green channel in remote sensing of global vegetation from EOS-MODIS. Remote Sensing of Environment, 58, 289-298.

GITELSON, A.A., MERZLYAK, M.N., 1998. Remote sensing of chlorophyll concentration in higher plant leaves. Advances in Space Research, 22, 689-692.

HANSEN, P.M., SCHJOERRING, J.K., 2003. Reflectance measurement of canopy biomass and nitrogen status in wheat crops using normalized difference vegetation indices and partial least square regression. Remote Sensing of Environment, 86, 542-553.

JIA, L.L., BUERKERT, A., CHEN, X.P., RÖMHELD, V., ZHANG, F.S., 2004. Low-altitude aerial photography for optimum N fertilization of winter wheat on the North China Plain. Field Crops Research, 89, 389-395.

JORDAN, C.F., 1969. Derivation of leaf area index from quality of light on the forest floor. Ecology, 50, 663-666.

JU, X.T., KOU, C.L., ZHANG, F.S., CHRISTIE, P., 2006. Nitrogen balance and groundwater nitrate

contamination: comparison among three intensive cropping systems on the North China Plain. Environmental Pollution, 143, 117-125.

JUSTES, E., MARY, B., MEYNARD, J.M., MACHET, J.M., THELIER-HUCHE, L. 1994. Determination of a critical nitrogen concentration dilution curve for winter wheat. Crops Annals of Botany, 74, 397-407.

LARGE, E.C., 1954. Growth stage in cereals. Plant Pathology, 3, 128-129.

LAUDIEN, R., BARETH, G., 2006. Multitemporal Hyperspectral Data Analysis for Regional Detection of Plant Diseases by using a Tractor- and an Airborne-based Spectrometer. Photogrammetrie Fernerkundung Geoinformation, 2006 (3), 217-228.

LI, X.X., HU, C.S., DELGADO, J.A., ZHANG, Y.M., OUYANG, Z.Y., 2007. Increased nitrogen use efficiencies as a key mitigation alternative to reduce nitrate leaching in North China Plain. Agricultural Water Management, 89, 137-147.

LIU, X.J., JU, X.T., ZHANG, F.S., CHEN, X.P., 2003. Nitrogen recommendation for winter wheat using N-min test and rapid plant tests in North China Plain. Communications in Soil Science and Plant Analysis, 34, 2539-2551.

LUKINA, E.V., FREEMAN, K.W., WYNN, K.J., THOMASON, W.E., MULLEN, R.W., STONE, M.L., SOLIE, J.B., KLATT, A.R., JOHNSON, G.Y., ELLIOT, R.L., RAUN, W.R., 2001. Nitrogen fertilization optimization algorithm based on in-season estimates of yield and plant nitrogen uptake. Journal of Plant Nutrition, 24, 885–898.

MOGES, S.M., RAUN, W.R., MULLEN, R.W., FREEMAN, K.W., JOHNSON, G.V., SOLIE, G.B., 2004. Estimating of green, red, and near infrared bands for predicting winter wheat biomass, nitrogen uptake, and final grain yield. Journal of Plant Nutrition, 27, 1431-1441.

NGUYEN, H.T., LEE, B.W., 2006. Assessment rice leaf growth and nitrogen status by hyperspectral canopy reflectance and partial least square regression. European Journal of Agronomy, 24, 349-356.

OSBORNE, S.L., SCHEPERS, J.S., FRANCIS, D.D., SCHLEMMER, M.R., 2002. Detection of phosphorous and nitrogen deficiencies in corn using spectral radiance measurement. Agronomy Journal, 94, 1215-1221.

RAUN, W.R., SOLIE, J.B., JOHNSON, G.V., STONE, M.L., MULLEN, R.W., FREEMAN, K.W., THOMASON, W.E., LUKINA, E.V., 2002. Improving nitrogen use efficiency in cereal grain production with optical sensing and variable rate application. Agronomy Journal, 94, 815-820.

REYNIERS, M., WALVOORT, D., BAARDEMAAKER J., 2006. A linear model to predict with a multispectral radiometer the amount of nitrogen in winter wheat. International Journal of Remote Sensing, 27, 4159-4179.

ROUSE, J.W., HAS, R.H., SCHELL, J.A., DEERING, D.W., 1974. Monitoring vegetation systems in the

Great Plains with ERTS. Third ERTS Symposium, NASA SP-351, Vol. 1. NASA, Washington, DC, 309-317.

SCHLEEF, K.H., KLEIHANSS, W., 1994. Mineral balance in agriculture in EU. Institute of farm economics, Federal Agricultural Research Centre, Braunchweig, Germany.

SEMBIRING, H., LEES, H.L., RAUN, W.R., JOHNSON, G.V., SOLIE, J.B., STONE, M.L., DELEON, M.J., LUKINA, E.V., COSSEY, D.A., LARUFFA, J.M., WOOLFOLK, C.W., PHILLIPS, S.B., THOMASON, W.E., 2000. Effect of growth stage and variety on spectral radiance in winter wheat. Journal of Plant Nutrition, 23, 141-149.

SERRANO, L., FILELLA, I., PEÑUELAS, J., 2000. Remote sensing of biomass and yield of winter wheat under different nitrogen supplies. Crop Science, 40, 723-731.

STONE, M.L., SOLIE, J.B., RAUN, W.R., WHITNEY, R.W., TAYLOR, S.L., RINGER, J.D., 1996. Use of spectral radiance for correcting in-season fertilizer nitrogen deficiencies in winter wheat. Transactions of ASAE, 39, 1623-1631.

THENKABAIL, P.S., SMITH, R.B., PAUW, E.D., 2000. Hyperspectral vegetation indices and their relationships with agricultural crop characteristics. Remote Sensing of Environment, 71, 158-182.

XUE, L.H., CAO, W.X., LUO, W.H., DAI, T.B., ZHU, Y., 2004. Monitoring leaf nitrogen status in rice with canopy spectral reflectance. Agronomy Journal, 96, 135-142.

YANG, C.M., CHEN, R.K., 2004. Modeling rice growth with hyperspectral reflectance data. Crop Science, 44, 1283-1290.

ZHANG, J.H., WANG, K., BAILEY, J.S., WANG, R.C., 2006. Predicting nitrogen status of rice using multispectral data at canopy scale. Pedosphere, 16, 108-117.

4. Evaluating multispectral and hyperspectral satellite remote sensing data for estimating winter wheat growth parameters at regional scale in the North China Plain

W. KOPPE [a, b], F. LI [c,d], M. L. GNYP [a], Y. MIAO [c], L. JIA [c, e], X. CHEN [c], F. ZHANG [c], G. BARETH [a]

received: October 2009, accepted: December 2009, published: May 2010
Photogrammetrie Fernerkundung Geoinformation 2010 (3), 167-178. DOI: 10.1127/1432-8364/2010/0047
Original accepted manuscript is used and embedded in dissertation format.

a. Institute of Geography, University of Cologne, 50923, Köln, Germany
b. Infoterra GmbH, Astrium Geo-Information Services, 88039 Friedrichshafen, Germany
c. College of Resources & Environmental Sciences, China Agricultural University, 100094, Beijing, China
d. College of Ecology & Environmental Science, Inner Mongolia Agricultural University, 010019, Hohhot, China
e. Institute of Agriculture Resource & Environment, Hebei Academy of Agricultural and Forestry Sciences, 050051, Shijiazhuang, China

*Corresponding author, Tel.: +49 7545-84226.
Email: wolfgang.koppe@infoterra-global.com (W. Koppe)

Abstract

Timely monitoring of crop growth status at large scale is crucial for improving regional crop management decisions. The main objective of the recent study is a model development to predict and estimate crop parameters, here biomass, plant N concentration and plant height, based on multi- and hyperspectral satellite data. In this contribution, the focus is on relating orbital multispectral (EO-1 ALI) and hyperspectral (EO-1 Hyperion) measurements to winter wheat parameters for regional level applications. The study was conducted in Huimin County, Shandong Province of China in the growing season of 2005/2006 involving three big winter wheat fields managed by different farmers. Winter wheat growth parameters including aboveground biomass, plant N concentration and plant height were collected at different growth stages. Three different predicting models were investigated: traditional vegetation indices calculated from broad and narrow bands, and Normalized Ratio Indices (NRI) calculated from all possible two-band combinations of Hyperion between 400 and 2500 nm. The results indicated that TVI performed best among the tested vegetation indices using either broad (R^2=0.69, 0.32 and 0.64 for biomass, N concentration and plant height, respectively) or narrow

(R^2=0.71, 0.33 and 0.65 for biomass, N concentration and plant height, respectively) bands. The best performing Normalized Ratio Index (NRI) selected through band combination analysis were significantly better than TVI, achieving R^2 of 0.83, 0.81 and 0.79 for biomass, plant N concentration and plant height, respectively. The different NRI models use wavebands from the near infrared (NIR) (centered at 874, 732, and 763 nm) and short wave infrared (SWIR) (centered at 1225 and 1305 nm) spectrum with varying bandwidth between 10 and 190 nm. The result of this study suggest that vegetation indices derived from NIR- and SWIR-Hyperion spectrum are better predictors of plant aboveground biomass, nitrogen concentration and plant height than indices derived from only visible spectrum. More studies are needed to further evaluate the results using data from more diverse conditions.

Keywords: Hyperion, ALI, vegetation indices, winter wheat, biomass, nitrogen concentration, imaging spectrometry, hyperspectral, multispectral

4.1 Introduction

Timely monitoring of crop growth status is important for dynamic in-season site specific crop management, detection of plant vitality, assessment of seasonal production as well as environmental pollution control and yield prediction (MIAO et al., 2009; LAUDIEN and BARETH 2006; ZHAO et al., 2004; HANSEN and SCHJOERING, 2003). Traditional techniques for the measurement of accurate crop parameters, such as plant aboveground biomass and nitrogen concentration are destructive, extremely cost and labour intensive and not able to provide spatial distributed data on regional level (LU, 2006). The estimation of these parameters can be done more efficiently by non-destructive spectral reflectance observations (DAUGHTRY et al., 2000), obtained from field-, airborne- or satellite based sensors. For the linkage of crop parameters with spectral reflectance measurements, a wide range of vegetation indices were developed (ZHAO et al., 2004, HABOUNDANE et al., 2004, BROGE and MORTENSEN, 2002).

Vegetation indices obtained from spectral reflectance measurements are designed to enhance the vegetation cover signal while minimizing the response of various background materials (SCHOWENGERDT, 2007). They are mainly based on the difference between low reflection due to strong absorptions by foliar pigments in the red spectrum and high reflection of structural components (cell walls) in the near infrared spectrum (KUMAR et al., 2003; LILLESAND et al., 2004). In the past decades, many attempts have been made to estimate crop parameters at regional level, either directly from remote sensing data or by assimilating remote sensing data into crop models (SCHNEIDER, 2003). A lot of earth observation satellites carrying multispectral imaging sensors are available (WOOSTER, 2007), providing data that can be used for the calculation of broad band vegetation indices (LU, 2006).

Vegetation indices calculated from the visible and near infrared bands of multispectral scanners have been used to estimate crop parameters, such as standing biomass and grain yield

(TUCKER, 1979; THENKABAIL et al., 1995; SINGH et al., 2002; DORALSWAMY et al., 2003), leaf area index (LAI) (CLOUTIS et al., 1999) and plant nitrogen content (REYNIERS and VRINDTS, 2004). At higher vegetation densities, standard broadband vegetation indices, such as Simple Ratio (SR) or Normalized Difference Vegetation Index (NDVI) are generally less accurate (JONGSCHAAP and SCHOUTEN, 2005) and tend to saturate (HABOUDANE et al., 2004; MUTANGA and SKIDMORE, 2004), which results in a limited prediction value of crop parameters when LAI exceeds two (HABOUDANE et al., 2004). Improvements could be achieved by using hyperspectral radiometers, which can acquire a continuous electromagnetic spectrum for each pixel between 350 and 2500 nm (HANSEN and SCHJOERING, 2003). The sensitivity of hyperspectral vegetation indices for estimation of crop parameters has already been demonstrated with significant improvements compared to broad bands by several authors during the past several decades (SINCLAIR, 1971; FILLELA et al., 1995; STRACHAN et al., 2002). Beyond narrow band standard vegetation indices, imaging spectroscopy provides the opportunity of using more adequate wavebands or waveband combinations to estimate biophysical parameters (CECCATO et al., 2002). According to this, different approaches for index calculation based on all waveband combinations were developed and successfully used for estimation of wheat grain yield (XAVIER et al., 2006), wheat biomass and nitrogen content (HANSEN and SCHJOERING, 2003; THENKABAIL et al., 2000) as well as land cover classification (THENKABAIL et al., 2004). Also, FERWERDA et al. (2005) used waveband selection method successfully for the estimation of leaf nitrogen content across different species. MUTANGA and SKIDMORE (2004) reported that waveband combinations different from the standard NDVI could overcome saturation effects of biomass estimation at full canopy cover.

A lot of studies have been conducted on improving the performance of hyperspectral vegetation indices both on excised leaves and in situ measurements, but there are only a few studies dealing with hyperspectral imaging on regional level (e.g. SMITH et al., 2003; GALVAÕ et al., 2005; DATT et al., 2003). By using high spectral resolution space born radiometers (e.g. Hyperion sensor on Earth Observation-1 satellite), detailed variation in the electromagnetic spectrum between 400 and 2500 nm can be measured over a wide area (BROGE and LEBLANC, 2000), making this approach more efficient for large scale precision crop management.

The objective of this study was to analyse, compare and evaluate satellite based multispectral and hyperspectral images in terms of broad band and narrow band vegetation indices for the estimation of winter wheat aboveground biomass, plant N concentration and plant height. For this research interest, the optical sensors Hyperion and ALI, mounted on Earth Observation-1 satellite were selected, because they can provide multispectral and hyperspectral data simultaneously. Three different types of vegetation indices were calculated to estimate crop parameters: (1) standard broad band vegetation indices derived from multispectral sensor ALI; (2) standard narrow band vegetation indices derived from Hyperion; and, (3) systematic identification of best waveband combinations in the Hyperion reflectance spectrum from 400 to 2500 nm using Normalized Ratio Indices (NRI)

following (THENKABAIL et al., 2000) and (SIMS and GAMON, 2002).

4.2 Material and methods

4.2.1 Study area

The research was accomplished in the North China Plain during the winter wheat growing season of 2006. The test fields were located in Huimin County (37.3° latitude, 117.4° longitude), Shandong Province. This area is characterized by a continental climate with precipitation maxima between June and September, typical for the warm-temperature subhumid continental monsoon climate. The average temperature is 12.3 °C and annual average precipitation sums up to 580 mm. The dominant crop rotation, up to 66% of the cultivated area, is winter wheat followed by maize enabling two harvests per year. Huimin County was chosen because of the existence of long term field experiments managed by the Dept. of Plant Nutrition (CAU) and availability of collecting ground truth data from selected fields. Three big fields, each of which is about 5 ha and managed by different farmers, were selected for collecting ground truth information. The fields are located in the villages of Xili, Xujia, and Shizhang in Huimin County. Winter wheat in the three villages was sowed from September 17th to October 26th, 2005 and harvested in the beginning of June, 2006. All the fields were managed by the farmers according to their common practices.

4.2.2 Hyperion and ALI image data

Three Hyperion and ALI images were acquired on April 19, May 6 and May 31, 2006. The optical sensors Hyperion and ALI are mounted on the Earth Observing One (EO-1) Satellite that follows the World Reference System-2 (WRS-2) with a 16 day repeat cycle for nadir mode. Both sensors are push broom imaging spectrometers that are capable of cross-track pointing (Earth Observation-1, 2003). The multispectral Advanced Land Imager (ALI) acquires information in nine discrete bands with a spatial resolution of 30 m. An additional panchromatic channel has a resolution of 10 m. The Hyperion hyperspectral sensor collects continuous data with a VNIR and a SWIR spectrometer in the 400-2400 nm wavelength domain. Each frame taken captures images in a 7.7 km wide and 42 km (resp. 185 km) long area (UNGAR et al., 2003). Similar to the multispectral ALI, Hyperion provides also a spatial resolution of 30 m. EO-1 Hyperion images are radiometric calibrated (Level 1R) and delivered in 16-bit radiance data (PEARLMAN et al., 2003).

4.2.3 Groundtruth measurements

Winter wheat canopy spectral reflectance was measured in the field using an ASD Fieldspec©HandHeld Pro optical sensor (Analytical Spectral Devices, Inc., Boulder, CO, USA; www.asdi.com) between 10 am to 2 pm under cloudless conditions. The HandHeld Pro device measures the visible (VIS) and near infrared (NIR) spectrum with 512 channels in the 325–1075 nm wavelength domain. In the context of this research, the in-Situ spectral measurements were only used

for calibrating orbital reflectance data. After field canopy spectral data collection, crop samples were collected for aboveground biomass and plant nitrogen concentration determination on four dates: 19 April, 28 April, 12 May and 30 May, with the corresponding growth stages from shooting to ripening stage. The measurements on April 19 and May 30 matched EO-1 satellite image collection very well; however, no ground measurements could match the EO-1 data acquisition on May 6. Therefore, agronomic measurements on 28 April and 12 May had to be interpolated to coincide with EO-1 acquisition on 6 May. Aboveground biomass was destructively collected by cutting the vegetation on ground level within an area of 100 cm by 30 cm. Then the samples were dried at 70°C to constant weight. Plant nitrogen concentration was then determined by the Kjeldahl digestion method (BREMNER, 1960). Around 39 to 45 measurements per field were sampled.

4.2.4 Satellite image pre-processing

Satellite image pre-processing of Hyperion and ALI data included (a) a correction for sensor artifacts, (b) an atmospheric correction as well as (c) a geometric correction. The performed pre-processing steps (LILLESAND et al., 2004; KHURSHID et al., 2006) were aimed to improve the quality of the images for multitemporal data analysis. For correction of sensor artifacts, uncalibrated and corrupted Hyperion bands were eliminated by applying the Flag-Mask that was delivered with the data product. A Flag-Mask indicates detectors which are unresponsive and unreliable (USGS, 2007). 158 of the original 242 bands had remained for subsequent destriping (described in DATT et al., 2003). During the destriping process periodic along track stripes in image data, caused by detector errors were removed. Since some of the bands were not repairable, another 17 bands had to be excluded. The destriping and exclusion of image channels was performed with ENVI software (ITT Visual Information Solutions).

For some application using single satellite observations, it is of no importance to atmospherically correct image data (SCHOWENGERDT, 2007). However, in the present work, the focus was set on multi-temporal analysis as well as on matching image data to canopy spectral reflectance that was measured using a portable spectroradiometer (Fieldspec® Pro by ASD). The measured at-sensor radiance L of Hyperion and ALI data consists of reflectance from the surface and scattering from the atmosphere. Major sources of distortions of remotely sensed imagery are water vapor and aerosols (CAIRNS et al., 2003). To convert the Hyperion and ALI at-sensor radiance data to surface reflectance data, the MODTRAN-based radiative transfer algorithm implemented in the FLAASH module of ENVI software was used.The radiative transfer algorithm that applies for Lambertian materials, converts the at-sensor radiance L to surface reflectance ρ on a pixel-by-pixel basis as

$$\rho = \frac{L - L_a}{(L - L_a)S + T_2 \frac{E_s * \cos(\theta_s)}{\pi}} \qquad \text{(Eq. 4.1)}$$

where L_a is the radiance caused by atmospheric scattering; T_2 is the two-way transmittance; S is the albedo of the atmosphere; θ_S is the solar zenith angle and E_S is the exoatmospheric solar irradiance. The radiative transfer algorithm is described in (BERK et al., 2000).

According to equation 4.1, atmospheric scattering effects were compensated and a surface reflectance spectrum for each pixel was retrieved. The comparison of single pixel at sensor radiance and surface reflectance from fully developed winter wheat is shown in Fig. 4.1.

The last step of the Hyperion and ALI pre-processing chain is the geometric correction, which was undertaken to rectify geometric distortions using ground control points (GPCs), sensor parameters and a digital elevation model. For orthorectification process of each scene, 25 GCPs distributed across the area of interest were selected and the image rectification was carried out by bilinear resampling method using ENVI. For evaluation purpose, other 20 independent check points were used, which resulted in overall RMSE of around 0.5 pixels (15 m) for each image.

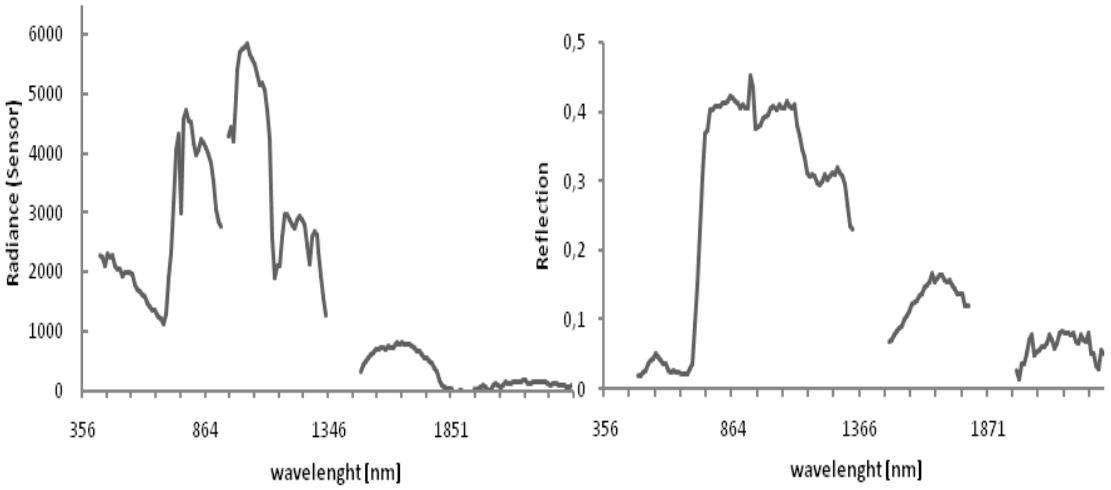

Fig. 4.1 Comparison of single pixel spectra before (a) and after (b) atmospheric correction. Spectra were acquired on April 19, 2006.

4.2.5 Vegetation index calculation and model development for crop parameter estimation

In this study, the reflectance spectra from multi-temporal Hyperion and ALI data were extracted on a pixel basis (cell size 30m) on the farmers' fields in the three villages. Pixel based reflectance spectra were then used for the calculation of (1) standard broad band vegetation indices, (2) standard hyperspectral vegetation indices, and (3) narrow band Normalized Ratio Indices (NRI; SCHMIDT and SKIDMORE, 2003; SIMS and GAMON, 2002). To compare the prediction power of broad band and narrow band crop parameter estimations, the following vegetation indices were calculated: Simple Ratio (SR), Normalized Difference Vegetation Index (NDVI), Soil Adjusted Vegetation Index (SAVI) and Triangular Vegetation Index (TVI). The SR, NDVI and SAVI vegetation indices are based on the difference between strong absorption of solar radiation in the red, caused by chlorophyll pigments and the high leaf cellular reflection in the near infrared. Unlike the Simple Ratio Index, the NDVI is normalized which reduces the effects of variable illuminations and limits the NDVI to values

from -1 to 1 (BARET and GYOT, 1991). The SAVI is intended to minimize influences due to soil optical properties. The included background factor L depends on vegetation density and requires information about the relationship between soil background and vegetation (HUETE, 1988). The TVI was developed by BROGE and LEBLANC (2000) and is defined additionally to red and near infrared reflectance by the magnitude in the green region. The detailed expressions and the notable references of the mentioned vegetation indices are provided in Table 4.1.

Table 4.1 Standard vegetation indices evaluated in this study.

Index	Name	Formula	References
SR	Simple Ratio	$SR=\rho_{NIR}/\rho_R$	(BARET and GUYOT, 1991)
NDVI	Normalized Difference	$NDVI=(\rho_{NIR}-\rho_R)/(\rho_{NIR}+\rho_R)$	(ROUSE et al., 1974)
SAVI	Soil_Adjusted Vegetation Index	$SAVI=(1+L)\ (\rho_{NIR}-\rho_R)/(\rho_{NIR}+\rho_R+L)$	(HUETE, 1988)
TVI	Triangular Vegetation Index	$TVI=0.5*[120*(\rho_{NIR}-\rho_{Green})-200(\rho_R-\rho_{Green})]$	(BROGE and LEBLANC, 2000)

In addition to standard vegetation indices, a specific waveband selection method suggested by THENKABAIL et al. (2000) and SIMS and GAMON (2002) was used to determine best band combinations suitable for crop parameter estimation (see also SCHMIDT and SKIDMORE, 2003). The two-band Normalized Ration Index (NRI) is defined as (SIMS and GAMON, 2002):

$$NRI_{(band\,1,band\,2)} = \frac{(\rho_{band1} - \rho_{band\,2})}{(\rho_{band\,1} + \rho_{band\,2})} \qquad band\,1 \geq band\,2 \qquad \text{(Eq. 4.2)}$$

where ρ_{band1} and ρ_{band2} are reflectance of Hyperion narrow bands in the wavelength range between 400 and 2500 nm. The hyperspectral Hyperion sensor allows the calculation of a total number of 9870 (141*140/2) possible two-band combinations for each agronomic parameter. A linear regression between each vegetation index and crop parameter was performed.

4.3 Results

4.3.1 Variation of crop parameters

Due to different farmers' management practices, the investigated fields were different in terms of seeding time, plant density, and nitrogen application rates. As expected, the differences in management practices resulted in a wide range of variation in crop parameters (aboveground biomass, plant nitrogen concentration and plant height). Within-field variation of plant height and aboveground biomass at shooting stage (heading stage) ranged from 31.3 to 51 cm (70.3 to 90 cm), and from 0.28 to 0,79 kg/m^2 (0.72 to 1.55 kg/m^2), respectively. Plant nitrogen concentration varied from 17.1 to 37.42 g/kg at shooting stage and from 13.1 to 19.5 g/kg at heading stage. The decrease of plant nitrogen concentration during the vegetation period is due to dilution effect.

4.3.2 Relationship of standard vegetation indices with crop parameters

The relationships of the different vegetation index types (broad band and narrow band) with the three crop parameters showed different results. Best individual R^2 values for broad band and narrow band standard vegetation indices were achieved for TVI (Table 4.2). The narrow band TVI has high coefficient of determination values for aboveground biomass (R^2=0.71) and plant height (R^2=0.65), but low values for plant nitrogen concentration (R^2=0.33). NDVI generally has lower R^2 values than TVI. Narrow band vegetation indices did not improve the relationships significantly compared with broad band vegetation indices. None of the evaluated broad or narrow band vegetation indices performed well for plant nitrogen concentration, with R^2 being less than 0.35 (Table 4.2).

Table 4.2 Coefficient of determination (R2) between ALI broad band, Hyperion narrow band vegetation indices and measured agronomic parameters.

Sensor	Index	ALI Band / Hyperion wavelength			Coefficient of Determination R^2		
		λ_1	λ_2	λ_3	biomass	plant N	pl. height
ALI broad band	SR	Red (4)	NIR (5)		0.35	0.25	0.41
	NDVI	Red (4)	NIR (5)		0.4	0.28	0.43
	SAVI	Red (4)	NIR (5)		0.55	0.21	0.49
	TVI	Red (4)	NIR (5)		0.69	0.32	0.64
Hyperion narrow band	SR	671	803		0.41	0.3	0.41
	NDVI	671	803		0.41	0.29	0.4
	SAVI	671	803		0.58	0.22	0.56
	TVI	671	803	549	0.71	0.33	0.65
Hyperion best waveband combinations	NRI_1	874	1225		0.83		
	NRI_2	732	1305			0.81	
	NRI_3	763	1225				0.79

4.3.3 Relationship of narrow band Normalized Ratio Index (NRI) with crop parameters

A total number of 9,870 narrow band NRIs according to equation 2 were calculated from multi-temporal Hyperion data. Correlation matrices between each agronomic parameter and two-band vegetation indices were constructed. In each correlation matrix, the wavelengths of the two bands were plotted on the x and y axes and the classified coefficients of determination (R^2) between crop parameters and all possible two-band vegetation indices were plotted on a color scale (Fig. 4.2).

The correlation matrices are only displayed below the diagonal because R^2 values are symmetrical. The R^2 values for aboveground biomass and plant nitrogen concentration ranged from 0.08 to 0.83, and several clusters of high R^2 values could be recognized in the two matrix plots (Fig. 4.2). Wavebands used for broadband NDVI calculation from the red and near infrared spectrum (which match red and near infrared ALI bands), are labeled in the matrix plot. This area shows very low correlation coefficients R^2 compared to waveband pairs forming the clusters with high correlation coefficients. Best center wavelengths of band 1 and band 2 for these patches for aboveground biomass estimation were extracted from the matrices and listed in Table 4.2. Following the same approach, best waveband pairs and bandwidth were determined for the estimation of plant nitrogen concentration (cf. Fig. 4.2b and Tab. 4.3). Similar to aboveground biomass, best waveband centers were not located in

the R and NIR spectrum. The best best values of NRIs for aboveground biomass, plant N concentration and plant height were 0.83, 0.81 and 0.79, respectively. The selected wavebands were centered at 874, 732 and 763 nm for band 1, and 1225 and 1305 nm for band 2 with bandwidth between 10 to 30 nm (Table 4.2).

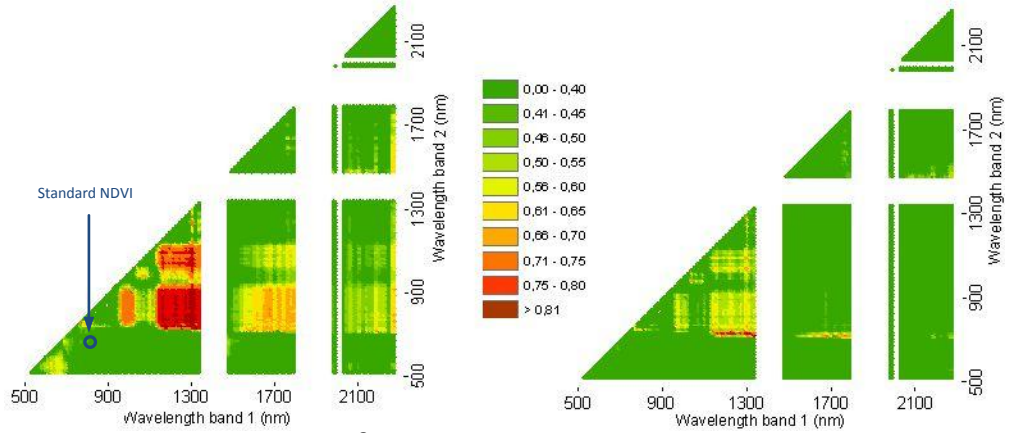

Fig. 4.2 Coefficient of determination (R^2) between Hyperion narrow band vegetation indices calculated from all possible two-band combinations according to equation 2 and measured agronomic parameters. (a) Biomass and (b) total nitrogen content.

4.4 Discussion

4.4.1 Pre-processing of EO-1 data

For the presented study Hyperion and ALI Level 1R data were used which are radiometrically corrected with no geometric correction applied (USGS, 2007). This low level of correction assures no resampling and gives the possibility to bear a complete pre-processing chain to retrieve surface reflectance from at-sensor radiance measured with ALI multispectral and Hyperion hyperspectral sensor. Several authors (BIGGAR et al., 2003; DATT et al., 2003; COOPS et al., 2003) pointed out the importance of correction of artefacts or atmospheric effects. A full processing chain for EO-1 Hyperion data was described by KHURSHID et al. (2006). In comparison to KHURSHID et al. (2006), the misregistration of VNIR and SWIR wavebands, which include spatial and angular shift, has been solved by a co-registration of the wavebands from the two VNIR and SWIR detectors. Due to the lack of detailed atmospheric information, the atmospheric correction was performed with a standard atmosphere implemented in FLAASH (ENVI). The applied atmospheric correction resulted in a good agreement with ASD field data that were taken close to satellite overpass. Similar correction method and observed results were presented by DATT et al. (2003) as well as by CHEN and TIAN (2006).

4.4.2 Standard vegetation indices

In the first step of the study three different two-band indices (SR, NDVI, SAVI) and one three-band index (TVI) were compared in order to evaluate the capability of broad band and narrow band standard vegetation indices for crop parameter estimation. The narrow bands of Hyperion sensor for these indices were centered at green (559 nm), red (681 nm) and near infrared (803 nm) with

bandwidth of 10 nm. The corresponding ALI broadband channels were 4, 5 and 6 with a bandwidth between 40 and 80 nm.

Comparing vegetation indices based on different sources (ALI and Hyperion), only a slight improvement of hyperspectral narrow bands was observed for the three measured crop variables compared to broad band indices. Similar results were found by ZHAO et al. (2007) and LEE et al. (2004), who tested the ability of different multispectral airborne and orbital sensor data for LAI prediction in an agricultural environment. Also HANSEN and SCHJOERRING (2003) found a slightly improved performance of narrow bands for biomass and nitrogen status of wheat crops. On the contrary, BROGE and MORTENSEN (2002) and BROGE and LEBLANC (2000) showed that hyperspectral vegetation indices did not perform better than their simulated multispectral counterparts. Whether broad or narrow bands were used, the standard vegetation indices had limited capability for crop parameter estimation due to canopy closure at high plant densities, which was also observed in the recent study. This saturation effect of standard vegetation indices at high canopy cover is evident for multispectral space based imaging (TUCKER, 1977), airborne hyperspectral imaging (OPPELT and MAUSER, 2004) and ground-based measurements (MUTANGA and SKIDMORE, 2004).

4.4.3 Narrow band normalized difference indices

In this study we evaluated the performance of these calculated band ratios that are widely used and readily adaptable in vegetation studies (SCHOWENGERDT 2007; GONG et al., 2003; THENKABAIL et al., 2000). The results in Fig. 4.2 show that the two-band combinations respond in a wide range to variations in biomass. High coefficients of determination (R^2) between narrow band indices and aboveground biomass are mainly clustered in the red edge, NIR and the SWIR spectra domain. These wavebands are centered in the red edge (720 nm), the NIR peak (874 nm) as well as in the SWIR (1225 nm and 1750 nm) with varying spectral range between 10 and 180 nm. Similar findings for biomass estimation are summarized in THENKABAIL et al. (2004) and MUTANGA and SKIDMORE (2004). These spectral regions of the NIR peak and the SWIR in the electromagnetic spectrum are among others sensitive to plant water content (KUMAR et al., 2001), and consequently they have a close relationship to biomass (HUNT, 1991). The best waveband combination for estimating aboveground biomass was obtained using wavebands centered at 874 nm and 1225 nm. Similar approaches in different types of vegetation cover showed that band combinations from the red edge (ZHAO et al., 2007; MUTANGA and SKIDMORE, 2004) as well as NIR and SWIR (MUTANGA and SKIDMORE 2004; XAVIER et al., 2006) had a close relationship to LAI and aboveground biomass and performed much better than spectral bands used in standard vegetation indices.

Analog to biomass, the regression analysis between NRI and plant nitrogen concentration resulted in a wide range of R^2 values. The best correlation was achieved by combining bands from the red edge region (702 to 732 nm) with wavebands centered between 1138 and 1332 nm, which is in accordance to findings of SMITH et al. (2003). In addition to this, several authors showed that the VIS

region had a close relationship to plant nitrogen concentration (DAUGHTRY et al., 2000, NGUYEN and LEE, 2006). It is well known that canopy spectral reflectance of the VIS (400 to 700 nm) is mainly governed by foliar pigments, such as chlorophyll, which is induced by plant nitrogen concentration (KUMAR et al., 2003; OPPELT and MAUSER, 2004). In addition to the VIS region some authors proved a sensitivity of red edge (LACAPRA et al., 1996; STRACHAN et al., 2002) as well as NIR (LACAPRA et al., 1996; HANSEN and SCHJOERING, 2003) for nitrogen status detection, which is coincident with the best wavebands used for NRI index calculation in our study. Furthermore, the study of FERWERDA et al. (2005) indicated significant differences in the estimation potential of indices for nitrogen concentration across different species.

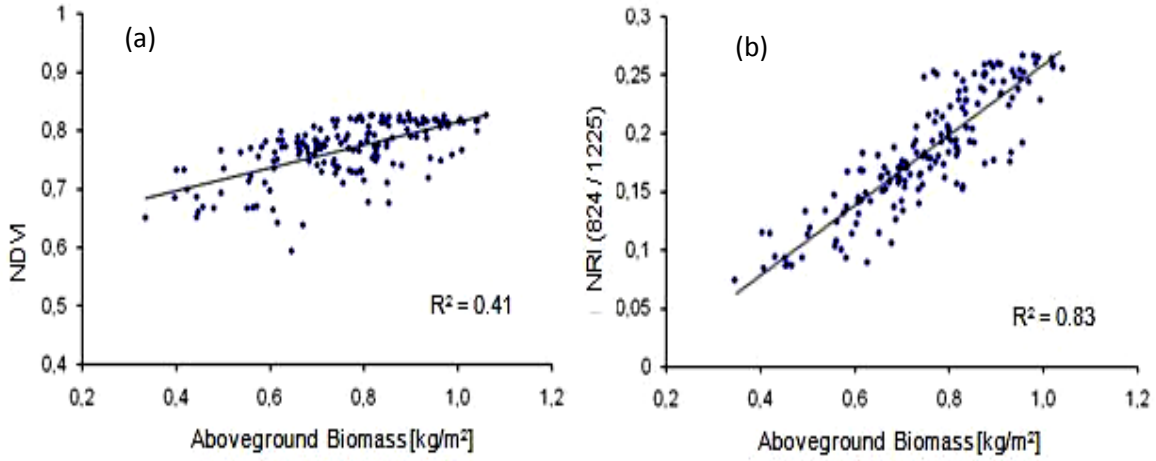

Fig. 4.3 Scatterplot of aboveground biomass against (a) standard narrow band NDVI (671 nm and 803 nm) and (b) best waveband combination from NRI (874 nm and 1225 nm).

4.5 Conclusions

This study compared vegetation indices calculated from multispectral and hyperspectral satellite remote sensing data for estimating winter wheat aboveground biomass, plant nitrogen concentration and plant height in North China Plain, and identified better vegetation indices by systematically evaluating all possible two band combinations using Hyperion satellite hyperspectral remote sensing data from 400 to 2500 nm. The results indicated that TVI performed best among the tested vegetation indices using either broad (R^2=0.69, 0.32 and 0.64 for biomass, N concentration and plant height, respectively) or narrow (R^2=0.71, 0.33 and 0.65 for biomass, N concentration and plant height, respectively) bands. For the evaluated standard vegetation indices, narrow band indices only had slight improvements over corresponding broad band indices. The best performing Normalized Ratio Indices (NRI) selected through band combination analysis were significantly better than TVI, achieving R^2 of 0.83, 0.81 and 0.79 for biomass, plant N concentration and plant height, respectively. They all used wavebands from the near infrared (NIR) (centered at 874, 732, and 763 nm) and short wave infrared (SWIR) (centered at 1225 and 1305 nm) spectrum with varying bandwidth between 10

and 190 nm. The results of this study suggest that is important to include SWIR bands in multispectral satellite sensors for agricultural crop growth status monitoring. More studies are needed to further evaluate the results using data from more diverse conditions.

We can conclude that narrow band vegetation indices calculated from all possible waveband combination from Hyperion data perform much better for winter wheat parameters estimation on a regional level than standard vegetation indices calculated from red and NIR wavebands. Comparing all three index calculations, it was observed that two-band indices calculated according to Eq. 4.2 performed much better for estimation of aboveground biomass and total nitrogen content with at least 12% improvement for aboveground biomass and 48% for plant nitrogen content for winter wheat in the North China Plain. Because satellite image data were acquired at shooting and heading stage with a canopy closure of almost 100%, the saturation effect was obvious. This saturation effect is pointed out in a flat slope for regression between standard NDVI and aboveground biomass in Fig. 4.3. Compared to this, the slope of the regression line is much steeper using bands from the NIR and SWIR for index calculation. The results of band combination showed, that the saturation problem occurred for standard vegetation indices can be overcome by using different combinations for narrow band indices.

References* (* for chapter 4)

BERK, A., ANDERSON, G.P., ACHARYA, P.K., CHETWYND, J.H., BERNSTEIN, L.S., SHETTLE, E.P., MATTHEW, M.W., ADLER-GOLDEN, S.M., 2000: MODTRAN4 User's Manual. Hanscom AFB, MA: Air Force Res. Lab., 1–93.

BIGGAR, S.F., THOME, K.J., WISNIEWSKI, W., 2003. Vicarious radiometric calibration of EO-1 sensors by reference to high-reflectance ground targets. IEEE Transactions on Geoscience and Remote Sensing, 41 (6), 1174-1179.

BREMNER, J.M., 1960. Determination of nitrogen in soil by the Kjeldahl method. Journal of Agricultural Science, 55, 11-33.

BROGE, N.H., LEBLANC, E., 2000. Comparing predicting power and stability of broadband and hyperspectral vegetation indices for estimation of green leaf area index and canopy chlorophyll density. Remote Sensing of Environment, 76, 156-172.

BROGE, N.H., MORTENSEN, J.V., 2002. Deriving green crop area index and canopy chlorophyll density of winter wheat from spectral reflectance data. Remote Sensing of Environment, 81, 45-57.

CAIRNS, B., 2003. Special Issues Papers. Atmospheric correction and its application to an analysis of Hyperion Data. IEEE Transactions on Geoscience and Remote Sensing, 41 (6), 1232-1245.

CECCATO, P., GOBRON, N., FLASSE, S., PINTY, B., TARANTOLA, S., 2002. Designing a spectral index to estimate vegetation water content from remote sensing data: Part 1 Theoretical approach. Remote Sensing of Environment, 82, 188-197.

CHEN, J., TIAN, Q., 2006: Estimating canopy chlorophyll and nitrogen concentration of rice from EO-1 Hyperion data. Remote Sensing for Agriculture. Proceedings of the SPIE 6359.

COOPS, N.C., SMITH, M.-C., MARTIN, M.E., OLLINGER, S.V., 2003. Prediction of eucalypt foliage nitrogen content from satellite-derived hyperspectral Data. IEEE Transactions on Geoscience and Remote Sensing, 41 (6), 1338-1346.

CLOUTIS, E.A., CONNERY, D.R., DOVER, F.J., 1999. Agricultural crop monitoring using airborne multi-spectral imagery and C-band synthetic aperture radar. International Journal of Remote Sensing, 20, 767-787.

DATT, B., MCVICAR, T.R., VAN NIEL, T.G., JUPP, D.L.B., PEARLMAN, J.S., 2003. Pre-processing EO-1 Hyperion hyperspectral data to support the application of agricultural indexes. IEEE Transactions on Geoscience and Remote Sensing, 41 (6), 1246-1259.

DAUGHTRY, C.S.T., WALTHALL, C.L., KIM, M.S., DE COLSTOUN, E.B., MCMURTREY, J.E., 2000. Estimating corn leaf chlorophyll concentration from leaf and canopy reflectance. Remote Sensing of Environment, 74, 229-239.

FERWERDA, J.G., SKIDMORE, A.K., MUTANGA, O., 2005. Nitrogen detection with hyperspectral normalized ratio indices across multiple plant species. International Journal of Remote Sensing, 26, 4083-4095.

GALVAÕ, L.S., FORMAGGIO, A.R., TISOT, D.A., 2005. Discrimination of sugarcane varieties in Southeastern Brazil with EO-1 Hyperion data. Remote Sensing of Environment, 94, 523-534.

GONG, P., PU, R., BIGING, G.S., LARRIEU, M.R., 2003. Estimation of forest leaf area index using vegetation indices derived from Hyperion hyperspectral data. IEEE Transactions on Geoscience and Remote Sensing, 41 (6), 1355-1362.

HABOUDANE, D., MILLER, J.R., PATTEY, E., ZARCO-TEJADA, P.J., STRACHAN, I.B., 2004. Hyperspectral vegetation indices and novel algorithms for predicting green LAI of crop canopies: Modeling and validation in the context of precision agriculture. Remote Sensing of Environment, 90, 337-352.

HANSEN, P.M., SCHJOERRING, J.K., 2003. Reflectance measurement of canopy biomass and nitrogen status in wheat crops using normalized difference vegetation indices and partial least square regression. Remote Sensing of Environment, 86, 542-553.

HUETE, A.R., 1988. A soil-adjusted vegetation index (SAVI). Remote Sensing of Environment, 25, 295-309.

JONGSCHAAP, R.W.W., SCHOUTEN, L.S.M., 2005. Predicting wheat production at regional scale by integration of remote sensing data with a simulation model. Agronomy for Sustainable Development, 25, 481-489.

KHURSHID, K., STAENZ, K., SUN, L., NEVILLE, R., WHITE, H.P., BANNARI, A., CHAMPAGNE, C.M.,

HITCHCOCK, R., 2006. Preprocessing of EO-1 Hyperion data. Canadian Journal of Remote Sensing, 32, 84-97.

KUMAR, L., SCHMIDT, K., DURY, S., SKIDMORE, A., 2003. Imaging spectrometry and vegetation science. In: F.D., VAN DER MEER, S.M., DE JONG, (Eds.), Imaging Spectrometry. Dordrecht, pp. 111-156.

LAUDIEN, R., BARETH, G., 2006. Multitemporal hyperspectral data analysis for regional detection of plant diseases by using a tractor-and an airborne-based spectrometer. Photogrammetrie, Fernerkundung, Geoinformation, 2006 (3), 217-228.

LEE, K.-S., COHAN, W.B., KENNEDY, R.E., MAIERSPERGER, T.K., GOWER, S.T., 2004. Hyperspectral versus multispectral data for estimation leaf area index in four different biomes. Remote Sensing of Environment, 91, 508-520.

LI, F., GNYP, M.L., JIA, L., MIAO, Y., YU, Z., KOPPE, W., BARETH, G., CHEN, X., ZHANG, F., 2008. Estimating N status of winter wheat using a handheld spectrometer in the North China Plain. Field Crops Research, 106, 77-85.

LILLESAND, T.M., KIEFER, R.W., CHIPMAN, J.W., 2004. Remote Sensing and Image Interpretation. 5th Edition. New York, Chichester, Brisbane, Toronto, Singapore, 763 pages.

LU, D., 2006. The potential and challenge of remote sensing-based biomass estimation. International Journal of Remote Sensing, 27, 1297-1328.

MIAO, Y., MULLA, D.J., RANDALL, G.W., VETSCH, J.A., VINTILA, R., 2009. Combining chlorophyll meter readings and high spatial resolution remote sensing images for in-season site-specific nitrogen management of corn. Precision Agriculture, 10, 45-62.

MUTANGA, O., SKIDMORE, A.K., 2004. Narrow band vegetation indices overcome the saturation problem in biomass estimation. International Journal of Remote Sensing, 25, 3999-4014.

NGUYEN, H.T., LEE, B.-W., 2006. Assessment of rice leaf growth and nitrogen status by hyperspectral canopy reflectance and partial least square regression. European Journal of Agronomy, 24, 349-356.

OPPELT, N., MAUSER, W., 2004. Hyperspectral monitoring of physiological parameters of wheat during a vegetation period using AVIS data. International Journal of Remote Sensing, 25, 145-159.

PEARLMAN, J.S., BARRY, P.S., SEGAL, C.C., SHEPANSKI, J., BEISO, D., CARMAN, S.L., 2003. Hyperion, a Space-Based Imaging Spectrometer. IEEE Transactions on Geoscience and Remote Sensing, 41 (6), 1160-1173.

REYNIERS, M., VRINDTS, E., 2006. Measuring wheat nitrogen status from space and ground-based platform. International Journal of Remote Sensing, 27, 549-567.

ROUSE, J.W., HAAS, R.H., SCHELL, J.A., DEERING, D.W., HARLAN, J.C., 1974. Monitoring the vernal advancements and retrogradation of natural vegetation. In: NASA/GSFC, Final Report, Greenbelt, USA, 1-137.

SERRANO, L., FILELLA, I., PEÑUELAS, J., 2000. Remote sensing of biomass and yield of winter wheat under different nitrogen supplies. Crop Science, 40, 723-731.

SCHMIDT, K.S., SKIDMORE, A.K., 2003. Spectral discrimination of vegetation types in a coastal wetland. Remote Sensing of Environment, 85, 92-108.

SCHNEIDER, K., 2003. Assimilating remote sensing data into a land surface process model. International Journal of Remote Sensing, 24, 2959-2980.

SCHOWENGERDT, R.A., 2007. Remote sensing: models and methods for image processing. 3rd ed. Amsterdam, Elsevier Academic Press, The Netherlands, 515 pages.

SIMS, D.A., GAMON, J.A., 2002. Relationships between leaf pigment content and spectral reflectance across a wide range of species, leaf structures and development stages. Remote Sensing of Environment, 81, 337-354.

SMITH, M.-L., MARTIN, M.E., PLOURDE, L., OLLINGER, V., 2003. Analysis of hyperspectral data for estimation of temperate forest canopy nitrogen concentration: Comparison between an airborne (AVIRIS) and a spaceborne (Hyperion) sensor. IEEE Transactions on Geoscience and Remote Sensing, 41 (6), 1332-1337.

STRACHAN, I.B., PATTEY, E., BOISVERT, J.B., 2002. Impact of nitrogen environmental conditions on corn as detected by hyperspectral reflectance. Remote Sensing of Environment, 80, 213-224.

THENKABAIL, P.S., ENCLONA, E.A., ASHTON, M.S., VAN DER MEER, B., 2004. Accuracy assessment of hyperspectral waveband performance for vegetation analysis application. Remote Sensing of Environment, 91, 354-376.

THENKABAIL, P.S., SMITH, R.B., DE PAUW, E., 2000. Hyperspectral vegetation indices and their relationships with agricultural crop characteristics. Remote Sensing of Environment, 71, 158-182.

TUCKER, C.J., 1979. Red and photographic infrared linear combinations for monitoring vegetation. Remote Sensing of Environment, 8, 127-150.

USGS, 2007. EO-1 User's Guide, http://eo1.usgs.gov/userGuide/index.php

WOOSTER, M., 2007. Remote sensing: sensors and systems. Progress in Physical Geography, 31, 95-100.

XAVIER, A.C., RUDORFF, B.F.T., MOREIRA, M.A., ALVARENGA, B.S., DE FREITAS, J.G., SALOMON, M.V., 2006. Hyperspectral field reflectance measurements to estimate wheat grain yield and plant height. Scientia Agricola, 63, 130-138.

ZHAO, D., LI, J., QI, J., 2004. Hyperspectral characteristic analysis of a developing cotton canopy under different nitrogen treatments. Agronomy Journal, 24, 463-471.

ZHAO, D., HUANG, L., LI, J., QI, J., 2007. A comparative analysis of broadband and narrowband derived vegetation indices in predicting LAI and CCD of a cotton canopy. ISPRS Journal of Photogrammetry & Remote Sensing, 62, 25-33.

5. Development and implementation of a multiscale biomass model using hyperspectral vegetation indices for winter wheat in the North China Plain

M.L. GNYP[a, b,*], G. BARETH[a, b], F. LI[b, c], V.I.S. LENZ-WIEDEMANN[a, b], W. KOPPE[a, e], Y. MIAO[b, d], S.D. HENNIG[e], L. JIA[d, f], R. LAUDIEN[g], X. CHEN[b, d], F. ZHANG[d]

received: 16 October 2013, received in revised form: 8 May 2014, accepted: 9 May 2014
International Journal of Earth Observation and Geoinformation (accepted)
Original submitted manuscript is used and embedded in dissertation format.

a. Institute of Geography, University of Cologne, 50923 Cologne, Germany
b. International Center for Agro-Informatics and Sustainable Development (ICASD), www.icasd.org
c. Collge of Ecology and Environmental Science, Inner Mongolia Agricultural University, Hohhot, 010019, China
d. College of Resources and Environmental Science, China Agricultural University, Beijing, 100193, China
e. Infoterra GmbH, Astrium Geo-Information Services, 88039 Friedrichshafen, Germany
f. Institute of Agricultural Resources & Environment, Hebei Academy of Agricultural and Forestry Sciences, Shijiazhuang, 050051, China
g. ESRI Germany GmbH, 85402 Kranzberg, Germany

*Corresponding author, Tel.: +49-221-4706551; fax: +49-221-4701638.
Email: mgnyp1@uni-koeln.de, martingnyp@yahoo.de (M. L. Gnyp)

Abstract

Crop monitoring during the growing season is important for regional management decisions and biomass prediction. The objectives of this study were to develop, improve and validate a scale independent biomass model. Field studies were conducted in Huimin County, Shandong Province of China, during the 2006-2007 growing season of winter wheat (*Triticum aestivum L.)*. The field design had a multiscale set-up with four levels, which differed in their management, such as nitrogen fertilizer inputs and cultivars, to create different biomass conditions: small experimental fields (L1), large experimental fields (L2), small farm fields (L3), and large farm fields (L4). L4, planted with different winter wheat varieties, and was managed according to farmers' practice while L1 through L3 represented controlled field experiments. Multitemporal spectral measurements were taken in the fields, and biomass was sampled for each spectral campaign. In addition, multitemporal Hyperion data were obtained in 2006 and 2007. L1 field data were used to develop biomass models based on the

relation between the winter wheat spectra and biomass: Several published vegetation indices, including NRI, REP, OSAVI, TCI, and NDVI, were investigated. A new hyperspectral vegetation index, which uses a four-band combination in the NIR and SWIR domains, named GnyLi, was developed. Following the multiscale concept, the data of higher levels (L2 through L4) were used stepwise to validate and improve the models of the lower levels, and to transfer the improved models to the next level. Lastly, the models were transferred and validated at the regional scale using Hyperion images of 2006 and 2007. The results showed that the GnyLi and NRI models, which were based on the NIR and SWIR domains, performed best with $R^2>0.74$. All the other indices explained less than 60% model variability. Using the Hyperion data for regionalization, GnyLi and NRI explained 81–89% of the biomass variability. These results highlighted that GnyLi and NRI can be used together with hyperspectral images for both plot and regional level biomass estimation. Nevertheless, additional studies and analyses are needed to test its replicability in other environmental conditions.

Keywords: multiscale, biomass, model development, hyperspectral, vegetation index, winter wheat

5.1 Introduction

Knowledge about crop characteristics during its growing season is very important for disease monitoring, yield prediction, and for adapting agricultural management to optimize yield and to avoid over-fertilization (LAUDIEN et al., 2006; MIAO et al., 2009; OERKE et al., 2010). Traditionally, expensive field-based destructive measuring of agronomic parameters, such as biomass, plant and soil nitrogen content, and Leaf Area Index (LAI) is necessary in order to accurately describe crop growth (ATZBERGER, 1998; THENKABAIL et al., 2000). Alternatively, agronomic parameters can be monitored using non-destructive spectral reflectance observations (KUMAR et al., 2003) obtained from satellite, airborne or hand-held imaging spectrometers. In-season and within-field crop development and growth can be described using crop reflectance. The prediction of crop parameters with remote and close range sensing data have become very common in the last decade (ADDINK et al., 2007; OERKE et al., 2010). Various airborne sensors (e.g. APEX, AVIRIS, CASI, and HyMap) and satellite sensors (e.g. CHRIS-PROBA, HJ-1/HSI, and Hyperion) are available for this purpose or will be launched in the near future (e.g. EnMAP, HyspIRI, and PRISMA).

One major advantage of hyperspectral spectrometers is their high spectral resolution (bandwidth ≤3 nm) and continuous acquisition of reflectance values between 350 nm and 2500 nm. Numerous vegetation indices (VIs), mainly situated in the red and near infrared (NIR), and sometimes in the green spectral region, were published (CLEVERS and JONGSCHAAP, 2001; TODD et al., 1998). These VIs use the wavelengths around the minima and maxima of crop reflectance caused by leaf pigments and cell structure (ROBERTS et al., 2011). Combined with agronomic parameters, such as biomass or nitrogen concentration, crop models can be developed (CLEVERS and JONGSCHAAP, 2001;

GNYP et al., 2014; TODD et al., 1998). In the simplest approach, single or multiple time-integrated VIs were used to estimate crop parameters by regression modeling (SERRANO et al., 2000).

Canopy reflectance is mainly determined by LAI and other properties (e.g. leaf angle, soil optical properties). When LAI shows a close relation to biomass, a good relation between canopy reflectance and biomass can be expected (GNYP et al., 2013; LIU, et al., 2010; SERRANO et al., 2000). High correlations between biomass and reflectance are shown in hyperspectral data collected by field spectrometer, airborne, and satellite sensors (BABAR et al., 2006; CHO et al., 2007; PSOMAS et al., 2011). Narrow-band VIs have already demonstrated excellent relations with wheat biomass (XAVIER et al., 2006) or Green LAI (HABOUDANE et al., 2004; HINZMAN et al., 1986).

THENKABAIL et al. (2000) introduced the Normalized Ratio Index (NRI) based on the visible (VIS) and NIR spectra without using shortwave infrared (SWIR) domain. According to VAN LEEUWEN (2009), the NIR domain is defined from 700 nm to 1100 nm and the SWIR from 1100 nm to 2500 nm. The NRI represents the best band combination. Using 2006 EO-1 Hyperion data, KOPPE et al. (2010) found the NRI calculated from the NIR and SWIR bands (centered at 874 nm and 1225 nm) performed much better than broad-band or other narrow-band VIs in regional winter wheat biomass estimation.

Although the importance of monitoring agricultural production at regional scales has been identified as a key task (BOUMAN, 1995; CLEVERS and JONGSCHAAP, 2001), yield and biomass estimation were rarely addressed at the regional scale using multispectral and hyperspectral data due to uncertainties in prediction associated with this scale and limited data availability (BARETH, 2009; LOBELL et al., 2003; MA et al., 2008). However, this situation has changed rapidly in recent years (LU, 2006). For example, CHO et al. (2007) estimated grass biomass in Southern Italy using HyMap data. PSOMAS et al. (2011) studied grassland in the Swiss Plateau. In the North China Plain, REN et al. (2008) predicted winter wheat yield; BAO et al. (2009) monitored winter wheat biomass using MODIS data; and KOPPE et al. (2012) estimated winter wheat biomass using Hyperion data. Remote sensing has proved to be an effective alternative for mapping aboveground biomass in remote areas at the regional scale (JI et al., 2012).

For the development and implementation of a multiscale biomass, the NRI was tested. The index was derived by KOPPE et al. (2010) based on 2006 Hyperion imagery against 2007 spectral field measurements in the same study area for winter wheat biomass estimation. Several selected VIs were also compared to the NRI. Moreover, a new index, the GnyLi (named in this study by the authors Gnyp and Li who did most of the field and data analyses work), was introduced using the absorption and reflectance features in the NIR and SWIR spectral regions. The VIs were used to build the biomass models based on a newly proposed bottom-up approach. Finally, the models were tested against independent field-observed datasets. Due to the increasing availability of hyperspectral satellite data, the importance of developing validated algorithms and models for field and regional applications, especially in crop production, is apparent.

5.2 Study site and data

5.2.1 Study site description

The study site Huimin County (~1,400 km²) is located in the North China Plain (117.4°E, 37.3°N), at the lower stretch of the Yellow River (Huang He), approximately 100 km west of the Bo Hai Sea in the Northeastern Shandong Province (Fig. 5.1). This area is characterized by the warm-temperature sub-humid continental East Asian monsoon climate controlled by the thermal low-pressure area at the Tibetan Plateau. A clear seasonal change between arid, cool winter and humid, hot summer days exists. The annual average temperature is 12.5°C and the total annual precipitation is 600 mm with a summer maximum. Yellow loamy fluvisols with the alluvial loess as subsoil substrate are typical for the area. Soil and climate allow double-cropping per year. The dominant cropping system is a summer maize and winter wheat rotation. Winter wheat is sown in October and harvested in early June of the following year. The specific study fields (L1-L3) are located in Xizhangliu village and L4 in the Xili, Xujia and Donjie villages.

5.2.2 Multiscale set-up of the study fields

5.2.2.1 Level 1 (L1): Small experimental fields

The small experimental field plots (L1) included 48 plots in total, each in a size of 4.5 m by 7.5 m. Two cultivar experiments with four replications and six nitrogen (N) fertilizer treatments were set up. The cultivars were *Kenong9204* (new cultivar) and *Lumai23* (local cultivar). Each replication consisted of six N treatments: (1) *Control* (no N input), (2) 40% of optimum N rate (*Opt*), (3) 70% of *Opt*, (4) 100% of *Opt*, (5) 130% of *Opt*, and (6) conventional N fertilization. The last one represents the local farmers' practice with a total N input of approximately 300 kg N/ha. The optimal rate was plot-specific based on expected plant N demand and measured soil N supply for the growing periods from the sowing through harvest (LI et al., 2008).

5.2.2.2 Level 2 (L2): Large experimental fields

The large experimental field plots (L2) had a size of 10 m by 15 m with four replicates of five differently fertilized plots. The application rate of nitrogen fertilizer like urea $(NH_2)_2CO$ was either 0, 25, 50, 75 or 100 kg N/ha before sowing the local winter wheat cultivar *Weimei8* in early October of 2006. When the phenological stage of BBCH 30 was reached, each plot was divided into two parts (7.5 m by 10 m), one with and one without N topdressing. L2 includes 20 plots before topdressing and 40 after topdressing.

5.2.2.3 Level 3 (L3): Small farm fields

The L3 experiment comprised farm fields with both controlled and conventional management. For *Control* and *Opt* plots, the plot size was 150 m². The conventionally managed plots' size ranged from 150 m² to 1750 m². Totally, 14 small farm fields were selected with different management

strategies (planting dates, cultivars, and especially different N inputs). Each field was divided into three plots according to the applied amount of N: *Control* (no N), *Opt* (using N_{min} method), and conventionally fertilized plots with a fertilizer input of 200 – 400 kg N/ha. The farmers sowed several winter wheat cultivars including *Lumai8*, *Lumai23*, and *Zimai12*. This level comprised 42 plots in total.

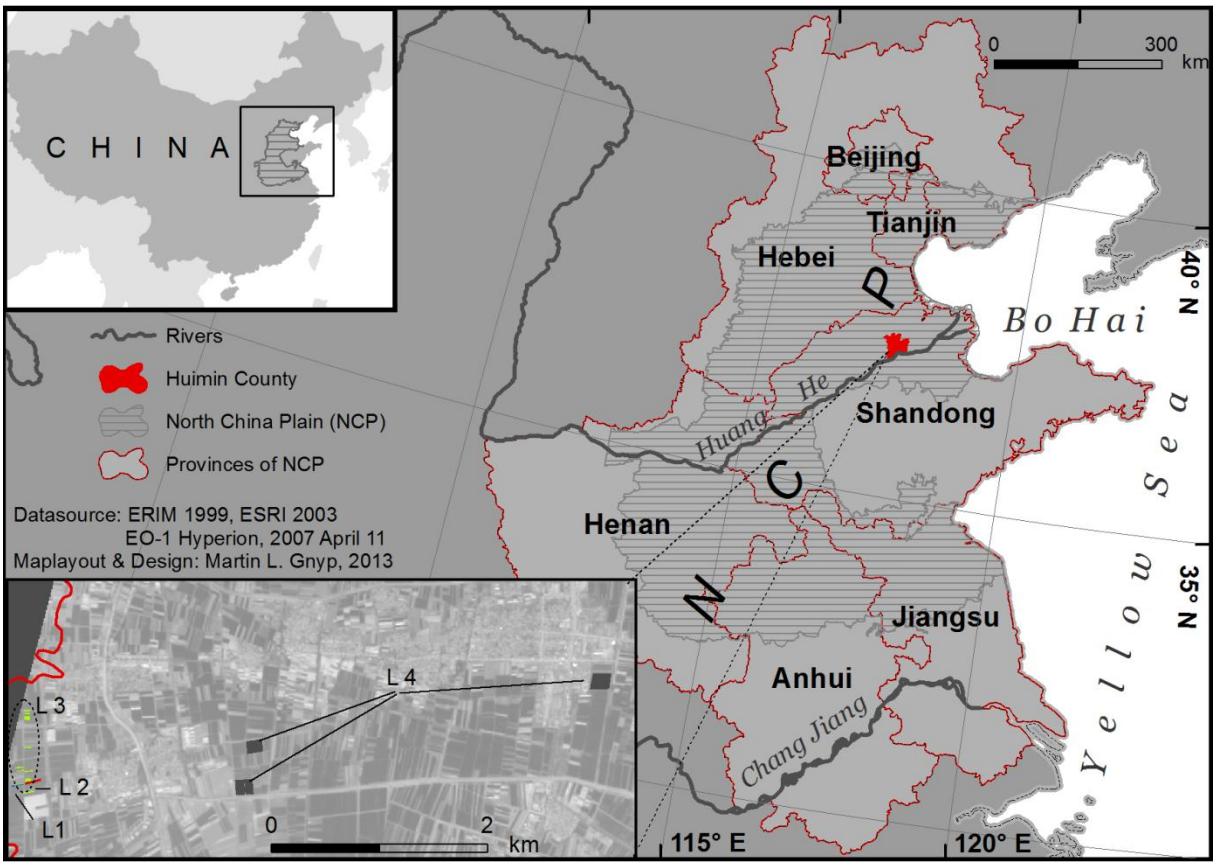

Fig. 5.1 Study site Huimin County in the North China Plain and the locations of the test sites (L1-L4).

5.2.2.4 Level 4 (L4): Large farm fields

The large farm fields (L4) were located within a distance of less than 4 km (Fig. 5.1). The fields were conventionally managed by the farmers. The field sizes varied from 1 ha to 3 ha, and totally 56 plots were investiged. The smallest plots size was 10 m by 100 m. Winter wheat cultivars *Jimai20*, *Jimai21*, and *Weimai8* were planted.

5.2.3 Field measurements

5.2.3.1 Spectral reflectance measurements

Canopy spectral reflectance was collected in 2007 using a QualitySpec Pro (350–1800 nm). The device is a product of Analytical Spectral Devices Inc., Boulder, CO, USA. The default field of view angle of 25° was used. The sensor was fixed by an orthogonal construction 1 m above the crop canopy. The acquisition geometry resulted in a diameter for each measurement of approximately 44

cm and an area of canopy of 0.15 cm². The construction consisted of three brass-poles, which were combined to a triangle with moveable joins (LAUDIEN et al., 2006). Continuous calibration measurements with a white reference panel ($BaSO_4$) and dark current were taken depending on illumination changes. The measurements were carried out near noon ± 2 hours under mostly cloudless conditions. Ten sample counts for spectral reflectance were collected and repeated at three scanning positions. The spectral scanning positions were taken randomly in the center of each plot in order to reduce influences caused by plant density and plant row orientation variations, and boundary disturbances. The spectral data were collected at five different BBCH phenological stages 30, 31, 32, 39 and 45 (Table 5.1). In total, approximately 4,000 winter wheat canopy spectra were collected during the field campaign in 2007. ASD Indico Pro Tools software was used for pre-processing. The spectra information was averaged for each plot.

Table 5.1 Dates of spectral and biomass measurements for L1 to L4 and corresponding phenological stages according to the BBCH scale (MEIER, 2001).

BBCH scale	30	30	31	32	39	45
Level 1 (L1)	26/03/2007	31/03/2007	17/04/2007	26/04/2007	05/05/2007	18/05/2007
Level 2 (L2)	20/03/2007	31/03/2007	17/04/2007	26/04/2007	05/05/2007	18/05/2007
Level 3 (L3)	27/03/2007	06/04/2007	18/04/2007	27/04/2007	05/05/2007	19/05/2007
Level 4 (L4)	27/03/2007	01/04/2007	11/04/2007	21/04/2007	04/05/2007	19/05/2007

5.2.3.2 Biomass measurements

After taking reflectance measurements (Table 5.1), aboveground biomass was sampled by randomly cutting a representative area of at least 30 cm by 100 cm (two rows, each 1 m long) in each plot. Considering the different plot sizes and conditions, the number of biomass samples varied per plot: one for L1, L2, and L3, and two for L4. Since winter wheat is irrigated during its growing season, biomass samples could not be collected for each plot at each growth stage. In total, 901 biomass samples were taken (L1: n=240, L2: n=159, L3: n=221, L4: n=281). All samples were oven dried at 70°C to constant weight to determine dry matter. This weight was multiplied by number of plants in 1 m² and then scaled to the real unit of each plot to obtain biomass (t/ha).

5.2.4 EO-1 Hyperion images and pre-processing

Six Hyperion images with different view angles were acquired on April 19, May 6, May 31, 2006 and on April 11, April 21, and May 6, 2007. The optical sensor is mounted on the Earth Observing One (EO-1) satellite that follows the World Reference System-2 with a 16 day revisit time for nadir mode. Hyperion collects continuous data with a VNIR and a SWIR spectrometer using 220 bands in the 400–2400 nm wavelength domain. Each image covers a 7.5 km wide and 100 km long area, with a spatial resolution of 30 m. The images were radiometrically calibrated (Level 1R) and delivered in 16-bit radiance data.

Satellite image pre-processing of Hyperion data included (a) a correction of sensor artifacts,

b) an atmospheric correction, and (c) a geometric correction. The pre-processing aimed to improve the quality of the images for multitemporal data analysis (KHURSHID et al., 2006). Totally, to analyze the relationship between spectral reflectance and measured biomass collected in L4, 162 and 108 pixel samples (30 m x 30 m) were extracted from the 2006 and 2007 imagery, respectively. Mixed pixel information caused by plot boundaries were excluded for further analysis. More detailed information about Hyperion image pre-processing for the study area is given by KOPPE et al. (2010).

Table 5.2 VIs evaluated in this study. R is the reflectance value (%) at a specific wavelength (nm).

VI	Name	Formula	Reference
NDVI	Normalized Difference Vegetation Index	$\frac{R_{NIR}-R_{RED}}{R_{NIR}+R_{RED}}$	ROUSE et al. (1974)
RVI	Ratio Vegetation Index	R_{NIR}/R_{RED}	PEARSON and MILLER (1972)
SAVI	Soil Adjusted Vegetation Index	$(1+L)*(R_{800}-R_{670})/(R_{800}+R_{670}+L)$	HUETE (1988)
MSAVI	Modified SAVI	$0.5(2R_{800}+1-\sqrt{(2*R_{800}+1)^2-8(R_{800}-R_{670})})$	QI et al. (1994)
OSAVI	Optimized Soil-Adjusted Vegetation Index	$(1+0.16)*\frac{R_{800}-R_{670}}{R_{800}+R_{670}+0.16}$	RONDEAUX et al. (1996)
HVI	Hyperspectral Vegetation Index	R_{750}/R_{700}	GITELSON et al. (1996)
HNDVI	Hyperspectral Normalized Difference Vegetation Index	$\frac{R_{827}-R_{668}}{R_{827}+R_{668}}$	OPPELT and MAUSER (2004)
GI	Greennees Index	R_{554}/R_{677}	ZARCO-TEJADA et al. (2005)
TVI	Triangular Vegetation Index	$0.5*[120*(R_{750}-R_{550})-200*(R_{670}-R_{550})]$	BROGE and LEBLANC (2000)
MCARI2	Modified Chlorophyll Absorption Ratio Index	$\frac{1{,}5*[2.5*(R_{800}-R*_{670})-1.3*(R_{800}-R_{550})]}{\sqrt{(2*R_{800}+1)-(6*R_{800}-5*\sqrt{R_{670}})-0.5}}$	HABOUDANE et al. (2004)
TCI	Triangle Chlorophyll Vegetation Index	$\frac{(R_{800}+1.5*R_{550})-R_{675}}{R_{800}-R_{700}}$	GAO (2006)
RRE	Reflexion in Red Edge	$(R_{670}+R_{780})/2$	GUYOT and BARET (1988)
REP	Red Edge Position	$700+(740-700)*\frac{R_{RRE}-R_{700}}{R_{740}-R_{700}}$	GUYOT and BARET (1988)
NRI	Normalized Ratio Index	$\frac{R_{874}-R_{1225}}{R_{874}+R_{1225}}$	KOPPE et al. (2010)
GnyLi	Named by the authors Gnyp and Li	$\frac{R_{900}*R_{1050}-R_{955}*R_{1220}}{R_{900}*R_{1050}+R_{955}*R_{1220}}$	This paper

5.3 Methods

5.3.1 Vegetation indices (VIs)

Vegetation indices (VIs) are usually used to identify plant vitality during different phenological stages or to quantify biomass under various growth conditions (e.g. caused by fertilizer input, water availability). This study examined 15 VIs using broad and narrow bands (Table 5.2). Most of them were reported in the literature to be well correlated with biomass or LAI. For the NDVI and RVI, the mean reflectance values in the red (600-700 nm) and in the NIR domains (700-1100 nm) were calculated. The adjustment for the constant L in the SAVI equation was set to 0.5, which was suggested for intermediate vegetation density by HUETE (1988).

5.3.2 New developed VI GnyLi

The GnyLi index follows the NRI equation, and considers two reflection and absorption features in the NIR and SWIR domains between 800 and 1300 nm. Those features were detected as peaks in almost all spectra, which represent one absolute ($R_{absolute.max}$) and one local reflectance ($R_{local.max}$) maximum in the NIR domain as well as the absorption features of the local minima ($R_{local.min.1}$ and $R_{local.min.2}$) in the NIR and SWIR domains (Fig. 5.2 and Eq. 5.1). The numerator and denominator of the ratio equation consist of two peaks' product. Product P1 uses the two highest reflectance values in the NIR domain and P2 uses the lowest reflectance values in the NIR and SWIR domains.

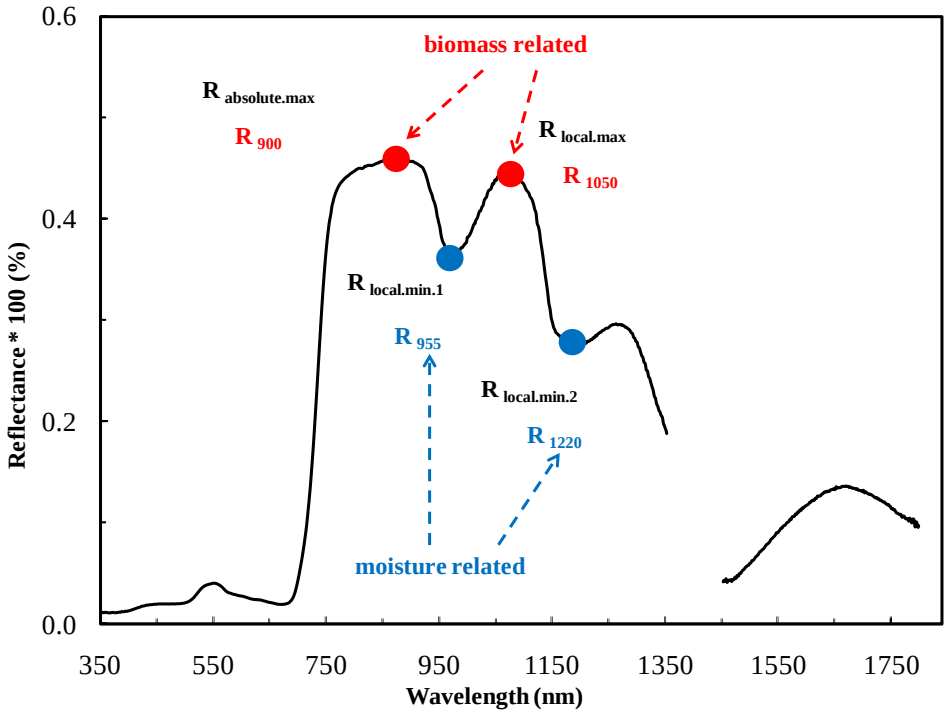

Fig. 5.2 Reflectance of winter wheat and its characteristic peaks and troughs with the reflectance maxima and minima in the NIR and SWIR domains. These peaks were used to compute the VI GnyLi. R is the reflectance value (%) at a specific wavelength (nm).

$$\mathrm{GnyLi} = \frac{P1 - P2}{P1 + P2} = \frac{R_{absolute.\max} * R_{local.\max} - R_{local.\min.1} * R_{local.\min.2}}{R_{absolute.\max} * R_{local.\max} + R_{local.\min.1} * R_{local.\min.2}} \qquad \text{(Eq. 5.1)}$$

where P1 represents product 1 and P2 is product 2, and P1>P2; R denotes reflectance

In those wavelength domains, the high reflection is caused by the intercellular structure of plants (KUMAR et al., 2003). The absorption characteristics of fresh leaves around 970 nm and 1200 nm are affected by plant moisture, cellulose, starch, lignin, and leaf water content dominates the absorption strength (CURRAN, 1989; PU et al., 2003). Only the effective wavelength domains of 350–1330 nm and 1450–1770 nm were used in the permutation to identify the best 4-band for the GnyLi index. The spectral regions of 1331–1449 nm and 1771–1800 nm were excluded due to their

association with water absorption. Hence, totally 1300 bands allowed a permutation of 1300^4 four-band combinations. The permutation process was optimized by selecting only the first hundred best combinations to minimize the large storage capacity and the attended time in the calculation process. The calculation was performed by the HyperCor tool, which was developed by AASEN et al. (2014). The highest correlation with biomass was achieved with a combination of four narrow bands centered at 900 nm, 955 nm, 1050 nm and 1220 nm in the form of normalized difference of the products of local maximum or minimum values as shown in Eq. (5.1). Specifically, two of the identified spectra near the peak reflectance (900 nm and 1050 nm) are sensitive to biophysical quantities, such as biomass (PEÑUELAS and FILLELA, 1988, THENKABAIL et al., 2011), and the other two identified spectra close to the local reflectance troughs (955 nm and 1220 nm) are sensitive to plant or leaf moisture (CLEVERS et al., 2010; PU et al., 2003; THENKABAIL et al., 2011).

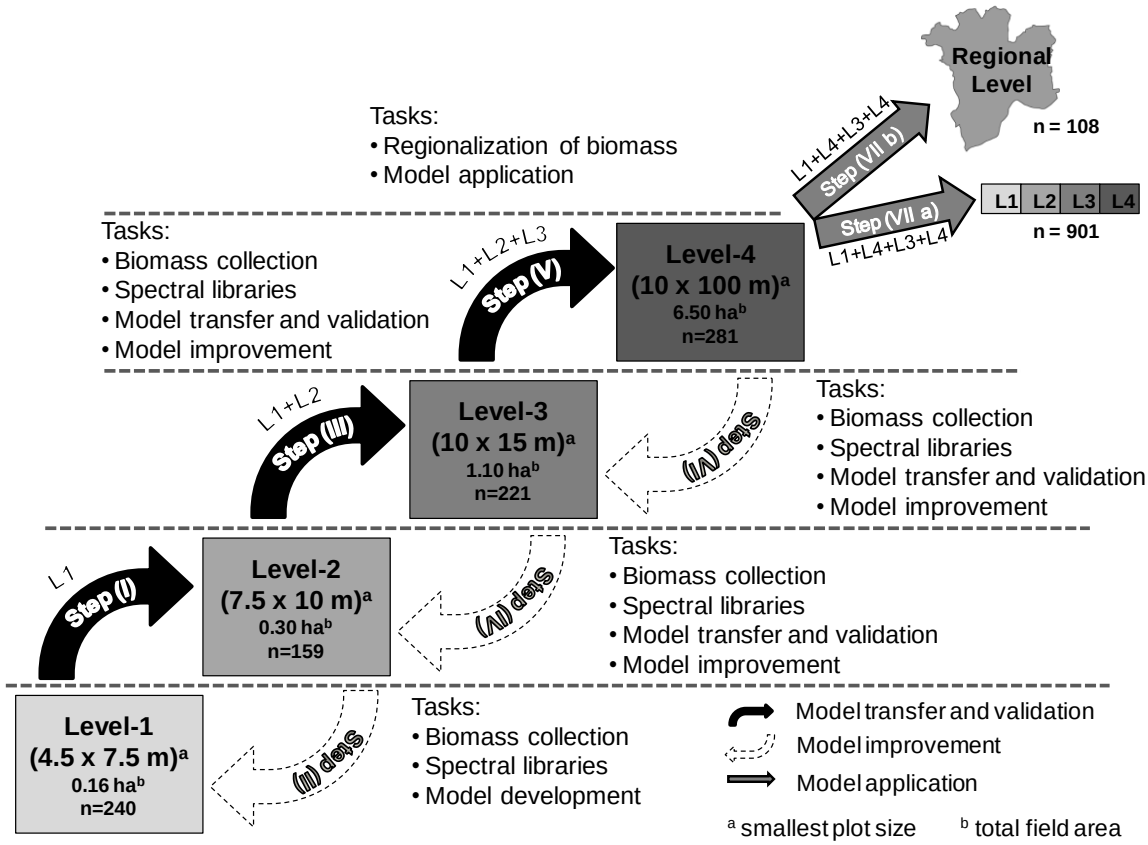

Fig. 5.3 Concept of the multiscale biomass model development with a bottom-up design (n=number of biomass samples). Biomass samples from Level-1 (L1) to Level-4 (L4) were measured and samples at the regional level were extracted from the Hyperion imagery.

5.3.3 Multiscale biomass model development

Our bottom-up multiscale approach was based on regression modeling. Biomass measurements and VIs calculated from hyperspectral field measurements were regressed. The field data were obtained from a multiscale field design of four levels, with L1 and L2 representing experimental fields of different plot sizes, and L3 and L4 representing farm fields under controlled and

conventional management. The plot size increases from L1 to L4. Different N management strategies were applied to create diverse biomass conditions.

Fig. 5.3 illustrates the multiscale approach in a stepwise procedure. Following a bottom-up concept, each step represents a model development level (L1 to L4), ending with the model application at the regional level (Huimin County). There were two development steps for each level as shown by the arrows in Fig. 5.3. Each step included several tasks: biomass collection, establishment of spectral libraries, model development, model validation and improvement, and finally, model application and regionalization. Steps (I), (III), and (V) stand for model transfer and validation for the higher level. Steps (II), (IV), (VI), and (VII a) represent model improvement. Additionally, step (VII b) indicates model application at the regional level. In particular, in step (I), a model was developed by a regression analysis of biomass and hyperspectral data (VIs) for L1. When the statistical analysis exhibited satisfying results, the computed regression equation was then used to estimate biomass for the next higher level L2. Field biomass data of L2 were used for the model validation. Step (II) was applied if the validation was successful. In step (II), biomass and hyperspectral data of L1 and L2 were combined in a new regression analysis. Again, if the statistical analysis showed satisfying results, the regression model was applied to estimate the biomass for the next higher level L3. Recursively, a positive model validation result led to a L4 model development (step (IV)) using biomass and hyperspectral data of L1 through L3. The development of the regional model (step (VI)) relied on all available data from L1 through L4. The result of step (VI) was the regional model, which was tested in step (VII a) in order to estimate biomass for all levels and was transferred to Hyperion data in step (VII b).

5.3.4 Statistical analyses

For the correlation and regression analyses SPSS 13.0 (SPSS, Inc., Chicago, IL, USA) and STATISTICA 6.0 (StatSoft, Inc., Tulsa, OK, USA) were used. Based on the calculated VI values and corresponding measured biomass (dry matter) values, regression equations were derived for each VI. The performance of the VIs was evaluated by the coefficient of determination (R^2). The regression model was then used to estimate biomass for the next higher level. Model performance was quantified by root mean square error (RMSE), relative error (RE in %), and standard error (SE). The higher the R^2 and the degrees of freedom (n) of the regression model, the higher the accuracy and the level of significance.

5.4 Results

5.4.1 Selected VIs for biomass model development

The coefficients of determination (R^2) for all the regression models of L1 are shown in Table 5.3. The results were classified in three categories: low correlation ($R^2<0.5$), medium correlation ($0.5<R^2<0.7$), and high correlation ($R^2>0.7$). Only the GnyLi, NRI, and REP-based regression models

showed high correlations. Medium correlations occurred in the TCI, OSAVI and NDVI-based models. Low correlations were found in the rest of the models. Hence, those six VIs with high to medium R^2 values were chosen for biomass model development. The following sections consider only these six VIs for the scale independent biomass model development and performance evaluation.

Table 5.3 Coefficient of determination (R^2) for the relationships between VIs and biomass at phenological stages 30–45 (BBCH scale) for L1.

VI	R^2	VI	R^2	VI	R^2
NDVI	0.524**	HVI	0.414*	TCI	0.642**
RVI	0.526**	HNDVI	0.525**	RRE	0.477*
SAVI	0.603**	GI	0.327*	REP	0.863***
MSAVI	0.619**	TVI	0.450*	NRI	0.875***
OSAVI	0.602**	MCARI2	0.587**	GnyLi	0.892***

*low, **medium, *** high correlation ; all R^2 significant at 0.01 probability level

5.4.2 Step (I): Model L1 versus biomass on L2

In the first step, we developed the models based on the observed data of L1 experiment in order to estimate the biomass for L2 experiment. The model equations, derived from the relationships between observed biomass of L1 and the corresponding VIs (calculated from the field spectrometer data), are shown in Table 5.4. The newly developed GnyLi-based model performed the best. It produced the highest R^2, the lowest RMSE, RE, and SD (R^2=0.84; RMSE=2.29 t/ha; RE=41.65%; SE=0.18 t/ha). The second best model was the NRI-based one (R^2=0.77; RMSE=2.68 t/ha; RE=48.82%; SE=0.23 t/ha). OSAVI and NDVI-based models had the lowest fitting.

Table 5.4 Characteristics of the regressions between observed and predicted biomass for L2, L3, and L4.

VI	Regression Models	SE (t/ha)	Intercept	R^2	RMSE (t/ha)	RE (%)
		L2 with n=159 (step I)				
(a) NRI	Biomass = 0.529*exp (12.28*NRI_{L2})	0.228	+1.023	0.77	2.68	48.82
(b) GnyLi	Biomass = 0.357*exp (11.39*$GnyLi_{L2}$)	0.182	+1.020	0.84	2.29	41.65
(c) REP	Biomass = 7E-83*exp (0.261*REP_{L2})	0.277	+1.330	0.67	3.10	56.44
(d) OSAVI	Biomass = 0.015*exp (7.303*$OSAVI_{L2}$)	0.541	+1.063	0.33	3.40	61.91
(e) TCI	Biomass = 9056*exp (-5.99*TCI_{L2})	0.425	+0.444	0.52	2.62	47.62
(f) NDVI	Biomass = 0.002*exp (8.782*$NDVI_{L2}$)	0.527	+1.009	0.35	3.27	59.55
		L3 with n=221 (step III)				
(a) NRI	Biomass = 0.931*exp (9.029*NRI_{L3})	0.266	-0.539	0.75	1.74	30.82
(b) GnyLi	Biomass = 0.518*exp (9.636*$GnyLi_{L3}$)	0.215	+0.584	0.77	1.62	28.76
(c) REP	Biomass = 9E-73*exp (0.23*REP_{L3})	0.273	+0.529	0.67	1.99	35.24
(d) OSAVI	Biomass = 0.036*exp (6.343*$OSAVI_{L3}$)	0.817	+1.347	0.12	3.15	55.89
(e) TCI	Biomass = 342.7*exp (-3.407*TCI_{L3})	0.909	-5.807	0.42	2.89	51.26
(f) NDVI	Biomass = 0.012*exp (6.882*$NDVI_{L3}$)	0.997	-0.996	0.18	3.19	56.63
		L4 with n=281 (step V)				
(a) NRI	Biomass = 0.891*exp (9.272*NRI_{L4})	0.217	+0.122	0.73	1.74	30.52
(b) GnyLi	Biomass = 0.535*exp (9.482*$GnyLi_{L4}$)	0.163	+0.722	0.80	1.66	31.92
(c) REP	Biomass = 4E-72*exp (0.227*REP_{L4})	0.273	+1.784	0.46	2.57	47.09
(d) OSAVI	Biomass = 0.037*exp (6.265*$OSAVI_{L4}$)	0.544	-0.522	0.32	2.58	47.46
(e) TCI	Biomass = 481.3*exp (-3.675*TCI_{L4})	0.718	-2.213	0.30	2.63	48.31
(f) NDVI	Biomass = 0.01*exp (7.146*$NDVI_{L4}$)	0.689	-0.319	0.21	2.76	50.58

n = Number of samples for model validation

5.4.3 Step (II): Model improvement (L1+L2) versus biomass on L1+L2

In the second step, field data from L1 and L2 were merged to one dataset (n=399). The new correlations between the observed biomass and the VIs were derived. Table 5.5 displays the coefficients of determination (R^2) for the six indices. Again, the same three models based on REP, NRI, and GnyLi achieved the highest R^2 values (0.79–0.87). The other three models showed medium correlations ($0.53 \leq R^2 \leq 0.57$).

5.4.4 Step (III): Model L1+L2 versus biomass on L3

In step (III), the model L1+L2 was applied to the L3 observations. Regression characteristics for the observed and predicted biomass are listed in Table 5.4. The best model was GnyLi (R^2=0.77), slightly better than the NRI model (R^2=0.75, RMSE=1.74 t/ha), then followed by the REP model (R^2=0.67, RMSE=1.99 t/ha, and RE=35.24%). The OSAVI and NDVI models had low R^2 values (<0.2) and high errors (RE>55%). Especially, the SE increased about 50% from step (I) to step (III). For the TCI model, all statistical measures indicated a weak worsening of the model accuracy, given the rising RMSE and RE values. The SE has doubled from 0.43 t/ha in step (I) to 0.91 t/ha in step (III) for this model. At this step, it can be concluded that the OSAVI, TCI and NDVI models were not suitable to predict biomass of a higher scale.

5.4.5 Step (IV): Model improvement (L1+L2+L3) versus biomass on L1+L2+L3

In this step, data from L1 through L3 were merged to one database (n=620) for a second model improvement. As in step (II), three models achieved high precision (R^2=0.86 for GnyLi, R^2=0.80 for REP and NRI), while the other three had lower R^2 ($\leq$0.50). These results showed that models based on the OSAVI, TCI, and NDVI from the L1 and L2 experimental fields could not be transferred to farm fields (L3). Although a medium correlation in L1 was detected in these models, the results indicated that using data from different levels evidently reduced model accuracies (Table 5.5).

Table 5.5 Coefficient of determination (R^2) for the cross-validation relationships between observed biomass and vegetation indices (step II, step IV, step VI).

	R^2		
	Step (II) n=399	Step (IV) with n=620	Step (VI) with n=901
(a) NRI	0.79	0.80	0.78
(b) GnyLi	0.87	0.86	0.84
(c) REP	0.82	0.80	0.70
(d) OSAVI	0.57	0.50	0.49
(e) TCI	0.53	0.50	0.47
(f) NDVI	0.53	0.48	0.44

n = Number of samples

5.4.6 Step (V): Model L1+L2+L3 versus biomass on L4

The L1+L2+L3 models were applied to large farm fields (L4). L4 data comprised farmers' management practices that incorporating different sowing dates, fertilizer inputs, cultivars, and large

areas. Statistical characteristics of the regressions between observed and predicted biomass for L4 (281 samples) are listed in Table 5.4. Again, the two NRI and GnyLi models showed a high performance ($R^2 \leq 0.80$) with lower RMSE ($\leq$1.74t/ha) and RE (<32%). In contrast to step (I) and (III), the validation indicators of the transferred GnyLi model of L4 showed a smaller change. For the NRI model, the indicators slightly changed compared with those in step (I) and step (III). For the REP model, a higher coefficient of determination was reached through model up-scaling from L1 to L3. However, transferring the model to L4 resulted in a lower accuracy (R^2=0.46). In comparison to the first and second model up-scaling, the RMSE and RE values decreased for the TCI, OSAVI and NDVI models. These models explained 21–32% of biomass variability and their intercept became negative.

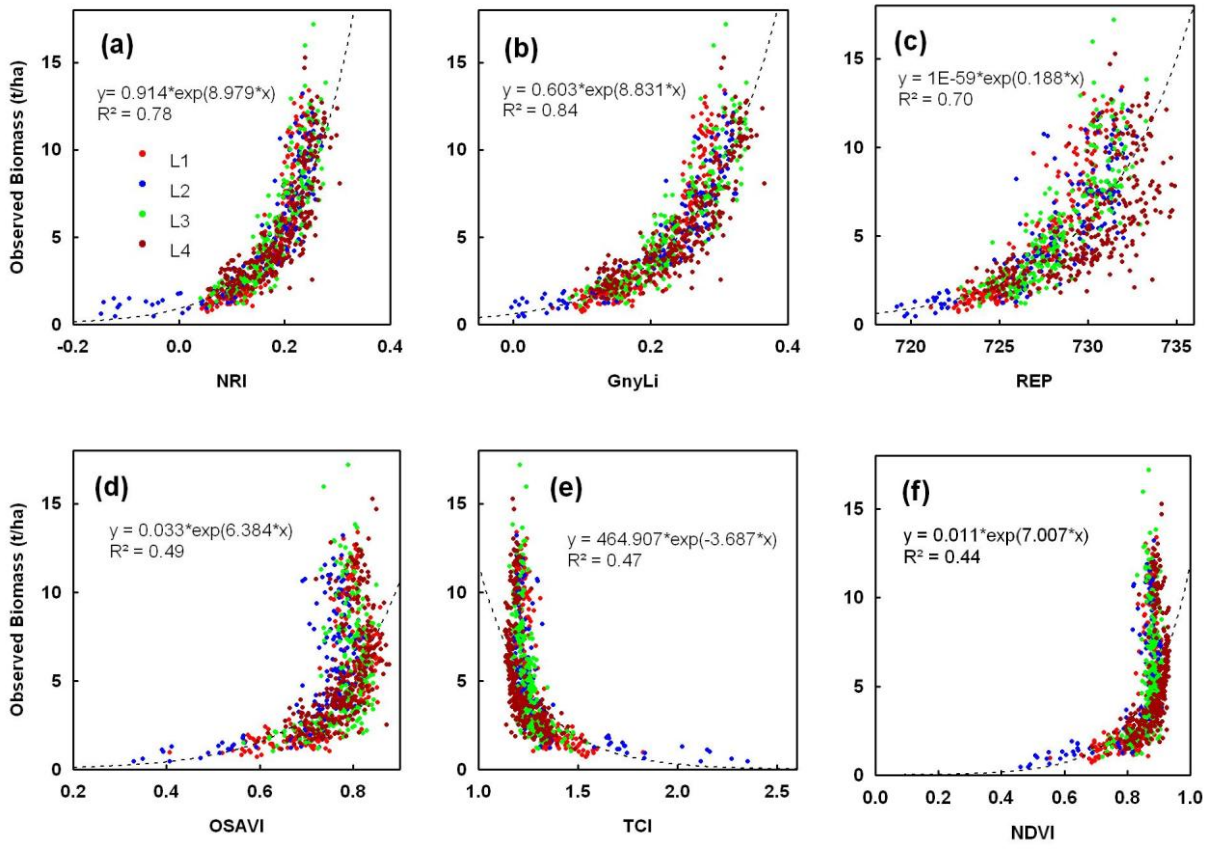

Fig. 5.4 Step (VI): Cross-validation relationship between observed biomass and vegetation indices (a) NRI. (b) GnyLi, (c) REP, (d) OSAVI, (e) TCI, and (f) NDVI. The graphs show the model improvement with the combined (L1+L2+L3+L4) biomass data (sample number n=901).

5.4.7 Step (VI): Model improvement (L1+L2+L3+L4) versus biomass on L1+L2+L3+L4

Step (VI) represents the final model improvement which included data across all levels from L1 to L4 with 901 observations (Table 5.5, Fig. 5.4). All six regressions had an exponential trend. The GnyLi and NRI models ($R^2 \geq 0.78$) outperformed the other models again ($R^2 \leq 0.70$). Their values scattered closer to the regression line and reached the saturation when the biomass was higher than 10 t/ha. Given the high biomass variability during the growing season, the performance of these two models was satisfactory. In comparison, the OSAVI, TCI and NDVI models were saturated at a lower

biomass level (>7.5 t/ha). Lower biomass values were commonly observed at the jointing stage (BBCH scale 32–39).

5.4.8 Step (VII): Model application on regional level

All models were applied at the regional level for biomass regionalization. This process was conducted in two steps (Fig. 5.3): (a) model application with ground truth data for L1+L2+L3+L4 and (b) model application with hyperspectral Hyperion satellite data.

(a) At the regional level, high model accuracy ($R^2 \geq 0.74$, RMSE$\leq$1.74 t/ha, and RE<34%) occurred with the GnyLi and NRI based models (Fig. 5.5 and Table 5.6). The scatter plots for these models demonstrated a linear correlation between observed and predicted biomass (901 observations). For both models, the regression line fitted the 1:1 line very well, with the trend line of the GnyLi model being significantly closer to the 1:1 line. The other models based on REP, OSAVI, TCI, NDVI were much less accurate with $R^2<0.52$, and their RMSE and RE values were more than doubled comparatively. OSAVI, TCI and NDVI were logarithmically correlated with biomass. In general, from L1 to the regional level, the performance of the GnyLi and NRI models decreased relatively 9–10% while the performance dropped 12–13% and 17–28% respectively for the NDVI and OSAVI models and the TCI and REP models (Table 5.6).

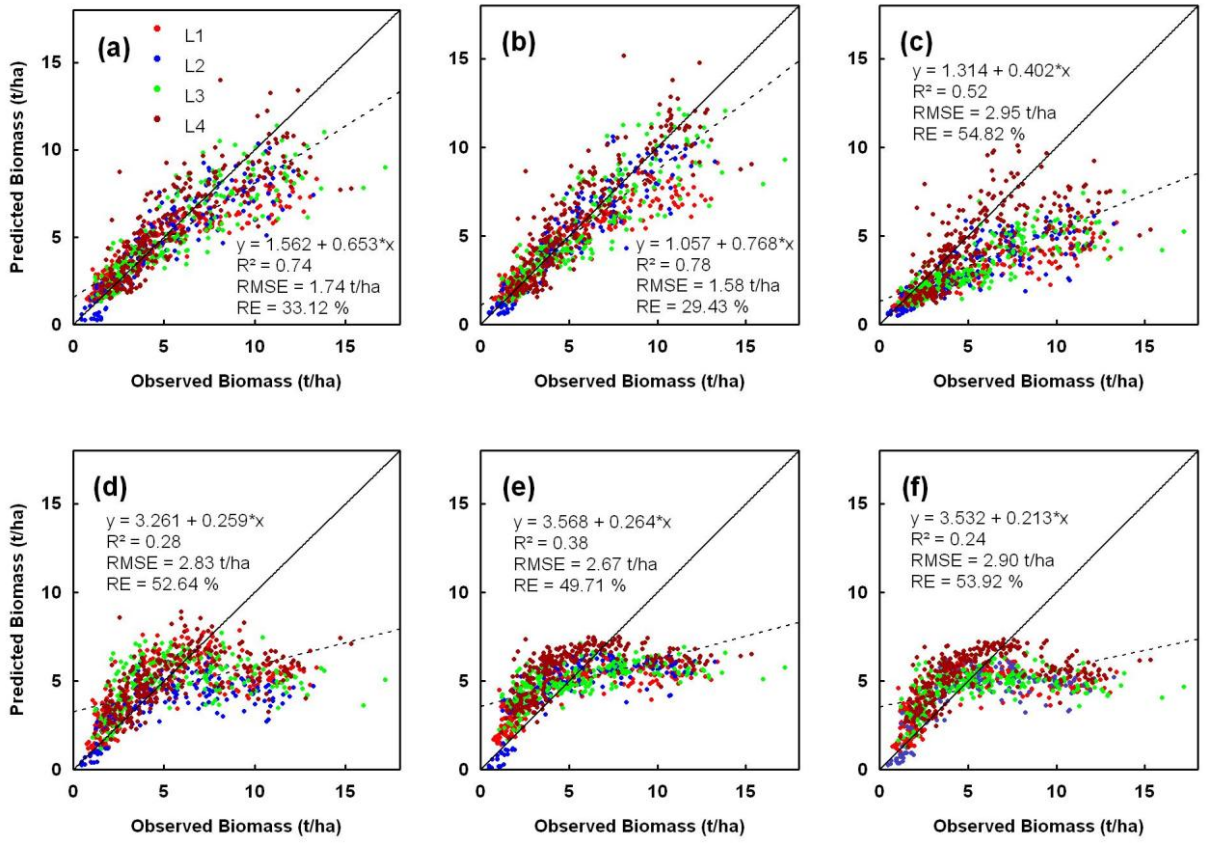

Fig. 5.5 Step (VII a): Cross-validation scatter plots with observed biomass versus predicted biomass for L1+L2+L3+L4. The total sample size was 901. The six models are: (a) NRI model, (b) GnyLi model, (c) REP model, (d) OSAVI model, (e) TCI model, and (f) NDVI model. The solid line indicates the 1:1 line and the dashed line indicates the regression line.

Table 5.6 Statistics for the biomass model application on regional level (L1+L2+L3+L4) and on each level.

VI	Regression Models	All (n=901)	Validation indicators	L1 (n=240)	L2 (n=159)	L3 (n=221)	L4 (n=281)
		0.74	R^2	0.84	0.77	0.75	0.73
(a) NRI	0.914*exp (8.979*NRI)	1.74	RMSE (t/ha)	1.85	2.13	1.79	1.62
		33.12	RE (%)	37.25	38.79	31.77	29.66
		0.78	R^2	0.87	0.85	0.78	0.80
(b) GnyLi	0.603*exp (8.831*GnyLi)	1.58	RMSE (t/ha)	1.70	1.73	1.63	1.48
		29.43	RE (%)	34.19	31.42	28.80	27.08
		0.52	R^2	0.80	0.68	0.68	0.47
(c) REP	1E-59*exp (0.188*REP)	2.95	RMSE (t/ha)	3.25	3.13	3.29	2.47
		54.82	RE (%)	65.24	57.00	58.32	45.27
		0.28	R^2	0.41	0.34	0.12	0.32
(d) OSAVI	0.033*exp (6.384*OSAVI)	2.83	RMSE (t/ha)	2.67	3.26	3.20	2.61
		52.64	RE (%)	53.62	59.27	56.61	47.77
		0.38	R^2	0.55	0.49	0.43	0.30
(e) TCI	464.907*exp (-3.687*TCI)	2.67	RMSE (t/ha)	2.74	2.93	2.96	2.64
		49.71	RE (%)	55.07	53.29	52.38	48.35
		0.24	R^2	0.36	0.36	0.17	0.21
(f) NDVI	0.011*exp (7.007*NDVI)	2.90	RMSE (t/ha)	2.98	5.11	3.32	2.79
		53.92	RE (%)	59.84	92.84	58.80	58.08

n=Number of samples

(b) In order to evaluate their performance at the regional level, the models were tested using Hyperion images. The regression equations based on the L1 through L4 field data were applied to the three Hyperion images acquired during the 2007 growing season. The results are listed in Table 5.7.

Table 5.7 Statistics for the biomass models application to the Hyperion images data (2006 and 2007).

		2006			2007		
		R^2	RMSE	RE	R^2	RMSE	RE
VI	Regression Models		(t/ha)	(%)		(t/ha)	(%)
(a) NRI	0.914*exp (8.979*$NRI_{Hyperion}$)	0.84	1.67	24.04	0.89	2.34	33.08
(b) GnyLi	0.603*exp (8.831*$GnyLi_{Hyperion}$)	0.81	2.13	30.69	0.86	3.10	43.81
(c) REP	1E-59*exp (0.188*$REP_{Hyperion}$)	0.52	5.16	76.43	0.02	4.86	68.64
(d) OSAVI	0.033*exp (6.384*$OSAVI_{Hyperion}$)	0.49	21.60	300.96	0.71	10.63	150.13
(e) TCI	464.907*exp (-3.687*$TCI_{Hyperion}$)	0.28	3.25	46.76	0.81	4.82	68.05
(f) NDVI	0.011*exp (7.007*$NDVI_{Hyperion}$)	0.43	3.24	46.72	0.69	5.68	80.26
n=Number of samples			n=162			n=108	

The NRI model showed the best performance while the opposite was true for the NDVI and TCI model. Specifically, the NRI model had a R^2 of 0.90, RMSE of 2.34 t/ha, and RE of 33.07%. The GnyLi model had a compatible performance (R^2=0.86, RMSE=3.10 t/ha, and RE=43.80%). Although NRI worked better for Hyperion data, GnyLi was better for ground field data. Both models explained a large portion of the biomass variability in the Hyperion imagery. The other models achieved a moderate performance ($R^2 \geq 0.69$), but had relatively high RMSE (>4 t/ha) and RE (63–80%). Especially, the REP and OSAVI models were very imprecise at regional level. Similar high

performance (R^2>0.81, RMSE<2.2 t/ha, and RE<31%) occurred with the NRI and GnyLi models when they were applied to the 2006 Hyperion imagery.

5.5 Discussion

In this study, the major objective of developing a scale-independent remote sensing-based biomass model was achieved. Once the regression model is developed, it can be used to estimate biomass at several spatial levels. In general, the multiscale set up was based on a total sample number of n=901. However, the number of samples for each level (L1, L2, L3, and L4) differed (n=240, n=159, n=221 to n=281). The results of the multiscale model development revealed that the components of the regression equations could remain relatively consistent if the models had a high goodness of fit. The analyses of the linear regression models from L2 to L4 (Table 5.3 to Table 5.4) and across L1 to L4 (Table 5.6) demonstrated the superiority of the NRI and GnyLi models over other investigated VIs. While the R^2 values of the NRI and GnyLi models changed slightly from step (I) to step (V) (between 0.73 and 0.77, and 0.77 and 0.84, respectively), they decreased remarkably in other four models during the up-scaling process.

The biomass estimation models were developed from plot level, presenting a cultivar experiment. Different associations were identified between biomass and VIs for the two varieties *Kenong9204* and *Lumai23* of L1, with a more significant association found in the cultivar *Kenong9204* (GNYP et al., 2009). Cultivar's influence on reflectance and consequent models were reported for winter wheat by BABAR et al. (2006), KIPP et al. (2014), and OPPELT and MAUSER (2004). However, different cultivars were not considered separately in this study. The study area is known for small scale farming. Thus, field data of various cultivars were chosen to represent the reality. Especially for the regionalization purpose, it is impracticable to develop a model being only valid for one cultivar (FERRIO et al., 2005). This study showed that the regression models were improved resulting in lower estimation errors when several cultivars were included in the regression models (Table 5.4).

In addition to the cultivar effect, the results indicated the need to use of observations that fully represent real farm situations. LI et al. (2010) reported similar developing models for practical nitrogen fertilizer application. Models developed and validated based on laboratory measurements may not be transferable to farmers scale. On the other hand, this study highlighted the transferability from small plot level to regional level using VIs based on NIR and SWIR domains.

KOPPE et al. (2010) found that NRI based on NIR and SWIR bands were of more value than other VIs. Their findings were based on the 2006 Hyperion image, but validated using the 2007 hyperspectral field data. The newly developed GnyLi index uses some similar wavelengths. However, the GnyLi uses four bands of the NIR and SWIR domains (900, 955, 1050 and 1220 nm) rather than two. Using two products of the local peak/trough spectra in the NIR and SWIR domains in the equation of GnyLi helped avoid saturation problem, which is a major advantage of the GnyLi index.

As shown in the results (Table 5.4), only the NRI and GnyLi models performed constantly well at all four levels. Therefore, they enabled scale-independent model development and offered promising biomass estimates across several growth stages (BBCH 30–45). Nevertheless, further studies are needed to test the four-band GnyLi and two-band NRI at a single growth stage of winter wheat.

In other studies, high relationships between biomass and VIs were also found for three wavelengths clustered in the SWIR region (1205, 1325, and 1710 nm) for grassland (PSOMAS et al., 2011) and at 1100 nm along with 660 nm for wheat (ZHU et al., 2008). MARIOTTO et al. (2013) observed different crops and found higher correlation for cotton and a lower correlation for wheat biomass using the SWIR domain. Their results revealed better biomass predictability by field spectrometers than by Hyperion. The plant spectra in the SWIR region are strongly related to leaf water content, cellulose, lignin, and starch (CURRAN, 1989; PU et al., 2003). The water content is a main component of fresh weight and is associated with dry weight. However, factors such as crop type, phenology, and growth condition also have an impact (CLEVERS et al., 2008). Generally, the use of SWIR domain for biomass estimation was not very common in the past.

The two models transferred to the regional level using Hyperion data showed an excellent performance (R^2=0.89 for NRI, R^2=0.86 for GnyLi) in this study. Other validation indicators, such as RMSE, ranging from 2.3 t/ha to 3.1 t/ha, and RE, ranging from 33% to 43%, were higher than the applied models at the L1+L2+L3+L4 level, which revealed some uncertainties that might be caused by the mixed pixel problem (30 m by 30 m) of the Hyperion data. These uncertainties were apparent in the imprecise biomass estimation using REP and OSAVI. Hazy conditions at the early growth stages caused a three times higher reflectance value at 670 nm wavelength in two of the three Hyperion images than the field spectrometer reflectance (KOPPE et al., 2012). The visible part of the electromagnetic spectrum is particularly affected by hazy atmospheric conditions (KUMAR et al., 2003). LIU et al. (2012) proposed a piecewise function to correct Hyperion's reflectance to ASD reflectance in the up-scaling approach. KOPPE et al. (2010)'s model explained 83% of the winter wheat biomass variability based on the 2006 Hyperion data. Our study conformed to their results. Both studies showed that models based on ground spectrometer data can be transferred to the regional level using hyperspectral satellite image data. A stronger model performance was found by LIU et al. (2010) using a "radiation use efficiency index" derived from CASI and Landsat TM data. Their model explained 96% of the biomass variability for corn with a low model RMSE (1.33 t/ha) over two years. Besides, REN et al. (2008) achieved higher model accuracy in the regionalization of a MODIS-NDVI model. However, their model was based on lower-resolution image (250 m). By contrast, DAVIDSON et al. (2006) yielded a less accurate model (R^2=0.53) using CropScan (0.5 m) at the plot scale and Landsat TM (30 m) at the regional scale. Our models were improved and validated at different scales.

Compared to the NRI and GnyLi models, the other investigated models reached an earlier saturation. The NDVI is known to be saturated with high biomass or LAI observations. The findings of our study conform to those of PSOMAS et al. (2011) who reported weak model performances for

SAVI and NDVI (R^2<0.3) at the regional level. Additionally, KOPPE et al. (2010) also concluded that NDVI performed worse (R^2<0.4) for biomass estimation using Hyperion data. Similar results were reported by CHO et al. (2007) using the NDVI model (R^2=0.42, RMSE=2.98 t/ha) for grass biomass. Using REP and the best band combination NDVI (771 and 740 nm) model, they estimated biomass from HyMap imagery for green grass/herb. However, their estimates offered a better biomass explanation, where R^2=0.7 and RMSE=2.16 t/ha for the REP model and R^2=0.7 and RMSE 14 t/ha for the best NDVI model. Their results are only similar to our REP model at the L1+L2+L3+L4 level (R^2=0.52 and RMSE=2.95 t/ha).

In summary, because of the saturation problem, the standard narrow-band indices have a low potential for biomass regionalization. Instead, the indices based on NIR and SWIR domains are proposed.

5.6 Conclusions and outlook

The results of this study indicated the potential applications of the NIR and SWIR domains for biomass estimation. The two best performed models (NRI and GnyLi) explained 73–87% and 81–89% winter wheat biomass variability using field spectrometer measurements (L1+L2+L3+L4) and Hyperion data at the regional level, respectively. In comparison, the models using the VIS and NIR domains (REP, OSAVI, TCI, and NDVI) explained less biomass variability with higher model errors. These models were only useful during a short time of the critical growth stages.

We found that the best NIR and SWIR band combination (874 nm and 1225 nm) identified by KOPPE et al. (2010) based on Hyperion data could be transferred to spectrometer bands, with similar results of biomass prediction at the regional level. The analysis results based on the two Hyperion images of 2006 and 2007 were comparable. The newly developed four-band GnyLi index performed consistently well across the scales for biomass estimation. Finally, we conclude that NIR and SWIR spectra are more useful for biomass estimation since they are sensitive to absorption characteristics of plant water content, cellulose, lignin, and starch. The biomass models, based on hyperspectral NRI and GnyLi indices, are excellent predictors at the regional level. Compared with standard indices, these two indices can be applied in a longer period of the winter wheat growing season.

Future studies are needed to confirm the findings using multitemporal hyperspectral data acquired from other years or other study sites. Besides, an investigation of the findings at diverse growth stages would be interesting. The developed multiscale framework could be applied to estimate biomass of different crops based on diverse types of remote sensing data. Above all, additional quantitative analyses, such as Multiple Linear Regression, Partial Least Squares, and Neural Network may also be valuable.

Acknowledgements

This study was financially supported by the International Bureau of the German Federal Ministry of Research and Technology (BMBF, Project number CHN 06/003), the Natural Foundation of China (Project number: 30571080), Program for Changjiang Scholars and Innovative Research Team in University (IRT 0511), and the GIS & RS Group of the Institute of Geography, University of Cologne. Continuous funding support for the field work was provided by the Agricultural Bureau of Huimin County (Director Kang). The authors also want to thank Dr. Fei Yuan from the Minnesota State University for her comments and edits.

References * (* for chapter 5)

AASEN, H., GNYP, M.L., MIAO, Y., BARETH, G., 2014. Automated hyperspectral vegetation index retrieval from multiple correlation matrices with HyperCor. Photogrammetric Engineering and Remote Sensing (accepted).

ADDINK, E.A., DE JONG, S.M., PEBESMA, E.J., 2007. The importance of scale in object-based mapping of vegetation parameters with hyperspectral imagery. Photogrammetric Engineering and Remote Sensing, 73 (8), 905-912.

ATZBERGER, C., 1998. Estimates of winter wheat production through remote sensing and crop growth modeling. VWF Verlag für Wissenschaft und Forschung. Berlin. 270 pages.

BABAR, M.A., REYNOLDS, M.P., VAN GINKEL, M., KLATT, A.R., RAUN, W.R., STONE, M.L., 2006. Spectral reflectance to estimate genetic variation for in-season biomass, leaf chlorophyll, and canopy temperature in wheat. Crop Science, 46 (3), 1046-1057.

BARETH, G., 2009. GIS- and RS-based spatial decision support: structure of a spatial environmental information system (SEIS). International Journal of Digital Earth, 2 (2), 134-154.

BAO, Y., GAO, W., GAO, Z., 2009. Estimation of winter wheat biomass based on remote sensing data at various spatial and spectral resolutions. Frontiers of Earth Science in China, 3 (1), 118-128.

BOUMAN, B.A.M., 1995. Crop modeling and remote sensing for yield prediction. Netherlands Journal of Agricultural Sciences, 43 (2), 143-161.

BROGE, N.H., LEBLANC, E., 2000. Comparing prediction power and stability of broad-band and hyperspectral vegetation indices for estimating of green leaf area index and canopy chlorophyll density. Remote Sensing of Environment, 76 (2), 156-172.

CHO, M.A., SKIDMORE, A., CORSI, F., VAN WIEREN, S.E., SOBHAN, I., 2007. Estimation of green grass/herb biomass from airborne hyperspectral imagery using spectral indices and partial least squares regression. International Journal of Applied Earth Observation and Geoinformation, 9 (4), 414-424.

CLEVERS, J.P.G.W., JONGSCHAAP, R., 2001. Imaging Spectrometry for Agricultural Applications. In: F.D.,VAN DER MEER, S.M., DE JONG (Eds.), Imaging Spectrometry, Kluwer Academic Publishers, Dordrecht, The Netherlands, pp. 157-199.

CLEVERS, J.P.G.W., KOOISITRA, L., SCHAEPMAN, M.E., 2008. Using spectral information from the NIR water absorption features for the retrieval of canopy water content. International Journal of Applied Earth Observation and Geoinformation, 10 (3), 388-397.

CURRAN, P.J., 1989. Remote sensing of foliar chemistry. Remote Sensing of Environment, 30 (3), 271-278.

DAVIDSON, A., WANG, S., WILMSHURST, J., 2006. Remote sensing of grassland-shrubland vegetation water content in the shortwave domain. International Journal of Applied Earth Observation and Geoinformation, 8 (4), 225-236.

FERRIO, J.P., VILLEGAS, D., ZARCO, J., APARICIO, N., ARAUS, J.L., ROYO, C., 2005. Assessment of durum wheat yield using visible and near-infrared reflectance spectra of canopies. Field Crops Research, 94 (2-3), 126-148.

GAO, J. (2006). Canopy chlorophyll estimation by remote sensing. PhD Thesis, Manhattan, Kansas, USA. 192 pages.

GITELSON, A., MERZLYAK, M.N., LICHTENTHALER, K., 1996. Detection of red edge position and chlorophyll content by reflectance. Journal of Plant Physiology, 148 (3-4), 501-508.

GNYP, M.L., LI, F., MIAO, Y., KOPPE, W., JIA, L., CHEN, X., ZHANG, F., BARETH, G., 2009. Hyperspectral data analysis of nitrogen fertilization effects on winter wheat using spectrometer in North China Plain. In: Proceedings of First workshop on hyperspectral image and signal processing, Evolution in Remote Sensing, Grenoble, pp. 255-258.

GNYP, M.L., YU, K., AASEN, H., YAO, Y., HUANG, S., MIAO, Y., BARETH, G., 2013. Analysis of crop reflectance for estimating biomass in rice canopies at different phenological stages. Photogrammetrie Fernerkundung Geoinformation, 2013 (4), 351-365.

GNYP, M.L., MIAO, Y., YUAN, F., USTIN, S.L., YU, K., YAO, Y., HUANG, S., BARETH, G., 2014. Hyperspectral canopy sensing of paddy rice biomass at different growth stages. Field Crops Research, 155, 42-55.

GUYOT, G., BARET, F., 1988. Utilisation de la haute résolution spectrale pour suivre l'état des couverts végétaux. In: Proc. 4ème colloque internationales signature spectrales d'objets en télédétection, Aussois, France, 279-286.

HABOUDANE, D., MILLER, J.R., PATTEY, E., ZARCO-TEJADA, P.J., STRACHAN, I.B., 2004. Hyperspectral vegetation indices and novel algorithms for predicting green LAI of crop canopies: modeling and validation in the context of precision agriculture. Remote Sensing of Environment, 90 (3), 337-352.

HINZMAN, L.D., BAUER, M.E., DAUGHTRY, C.S.T., 1986. Effects of nitrogen fertilization on growth and reflectance characteristics of winter wheat. Remote Sensing of Environment, 19 (1), 47-61.

HUETE, A.R., 1988. A soil vegetation adjusted index (SAVI). Remote Sensing of Environment, 25 (2), 295-309.

JI, L., WYLIE, B.K., NOSSOV, D.R., PETERSON, B., WALDROP, M.P., MCFARLAND, J.W., ROVER, J., HOLLINGSWORTH, T.N., 2012. Estimating aboveground biomass in interior Alaska with Landsat data and field measurements. International Journal of Applied Earth Observation and Geoinformation, 18, 451-461.

KIPP, S., MISTELE, B., BARESEL, P., SCHMIDHALTER, U., 2014. High-troughput phenotyping early plant vigour of winter wheat. European Journal of Agronomy, 52, 271-278.

KOPPE, W, LI, F., GNYP, M.L., MIAO, Y., JIA, L., CHEN, X., ZHANG, F., BARETH, G., 2010. Evaluating multispectral and hyperspectral satellite remote sensing data for estimating winter wheat growth parameters at regional scale in the North China Plain. Photogrammetrie Fernerkundung Geoinformation, 2010 (3), 167-178.

KOPPE, W., GNYP, M.L., HENNIG, S.D., LI, F., MIAO, Y., JIA, L., BARETH, G., 2012. Multi-temporal hyperspectral and radar remote sensing for estimating winter wheat biomass in the North China Plain. Photogrammetrie Fernerkundung Geoinformation, 2012 (3), 281-298.

KUMAR, L., SCHMIDT, K., DURY, S., SKIDMORE, A., 2003. Imaging spectrometry and vegetation science. In: F.D., VAN DER MEER, S.M., DE JONG (Eds.), Imaging Spectrometry, Kluwer Academic Publishers, Dordrecht, The Netherlands, pp. 111-156.

KHURSHID, K., STAENZ, K., SUN, L., NEVILLE, R., WHITE, H.P., BANNARI, A., CHAMPAGNE, C.M., HITCHCOCK, R., 2006. Preprocessing of EO-1 Hyperion data. Canadian Journal of Remote Sensing, 32 (2), 84-97.

LAUDIEN, R., BÜRCKY, K., DOLUSCHITZ, R., BARETH, G., 2006. Establishment of a Web-based spectral database for the analysis of hyperspectral data from Rhizoctonia solani-inoculated sugarbeets. Zuckerindustrie, 131 (3), 164-170, (in German).

VAN LEEUWEN, W.J.D., 2009. Visible, Near-IR, and shortwave IR spectral characteristics of the terrestrial surfaces. In: T.A., WARNER, M.D., NELLIS, G.M., FOODY, The sage handbook of remote sensing, Sage Publications Ltd, London, UK, pp. 33-50.

LI, F., GNYP, M.L., JIA, L., MIAO, Y., YU, Z., KOPPE, W., BARETH, G., CHEN, X., ZHANG, F., 2008. Estimating N status of winter wheat using a handheld spectrometer in North China Plain. Field Crops Research, 106 (1), 77-85.

LI, F., MIAO, Y., HENNIG, S.D., GNYP, M.L., CHEN, X., JIA, L., BARETH, G., 2010. Evaluating hyperspectral vegetation indices for estimating nitrogen concentration of winter wheat at different growth stages. Precision Agriculture, 11 (4), 335-357.

LIU, J., PATTEY, E., MILLER, J.R., MCNAIRN, H., SMITH, A., HU, B., 2010. Estimating crop stresses, aboveground dry biomass and yield of corn using multi-temporal optical data combined with a radiation use efficiency model. Remote Sensing of Environment, 114 (6), 1167-1177.

LIU, M., LIU, X., LI, J., LI, T., 2012. Estimating regional heavy metal concentration in rice by scaling up a field-scale heavy metal assessment model. International Journal of Applied Earth Observation and Geoinformation, 19, 12-23.

LOBELL, D.B., ASNER, G.P., ORTIZ-MONASTERIO, J.I., BENNING, T.L., 2003. Remote sensing of regional crop production in the Yaqui valley, Mexico: estimates and uncertainties. Agriculture Ecosystems and Environment, 94 (2), 205-220.

LU, D.S., 2006. The potential and challenge of remote sensing based biomass estimation. International Journal of Remote Sensing, 27 (7), 1297-1328.

MA, Y., WANG, S., ZHANG, L., HOU, Y., ZHUANG, L., HE, Y., WANG, F., 2008. Monitoring winter wheat growth in North China by combining a crop model and remote sensing data. International Journal of Applied Earth Observation and Geoinformation, 10 (4), 426-437.

MARIOTTO, I., THENKABAIL, P.S., HUETE, A., SLONECKER, E.T., PLATONOV, A., 2013. Hyperspectral versus multispectral crop-productivity modeling and type discrimination for the HyspIRI mission. Remote Sensing of Environment, 139, 291-305.

MEIER, U., 2001. Growth stages of mono-and dicotyledonous plants. Federal Biological Research Centre for Agriculture and Forestry. 158 pages.

MIAO, Y., MULLA, D.J., RANDALL, G.W., VETSCH, J.A., VINTILA, R., 2009. Combining chlorophyll meter readings and high spatial resolution remote sensing images for in-season site-specific nitrogen management of corn. Precision Agriculture, 10 (1), 45-61.

OERKE, E.C., GERHARDS, R., MENZ, G., SHIKORA, R.A., 2010. Precision crop protection - the challenge and use of heterogeneity. Springer, Heidelberg. 441 pages.

OPPELT, N., MAUSER, W., 2004. Hyperspectral monitoring of physiological parameters of wheat during a vegetation period using AVIS data. International Journal of Remote Sensing, 25 (1), 145-159.

PEARSON, J.S., MILLER, L.D., 1972. Remote mapping of standing crop biomass for estimation of the productivity of the shortgrass prairie, Pawnee national grassland, Colorado. In: Proceedings of the 8th International Symposium on Remote Sensing of the Environment, 1355-1379.

PEÑUELAS, J., FILLELA, I., 1998. Visible and near-infrared reflectance techniques for diagnosis plant physiological status. Trends in Plant Science 3 (4), 151-156.

PSOMAS, A., KNEUBÜHLER, M., HUBER, S., ITTEN, K., ZIMMERMANN, N.E., 2011. Hyperspectral remote sensing for estimating aboveground biomass and exploring species richness patterns of grassland habitats. International Journal of Remote Sensing, 32 (24), 9007-9031.

PU, R., GE, S., KELLY, M., GONG, P., 2003. Spectral absorption features as indicators of water status in coast live oak (Quercus agrifolia) leaves. International Journal of Remote Sensing, 24 (9), 1799-1810.

QI, J., CHEHBOUNI, A., HUETE, A.R., KEER, Y.H., SAROOSHIAN, S., 1994. A modified soil vegetation adjusted index. Remote Sensing of Environment, 48 (2), 119-126.

REN, J., CHEN, Z., ZHOU, Q., TANG, H., 2008. Regional yield estimation for winter wheat with MODIS-NDVI data in Shandong, China. International Journal of Applied Earth Observation and Geoinformation, 10 (4), 403-413.

ROBERTS, D.A., ROTH, K.L., PERROY, R.L., 2011. Hyperspectral vegetation indices. In: P.S., Thenkabail, J.G., Lyon, A., Huete (Eds.), Hyperspectral remote sensing of vegetation, CRC Press, Boca Raton, FL, USA, pp. 309-327.

RONDEAUX, G., STEVEN, M., BARET, F., (1996). Optimization of soil-adjusted vegetation indices. Remote Sensing of Environment, 55 (2), 95-107.

ROUSE, J.W., HAS, R.H., SCHELL, J.A., DEERING, D.W., 1974. Monitoring vegetation systems in the Great Plains with ERTS. In: Third ERTS Symposium, NASA SP-351, Vol. 1. NASA, Washington, DC, pp. 309-317.

SERRANO, L., FILELLA, L., PENUELAS, J., 2000. Remote sensing of biomass and yield of winter wheat under different nitrogen supplies. Crop Science, 40 (3), 723-731.

THENKABAIL, P.S., SMITH, R.B., PAUW, E.D., 2000. Hyperspectral vegetation indices and their relationships with agricultural crop characteristics. Remote Sensing of Environment, 71 (2), 158-182.

THENKABAIL, P.S., LYON, J.G., HUETE, A., 2011. Advance in hyperspectral remote sensing of vegetation of vegetation and agricultural croplands. In: P.S., Thenkabail, J.G., Lyon, A., Huete (Eds.), Hyperspectral remote sensing of vegetation, CRC Press, Boca Raton, FL, USA, pp. 3-36.

TODD, S.W., HOFFER, R.M., MILCHUNAS, D.G., 1998. Biomass estimation on grazed and ungrazed rangelands using spectral indices. International Journal of Remote Sensing, 19 (3), 427-438.

XAVIER, A.C., RUDORFF, B.F.T., MOREIRA, M.A., ALVARENGA, B.S., DE FREITAS, J.G., SALOMON, M. V., 2006. Hyperspectral field reflectance measurements to estimate wheat grain yield and plant height. Scientia Agricola, 63 (2), 130-138.

ZARCO-TEJADA, P.J., BERJÓN, A., LÓPEZ-LOZANO, R., MILLER, J.R., MARTÍN, P., CACHORRO, V., GONZÁLEZ, M.R., DE FRUTOS, A., 2005. Assessing vineyard condition with hyperspectral indices: Leaf and canopy reflectance simulation in a row-structured discontinuous canopy. Remote Sensing of Environment, 99 (3), 271-287.

ZHU, Y., YAO, X., TIAN, Y., LIU, X., CAO, W., 2008. Analysis of common canopy vegetation indices for indicating leaf nitrogen accumulations in wheat and rice. International Journal of Applied Earth Observation and Geoinformation, 10 (1), 1-10.

6. Analysis of crop reflectance for estimating biomass in rice canopies at different phenological stages

M. L. GNYP [a,b] *, K. YU [a,b], H. AASEN [b], Y. YAO [a,c], S. HUANG [a, c], Y. MIAO [a,c], G. BARETH [a,b]

received: December 2012, accepted: April 2013, published: August 2013
Photogrammetrie Fernerkundung Geoinformation, 2013 (4), 351-365. DOI: 10.1127/1432-8364/2013/0182
Original accepted manuscript is used and embedded in dissertation format.

a. International Center for Agro-Informatics and Sustainable Development (www.icasd.org)
b. Institute of Geography, University of Cologne, 50923, Cologne, Germany
c. College of Resources & Environmental Sciences, China Agricultural University, 100094, Beijing, China.

*Corresponding author, Tel.: +49-221-4706551; fax: +49-221-4701638.
Email: mgnyp1@uni-koeln.de (M. L. Gnyp)

Abstract

This paper contributes an assessment for estimating rice (*Oryza sativa L., irrigated lowland rice*) biomass by canopy reflectance in the Sanjiang Plain, China. Hyperspectral data were captured with field spectroradiometers in experimental field plots and farmers' fields and then accompanied by destructive aboveground biomass (AGB) sampling at different phenological growth stages. Best single bands, best two band-combinations, optimised simple ratio (SR), and optimised normalized ratio index (NRI), as well as multiple linear regression (MLR) were calculated from the reflectance for the non-destructive estimation of rice AGB. Experimental field data were used as the calibration dataset and farmers' field data as the validation dataset. Reflectance analyses display several sensitive bands correlated to rice AGB, e.g., 550, 670, 708, 936, 1125, and 1670 nm, which changed depending on the phenological growth stages. These bands were detected by correlograms for SR, NRI, and MLR with an offset of approx. ±10 nm. The assessment of the three methods showed clear advantages of MLR over SR and NRI in estimating rice AGB at the tillering and stem elongation stages by fitting and evaluating the models. The optimal band number for MLR was set to four to avoid overfitting. The best validated MLR model (R^2=0.82) at the tillering stage was using four bands at 672, 696, 814 and 707 nm. Overall, the optimized SR, NRI, and MLR have a great potential in non-destructive estimation of rice AGB at different phenological stages. The performance against the validation dataset showed R^2 of 0.69 for SR and R^2 of 0.70 for NRI, respectively.

Keywords: hyperspectral, biomass, rice, spectral indices, MLR

6.1 Introduction

In the field of crop science, the aboveground dry biomass (AGB) and nutrient use efficiency are considered to be the major factors for determining the final yield (RAUN and JOHNSON, 1999). AGB influences at each phenological stage the amount of grain production, since the yield is defined as the amount of grain, straw, and AGB. Furthermore, knowledge of crop development characteristics and its spatial and temporal variation in the field are useful for determining crop requirements, such as N-fertilisation as closely as possible and for achieving acceptable yields, e.g. for rice (FAGIERA, 2007).

Traditional methods to estimate AGB involve direct destructive measurements in the field, which are time-consuming, expensive, and require intensive field work. In the context of precision agriculture, proximal sensing is a promising and well investigated tool to avoid the destructive approach (GEBBERS and ADAMCHUK, 2010). Field canopy reflectance can be measured with portable handheld or mobile spectroradiometer, e.g. Yara N-Sensor (AGRICON, 2013) and can be used to support farmer's decisions on crop management, such as fertilisation, pest management, or irrigation.

Hyperspectral measurements in the field can also be used as groundtruth or for model development in analysing satellite imagery. The disadvantage of hyperspectral and multispectral satellite images is the high dependence on a clear sky at the image aquisition time, while spectroradiometers can be used in the field with some cloud cover for approximately 3–4 hours around solar noon. Spectroradiometers are fast and the most important non-destructive devices. They have a continuous acquisition of all reflectance values in a given spectral range of 350 nm–2500 nm with a high spectral resolution of < 2 nm–5 nm (MILTON et al., 2009; ORTENBERG, 2011).

In many studies, the in-field reflectance measurements are acquired and required for calibrating satellite-borne hyperspectral data using, e.g., EO-1 Hyperion imagery (PSOMAS et al., 2011; KOPPE et al., 2012) or of airborne-based data, e.g., HyMap imagery (CHO and SKIDMORE, 2009). The goal of these studies is to estimate AGB on a large scale using airborne or satellite-borne remote sensing data by applying evaluated models. The hyperspectral satellite EnMap, which is scheduled for 2016, will provide data with two separate sensors for the aquisition of VNIR and SWIR in the spectral domain of 420 nm–2450 nm with 30 m ground resolution similar to the Hyperion data (SCHWIND et al., 2012). By simulating the spectral properties of EnMap with field spectroradiometer data, models can be developed and evaluated for EnMap-based estimation of AGB (KAUFMANN et al., 2010).

The relationship between reflectance and agricultural crop characteristics has been investigated in many studies in the last decades (THENKABAIL et al., 2000). Most of those studies focused on nitrogen, leaf area index (LAI), or yield estimation, but rarely on AGB estimation, since there is a strong correlation between LAI and AGB (SHIBAYAMA and AKIYAMA,1989; FILLELA and PEÑUELAS, 1994). Studies that use hyperspectral ground data to estimate AGB have been carried out

for grass, wheat, and for rice (RICHARDSON et al., 1983; SHIBAYAMA and MUNAKATA, 1986; ANDERSON and HANSON, 1992; SERRANO et al., 2000; HANSEN and SCHJOERRING, 2003; LI et al., 2010; WANG et al., 2008; BAJWA et al., 2010).

The common method to estimate AGB from reflectance is based on the application, improvement, or development of spectral indices (SIs). Optimised or improved standard SIs, such as SR and NRI, represent best band selections based on correlograms (THENKABAIL et al., 2000; STROPPIANA et al., 2009; KOPPE et al., 2010). In addition, MLR has been applied in several studies, since this method provides flexibility in the choice of bands (SHIBAYAMA and AKIYAMA, 1989; TAKAHASHI et al., 2000; YU et al., 2013). Futhermore, MLR is more reliable than SIs that are saturated at high LAI levels (YANG and CHEN, 2004; HABOUDANE et al., 2004). It is simpler and more flexible for the adoption by growers and crop consultants than partial least square (PLS) (BAJWA et al., 2010).

Many AGB studies were conducted in greenhouses under controlled conditions or the spectral reflectance was measured in the laboratory (SONG et al., 2011), but not in the field. Furthermore, most results, proposed SIs, or developed models were not validated using an independent dataset to test the transferability of the models. Previous studies have often focused only on calibrating wavebands to a crop parameter, and have not adequately evaluated the performance of their results in an independent dataset (LU, 2006; CHO and SKIDMORE, 2009).

The main two objectives of this study are (i) to investigate the potential for rice AGB estimation from the canopy reflectance and (ii) to develop and evaluate the proposed AGB estimation models. The first step contains an analysis of the AGB variation, the analysis of the relationship between canopy reflectance and N-application and AGB. In a second step, three methods to estimate AGB by the reflectance are tested with a calibration dataset using experimental field data: Single bands, best two band-combinations (SR and NRI), and MLR. Finally, the three methods are transferred to an independent dataset using farmers' field data under conventional management.

6.2 Material and methods

6.2.1 Study area and experimental design

The research was carried out at the Qixing farm (47.2°N, 132.8°E) in Jiansanjiang, Heilongjiang Province, Northeast China. The farm is located in the Sanjiang Plain (Fig. 6.1), which is an alluvial plain from three rivers (Heilong, Songhua, Wusuli), and covers about 109,000 km². The area is characterised by a sub-humid continental monsoon climate. The mean annual temperature is about 2°C and the mean precipitation sums up to 550 mm per year. The frost-free period is about 130 days long. The rice fields belong to the northernmost cropping rice system in China and to the northernmost ones worldwide. The rice is sown in mid-April (in heated greenhouses), is transplanted after the frost period to the field from the middle to the end of May, and is harvested around end of September. The fields are controlled flooded and manured with N-fertiliser before transplanting the

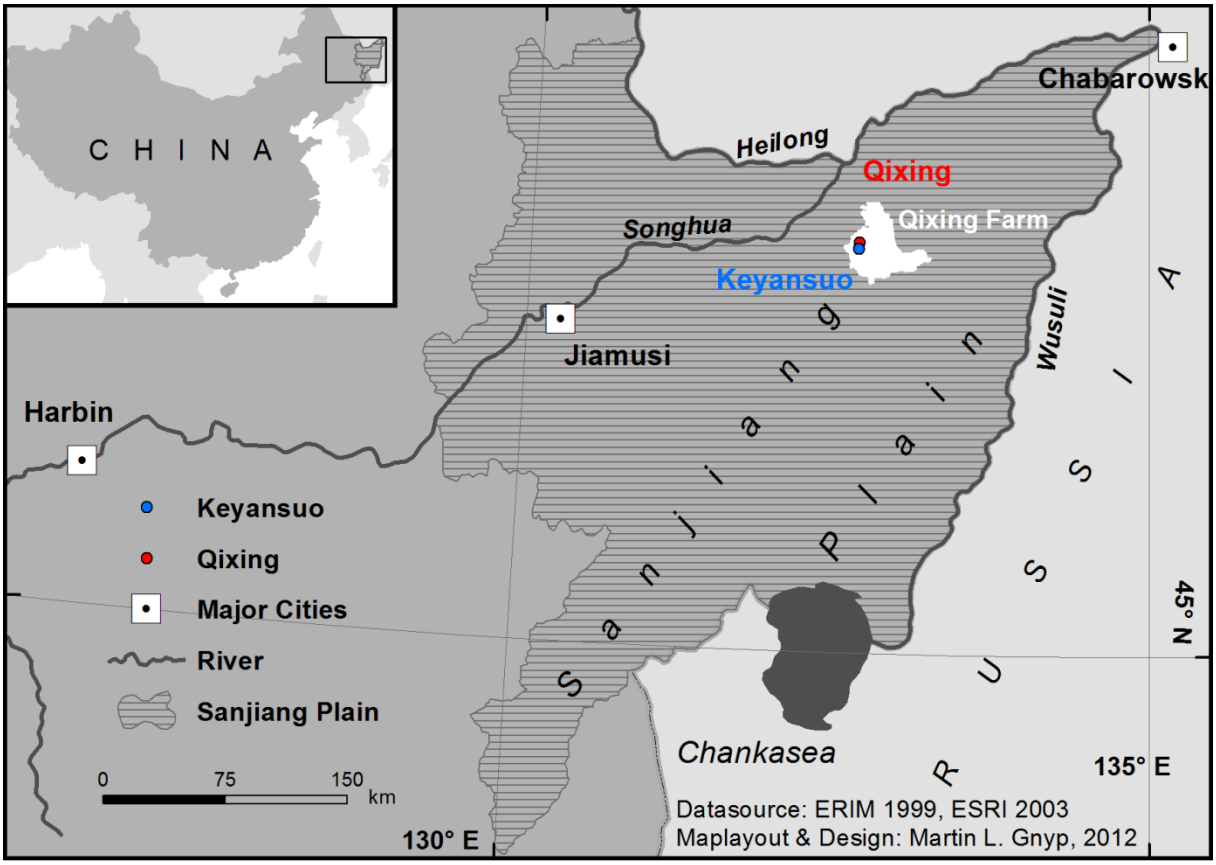

Fig. 6.1 Study area in the north-east corner of China.

seedlings. Four to five seedlings (120–150 seedlings/m²) are planted at one position forming a so-called hill. The irrigation is usually stopped 30 days before harvest.

Two field experiments were carried out at two sites (Keyansuo and Qixing research station) in Jiansanjiang and were used as the calibration dataset. They represented a wide range of growth conditions by N-fertiliser input conducted in a split-plot design: 0, 60, 75, 90, 105, 120, and 150 kg N ha^{-1} in 2007 (146 plots), and 0, 35, 70, 105, and 140 kg N ha^{-1} in 2008 (88 plots) and 2009 (95 plots). The plot size was approximately 20 m² each. The widely used rice variety *Kongyu131* (28 hills/m²) was cultivated in all experiments. In addition to the experimental fields, 9 farmers' fields were selected in 2007–2009 and used as the validation dataset. They were managed by the farmers according to their usual practices. The size of these fields varied from 12 to 27 ha, where each field contained several plots with a mean size of 1,400 m². In most cases, the cultivar *Kongyu131* was planted.

6.2.2 Hyperspectral data collection

Hyperspectral and agronomic data were collected in 2007–2009. Before taking the spectral reflectance, the average number of tillers in each hill was determined per plot in order to measure the reflectance of representative plants (Fig. 6.2). Canopy spectral reflectance was measured with two non-imaging passive sensors by ASD (Analytical Spectral Devices, Inc., Boulder, CO, USA):

Fig. 6.2 Hyperspectral data collection in paddy rice (distance to canopy: 0.3 m); Photo by Georg Bareth, 22 June 2012.

QualitySpec® Pro in the wavelength domain of 350 nm–1800 nm in 2007 and 2009, and FieldSpec3® Pro in the wavelength domain of 350 nm–2500 nm in 2008. Both devices have a sampling interval of 1.4 nm in the VNIR and 2 nm in the SWIR domain. The measurements were taken from 9 a.m. to 1 p.m. LMT, mostly under cloudfree conditions in the field. Every 10 to 15 minutes, calibration measurements were taken with a white reference panel ($BaSO_4$) and were repeated depending on illumination changes. A default viewing angle ($\propto$) of 25° and a measuring height (h) of 1 m above the canopy created a field of view (A) of 0.15 m² with a radius (r) of 22 cm (Eq. 6.1) and (Eq. 6.2).

$$r(m) = h \times \tan(\propto |2) \quad \text{(Eq. 6.1)}$$

$$A(m^2) = \pi \times r^2 \quad \text{(Eq. 6.2)}$$

Ten sample counts in the spectrum averaging (settings in the ASD software) were repeated at 6 positions per plot. They were averaged per plot in order to reduce the atmospheric influence, e.g. clouds and wind, and field conditions, e.g. planting in rows. Overall, approximately 14,000 spectra (unaveraged) were collected from 2007 to 2009.

6.2.3 Aboveground biomass (AGB) collection

The AGB was measured destructively by clipping three (booting to heading stage) to five (tillering to stem elongation stage) hills of the measured rice plants. All plant samples were rinsed with water, the roots were clipped, and then the samples were divided in their plant organs leaf, stem and head. They were oven dried at 105°C for 30 minutes, and dried at 70°C until constant weight. The AGB was weighed later. In this study, the combined total dry AGB was used and not the individual

AGBs from the different organs (leaf, stem, head). Altogether, 1,685 AGB samples were collected from the tillering to heading stages.

6.2.4 Spectral indices (SIs) and stepwise Multiple Linear Regression (MLR)

Single bands or combinations of up to four different bands were tested for their explanatory value. In addition, spectral indices representing two bands were analysed: simple ratio (SR) and normalised difference vegetation index (NDVI). They are widely used for the prediction of biophysical quantities of crops and were developed by JORDAN (1969) and ROUSE et al. (1974). In this study, the focus is on using the best band-combinations to optimise the SR and NDVI for AGB estimation due to the saturation of the NDVI (HABOUDANE et al., 2004). The optimised NDVI is also known as normalised ratio index (NRI) and was suggested to determine the best band-combinations (THENKABAIL et al., 2000; SIMS and GAMON, 2002). All possible combinations were computed from the wavelengths in the domain of 350 nm–1800 nm. The two band-combinations were calculated with a self-developed Java program, analysed and plotted as a contour diagram using MATLAB 7.0 software (MATLAB 2013). Due to the noises caused by water absorption in the SWIR domain, the bands from 1330 nm to 1480 nm, and 1770 nm to 1800 nm were excluded from the analyses. Only the best two band-combinations are presented in the results. The SR and NRI equations are defined as (Eq. 6.3) and (Eq. 6.4):

$$SR = \rho_1/\rho_2 \quad ; \text{where } \rho_1 > \rho_2 \tag{Eq. 6.3}$$

$$NRI = \frac{\rho_1-\rho_2}{\rho_1+\rho_2} \quad ; \text{where } \rho_1 > \rho_2 \tag{Eq. 6.4}$$

where ρ reflectance value

For the analysis of AGB in relation to one feature, irrespectively if a single band or index was used, correlation analysis was applied. The method attempts to model the relationship between two or more variables by fitting a linear regression equation to observed data. Single bands, but also combination of two, three, and four different bands were tested using a stepwise multiple linear regression (MLR). This allows to select predictors of dependent variable based on statistical criteria. The observed data is the dependent variable of the model. In this study, the AGB is the dependent variable and the single bands are the independent variables. In total, 1,250 bands were analysed in SPSS 20.0 (SPSS 2013) and the best MLR models are presented in the results. The MLR equation is defined as (Eq. 6.5):

$$y = a + b_1 \times \rho_{b_1} + b_2 \times \rho_{b_2} + \quad ... \quad + b_i \times \rho_{b_i} \tag{Eq. 6.5}$$

where y multiple linear regression (MLR) a mathematical constant
$b_1, b_2, \ldots, b_i$ coefficients $\rho_{b1}, \rho_{b2}, \ldots, \rho_{bi}$ reflectances

6.2.5 Data analysis and statistics

Original spectral data were used to average the six spectra per plot. The spectra were not smoothed, but significant outliers were excluded from the analysis. In addition, the stepwise MLR provided a method of feature reduction and a statement about the optimal band number to estimate AGB. Basic analyses were conducted like descriptive statistics of AGB, analyses of canopy spectra under different N-rates, and growth stages before using the data as a calibration dataset. The calibrated models were validated using an independent dataset to test the transferability of the models. The following statistic parameters, root-mean-square error (RMSE) and relative error (RE) against the observed mean, were used to calculate the fitness between the observed and estimated data. All statistical analyses were conducted in SPSS 20.0 and Statistica 6.0 (STATISTICA 2013).

Table 6.1 Descriptive statistics of AGB on the experimental fields.

	Stage	n	Min (t/ha)	Max (t/ha)	Mean (t/ha)	SD (t/ha)	CV (%)
2007	Tillering	146	0.1	2.0	0.9	0.46	46.5
	Stem Elongation	74	1.6	5.7	3.4	0.88	26.1
	Booting	49	2.9	7.5	5.6	1.05	18.8
	Heading	114	3.3	12.4	7.6	1.96	26.1
2008	Tillering	40	0.1	1.8	0.9	0.46	50.5
	Stem Elongation	40	0.9	2.9	1.6	0.49	31.3
	Booting	88	2.9	8.8	5.3	1.36	25.6
	Heading	88	4.4	14.1	9.0	1.83	20.4
2009	Tillering	91	0.2	1.6	0.8	0.34	41.3
	Stem Elongation	95	0.3	2.2	1.2	0.52	42.0
	Booting	95	1.4	6.6	3.5	1.26	36.1
	Heading	95	4.6	9.7	7.0	1.15	16.5
All	Tillering	277	0.1	2.0	0.9	0.43	46.3
	Stem Elongation	209	0.3	5.7	2.1	1.19	58.0
	Booting	232	1.4	8.8	4.7	1.57	34.0
	Heading	297	3.3	14.1	7.8	1.87	24.1

n = Number of samples, SD= Standard deviation, CV= Coefficient of variation

6.3 Results

6.3.1 Temporal AGB variation

AGB production and development are dependent on crop growth conditions, such as weather, soil and nutrition. Table 6.1 illustrates the temporal AGB variation in diverse years and growth stages for the experimental sites. Generally, AGB production tends to increase from the tillering to the heading stage. Overall, it ranges from 0.1 t/ha to 14.1 t/ha across all stages and years. The rice crop had a high variation in AGB (CV>30%), especially during the early growth stages. During the later stages booting and heading, the variation was lower (CV<30%). Temporal variation between the three years is significant. In 2009, the temperature was lower than in the previous years, so the AGB production was lower with a mean AGB value of 0.8 t/ha–7.0 t/ha. Highest values were observed in 2008.

6.3.2 Canopy reflectance spectra under different N-rates and at different growth stages

The reflectance spectra of the rice canopies clearly indicated differences in AGB or LAI that resulted from different N-rates and at various phenological growth stages. The spectra of the experiment plots with five different N-rates at the booting stage in 2008 were taken as an example to display the response pattern of canopy reflectance (Fig. 6.3, left). Generally, the reflectance spectra tended to increase with rising LAI in the NIR (700 nm–1100 nm) and SWIR (1100 nm–1800 nm) regions, whereas the opposite occurred in the VIS (500 nm–700 nm) region. The canopy LAI responded to N-application. Higher reflectance response occurred with lower N-application. Especially, in the green (500 nm–600 nm) and red (600 nm–700 nm) regions, obvious visible differences were detected. There was a high increase in the five spectra in the RedEdge region (670 nm–740 nm), which were clustered here as one spectrum. Mostly, the differences between the first (0 kg·N/ha) and the second N-rate (35 kg·N/ha) were not significant in the reflectance. Similarities were also observed for the fourth (105 kg·N/ha) and fifth (140 kg·N/ha) N-rate.

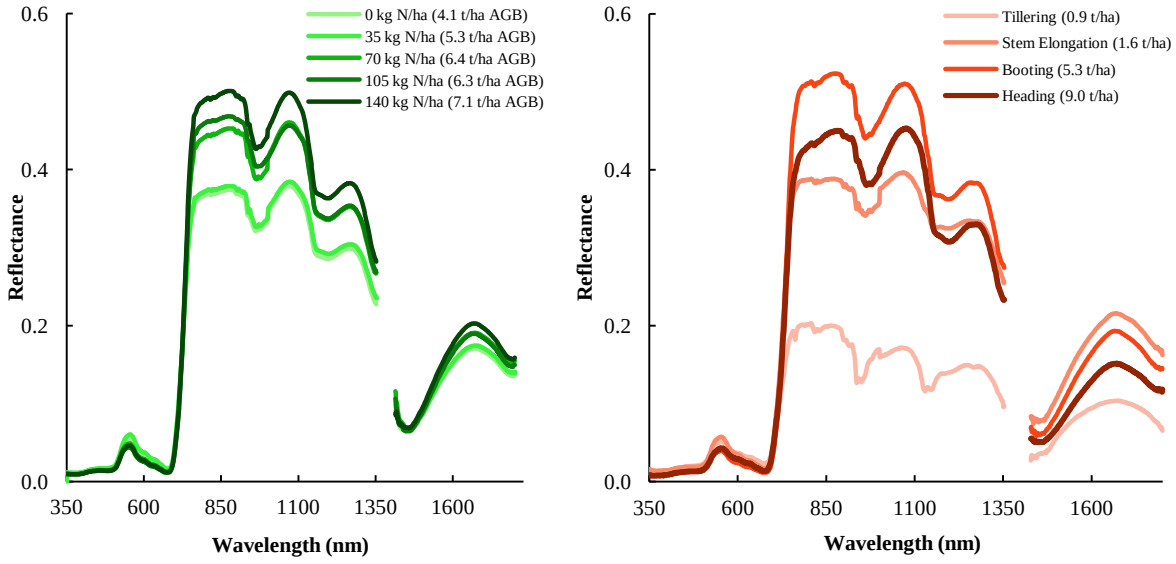

Fig. 6.3 Left: changes of rice canopy reflectance with varied N-rates at the booting stage in 2008, right: changes in reflectance at different growth stages in 2008.

Rice canopies showed a diverse reflectance at different growth stages. As an example, a dataset of four stages in 2008 was used to display the response of a rice crop from the tillering to the heading stage (Fig. 6.3, right). At an early phenological stage, the reflectance was mainly influenced by the soil and water of the paddy field, where the AGB production was low due to low LAI.

Generally, the reflectance increased from the tillering to the booting stage and decreased from the heading stage due to starting senescence of the plant. Maximum reflectance was observed at the booting stage. The canopy LAI and the biochemical components of the plant changed at different growth stages, which evidently influenced the reflectance.

6.3.3 Relationship between AGB and spectral reflectance

The correlation coefficients between AGB and canopy reflectance at different phenological stages and in different years are presented in Fig. 6.4. First of all, the correlation between AGB and reflectance at different stages is described (Fig. 6.4, left). The pattern of the R (correlation coefficient) curves was similar at the different stages and across all stages except for the heading stage. Lowest absolute R values were observed at the tillering stage as a result of low crop development at this growth stage. Highest R values were recorded at the stem elongation stage and across all stages. Maximum negative R values were observed at tillering and across all stages at wavelengths of 670 nm, which corresponds to high solar radiation absorption by chlorophyll pigments. In the RedEdge region, a high increase of R values was detected, which is coincident with reflectance increase of vegetation in this domain.

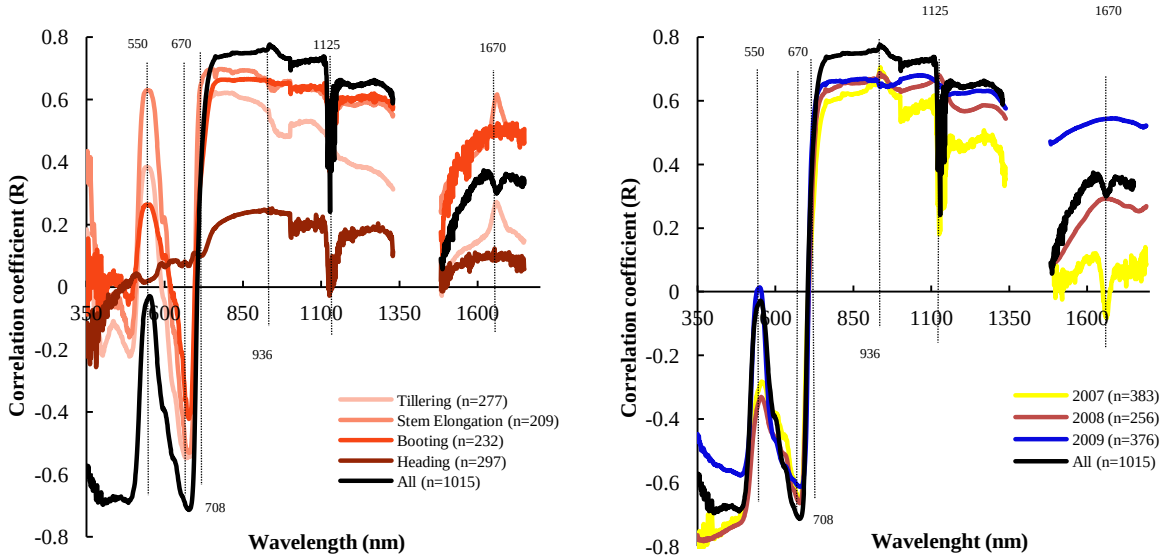

Fig. 6.4 Left the correlation coefficients (R) between AGB and canopy reflectance at different phenological stages, right: in different years.

Greatest positive R values were observed in the NIR shoulder at the stem elongation stage and at wavelengths of 936 nm across all stages. Two peaks are noticeable in the SWIR domain. The first one is located as a local minimum in the reflectance at wavelengths of 1125 nm at the booting and heading stages, which is not detected in the early stages of tillering and stem elongation. Additionally, the plotted R curves show some noises in the SWIR domain for the booting and heading stage. The noises were only observed in the 2007 data due to partly cloudy sky during the measurements. As a second peak, a local maximum in the R curves is observed at wavelengths of 1670 nm at tillering and stem elongation.

The plotted curves for the correlation coefficients (R) between AGB and canopy reflectance show strong differences from year to year (Fig. 6.4, right). In general, the relationship seems to be diverse in all three years. Across all years, the highest R values are observed (R>0.75), and in 2007 the

lowest (R>0.6). In summary, sensitive bands are located at around 550, 670, 708, 936, 1125, and 1670 nm.

6.3.4 Model calibration by single Bands, SR and NRI

The coefficient of determination between AGB and single bands, best SR, and best NRI was calculated. The best single bands and two band-combinations are shown in Table 6.2 at each growth stage and across all three years. Generally, the best SR and NRI always produce higher R^2 values as one single band. SR and NRI show a very similar performance in R^2 values except at the stem elongation stage. Moreover, they are similar in the band-combinations (±20 nm). At the tillering stage, the SR (ρ_{822}, ρ_{716}) has the best performance (R^2=0.58). At the stem elongation stage, the NRI (ρ_{1678}, ρ_{1575}) displayed the best results (R^2=0.75) versus other stages (Table 6.2, Fig. 6.5). At the booting stage, SR (ρ_{695}, ρ_{513}) and NRI (ρ_{695}, ρ_{515}) performed similarly (R^2=0.54) using almost equal bands. Due to the changes in the canopy reflectance by biochemical components of the plant, all AGB predictors result in lower R^2 values (<0.3) at the heading stage. However, across the whole monitored season, high R^2 values were observed (R^2>0.6) for a high sample number (n=1,015). SR (ρ_{713}, ρ_{550}) showed its best performance here (R^2=0.75). The best single band was 936 nm (R^2=0.62), which is also important

Table 6.2 Single bands, SR and NRI model calibration at different growth stages (2007–2009 pooled data).

Stages (2007-2009)	n	Single Band ρ_1		SR ρ_1/ρ_2		NRI $(\rho_1-\rho_2)/(\rho_1+\rho_2)$	
		ρ_1	R^2	ρ_1, ρ_2	R^2	ρ_1, ρ_2	R^2
Tillering	277	672	0.344	822,716	0.582	799,711	0.559
Stem Elongation	209	780	0.487	1760,1325	0.528	1678,1575	0.758
Booting	232	854	0.443	695,513	0.541	695,515	0.541
Heading	297	380	0.066	800,789	0.218	800,789	0.293
All	1015	936	0.629	713,550	0.757	713,533	0.743

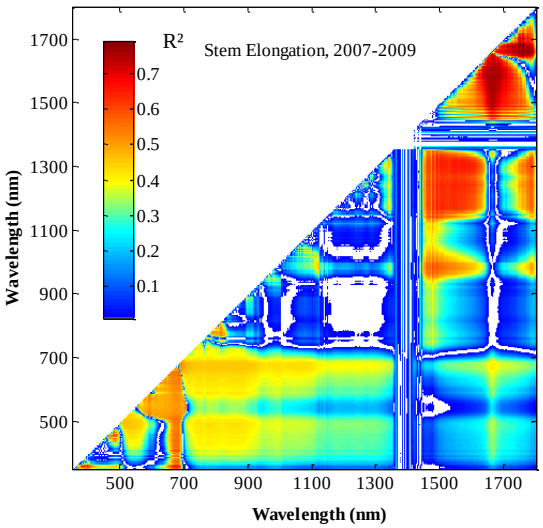

Fig. 6.5 Best two band-combinations for NRI at the stem elongation stage.

for the MLR models.

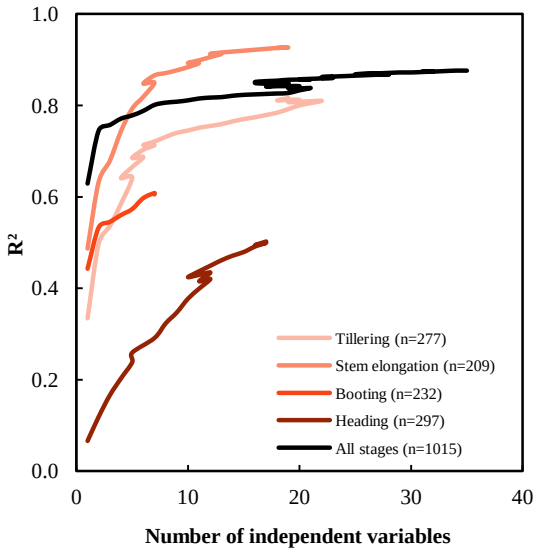

Fig. 6.6 Relationship between band number and performance (R^2) of the MLR models.

6.3.5 MLR model calibration

MLR analyses were conducted in two directions: i) assessment of the optimal band number, ii) MLR-models with 1–4 single bands. Generally, with respect to the first direction, the MLR models explain 50–93% of the variation in AGB (Fig. 6.6). The highest performance was observed at the stem elongation stage (R^2=0.93 with 18 bands), the lowest at the heading stage (R^2=0.50 with 17 bands). At the tillering stage, the R^2 reached a value of 0.82 with 19 bands and at the booting stage, a value of 0.60 with 7 bands. The accuracy of the MLR models was quite good. Across all stages, 35 bands explained 88% of the biomass variability. However, the results indicated that the best MLR model was dependent on the number of independent variables. A higher number of variables causes higher R^2 values, but the number of bands has a limit. Fig. 6.6 demonstrates the relationship between the band number and the performance of the MLR models at each stage. The relation is illustrated as a curve for each stage. The curves are characterised by four features: Linear rise, saturation, again linear rise and finally asymptotic trend. Despite the stepwise increasing of bands, the performance of the models showed an indication of overfitting (after 2–3 bands). ii) For this reason, the optimal number was set to four. The best MLR models are listed in Table 6.3 separately for each stage and across all results indicate that regression equations and the significant bands vary between the phenological stages. The performance of the models was improved by adding stepwise an additional independent band. For example at stem elongation, the R^2 values increased from 0.48 (MLR-1) to 0.74 (MLR-4) and across all stages from 0.62 (MLR-1) to 0.77 (MLR-4). Due to the high sample number, all results are significant at $p<0.0001$ except for the heading stage. It is striking that many of the bands are located in the NIR and SWIR domain, but only some in the VIS domain.

Table 6.3 Stepwise MLR models at diverse growth stages (MLR=multiple linear regression, adj.=adjusted, SE=Standard error of the estimator).

Stage	Model	Bands	Regression equation	R^2	$R^2_{adj.}$	SE
Tillering	MLR-1	1	$1.638 - 19.715\ \rho_{672}$	0.334	0.332	0.348
n=277	MLR-2	2	$1.051 - 16.182\ \rho_{672} + 2.369\ \rho_{1052}$	0.498	0.494	0.303
	MLR-3	3	$1.189 + 12.021\ \rho_{672} + 4.321\ \rho_{1052} - 28.093\ \rho_{696}$	0.536	0.530	0.292
	MLR-4	4	$0.824 - 31.879\ \rho_{672} + 70.423\ \rho_{696} + 12.658\ \rho_{814} - 60.408\ \rho_{707}$	0.641	0.636	0.257
Stem	MLR-1	1	$-0.190 + 9.658\ \rho_{780}$	0.487	0.485	0.858
Elongation	MLR-2	2	$0.220 + 91.228\ \rho_{780} - 86.560\ \rho_{763}$	0.633	0.629	0.728
n=209	MLR-3	3	$0.518 + 72.709\ \rho_{780} - 63.048\ \rho_{763} - 22.077\ \rho_{1489}$	0.679	0.674	0.682
	MLR-4	4	$1.277 + 26.058\ \rho_{780} - 24.207\ \rho_{763} - 66.429\ \rho_{1489} + 30.298\ \rho_{1662}$	0.744	0.739	0.611
Booting	MLR-1	1	$1.374 + 8.697\ \rho_{854}$	0.443	0.441	1.180
n=232	MLR-2	2	$1.772 + 17.572\ \rho_{854} - 19.088\ \rho_{729}$	0.533	0.529	1.083
	MLR-3	3	$1.555 + 24.049\ \rho_{854} - 14.718\ \rho_{729} - 10.531\ \rho_{1172}$	0.545	0.539	1.071
	MLR-4	4	$1.147 + 28.131\ \rho_{854} - 20.997\ \rho_{729} - 12.945\ \rho_{1172} + 69.257\ \rho_{377}$	0.560	0.552	1.056
Heading	MLR-1	1	$9.970 - 256.497\ \rho_{380}$	0.066	0.062	1.816
n=297	MLR-2	2	$7.798 - 255.759\ \rho_{380} + 5.190\ \rho_{1083}$	0.119	0.113	1.766
	MLR-3	3	$7.842 - 263.838\ \rho_{380} + 20.485\ \rho_{1083} - 16.632\ \rho_{1003}$	0.166	0.157	1.722
	MLR-4	4	$6.445 - 488.717\ \rho_{380} + 26.101\ \rho_{1083} - 23.102\ \rho_{1003} + 349.618\ \rho_{406}$	0.203	0.192	1.686
All	MLR-1	1	$-1.534 + 20.179\ \rho_{936}$	0.629	0.628	1.889
n=1015	MLR-2	2	$-0.111 + 29.231\ \rho_{936} - 25.930\ \rho_{1659}$	0.745	0.745	1.565
	MLR-3	3	$0.137 + 46.188\ \rho_{936} - 24.244\ \rho_{1659} - 18.150\ \rho_{762}$	0.757	0.756	1.529
	MLR-4	4	$0.481 + 37.904\ \rho_{936} - 30.875\ \rho_{1659} - 27.087\ \rho_{762} + 18.429\ \rho_{1027}$	0.771	0.770	1.485

6.3.6 Calibration against validation

The calibrated (SR-, NRI-, MLR-) models were validated by an independent dataset (Table 6.4). Generally, the models using 2–4 single bands are the most promising for estimating AGB. Only one band explained AGB variability the least. In the case of MLR, the models tended to overfit already when fitting with 2–3 bands. This caused a slight increase of the R^2 and the RMSE values, though more bands were used for modeling.

At the tillering stage, the top identified models all used RED (672 nm, 692 nm) and NIR bands (707 nm–1052 nm), while at the stem elongation stage NIR bands (763 nm, 780 nm) and SWIR bands (1325 nm–1760 nm) dominated, and across all stages GREEN bands (533 nm, 550 nm), NIR bands (713 nm–1027 nm) and a SWIR band (1659 nm) were selected. In most cases, the validated MLR-models provided the best results with highest R^2 values (R^2=0.82 at the tillering stage, R^2=0.51 at the stem elongation stage). The performance of the models at the booting and heading stages was worse (R^2<0.19). In addition, the RMSE values increased till to 3.49 t/ha. These models are useless for regionalisation. Across all stages, the SR showed its best performance (R^2=0.70). The RMSE values are reasonable, but the RE shows relatively high values (RE>40%). This fact can be explained through the different management of the experimental fields (manual work by fieldworkers) and farmers' fields (mechanical work by tractors and airplanes) and the different plot size (small scale farming in experiments and large scale in farmers' fields). When the SR-, NRI-, and MLR-models were evaluated with data from farmers' fields, the R^2 values were significantly smaller (0.38–0.51 at the stem elongation stage and 0.42–0.70 across all stages). However, at the tillering stage, the R^2 values were significantly higher (0.62–0.82) than the calibration values.

Table 6.4 Calibration results versus validation results (NRI=normalized ratio index, SR=simple ratio, MLR=multiple linear regression).

Calibration dataset		(2007-2009)	Validation dataset			
Stage	R^2	Model (ρ)	RMSE	RE	R^2	Stage
	0.56	NRI $_{(799, 711)}$	0.58	54.8	0.70	
	0.58	SR $_{(822, 716)}$	0.57	53.9	0.69	
Tillering	0.30	MLR-1$_{(672)}$	0.66	57.6	0.29	Tillering
n=277	0.44	MLR-2 $_{(672, 1052)}$	0.61	53.0	0.55	n=92
	0.47	MLR-3 $_{(672, 1052, 696)}$	0.56	53.0	0.62	
	0.56	MLR-4 $_{(672, 696, 814, 707)}$	0.47	44.5	0.82	
	0.76	NRI $_{(1678, 1575)}$	1.25	59.4	0.38	
	0.53	SR $_{(1760, 1325)}$	1.36	64.8	0.45	
Stem Elongation	0.49	MLR-1 $_{(780)}$	1.88	89.3	0.18	Stem Elongation
n=209	0.63	MLR-2 $_{(780, 763)}$	1.28	60.8	0.31	n=130
	0.68	MLR-3 $_{(780, 763, 1489)}$	1.15	54.8	0.51	
	0.74	MLR-4 $_{(780, 763, 1489, 1662)}$	1.16	55.1	0.42	
	0.54	NRI $_{(695, 515)}$	1.89	49.3	0.00	
	0.54	SR $_{(695, 513)}$	3.49	90.8	0.00	
Booting	0.44	MLR-1 $_{(854)}$	1.89	49.3	0.14	Booting
n=232	0.53	MLR-2 $_{(854, 729)}$	2.07	53.8	0.06	n=257
	0.54	MLR-3 $_{(854, 729, 1172)}$	1.98	49.7	0.12	
	0.56	MLR-4 $_{(854, 729, 1172, 377)}$	1.86	48.4	0.11	
	0.29	NRI $_{(800, 789)}$	2.73	51.3	0.19	
	0.22	SR $_{(800, 789)}$	2.76	51.9	0.19	
Heading	0.02	MLR-1 $_{(380)}$	3.12	58.6	0.01	Heading
n=297	0.04	MLR-2 $_{(380, 1083)}$	3.12	58.6	0.01	n=191
	0.05	MLR-3 $_{(380, 1083, 1003)}$	3.09	58.1	0.02	
	0.06	MLR-4 $_{(380, 1083, 1003, 406)}$	2.86	53.8	0.12	
	0.74	NRI $_{(713, 533)}$	2.86	76.0	0.42	
	0.76	SR $_{(713, 550)}$	2.76	77.9	0.70	
All	0.60	MLR-1 $_{(936)}$	2.57	72.7	0.48	All
n=1015	0.72	MLR-2 $_{(936, 1659)}$	2.42	68.4	0.53	n=670
	0.74	MLR-3 $_{(936, 1659, 762)}$	2.44	68.9	0.54	
	0.75	MLR-4 $_{(936, 1659, 762, 1027)}$	2.49	70.2	0.55	

6.4 Discussion and conclusion

In comparison to reflectance-based estimation of AGB for wheat or other cereals, the estimation of rice AGB is linked with a lower relationship between reflectance and AGB resulting in a lower R^2 performance of the models. Single bands, optimised SR and NRI, as well as MLR-based methods were able to explain 80–90% of the biomass variability in wheat, e.g. ZHU et al. (2008), BAO et al. (2009), KOPPE et al. (2010), but only 60–80% in rice, e.g. PATEL et al. (1985), SHIBAYAMA and AKIYAMA (1989), TAKAHASHI et al. (2000), WANG et al. (2008), and BAJWA et al. (2010).

In this study, the performance of the investigated indices SR and NRI (R^2=0.75) was in the range of published studies, while MLR performed better (R^2=0.93). The bands of NRI were similar as in the study of STROPPIANA et al. (2009) for rice AGB across all stages. Their analysis indicated highly correlated AGB (R^2>0.9) in the RedEdge. In the case of MLR, the optimal bands in this investigation were comparable to those by WANG et al. (2008). They also set the optimal band number to four to estimate AGB of rice, and they detected several bands in the SWIR domain. There was a clear cluster of SWIR bands, especially at the stem elongation stage, when the rice AGB was highly

correlated with LAI (GNYP et al., 2012). These bands represent the maximum reflectance in the 1500 nm–1800 nm domain and are sensitive to lignin, starch and protein (KUMAR et al., 2003).

Furthermore, one key objective of our study was the transfer of the optimised SIs and newly developed MLR models, which were investigated from data collected in field experiments, to real practice: Farmers' rice fields under conventional management. In this study, the up-scaling from the experimental to the farmers' field level was promising using 2–4 bands by SR, NRI and MLR at the tillering (R^2=0.82) and the stem elongation stage (R^2=0.51). Prosperous scaling approaches from plots to the regional level were demonstrated to estimate LAI (LAUSCH et al., 2012), plant diseases (LAUDIEN and BARETH, 2006), or AGB in wheat (KOPPE et al., 2012). But also high resolution and multi-temporal TerraSAR-X images indicated a high potential (R^2=0.80) of estimating rice AGB, e.g. KOPPE et al. (2013). However, these studies focused on SIs or radar backscatter to transfer the models.

Several problems occurred during up-scaling in this study, e.g., RedEdge shift and model overfitting. Best performing bands changed at different growth stages due to an increase or decrease of canopy reflectance in diverse spectral regions. Probably, the shift of the RedEdge and changes in the chlorophyll concentration due to the different N-application or different management in experimental and farmers' fields caused problems in model transferability. Temporal changes in RedEdge and chlorophyll concentration are a known fact, e.g. HORLER et al. (1983) and FILLELA and PEÑUELAS (1994). The overfitting occurred with 2–3 bands and reduced the model predictability by MLR. Therefore, more bands improved the statistical relation, but not the model transferability. Nevertheless, since MLR is widely used for AGB estimation, PLS could probably improve the results. HANSEN and SCHJOERRING (2003) showed that PLS performed better in predicting AGB compared to SIs. In a study for AGB estimation of rice, THAKASHAKI et al. (2000) achieved a better fitting by MLR, but a worse predictability than by PLS. Their results are comparable to this study at the stem elongation stage. In addition, the AGB variability is also diverse at each stage. The highest variability in AGB was observed, especially at the stem elongation stage. Probably, the water of the paddy field, but also wet soil could partly had some impact in the models at the tillering and stem elongation stages, when the plant cover was low. Since the same rice cultivar was planted in the experimental as well as in the farmers' fields, it should have no influence on the models. The different management, such as controlled conditions, in experimental and uncontrolled ones in farmers' fields might be a problem. Up-scaling from small experimental to larger farmers' fields often yielded lower model predictability, e.g. LI et al. (2010) and PSOMAS et al. (2011), like in this study at the stem elongation stage.

Several different calculations could have been carried out in this study to partially avoid overfitting with MLR. For example, prior studies have shown that PLS, support vector machine (SVM), principle component analysis (PCA) and neural network approaches can also partly help to avoid this problem. In addition, the comparison of estimation of fresh and dry AGB would be of great value, since several studies displayed a better predictability of fresh rice AGB, e.g. YANG and CHEN

(2004). Due to the changing of the reflectance characteristics in the different plant organs, the AGB estimation should be investigated in the different organs leaf, stem and head as well. Future studies should involve data from large fields for calibration and for validation, which should be independent of each other. Moreover, sensor fusion could improve the validation as well, as shown for the radar and hyperspectral data combination by KOPPE et al. (2012). Better development or validation of reliable models could be also achieved by cross-validation and bootstrapping (RICHTER et al., 2012).

After several improvements, the models of this study, especially these with high predictability at the tillering and stem elongation stages, could be tested by EnMap or other sensors from the space. This study showed the high potential in estimating dry AGB by MLR with 3–4 independent bands, but also by SR and NRI. These bands could be easily tested and evaluated for a larger area by UAVs (unmanned aerial vehicles) carrying hyperspectral sensors or cameras, or by satellite-borne hyperspectral sensors, such as EO-1 Hyperion and EnMap, or the airborne sensor HyMap.

Acknowledgements

The authors wish to thank ELKE DORNAUF, LEI GAO, CHRISTOPH HÜTT, XIUHUA LI, JOHANNES WESKAMM, GUANMING ZHAO and Q. ZHAO, who actively participated in the field campaigns from 2007 to 2009. Financial support came from the International Bureau of the German Federal Ministry of Education and Research (BMBF, Project number CHN 08/051), Natural Science Foundation of China (31071859), National Basic Research Program (973-2009CB118606), the Innovative Group Grant of Natural Science Foundation of China (31121062), the Qixing Research and Development Centre in Heilongjiang, China, and the Jiansanjiang Agricultural Research Station in Heilongjiang, China. The authors acknowledge the funding of the CROP.SENSe.net project in the context of Ziel 2-Programms NRW 2007-2013 "Regionale Wettbewerbsfähigkeit und Beschäftigung (EFRE)" by the Ministry for Innovation, Science and Research (MIWF) of the state North Rhine Westphalia (NRW) and European Union Funds for regional development (EFRE) (005-1103-0018) while the preparation of the manuscript. We would also like to thank the anonymous reviewers and the editor for the improvement of this manuscript.

References * (*for chapter 6)

AGRICON, 2013. www.agricon.de (4.5.2013).

ANDERSON, G.L., HANSON, J.D., 1992. Evaluating hand-held radiometer derived vegetation indices for estimating above ground biomass. Geocarto International, 7, 171-78.

BAJWA, S.G., MISHRA, A.R., NORMAN, R.J., 2010. Canopy reflectance response to plant nitrogen accumulation in rice. Precision Agriculture, 11(5), 488-506.

BAO, Y., GAO, W., GAO, Z., 2009. Estimation of winter wheat biomass based on remote sensing data at various spatial and spectral resolutions. Frontier of Earth Science in China, 3 (1), 118-128.

CHO, M.A., SKIDMORE, A.K., 2009. Hyperspectral predictors for monitoring biomass production in

Mediterranean grasslands: Majella National Park, Italy. International Journal of Remote Sensing, 30 (2), 499-515.

FAGIERA, N.K., 2007. Yield physiology of rice. Journal of Plant Nutrition, 30 (6), 843-879.

FILLELA, I., PEÑUELAS, J., 1994. The red edge position and shape as indicators of plant chlorophyll content, biomass and hydric status. International Journal of Remote Sensing, 15 (7), 1459-1470.

GEBBERS, R., ADAMCHUK, V.I., 2010. Precision agriculture and food security. Science, 327 (12), 828-831.

GNYP, M.L., YAO, Y., YU, K., HUANG, S., AASEN, H., LENZ-WIEDEMANN, V.I.S., MIAO, Y., BARETH, G., 2012. Hyperspectral analysis of rice phenological stages in Northeast China. ISPRS Annals of the Photogrammetry, Remote Sensing and Spatial Information Science, Melbourne, Australia, Volume I-7, 77-82.

HABOUDANE, D., MILLER, J.R., PATTEY, E., ZARCO-TEJADA, P.J., STRACHAN, I.B., 2004. Hyperspectral vegetation indices and novel algorithms for predicting green LAI of crop canopy: Modeling and validation in the context of precision agriculture. Remote Sensing of Environment, 90 (3), 337-352.

HANSEN, P.M., SCHJOERRING, J.K., 2003. Reflectance measurement of canopy biomass and nitrogen status in wheat crops using normalized difference vegetation indices and partial least squares regression. Remote Sensing of Environment, 86 (4), 542–553.

HORLER, D.N.H., DOCKRAY, M., BARBER, J., 1983. The red edge of plant leaf reflectance. International Journal of Remote Sensing, 4 (2), 273-288.

JORDAN, C.F., 1969. Derivation of leaf area index from quality of light on the forest floor. Ecology, 50, 663-666.

KAUFMANN, H., SEGL, K., ITZEROTT, S., BACH, H., WAGNER, A., HILL, J., HEIM, B., OPPERMANN, K., HELDENS, W., STEIN, E., MÜLLER, A., VAN DER LINDEN, S., LEITAO, P.J., HOSTERT, P., 2010. Hyperspectral algorithms. Report in the frame of EnMAP preparation activities. Deutsches GeoForschungsZentrum GFZ, 10 (8), 1-268.

KOPPE, W., LI, F., GNYP, M.L., MIAO, Y., JIA, L., CHEN, X., ZHANG, F., BARETH, G., 2010. Evaluating multispectral and hyperspectral satellite remote sensing data for estimating winter wheat growth parameters at regional scale in North China Plain. Photogrammmetrie Fernerkundung, Geoinformation, 2010 (3), 167-178.

KOPPE, W., GNYP, M.L., HENNIG, S.D., LI, F., MIAO, Y., CHEN, X., JIA, L., BARETH, G., 2012. Multi-temporal hyperspectral and radar remote sensing for estimating winter wheat biomass in the North China Plain. Photogrammmetrie Fernerkundung Geoinformation, 2012 (3), 281-298.

KOPPE, W., GNYP, M.L., HÜTT, C., YAO., Y., MIAO, Y., CHEN, X., BARETH, G., 2013. Rice monitoring with multi-temporal and dual-polarimetric TerraSAR-X data. International Journal of Applied Earth Observation and Geoinformation, 21, 568-576.

KUMAR, L., SCHMIDT, K., DURRY, S., SKIDMORE, A., 2003. Imaging spectrometry and vegetation science. In: F.D., VAN DER MEER, S.M., DE JONG, (Eds.): Imaging Spectrometry, Dordrecht, The Netherlands, pp. 111-156.

LAUDIEN, R., BARETH, G., 2006. Multitemporal hyperspectral data analysis for regional detection of plant diseases by using a tractor- and an airborne-based spectrometer. Photogrammetrie Fernerkundung Geoinformation, 2006 (3), 217-227.

LAUSCH, A., PAUSE, M., MERBACH, I., GWILLYM-MARGIANTO, S., SCHULZ, K., ZACHARIAS, S., SEPPELT, R., 2012. Scale-specific hyperspectral remote sensing approach in environmental research. Photogrammetrie Fernerkundung Geoinformation, 2012 (5), 589-602.

LI, F., MIAO, Y., HENNIG, S.D., GNYP, M.L., CHEN, X., JIA, L., BARETH, G., 2010. Evaluating hyperspectral vegetation indices for estimating nitrogen concentration of winter wheat at different growth stages. Precision Agriculture, 11 (4), 335-357.

LU, D., 2006. The potential and challenge of remote sensing-based biomass estimation. International Journal of Remote Sensing, 27 (7), 1297-1328.

MATLAB, 2013. MathWorks Inc., Natick, MA, USA, www.mathwork.de (4.5.2013).

MILTON, E.J., SCHAEPMAN, M.E., ANDERSON, K., KNEUBÜHLER, M., FOX, N., 2009. Progress in field spectroscopy. Remote Sensing of Environment, 113 (1), S92-S109.

ORTENBERG, F., 2011. Hyperspectral sensor characteristics: airborne, spaceborne, hand-held, and truck-mounted; Integration of hyperspectral data with Lidar. In: P.S., THENKABAIL, J.G., LYON, A., HUETE (Eds.): Hyperspectral remote sensing of vegetation. Boca Raton, FL, USA, pp. 39-68.

PATEL, N.K., SINGH, P., SAHAI, B., PATEL, M.S., 1985. Spectral response of rice crop and its relation to yield and yield attributes. International Journal of Remote Sensing, 6 (5), 657-664.

PSOMAS, A., KNEUBÜHLER, M., HUBER, S., ITTEN, K., ZIMMERMANN, N.E., 2011. Hyperspectral remote sensing for estimating aboveground biomass and for exploring species richness patterns of grassland habitats. International Journal of Remote Sensing, 32 (24), 9007-9031.

RAUN, W.R., JOHNSON, G.V., 1999. Improving nitrogen use efficiency for cereal production. Agronomy Journal, 91 (3), 357-363.

RICHARDSON, A.J., EVERITT, J.H., GAUSMAN, H.W., 1983. Radiometric estimation of biomass and nitrogen content of Alicia Grass. Remote Sensing of Environment, 13 (2), 179-185.

RICHTER, K., ATZBERGER, C., HANK, T.B., MAUSER, W., 2012. Derivation of biophysical variables from Earth observation data: validation and statistical measures. Journal of Applied Remote Sensing, 6 (1), 179-185.

ROUSE, J.W., HAS, R.H., SCHELL, J.A., DEERING, D.W., 1974. Monitoring vegetation systems in the Great Plains with ERTS. Third ERTS Symposium, NASA Sp-3511, 309-317.

SCHWIND, P., MÜLLER, R., PALUBINSKAS, G., STORCH, T., 2012. An in-depth simulation of EnMAP acquisition geometry. ISPRS Journal of Photogrammetry and Remote Sensing, 70 (1), 99-106.

SERRANO, L., FILELLA, I., PENUELAS, J., 2000. Remote sensing of biomass and yield of winter wheat under different nitrogen supplies. Crop Science, 40 (3), 723-731.

SHIBAYAMA, M., MUNAKATA, K., 1986. A spectroradiometer for field use III: A comparison of some vegetation indices for predicting luxuriant paddy rice biomass. Japanese Journal of Crop Science, 55 (1), 47-52.

SHIBAYAMA, M., AKIYAMA, K., 1989. Seasonal visible, near-infrared and mid-infrared spectra of rice canopies in relation to LAI and above-ground dry phytomass. Remote Sensing of Environment, 27 (2), 119-127.

SIMS, D.A., GAMON, J.A., 2002. Relationship between leaf pigment content and spectral reflectance across a wide range of species, leaf structure and development stages. Remote Sensing of Environment, 81 (2-3), 337-354.

SONG, S., GONG, W., ZHU, B., HUANG, X., 2011. Wavelength selection and spectral discrimination for paddy rice with laboratory measurements of hyperspectral leaf reflectance. ISPRS Journal of Photogrammetry and Remote Sensing, 66 (5), 672-682.

SPSS, 2013. IBM SPSS Inc., Armonk, NY, USA, www-01.ibm.com/software/analytics/spss (4.5.2013).

STATISTICA, 2013. StatSoft, Tulsa, OK, USA, www.statsoft.com (4.5.2013).

STROPPIANA, D., BOSCHETTI, M., BRIVIO, P.A., BOCCHI, S., 2009. Plant nitrogen concentration in paddy rice from canopy hyperspectral radiometry. Field Crops Research, 111 (1-2), 119-129.

TAKAHASHI, W., NGUYEN-CONG, V., KAWAGUCHI, S., MINAMIYAMA, M., NINOMIYA, S., 2000. Statistical models for prediction of dry weight and nitrogen accumulation based on visible and near-infrared hyper-spectral reflectance of rice canopies. Plant Production Science, 3 (4), 377-386.

THENKABAIL, P.S., SMITH, R.B., PAUW, E.D., 2000. Hyperspectral vegetation indices and their relationship with agricultural crop characteristics. Remote Sensing of Environment, 71 (2), 152-182.

WANG, F., HUANG, J., WANG, X., 2008. Identification of optical hyperspectral bands for estimation of rice biophysical parameters. Journal of Integrative Plant Biology, 50 (3), 291-299.

YANG, C., CHEN, R., 2004. Modeling rice growth with hyperspectral reflectance data. Crop Science, 44 (4), 1283-1290.

YU, K., LI, F., GNYP, M.L., MIAO, Y., BARETH, G., CHEN, X., 2013. Remotely detecting canopy nitrogen concentration and uptake of paddy rice in Northeast China Plain. ISPRS Journal of Photogrammetry and Remote Sensing, 78, 102-115.

ZHU, Y., YAO, X., TIAN, Y., LIU, X., CAO, W., 2008. Analysis of common canopy vegetation indices for indicating leaf nitrogen accumulation wheat and rice. International Journal of Applied Earth Observation and Geoinformation, 10 (1), 1-10.

7. Hyperspectral canopy sensing of paddy rice aboveground biomass at different growth stages

M.L. GNYP [a,b], Y. MIAO [a*], F. YUAN[c], S.L. USTIN[d], K. YU [a,b], Y. YAO [a], S. HUANG [a,b], G. BARETH [b]

received: 14 August 2013, received in revised from: 26 September 2013, accepted: 27 September 2013
published in 2014: Field Crops Research, 155, 42-55. DOI: 10.1016/j.fcr.2013.09.023
Original accepted manuscript is used and embedded in dissertation format.

a. International Center for Agro-Informatics and Sustainable Development, College of Resources and Environmental Science, China Agricultural University, Beijing, 100193, China
b. Institute of Geography, University of Cologne, 50923 Cologne, Germany
c. Department of Geography, Minnesota State University, Mankato, MN 56001, USA
d. Center for Spatial Technologies and Remote Sensing (CSTARS), Department of Land, Air, and Water Resources, University of California, Davis, CA 95616, USA

*Corresponding author, Tel.: +86-10-6273-2865.
Email: ymiao@cau.edu.cn; ymiao2007@gmail.com (Y. Miao)

Abstract

Normalized Difference Vegetation Index and Ratio Vegetation Index obtained with the fixed band GreenSeeker active multispectral canopy sensor (GS-NDVI and GS-RVI) have been commonly used to non-destructively estimate crop growth parameters and support precision crop management, but their performance has been influenced by soil and/or water backgrounds at early crop growth stages and saturation effects at moderate to high biomass conditions. Our objective is to improve estimation of rice (*Oryza sativa L.*) aboveground biomass (AGB) with hyperspectral canopy sensing by identifying more optimal measurements using one or more strategies: (a) soil adjusted Vegetation Indices (VIs); (b) optimized narrow band RVI and NDVI; and (c) Optimum Multiple Narrow Band Reflectance (OMNBR) models based on raw reflectance, and its first and second derivatives (FDR and SDR).

Six rice nitrogen (N) rate experiments were conducted in Jiansanjiang, Heilongjiang province of Northeast China from 2007 to 2009 to create different biomass conditions. Hyperspectral field data and AGB samples were collected at four growth stages from tillering through heading from both experimental and farmers' fields. The results indicate that six-band OMNBR models (R^2=0.44–0.73) explained 21–35% more AGB variability relative to the best performing fixed band RVI or NDVI at different growth stages. The FDR-based 6-band OMNBR models explained 4%, 6% and 8% more variability of AGB than raw reflectance-based 6-band OMNBR models at the stem elongation (R^2=0.77), booting (R^2=0.50), and heading stages (R^2=0.57), respectively. The SDR-based 6-band

OMNBR models made no further improvements, except for the stem elongation stage. Optimized RVI and NDVI for each growth stage (R^2=0.34–0.69) explained 18–26% more variability in AGB than the best performing fixed band RVI or NDVI. The FDR- and SDR-based optimized VIs made no further improvements. These results were consistent across different sites and years. It is concluded that with suitable band combinations, optimized narrow band RVI or NDVI could significantly improve estimation of rice AGB at different growth stages, without the need of derivative analysis. Six-band OMNBR models can further improve the estimation of AGB over optimized 2-band VIs, with the best performance using SDR at the stem elongation stage and FDR at other growth stages.

Keywords: vegetation index; OMNBR, derivative spectral analysis, precision agriculture, water reflectance, crop canopy sensor

7.1 Introduction

Rice (*Oryza sativa* L.) is a major staple cereal crop, providing food for more than half of the world's population (CANTRELL and REEVES, 2002; NORMILE, 2008). Precision management of rice for high yield and high resource use efficiency is crucially important for global food security and sustainable development (ZHAO et al., 2013). Information on aboveground biomass (AGB) is needed for calculating critical nitrogen (N) concentrations, which are important for in-season assessment of crop N status (LEMAIRE et al., 2008). It is also an important indicator of crop population, growth and gross primary production (PATEL et al., 1985; HARRELL et al., 2011; PENG and GITELSON, 2011). Traditional sampling methods are based on taking physical samples from the paddy fields, an approach that is time consuming, labor intensive, and results in destroying parts of the crop. Non-destructive or non-intrusive methods using digital technologies can avoid these issues and provide more representative measurements, thus avoiding sampling bias.

Crop canopy sensors have been commonly used in precision agriculture to non-destructively estimate agronomic parameters, including AGB (HEEGE et al., 2008; SAMBORSKI et al., 2009; PENG and GITELSON, 2011; CAO et al., 2012, 2013; YAO et al., 2012; DIACONO et al., 2013). The GreenSeeker handheld sensor (Trimble Navigation Limited, Sunnyvale, CA, USA) is a widely adopted active crop canopy sensor with two fixed wavebands (660±10 nm and 770±15 nm) and produces two vegetation indices, Normalized Difference Vegetation Index (NDVI) and Ratio Vegetation Index (RVI). LI et al. (2010a) found GreenSeeker NDVI (GS-NDVI) correlated with biomass of winter wheat (*Triticum aestivum*) at Feekes stages 4 to 10, although correlations decreased with maturity because measurements became saturated when biomass reached 3,746 kg ha^{-1}, while the GreenSeeker RVI (GS-RVI) did not show such saturation effect. For irrigated rice, the influence of a water background on crop canopy reflectance poses a unique challenge for estimating rice biophysical parameters using canopy remote sensing, especially at early growth stages when the vegetation cover

is low (MARTIN and HEILMAN, 1986; SHIKADA and MIYAKITA, 1992; VAN NIEL and MCVICAR, 2004; TUBAÑA et al., 2011).

To reduce the influence of soil backgrounds on plant canopy reflectance, scientists have developed many soil-adjusted vegetation indices. The most widely used index is the Soil-Adjusted Vegetation Index (SAVI) by including a background adjustment factor L (HUETE, 1988). QI et al. (1994) developed a Modified SAVI (MSAVI) to account for soil background differences. HABOUDANE et al. (2004) proposed Modified Chlorophyll Absorption Ratio Index 2 (MCARI2) and Modified Triangular Vegetation Index 2 (MTVI2) to minimize the sensitivity of the indices to chlorophyll effects, maximize their responsiveness to green LAI variations, and make them more resistant to soil and atmosphere effects. Their results indicated that these two indices performed better than the existing VIs. Little has been reported on whether these VIs can: (a) reduce soil and water background influences on rice canopy reflectance at early growth stages, and (b) improve the performance of VIs for estimating rice AGB.

Derivative spectral analysis is another technique that can be used to reduce background signals (DEMETRIADES-SHAH et al., 1990; BECKER et al., 2005). Seeing the spectral reflectance as a polynomial function of degree d, the first-derivative of reflectance (FDR) expresses the slope of this function in dependence on the wavelength. Thereby, the FDR eliminates the influence of all constant terms (d=0) on that function. The spectral signal of soil or water surfaces can be considered as a linear function of wavelength. The FDR cannot completely remove background signals. With the second-derivative of reflectance (SDR), all linear influences (d=1) are removed, if the second derivative was equal to zero (DEMETRIADES-SHAH et al., 1990). Hence, in theory the SDR should be useful in reducing the water and soil background influences. Additional advantage of derivative spectra is that the SDR is relatively insensitive to variation in illumination intensity caused by changes in cloud cover or sun angle (TSAI and PHILPOT, 1998). This is important for rice farming because clouds are common in rice growing regions, which limits the application of remote sensing technology in rice management. Derivative analyses of hyperspectral data have been found to be more useful in estimating plant N or pest information in rice than raw reflectance (KOBAYASHI et al., 2001; LIU et al., 2010; ZHANG et al., 2011; HUANG et al., 2012). LIU et al. (2010) demonstrated that FDR and SDR explained 5% and 9% more variability than raw reflectance in detecting rice disease, respectively. Derivative analyses appeared to be very effective for retrieving attributes of vegetation at canopy level (IMANISHI et al., 2004).

One common approach to overcome the limitations of the fixed band VIs like NDVI is to identify the best narrow band combinations for different crop species or growth stages using correlograms (THENKABAIL et al., 2000; HANSEN and SCHOERRING, 2003; LI et al., 2010b; GNYP et al., 2013; YU et al., 2013). YU et al. (2013) found that RVI combinations (R_{730}, R_{808}; R_{752}, R_{840}; R_{774}, R_{780}) or NDVI (R_{774}, R_{780}; R_{750}, R_{840}) could explain more than 66% of rice plant N uptake variability. GNYP et al. (2013) found that the optimized narrow band RVI or NDVI indices also explained similar

percentages of rice AGB variability. Compared with multispectral crop sensors with limited fixed bands like GreenSeeker, hyperspectral canopy sensors capture much richer information about crop canopy characteristics with the continuous acquisition of reflectance at narrow wavelengths; therefore, they may improve crop growth parameter estimation results.

Most VIs use two or three bands, which unnecessarily constrains regression analysis (LAWRENCE and RIPPLE, 1998). THENKABAIL et al. (2000) proposed Optimum Multiple Narrow Band Reflectance (OMNBR) model to use stepwise multiple linear regression (SMLR) to identify sensitive band combinations to estimate crop wet biomass and LAI. They found that 4-band OMNBR models could explain up to 92% of the crop biophysical parameter variability, but they were only marginally better than optimized narrow band NDVI type models. YU et al. (2013) found that 6-band OMNBR models could significantly improve the accuracy of estimating rice leaf N concentration and plant N concentration relative to optimized narrow band NDVI or RVI. For such models, 4–6 bands are generally used, because when the ratio (M/N) of the number of independent variables or narrow bands (M) to that of total number of field samples (N) is higher than 0.15–0.20, over-fitting can become a serious problem.

So far, little research has been conducted to evaluate how much soil adjusted vegetation indices, optimized narrow band vegetation indices, OMNBR and derivative spectral analyses can improve the estimation of rice AGB at different growth stages compared to the fixed band NDVI and RVI. Therefore, the objectives of this study were to determine: (1) if and how much published soil adjusted VIs, optimized narrow band VIs (RVI and NDVI) and OMNBR models can improve rice AGB estimation using canopy hyperspectral reflectance data as compared with the fixed band VIs at different growth stages, and, (2) if derivative spectra (FDR and SDR) can further improve the above-mentioned methods for estimating rice AGB. Achieving both these objectives meets our goal of improving the fixed band RVI and NDVI approaches for estimating rice AGB.

7.2 Materials and methods

7.2.1 Study site

The study was conducted in the Sanjiang Plain (47.2° N, 132.8° E), Heilongjiang Province, Northeast China. It is an alluvial plain derived from three rivers (Heilong, Songhua, and Wusuli) and covers about 109,000 km². Bordered by Siberia in the north and east, it is characterized by a sub-humid continental monsoon climate with a warm summer and cold winter. The mean annual temperature is about 2°C and the mean precipitation amounts to 550 mm per year (WANG and YANG, 2001). About 70% of the precipitation occurs from June through September. The dominant soil type in this area is Albic soil, which is classified in the FAO-UNESCO system as mollic planosols and Typical Argialbolls in Soil Taxonomy (XING et al., 1994). The upper layer of this soil is generally thin (10–25cm) and low in soil nutrients. An albic layer below the surface layer is compact and

impermeable (YUAN et al., 2006). We selected two sites for this study in Jiansanjiang. Site 1 has been planted in rice since 1992, and Site 2 was first planted in rice in 2002 (Fig. 7.1).

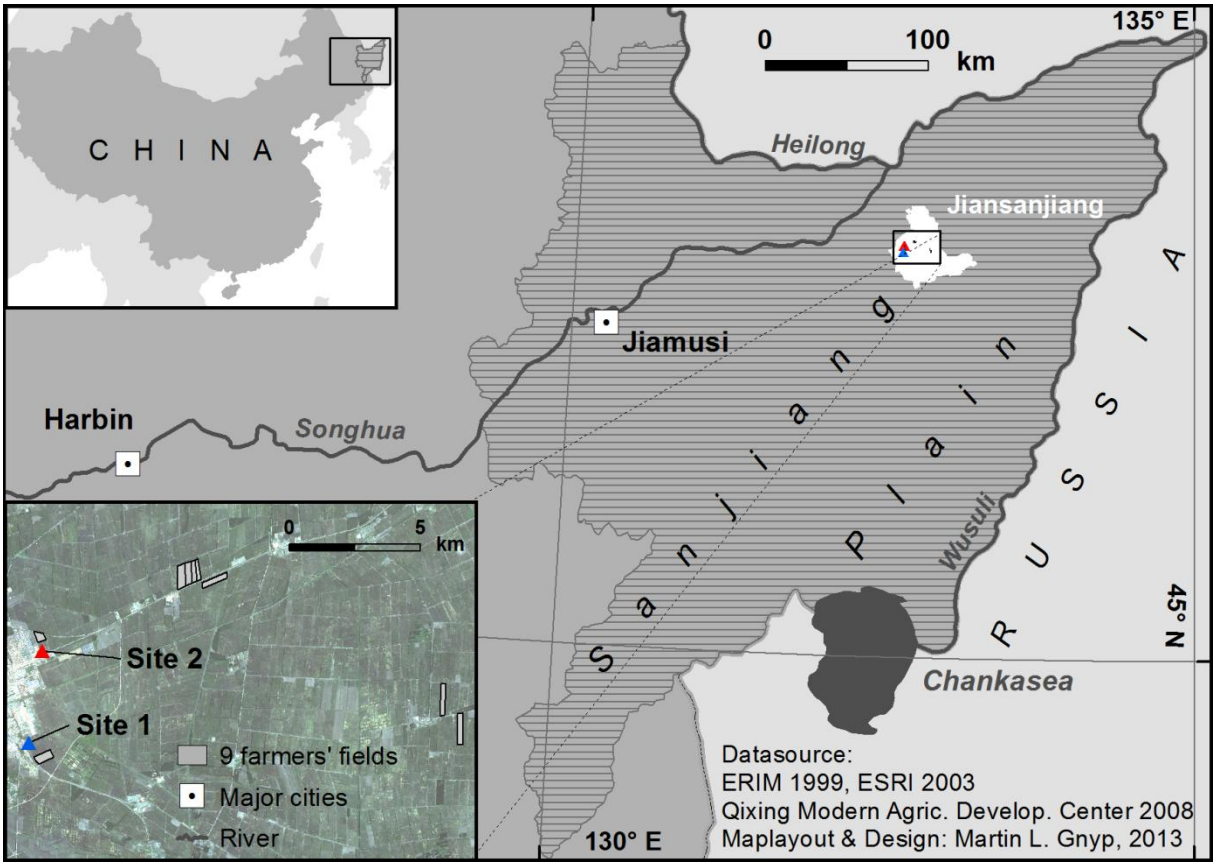

Fig. 7.1 Location of the Site 1, Site 2 and the 9 farmers' fields in the Sanjiang Plain, Heilongjiang Province, China.

7.2.2 Nitrogen rate experiments

7.2.2.1 Experiments 1 and 2

Experiments 1 and 2 were conducted in 2007 at Sites 1 and 2, respectively, in a randomized complete block design with four replications (Fig. 7.2, left). There were seven N rate treatments: 0, 60, 75, 90, 105, 120, and 150 kg N ha^{-1} that we used to obtain a large range of AGB. The N fertilizers were applied in the form of urea: 40% as basal fertilizer before transplanting, 30% at the tillering stage and 30% at the booting stage. The rice variety was Kongyu 131, with 11 leaves, 4 elongation nodes, and 127 maturity days. The rice seedlings were prepared in greenhouse and transplanted to the experimental fields at 3.1–3.5 leaf stage in mid-May, with a density of 0.12 m by 0.30 m and 4–5 plants per hill. For all the treatments, 60 kg P_2O_5 ha^{-1} and 75 kg K_2O ha^{-1} were applied as basal fertilizers before transplanting. The plot size was 5 m x 8 m. Other field management practices, such as irrigation, pesticide application, etc., followed local stand practices.

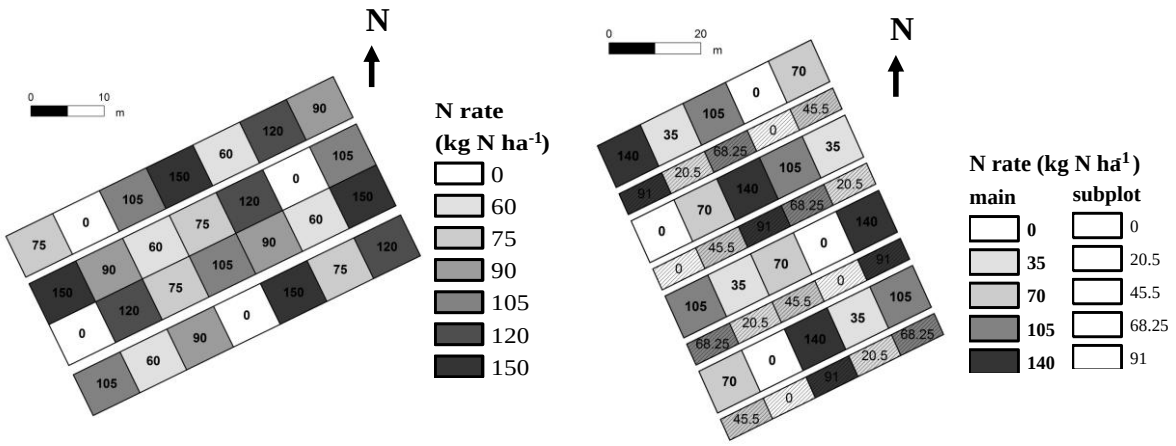

Fig. 7.2 Field plots layout for N rate experiments conducted in 2007 (left) and 2008–2009 (right).

7.2.2.2 Experiments 3–6

Experiments 3 and 4 were conducted in 2008 at Sites 1 and 2, respectively, with the same design and treatments. A randomized split plot design with four blocks was used. The main plot consisted of five N rates: 0, 35, 70, 105 and 140 kg N ha^{-1}, which were applied 45% as basal N before transplanting, 20% at the tillering stage, and 35% at the stem elongation stage. Each plot was 15 m x 10 m, and was divided into two parts: 10 m x10 m as the main plot and 5 m x 10 m as the subplot without receiving the third N application (Fig. 7.2, right). Although YAO et al. (2012) developed this method for crop sensor-based precision N management research, we took advantage of the diverse growth status in treatments to evaluate different remote sensing methods to estimate rice biomass. Only data from the main plots were used, because AGB samples were not collected in the subplots. Other management practices, such as the rice variety, phosphorus and potassium fertilizer application and seedling preparation, irrigation and pesticide application, etc. were the same as Experiments 1 and 2.

Experiments 5 and 6 were conducted in 2009 at sites 1 and 2, respectively. They virtually duplicated Experiments 3 and 4.

7.2.2.3 Farmers' fields

In order to evaluate the established relationships with the N experimental data under on-farm conditions, nine farmers' fields were also selected for study in 2007–2009. These fields were managed by farmers on their own. They represented the common practice of large scale faming in rice paddies in Northeast China. The size of these fields ranged from 12 to 27 ha.

7.2.3 Reflectance measurements

Rice canopy reflectance was measured with ASD QualitySpec® Pro (Analytical Spectral Devices, Inc., Boulder, CO, USA) for Experiments 1 and 2 in 2007 and ASD FieldSpec® 3

(Analytical Spectral Devices, Inc., Boulder, CO, USA) for Experiments 3–6 in 2008 and 2009. The QualitySpec® Pro spectrometer acquired the reflectance data in the wavelength domain of 350–1800 nm with two detectors, one for the visible near infrared (VNIR) (350–1000 nm) and one for the shortwave-infrared (SWIR) (1000–1800 nm). Equipped with 19 silica glass fibers, each detector has a sampling interval of 1.4 nm in the VNIR range and 2 nm in the SWIR range. The ASD FieldSpec® 3 spectrometer was configured to collect reflectance from 350 nm to 2500 nm, with 1.4 nm sampling interval between 350 and 1050, and 2 nm sampling interval between 1000 and 2500 nm. The reflectance was taken with a 25° field of view at a height of about 0.3 m above the crop canopy, resulting in a sample area of 150 cm^2 with a 14 cm diameter at the canopy surface. To minimize the disturbance of the canopy structure, the sensors were carried along the rows of rice plants. Hyperspectral data were subdivided into 1 nm band width using a self-driven interpolation method of the ASD spectrometers.

Measurements were taken from 9 a.m. to 1 p.m. Local Mean Time (solar noon at 11 a.m.). Calibration measurements were done with a barium sulfate ($BaSO_4$) reference panel at least every 10–15 minutes, depending on illumination changes. Twenty sample counts were collected for the white reference panel and ten for each scanning position of the rice canopy. Within one plot, five–six scanning positions were selected randomly and the reflectance was averaged to represent each plot. The reflectance was measured in 2007–2009 at the growth stages of tillering, stem elongation, booting, and heading (Fig. 7.3).

Fig. 7.3 Rice growth stages (from left to right) – Tillering (T), Stem Elongation (SE), Booting (B), and Heading (H).

7.2.4 Plant sampling and measurements

After the reflectance measurements, the center of the scan positions was marked with sticks. Then three (booting and heading stage) to five (tillering and stem elongation stage) hills or clusters of the scanned plants with average number of tillers per plot were cut at ground surface. All plant samples were rinsed with water, and the roots were removed. They were put into the oven at 105°C for 30 minutes and then dried at 70°C to constant weight. Altogether, 1,685 AGB samples were collected (1,015 from experimental fields and 670 from farmers' fields) from tillering through heading stage.

7.2.5 Data preprocessing of hyperspectral data

The reflectance spectra were analyzed using ViewSpecPro software Version 5.0.19 (Analytical Spectral Devices, Inc., Boulder, CO, USA). The spectral regions of 1331–1449 nm and 1771–1800 nm were excluded from the analysis due to their association with water absorption. To be consistent with data obtained from QualitySpec® Pro, data from 1800–2500 nm collected with FieldSpec® 3 were also excluded from the analysis. After that, the averaged raw reflectance was smoothed by the Savitzky-Golay filter (SAVITZKY and GOLAY, 1964) in Origin Pro Version 8.5G (OriginLab Corporation, Northampton, MA, USA) with a frame size of 15 data points (2nd degree polynomial). This filter was adjusted for the local signal-to-noise ratio in order to smooth the target spectrum point by point (TSAI and PHILPOT, 1998).

After smoothing, the derivative spectra FDR and SDR were computed using MATLAB Version 7.0 (The Mathworks®, Inc, Natick, MA, USA). The effective spectral bands of FDR were in the range of 400–970, 1120–1310 and 1530–1750 nm and bands of SDR were 450–900 and 1550–1680 nm, respectively. The 1550–1680 nm region of SDR was also excluded from the booting and heading stages due to excess noise.

$$FDR=d^{1st}=(R_{i+1}-R_i)/(\lambda_{i+1}-\lambda_i) \quad \text{(Eq. 7.1)}$$

where d^{1st}, R_i and λ were first derivative, reflectance value (%) and wavelength (nm), respectively.

$$SDR=d^{2nd}=(d^{1st}_{i+1}-d^{1st}_{i})/(\lambda_{i+1}-\lambda_i) \quad \text{(Eq. 7.2)}$$

where d^{2nd} and λ were second derivative approximation and wavelength (nm), respectively.

Samples from the N experiments (n=1,015) and farmers' fields (n=670) were pooled (n=1,685). Then the pooled dataset was randomly divided into calibration dataset (75% of the observations) and validation dataset (25% of the observations).

7.2.6 Vegetation indices

The smoothed raw reflectance data were used to simulate the spectral bands of GreenSeeker sensor and calculate GS-NDVI and GS-RVI. Several published VIs related to LAI or AGB estimation and corrected for soil background influences were also selected to see if they could perform better than GS-NDVI and GS-RVI (Table 7.1).

To overcome limitations of fixed band NDVI and RVI, all possible two band combinations of RVI and NDVI for estimating rice AGB were calculated with a Java program using the effective band regions of the raw reflectance (350–1330 and 1450–1770 nm), FDR (400–970, 1120–1310 and 1530–1750 nm) and SDR (450–900 and 1550–1680 nm). The excluded regions of SDR (901–1549 nm)

correspond to strong environmental and instrument noise (e.g., water absorption bands, detector change at 1000 nm).

Table 7.1 Selected published VIs evaluated in this study. The indices were simulated by GreenSeeker bands.

Index	Equation	Reference
Simulated GreenSeeker VIs		
GS-RVI	$R_{GS\text{-}NIR}/R_{GS\text{-}RED}$	JORDAN (1969)
GS-NDVI	$(R_{GS\text{-}NIR}-R_{GS\text{-}RED})/(R_{GS\text{-}NIR}+R_{GS\text{-}RED})$	ROUSE et al. (1974)
Soil adjusted VIs with simulated GreenSeeker bands ($R_{800}=R_{GS\text{-}NIR}$ and $R_{670}=R_{GS\text{-}RED}$)		
SAVI	$(1+0.5)(R_{GS\text{-}NIR}-R_{GS\text{-}RED})/(R_{GS\text{-}NIR}+R_{GS\text{-}RED}+0.5)$	HUETE (1988)
MSAVI	$0.5[2R_{GS\text{-}NIR}+1-((2R_{GS\text{-}NIR}+1)^2-8(R_{GS\text{-}NIR}-R_{GS\text{-}RED}))^{0.5}]$	QI et al. (1994)
OSAVI	$(R_{GS\text{-}NIR}-R_{GS\text{-}RED})/(R_{GS\text{-}NIR}+R_{GS\text{-}RED}+0.16)$	RONDEAUX et al. (1996)
MCARI	$[(R_{700}-R_{GS\text{-}RED})-0.2(R_{700}-R_{550})](R_{700}/R_{GS\text{-}RED})$	KIM et al. (1994)
MTVI1	$1.2[1.2(R_{GS\text{-}NIR}-R_{550})-2.5(R_{GS\text{-}RED}-R_{550})]$	HABOUDANE et al. (2004)
MCARI2	$1.5[2.5(R_{GS\text{-}NIR}-R_{GS\text{-}RED})-1.3(R_{GS\text{-}NIR}-R_{550})]/[(2R_{GS\text{-}NIR}+1)^2-(6R_{GS\text{-}NIIR}-5\sqrt{R_{GS\text{-}RED}})-0.5]^{0.5}$	HABOUDANE et al. (2004)
MTVI2	$1.5[1.2(R_{GS\text{-}NIR}-R_{550})-2.5(R_{GS\text{-}RED}-R_{550})]/[(2R_{GS\text{-}NIR}+1)^2-(6R_{GS\text{-}NIR}\ 5\sqrt{R_{GS\text{-}RED}})-0.5]^{0.5}$	HABOUDANE et al. (2004)

R_i=Raw reflectance in band i

7.2.7 Optimum multiple narrow band reflectance (OMNBR) models

The OMNBR models were developed using SMLR method with raw reflectance, the FDR, and SDR by SPSS 21.0 (IBM SPSS Inc. Armonk, NY, USA) (THENKABAIL et al., 2000; YU et al., 2013). In this study, we only considered 1–6 band OMNBR models to prevent over-fitting problems. The "Collinearity diagnosis" option was selected in the SPSS software. The collinearity was checked by the condition index. When its value is greater than 15, it indicates potential problem of collinearity, while values of condition index higher than 30 indicate that the results are highly dubious. Condition indices were all less than 15 for models using 1–6 bands of FDR and SDR. For models using 1–4 bands of raw reflectance, condition indices were all less than 15. For models with 5–6 bands of raw reflectance, condition indices increased to 15–25 at some growth stages, but still less than 30. For models using more than 6 bands, the condition index increased exponentially and reached high values (>30). This is another reason that we did not use models with more than 6 bands.

7.2.8 Statistics of model calibration and validation

The VIs and OMNBR were used to develop models for estimating AGB. The goodness of fit and validation were evaluated by the differences in the coefficient of determination (R^2), the root mean square error (RMSE), and the relative error (RE). The RMSE and RE were calculated using Eqs. (7.3) and (7.4), respectively:

$$\text{RMSE} = \sqrt{\frac{1}{n}\sum_{i=1}^{n}\left(y_i-\hat{y}_i\right)^2} \qquad \text{(Eq. 7.3)}$$

$$RE\ (\%) = \frac{RMSE}{\bar{y}} \times 100 \qquad \text{(Eq. 7.4)}$$

where y_i, $\hat{y}_i$ and $\bar{y}$ were the measured, predicted and mean values of rice biomass, respectively, and *n* was the number of samples.

7.3 Results

7.3.1 Aboveground biomass variability

The AGB varied from 0.12 t ha^{-1} to 14.13 t ha^{-1} across growth stages for the whole dataset (Table 7.2). Average AGB increased from 0.95 t ha^{-1} at tillering stage to 2.08 t ha^{-1} at stem elongation stage, and increased to 4.23 t ha^{-1} and 6.83 t ha^{-1} at booting stage and heading stage, respectively. The standard deviation (SD) values increased from 0.52 t ha^{-1} at the tillering stage to 2.22 t ha^{-1} at the heading stage. At each stage, the calibration and validation datasets had similar mean and SD values (Table 7.2). The coefficient of variation (CV) decreased from tillering to the heading stage.

Table 7.2 Descriptive statistics of AGB for model calibration and validation at different growth stages.

Stage	n	Min	Max	Mean	SD	CV
Tillering						
Total	369	0.12	4.53	0.95	0.52	54.3
Calibration	276	0.12	4.53	0.95	0.52	54.8
Validation	93	0.14	3.15	0.94	0.50	53.3
Stem Elongation						
Total	339	0.34	5.72	2.08	1.05	50.4
Calibration	254	0.34	5.72	2.10	1.09	51.9
Validation	85	0.57	4.46	2.01	0.91	45.3
Booting						
Total	489	1.41	10.06	4.23	1.66	39.3
Calibration	366	1.41	10.06	4.18	1.68	40.3
Validation	123	2.07	10.18	4.38	1.58	36.2
Heading						
Total	488	2.37	14.13	6.83	2.22	32.5
Calibration	366	2.37	14.13	6.86	2.27	33.1
Validation	122	3.14	12.39	6.72	2.06	30.7
All stages						
Total	1685	0.12	14.13	3.83	2.75	71.9
Calibration	1262	0.12	14.13	3.81	2.78	72.9
Validation	423	0.14	11.70	3.91	2.69	68.7

n=Number of observations; SD=Standard deviation of the mean; CV=Coefficient of variation
Min, Max, Mean and SD values in t ha^{-1}; CV in %

7.3.2 Reflectance, first and second derivative spectra of rice canopy

The spectral reflectance of paddy rice canopy responded to the AGB development (Fig. 7.4) at different growth stages. From the early tillering to heading stage, the NIR and SWIR reflectance increased while the visible spectral reflectance decreased due to the decreasing chlorophyll content in the plants. The raw reflectance (Fig. 7.4) exhibited several local peaks or troughs at 550 nm, 670 nm, 880 nm, 970 nm, 1070 nm, 1180 nm, 1250 nm and 1670 nm. Inflection points were found around

515 nm, 600 nm, 730 nm, 930 nm, 1000 nm, 1125 nm and 1220 nm. These peaks changed with an offset of approximately +15 nm in the different growth stages. The highest reflectance was always observed at 1070 nm (+15 nm) (Fig. 7.4).

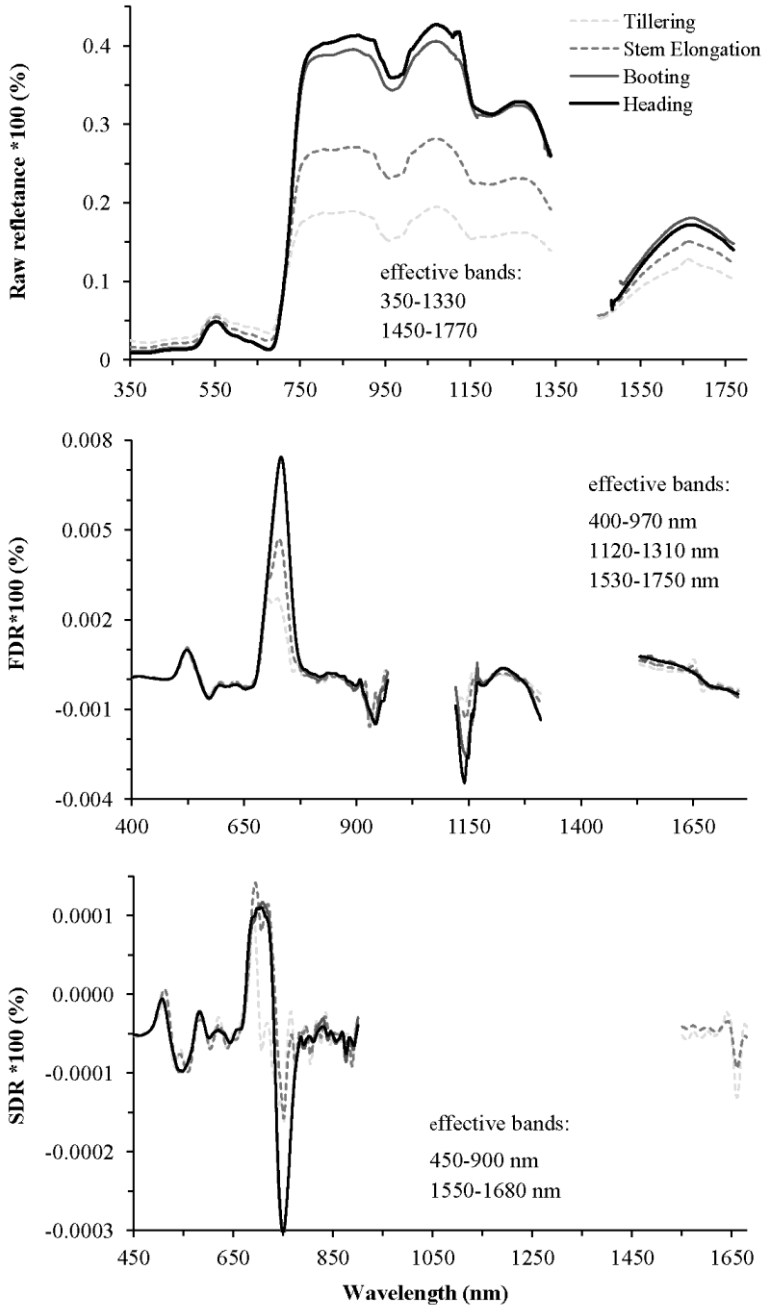

Fig. 7.4 Spectral reflectance, the first (FDR) and second-derivative of reflectance (SDR) at different growth stages: Tillering (T), Stem Elongation (SE), Booting (B), and Heading (H).

The inflection points of the raw reflectance illustrated peaks in the FDR spectra at 520 nm, 570 nm, 730 nm, 940 nm, 1140 nm, 1640 nm and 1670 nm (Fig. 7.4). Reflectance at 1640 nm and 1670 nm were peaks in the SWIR domain at the tillering and stem elongation stages. At booting and heading stages, reflectance at 1650 nm became an inflection point. The FDR clearly showed

differences between the early stages (tillering and stem elongation) and the later stages (booting and heading), especially in the NIR and SWIR domains. Compared to the tillering stage at the wavelength of 730 nm, the amplitude was three times higher at the booting and heading stages, and two times higher at stem elongation stage.

Much noise existed in the SDR's SWIR domain at the booting and heading stages. Consequently, that spectral region was completely excluded from further analysis (Fig. 7.4) for these two stages. Compared to the raw reflectance and FDR, the SDR was strongly characterized by a diverse pattern with peaks at different growth stages. In the VIS region, the SDR showed several peaks and inflection points, in about 20 nm steps. The red edge region was characterized by the largest increase and decrease in reflectance. Starting from 780 nm in the NIR domain, many peaks and inflection points alternated in 10 nm steps, which could be partially explained by background noises. At the tillering and stem elongation stages, two peaks occurred at 1640 and 1660 nm.

7.3.3 Estimating AGB with vegetation indices

7.3.3.1 Fixed band vegetation indices

The simulated GS-RVI had the strongest and weakest relationship with AGB at tillering and booting stages, respectively (Table 7.3). The simulated GS-NDVI had the strongest and weakest relationship with AGB at stem elongation and booting stage, respectively. Across growth stages, GS-NDVI was exponentially related to AGB, while GS-RVI performed best using a power model. However, GS-NDVI showed an obvious saturation effect even when AGB was less than 3 t ha^{-1} (Table 7.3 and Fig. 7.5), and the relationship between AGB and GS-RVI became more scattered as AGB increased (Fig. 7.5).

Table 7.3 Calibration results for the GS-RVI, GS-NDVI and soil adjusted VIs based on simulated GS wavelengths at different growth stages.

	Tillering (n=276)		Stem Elongation (n=254)		Booting (n=366)		Heading (n=366)		All stages (n=1262)	
Index	Model	R^2	Model	R^2	Model	R^2	Model	R^2	Model	R^2
GS-RVI	Q	0.48	P	0.47	P	0.08	E	0.25	P	0.68
GS-NDVI	Q	0.42	P	0.51	P	0.09	Q	0.25	E	0.64
SAVI	Q	0.31	P	0.54	Q	0.19	Q	0.04	E	0.58
MSAVI	Q	0.39	E	0.52	E	0.10	Q	0.23	E	0.60
OSAVI	Q	0.42	P	0.52	E	0.11	Q	0.21	E	0.64
MCARI	L	0.44	P	0.50	Q	0.13	E	0.11	P	0.69
MTVI1	Q	0.36	P	0.53	E	0.23	Q	0.04	E	0.66
MCARI2	Q	0.33	P	0.53	E	0.23	Q	0.04	E	0.65
MTVI2	L	0.27	E	0.43	E	0.24	L	0.05	E	0.60

E, L, P, Q denote exponential, linear, power, quadratic fit

7.3.3.2 Soil adjusted vegetation indices

In general, none of the selected soil adjusted VIs performed significantly better than GS-RVI or GS-NDVI, except at the stem elongation and booting stage (Table 7.3). At the stem elongation

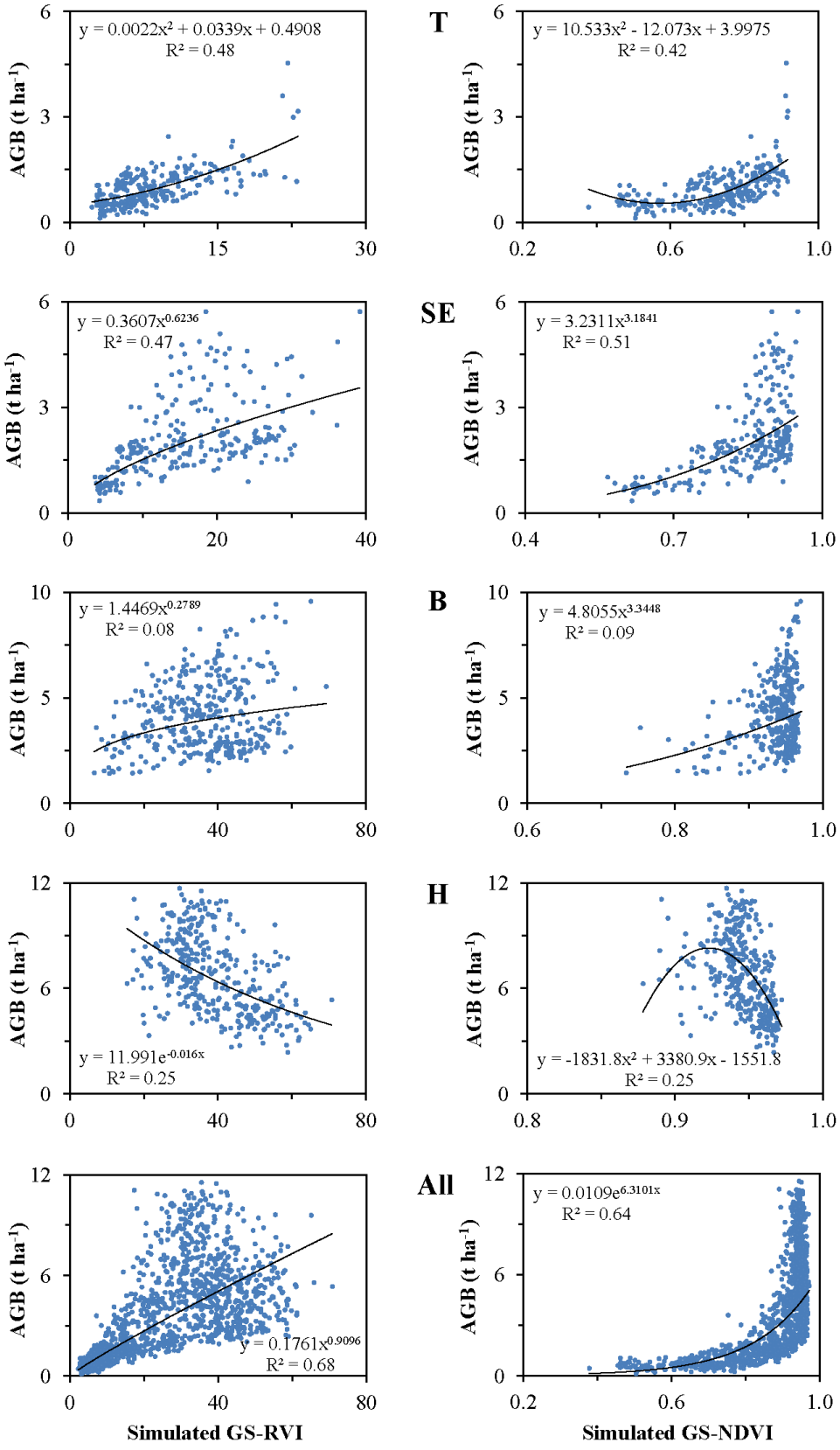

Fig. 7.5 Relationship between simulated GreenSeeker vegetation indices (RVI, left; NDVI, right) and aboveground biomass (AGB) at different growth stages. The simulated GreenSeeker bands were 660±10 nm (red) and 770±15nm (NIR). T, SE, B, H, and All represent tillering, stem elongation, booting, heading, and across all growth stages, respectively.

stage, indices such as SAVI, MTVI1 and MTVI2 slightly outperformed the GreenSeeker indices. All GS-RVI and GS-NDVI had the weakest relationships with AGB at the booting stage, while all the soil adjusted VIs again performed slightly better.

7.3.3.3 Optimized band combination vegetation indices

All the possible 2-band combinations were evaluated in the RVI and NDVI formulae for correlations with AGB at different growth stages (Table 7.4 and Fig. 7.6). The best RVI and NDVI were based on the same or similar bands at each of the four growth stages and explained the same or similar AGB variability at tillering, stem elongation, booting and heading stage, respectively. Across growth stages, the optimized RVI and NDVI were found from different bands, with NDVI performing slightly better. The optimized VIs used bands located in the SWIR domain at the stem elongation (R_{1484}, R_{1653}), booting (R_{1109}, R_{1160}) and across growth stages (R_{1112}, R_{1301}, R_{1581}, R_{1706}). At the tillering stage, the selected bands were from red edge (R_{729}, R_{730}) and NIR (R_{817}, R_{819}) regions, while at the heading stage, the selected bands were from green (R_{575}) and red edge (R_{696}) regions. These optimized narrow band RVIs and NDVIs consistently had higher R^2 than GS-RVI, GS-NDVI and the soil adjusted VIs (Tables 7.3 and 7.4).

The FDR- and SDR-based optimized VIs did not substantially improve the raw reflectance-based optimized VIs at any of the four growth stages (Table 7.4). The SDR-based optimized VIs performed worse than the FDR-based optimized VIs, except at the tillering stage when they performed similarly.

7.3.4 The OMNBR models

The 6-band OMNBR models produced better performance (Table 7.5) than optimized VIs (Table 7.4), except at the heading stage and across growth stages for optimized VIs. The largest improvement occurred at the booting stage, with OMNBR (Table 7.5) explaining 10% more variability of AGB than optimized VIs (Table 7.4). The OMNBR model explained 2% and 4% more variability of AGB at tillering and stem elongation stages, respectively.

The FDR-based 6-band OMNBR model did not make any improvements over raw reflectance-based 6-band OMNBR at the tillering stage, but could explain 4%, 6%, 8% and 5% more variability of AGB at the stem elongation, booting, heading and across growth stages, respectively (Table 7.5). The SDR-based 6-band OMNBR models did not further improve the FDR-based 6-band OMNBR models, expect at the stem elongation stage.

The FDR-based 6-band OMNBR model did not make any improvements over raw reflectance-based 6-band OMNBR at the tillering stage, but could explain 4%, 6%, 8% and 5% more variability of AGB at the stem elongation, booting, heading and across growth stages, respectively (Table 7.5). The SDR-based 6-band OMNBR models did not further improve the FDR-based 6-band OMNBR models, except at the stem elongation stage.

Table 7.4 Calibration results of optimized 2-band RVI and NDVI at different growth stages.

	Tillering (n=276)			Stem Elongation (n=254)			Booting (n=366)			Heading (n=366)			All stages (n=1262)		
Index	Bands	Model	R^2	Bands	Model	R^2	Bands	Model	R^2	Bands	Model	R^2	Bands	Model	R^2
RVI	$R_{(819,729)}$	Q	0.67	$R_{(1484,1653)}$	Q	0.69	$R_{(1160,1109)}$	P	0.34	$R_{(575,696)}$	P	0.51	$R_{(1112,1581)}$	E	0.66
NDVI	$R_{(730,817)}$	Q	0.67	$R_{(1484,1653)}$	L	0.68	$R_{(1109,1160)}$	E	0.34	$R_{(575,696)}$	E	0.51	$R_{(1301,1706)}$	E	0.74
RVI	$FDR_{(732,511)}$	Q	0.58	$FDR_{(1690,678)}$	Q	0.67	$FDR_{(497,680)}$	L	0.35	$FDR_{(532,695)}$	E	0.52	$FDR_{(702,526)}$	E	0.70
NDVI	$FDR_{(714,720)}$	E	0.59	$FDR_{(478,765)}$	Q	0.69	$FDR_{(497,680)}$	L	0.35	$FDR_{(532,695)}$	L	0.51	$FDR_{(526,702)}$	E	0.70
RVI	$SDR_{(711,671)}$	L	0.61	$SDR_{(1656,674)}$	Q	0.61	$SDR_{(991,1152)}$	E	0.31	$SDR_{(513,673)}$	E	0.43	$SDR_{(726,744)}$	E	0.55
NDVI	$SDR_{(715,756)}$	L	0.58	$SDR_{(553,1656)}$	Q	0.64	$SDR_{(853,1153)}$	E	0.28	$SDR_{(509,679)}$	E	0.44	$SDR_{(692,726)}$	E	0.64

E, L, P, Q denote exponential, linear, power, quadratic fit

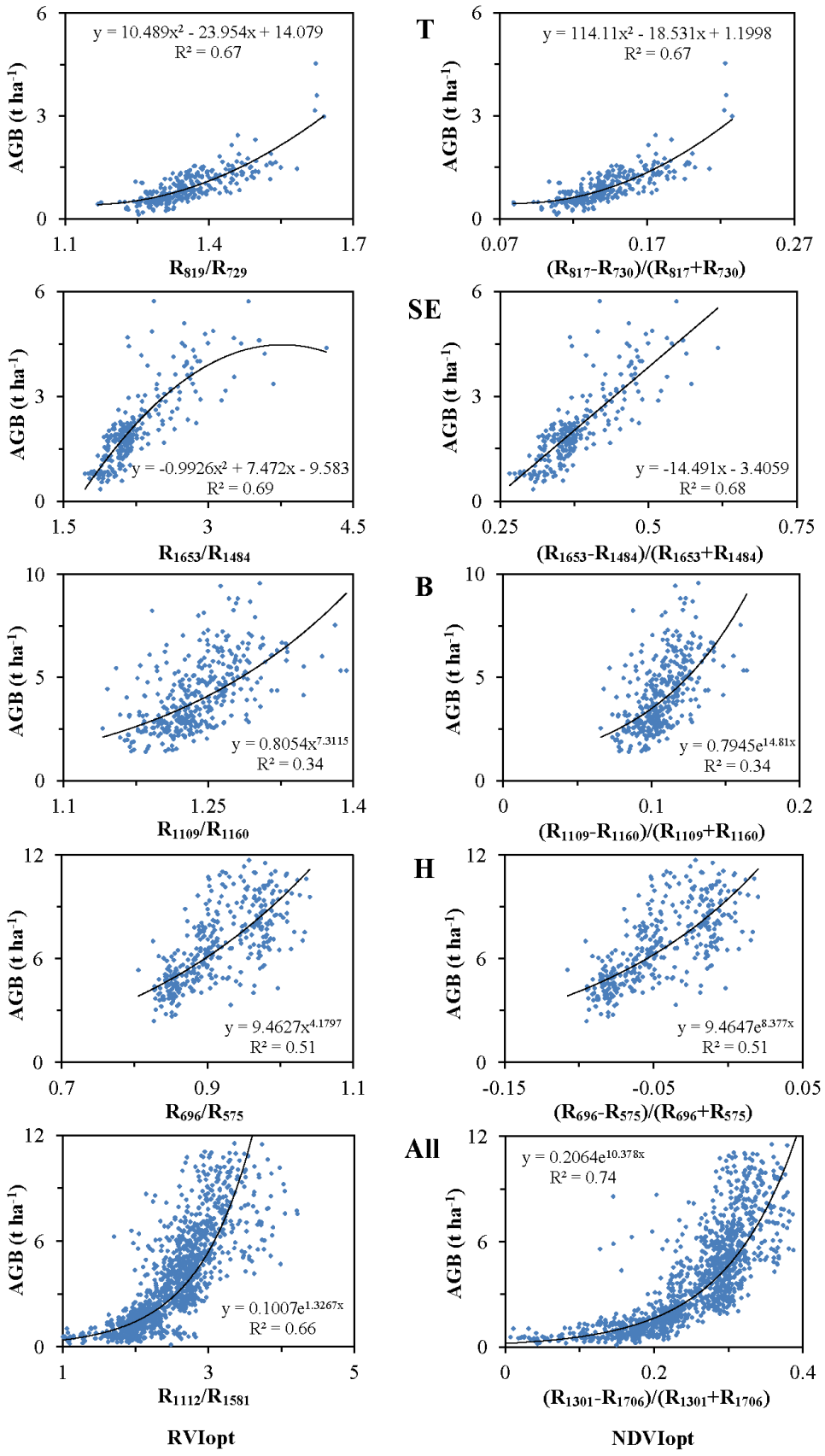

Fig. 7.6 Relationship between optimized RVI (left) and NDVI (right) and aboveground biomass (AGB) at different growth stages. T, SE, B, H, and All represent tillering, stem elongation, booting, heading and across all growth stages, respectively.

The largest improvement made with FDR was with the 1-band OMNBR model (Table 7.5). For example, R^2 of the 1-band OMNBR increased from 0.30 (raw reflectance) to 0.49 with FDR at the tillering stage. Corresponding increases at the stem elongation stage, booting stage, and heading stage occurred. The corresponding gain of R^2 ranged from 0.03 at the tillering and booting stages to 0.08 at the heading stage with 2–band OMNBR models, and from 0.01 at stem elongation to 0.09 at the heading stage with 3-band OMNBR models. With 4–6 band OMNBR models, FDR did not make any improvements at the tillering stage, but R^2 gained 0.03–0.04 at the stem elongation and 0.07–0.09 at the heading stage over raw reflectance. For the across growth stage models, FDR did not improve the 2-band OMNBR model, but increased R^2 by 0.03–0.06 for other models.

The SDR further increased the R^2 by 0.10–0.01 with 1–5-band OMNBR models over FDR, respectively, at the tillering stage. At the stem elongation stage, the SDR made no improvements relative to 1- and 2-band FDR-based OMNBR models, but R^2 increased slightly over other models. The SDR made no further improvements over FDR at booting, heading or across growth stages (Table 7.5).

7.3.5 Model validation

The validation results disclosed that at the tillering stage, the GS-RVI model explained 51% variability of AGB, with RMSE and RE being 0.35 t ha^{-1} and 37.2%, respectively (Table 7.6). The optimized VIs performed similarly better than GS-RVI, with R^2=0.62–0.63, RSME=0.31 and RE=32.8%. The FDR-based optimized VIs did not perform as well as raw reflectance-based optimized VIs. The SDR-based RVI performed the best (R^2=0.65, RMSE=0.30, RE=31.9%).

From stem elongation to the heading stage, GS-RVI and GS-NDVI became saturated, and failed to estimate AGB satisfactorily (Table 6). The raw reflectance-based optimized VIs consistently performed better than the fixed band RVI and NDVI, with R^2 being 0.50, 0.25–0.27 and 0.42 at the stem elongation, booting, and heading stage, respectively. At stem elongation and heading stages, the FDR-based optimized VIs performed slightly better than raw reflectance-based VIs, but SDR made no further improvements.

Across growth stages, GS-NDVI performed better than GS-RVI. The optimized RVI and NDVI using raw reflectance all performed better than GS-NDVI (Table 7.6). They explained 56–59% of the AGB variability with lower RE values compared to fixed band VIs. The best validated RVI and NDVI results based on raw reflectance are shown in Fig. 7.7. With rising AGB (>6 t ha^{-1}), the estimates yielded greater imprecision and they strongly scattered. The FDR- and SDR-based optimized VIs did not make any improvements over raw reflectance-based optimized VIs (Table 7.6).

The 6-band OMNBR models performed similarly as the best 2-band optimized VIs at tillering and heading stages, but significantly better at the stem elongation, booting and across growth stages (Tables 7.6 and 7.7). The FDR- and SDR-based 6-band OMBNR models made no remarkable improvements over the raw reflectance-based 6-band OMNBR models at any specific growth stage

Table 7.5 Calibration results for OMNBR models at different growth stages.

	Tillering (n=276)			Stem Elongation (n=254)			Booting (n=366)			Heading (n=366)			All stages (n=1262)		
Best	Factor type			Factor type			Factor type			Factor type			Factor type		
Model	R_i	FDR_i	SDR_i	R_i	FDR_i	SDR_i	R_i	FDR_i	SDR_i	R_i	FDR_i	SDR_i	R_i	FDR_i	SDR_i
1-Band															
R^2	0.30	0.49	0.59	0.36	0.59	0.53	0.22	0.34	0.20	0.27	0.32	0.28	0.51	0.55	0.19
Band	R_{939}	FDR_{751}	SDR_{712}	R_{775}	FDR_{766}	SDR_{554}	R_{786}	FDR_{944}	SDR_{744}	R_{687}	FDR_{676}	SDR_{631}	R_{929}	FDR_{630}	SDR_{770}
2-Band															
R^2	0.50	0.53	0.62	0.62	0.67	0.64	0.35	0.38	0.26	0.37	0.45	0.32	0.63	0.63	0.48
Band	R_{705}	FDR_{688}	SDR_{712}	R_{758}	FDR_{766}	SDR_{554}	R_{786}	FDR_{788}	SDR_{660}	R_{656}	FDR_{676}	SDR_{459}	R_{929}	FDR_{559}	SDR_{628}
	R_{939}	FDR_{751}	SDR_{1633}	R_{775}	FDR_{1181}	SDR_{1642}	R_{990}	FDR_{944}	SDR_{744}	R_{687}	FDR_{778}	SDR_{631}	R_{1707}	FDR_{630}	SDR_{770}
3-Band															
R^2	0.54	0.57	0.64	0.69	0.70	0.72	0.37	0.41	0.36	0.41	0.50	0.36	0.66	0.69	0.56
Band	R_{705}	FDR_{688}	SDR_{666}	R_{758}	FDR_{766}	SDR_{554}	R_{786}	FDR_{788}	SDR_{660}	R_{374}	FDR_{676}	SDR_{459}	R_{765}	FDR_{559}	SDR_{628}
	R_{822}	FDR_{732}	SDR_{712}	R_{775}	FDR_{866}	SDR_{772}	R_{990}	FDR_{818}	SDR_{744}	R_{656}	FDR_{778}	SDR_{631}	R_{929}	FDR_{630}	SDR_{673}
	R_{939}	FDR_{751}	SDR_{1633}	R_{1453}	FDR_{1181}	SDR_{1642}	R_{1326}	FDR_{944}	SDR_{835}	R_{687}	FDR_{870}	SDR_{783}	R_{1707}	FDR_{775}	SDR_{770}
4-Band															
R^2	0.66	0.62	0.65	0.70	0.73	0.75	0.39	0.44	0.45	0.42	0.53	0.40	0.68	0.74	0.58
Band	R_{705}	FDR_{565}	SDR_{666}	R_{758}	FDR_{766}	SDR_{554}	R_{786}	FDR_{788}	SDR_{660}	R_{374}	FDR_{676}	SDR_{459}	R_{765}	FDR_{559}	SDR_{628}
	R_{712}	FDR_{688}	SDR_{712}	R_{775}	FDR_{866}	SDR_{772}	R_{990}	FDR_{818}	SDR_{744}	R_{656}	FDR_{778}	SDR_{631}	R_{843}	FDR_{630}	SDR_{673}
	R_{822}	FDR_{732}	SDR_{871}	R_{1453}	FDR_{1181}	SDR_{1631}	R_{1167}	FDR_{875}	SDR_{835}	R_{687}	FDR_{787}	SDR_{783}	R_{929}	FDR_{775}	SDR_{770}
	R_{939}	FDR_{751}	SDR_{1633}	R_{1659}	FDR_{1240}	SDR_{1642}	R_{1326}	FDR_{944}	SDR_{862}	R_{938}	FDR_{870}	SDR_{805}	R_{1707}	FDR_{952}	SDR_{782}
5-Band															
R^2	0.67	0.65	0.66	0.72	0.75	0.77	0.43	0.47	0.48	0.48	0.55	0.43	0.70	0.75	0.60
Band	R_{678}	FDR_{565}	SDR_{666}	R_{758}	FDR_{416}	SDR_{554}	R_{786}	FDR_{408}	SDR_{521}	R_{374}	FDR_{676}	SDR_{459}	R_{765}	FDR_{559}	SDR_{628}
	R_{705}	FDR_{688}	SDR_{712}	R_{775}	FDR_{766}	SDR_{772}	R_{795}	FDR_{788}	SDR_{660}	R_{656}	FDR_{778}	SDR_{631}	R_{843}	FDR_{630}	SDR_{673}
	R_{712}	FDR_{732}	SDR_{811}	R_{1453}	FDR_{866}	SDR_{796}	R_{1109}	FDR_{818}	SDR_{744}	R_{687}	FDR_{787}	SDR_{668}	R_{911}	FDR_{775}	SDR_{717}
	R_{822}	FDR_{751}	SDR_{871}	R_{1659}	FDR_{1181}	SDR_{1631}	R_{1167}	FDR_{875}	SDR_{835}	R_{938}	FDR_{826}	SDR_{783}	R_{929}	FDR_{823}	SDR_{770}
	R_{939}	FDR_{848}	SDR_{1633}	R_{1667}	FDR_{1240}	SDR_{1642}	R_{1172}	FDR_{944}	SDR_{862}	R_{1719}	FDR_{870}	SDR_{805}	R_{1707}	FDR_{952}	SDR_{782}
6-Band															
R^2	0.69	0.66	0.66	0.73	0.77	0.80	0.44	0.50	0.49	0.49	0.57	0.45	0.71	0.76	0.67
Band	R_{637}	FDR_{565}	SDR_{666}	R_{665}	FDR_{416}	SDR_{554}	R_{362}	FDR_{408}	SDR_{521}	R_{374}	FDR_{676}	SDR_{459}	R_{765}	FDR_{559}	SDR_{628}
	R_{678}	FDR_{688}	SDR_{712}	R_{677}	FDR_{600}	SDR_{772}	R_{786}	FDR_{424}	SDR_{607}	R_{656}	FDR_{751}	SDR_{631}	R_{843}	FDR_{630}	SDR_{642}
	R_{705}	FDR_{732}	SDR_{811}	R_{758}	FDR_{766}	SDR_{796}	R_{795}	FDR_{788}	SDR_{660}	R_{687}	FDR_{778}	SDR_{668}	R_{911}	FDR_{775}	SDR_{673}
	R_{712}	FDR_{848}	SDR_{871}	R_{775}	FDR_{866}	SDR_{1584}	R_{1109}	FDR_{818}	SDR_{744}	R_{938}	FDR_{787}	SDR_{714}	R_{929}	FDR_{823}	SDR_{717}
	R_{822}	FDR_{1193}	SDR_{1557}	R_{1659}	FDR_{1181}	SDR_{1631}	R_{1167}	FDR_{875}	SDR_{835}	R_{1525}	FDR_{826}	SDR_{783}	R_{1485}	FDR_{868}	SDR_{770}
	R_{939}	FDR_{1695}	SDR_{1633}	R_{1667}	FDR_{1240}	SDR_{1642}	R_{1172}	FDR_{944}	SDR_{862}	R_{1719}	FDR_{870}	SDR_{805}	R_{1707}	FDR_{952}	SDR_{782}

Factor type: R_i=Raw reflectance, FDR_i=First-derivative of reflectance, SDR_i=Second-derivative of reflectance; All models with linear fit

Table 7.6 Validation results for selected vegetation indices at different growth stages.

	Tillering (n=93)			Stem Elongation (n=85)			Booting (n=123)			Heading (n=122)			All stages (n=423)		
Index	R^2	RMSE	RE	R^2	RMSE	RE	R^2	RMSE	RE	R^2	RMSE	RE	R^2	RMSE	RE
Simulated GreenSeeker vegetation index															
GS-RVI	0.51	0.35	37.2	0.24	0.81	40.1	0.05	1.61	36.8	0.14	1.97	29.4	0.34	2.24	57.3
GS-NDVI	0.49	0.36	38.0	0.28	0.77	38.3	0.05	1.60	36.7	0.21	1.84	27.4	0.45	2.11	54.1
Optimized vegetation index using raw reflectance															
RVI	0.63	0.31	32.8	0.50	0.64	31.9	0.25	1.69	38.7	0.42	1.61	24.0	0.56	1.78	45.5
NDVI	0.62	0.31	32.8	0.50	0.64	32.0	0.27	1.52	34.8	0.42	1.62	24.1	0.59	1.77	45.3
Optimized vegetation index using first derivative reflectance															
RVI	0.54	0.34	36.4	0.57	0.60	29.7	0.23	1.42	32.4	0.49	1.47	21.9	0.56	1.83	46.9
NDVI	0.56	0.34	35.8	0.57	0.61	30.1	0.22	1.43	32.7	0.49	1.47	21.9	0.58	2.01	51.3
Optimized vegetation index using second derivative reflectance															
RVI	0.65	0.30	31.9	0.50	0.66	33.0	0.23	2.30	52.6	0.39	1.64	24.5	0.37	2.12	54.1
NDVI	0.62	0.31	32.7	0.51	0.64	31.8	0.26	1.96	44.7	0.38	1.66	24.8	0.41	2.05	52.3

Table 7.7 Validation results for 6-band OMNBR, and FDR and SDR-based 6-band OMNBR models at different growth stages.

	Tillering (n=93)			Stem Elongation (n=85)			Booting (n=123)			Heading (n=122)			All stages (n=423)		
Best	Factor type			Factor type			Factor type			Factor type			Factor type		
Model	R_i	FDR_i	SDR_i	R_i	FDR_i	SDR_i	R_i	FDR_i	SDR_i	R_i	FDR_i	SDR_i	R_i	FDR_i	SDR_i
6-Band															
R^2	0.63	0.56	0.58	0.64	0.62	0.55	0.50	0.49	0.45	0.45	0.46	0.27	0.63	0.72	0.61
RMSE (t ha^{-1})	0.31	0.33	0.33	0.55	0.56	0.65	1.14	1.15	1.49	1.56	1.53	1.78	1.65	1.41	1.68
RE (%)	33.0	35.4	34.5	27.1	27.8	32.4	25.9	26.2	34.0	23.2	22.8	26.6	42.2	36.1	42.7

R_i= Raw reflectance, FDR_i= First-derivative of reflectance, SDR_i= Second-derivative of reflectance

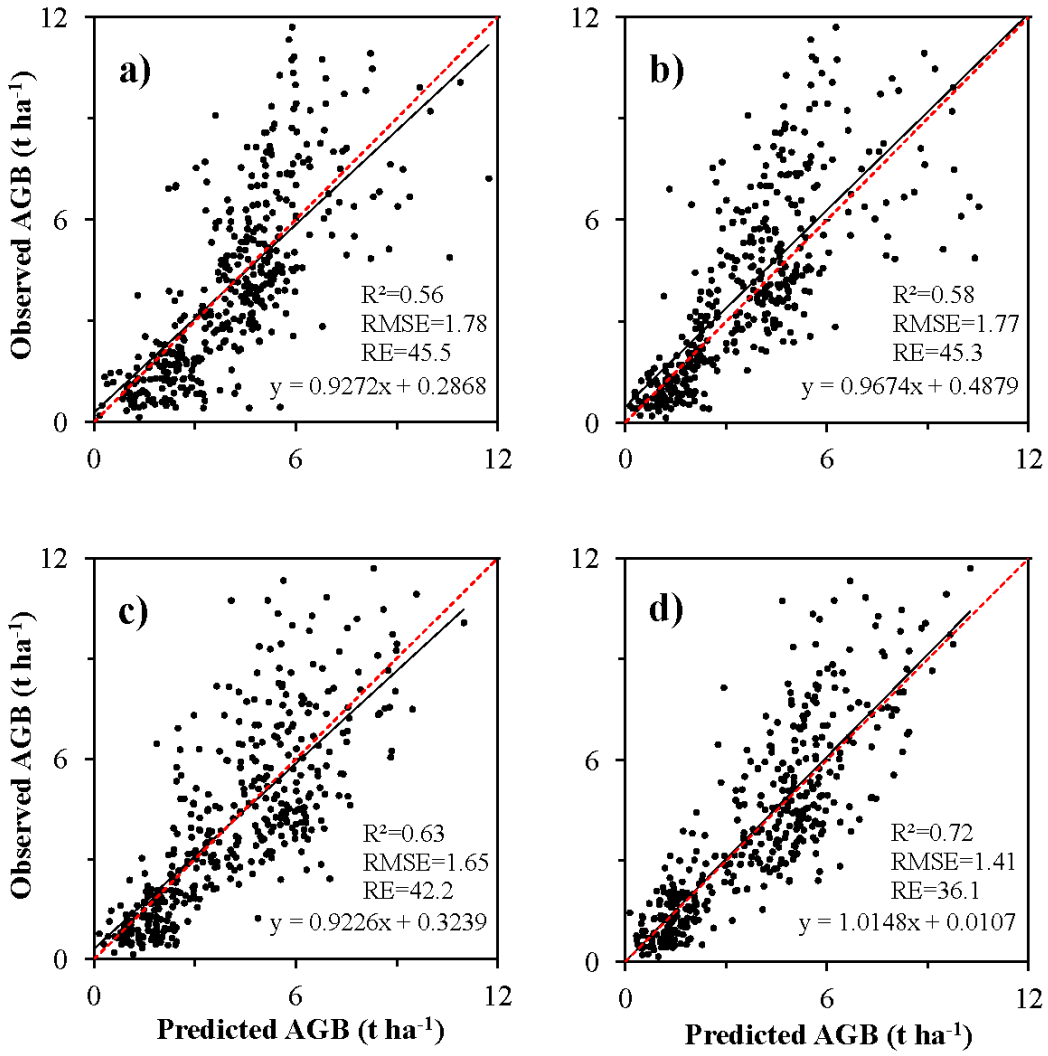

Fig. 7.7 Relationships between observed and predicted rice aboveground biomass across growth stages (n=423) using a) optimized RVI, b) optimized NDVI, c) 6-band OMNBR model, and d) first-derivative reflectance (FDR)-based 6-band OMNBR model. Black and red dash lines indicate the regression and the 1:1 line.

7.4 Discussion

7.4.1 Estimating rice AGB using vegetation indices

Growth stage has a strong influence on the sensitivity to different wavelengths and performance of VIs for estimating crop biophysical parameters (LI et al., 2010b, 2012; HATFIELD and PRUEGER, 2010; YU et al., 2013). Two important questions need to be addressed when using VIs to estimate rice biomass at different growth stages: (a) water and soil background influences before canopy closure; and (b) saturation of VIs above LAI of 2.5–3.0.

At the early growth stages (tillering and stem elongation), the rice canopy was not closed and the soil and water background could have a strong influence on canopy reflectance. The GS-RVI and GS-NDVI both use a red band and a NIR band, and explained approximately 50% of AGB variability

at most (Table 7.3). These results supported the findings that VIs calculated by simple combinations of visible and near infrared bands are sensitive to foliage density and biomass, but are susceptible to environmental and soil background effects, viewing geometry and soil view angles (SHIKADA and MIYAKITA, 1992; QI et al., 1994; RONDEAUX et al., 1996; YANG and CHEN, 2004). Our raw spectra in Fig. 7.4 indicate the rice plants were healthy, but exhibited different combinations of leaf chlorophyll and water absorption effects. In particular, the different reflectance responses in the NIR region of 750–1350 nm disclosed decreased water absorption from the tillering to the heading stage. None of the soil adjusted VIs performed better than the best performing GS VIs at the tillering stage, mostly due to the fact that water, rather than soil, dominates the background interference. CASANOVA et al. (1998) used reflectance values of water to replace reflectance of soil when calculating two VIs designed to eliminate soil background influences, because they found that reflectance of flooded soil was significantly lower than dry soil. More studies are needed to develop water adjusted vegetation indices to improve performance of spectral indices at early growth stages of rice.

The optimized NDVI and RVI, however, explained 62–68% of AGB variability at the early growth stages (Table 7.6). They used a red edge band (R_{729} or R_{730}) and a NIR band (R_{817} or R_{819}) at the tillering stage. This result agrees with the findings of HANSEN and SCHJOERRING (2003) on winter wheat, in which red edge bands were present in 87% of the selected indices related to variables based on quantities per unit surface area like AGB, LAI, leaf chlorophyll density and leaf N density. Even though their data were from early stem elongation to heading, their biomass range was similar to the range at the tillering stage in this study. In addition, the optimized VIs all used SWIR bands (R_{1484} and R_{1653}) at the stem elongation stage. The R_{1484} band was close to the band (R_{1445}) identified by THENKABAIL et al. (2004), which is sensitive to how much water is in a plant leaf. The R_{1653} band was close to R_{1650} as identified by SHIBAYAMA and AKIYAMA (1989) for estimating rice biomass. Our results indicate that with the appropriate bands (Red edge, NIR or SWIR), rice AGB at the tillering stage can be reliably estimated using either RVI or NDVI.

At later growth stages (booting and heading), the fixed band VIs performed significantly worse than at early stages. Fixed band NDVI obviously became saturated even at the stem elongation stage before biomass reached 3 t ha^{-1} or when fixed band NDVI was approximately 0.95. This differed slightly from LI et al. (2010a) who found that GS-NDVI saturated when winter wheat biomass reached 3.7 t ha^{-1} or when GS-NDVI reached about 0.8. This difference could be caused by the fact that our GS-NDVI was based on simulated GreenSeeker bands using passive hyperspectral data while LI et al. (2010a) used real GreenSeeker data. From the stem elongation through the heading stage, the NIR reflectance increased continuously while the red reflectance remained basically unchanged. Therefore, fixed band NDVI became saturated given the normalization effect embedded in the calculation formula of this index. Conversely, fixed band RVI with NIR/Red band ratio calculation avoided this saturation problem. The optimized VIs reduced the saturation effect using two far near-infrared (FNIR) bands (R_{1109} and R_{1160}) at the booting stage or two visible bands (R_{575} and R_{696}) at the heading

stage. These results support the observation that the saturation problems may be reduced by using wavelengths with similar penetration into the plant canopy (VAN NIEL and MCVICAR, 2004). They also confirm the importance of FNIR bands for estimating rice biomass as reported by previous researchers (SHIBAYAMA and MUNAKATA, 1986; SHIBAYAMA and AKIYAMA, 1989; THENKABAIL et al., 2004).

The optimized VIs did not perform as well as early growth stages. At the booting stage, the canopy is near closure; young panicles increase in size and cause the leaf sheath to bulge. It is already in reproductive stage dominated by grain development rather than plant growth (VAN NIEL and MCVICAR, 2004). In addition to saturation problem, interactions of stressed leaves and new leaves may also partly explain the poor performance of VIs at the booting stage. The stressed leaves due to low N application treatments are generally more compact and reflect less NIR light than healthy leaves of the same age, while young leaves are also more compact than mature leaves, and can result in differences in NIR reflectance outweighing those caused by N stresses (GAUSMAN, 1974). At the heading stage, panicles emerged from the sheath, making the canopy reflectance signal more complicated. The reflectance of rice panicles increased in the visible region but decreased in the NIR region with the growth stages (TANG et al., 2004). This may also explain the negative correlation between the AGB and the VIs at the heading stage shown in Fig. 7.5.

Across growth stages, the optimized RVI using one FNIR band (R_{1112}) and one SWIR band (R_{1581}) explained 66% of AGB variability. SHIBAYAMA and AKIYAMA (1989) also found that R_{1100} had the highest correlation with rice biomass for the whole season, either as single band, or in a VI format. The optimized NDVI using two SWIR bands (R_{1301} and R_{1701}) explained 74% AGB variability and possessed a much smaller saturation effect than fixed band NDVI.

The changes of sensitive spectral bands at different growth stages in response to crop growth and development demonstrate the limitations of fixed 2-band sensors like GreenSeeker. The good performances of the optimized RVI and NDVI revealed the importance of band selection for calculating VIs. HATFIELD and PRUEGER (2010) recommended different VIs for different crop growth parameters at different growth stages. Our results: (a) highlight the need to use different wavebands at different growth stages, and (b) illustrate the need to further explore the importance of FNIR and SWIR bands, which are missing from the current active crop canopy sensors developed for precision agriculture. These bands are particularly important for remote sensing of paddy rice to reduce the influence of water backgrounds. More studies are needed to evaluate different hyperspectral index optimization algorithms, especially those involving the combination of more than 2 wavebands (WANG et al., 2012; LI et al., 2013).

7.4.2 Estimating rice AGB with OMNBR models

The 6-band OMNBR models explained 5–9% more AGB variability than the best performing optimized VIs at the tillering through booting stage. The validation results revealed that the OMNBR

model performed similarly to the optimized VIs at the tillering and heading stages, but better at the stem elongation and booting stages. These results suggested that the OMNBR model may be a better approach than 2-band VIs, because they are simple to implement and more flexible in terms of band selection. Our results support the findings associated with wheat (XAVIER et al., 2006), maize (MIAO et al., 2009) and rice (YU et al., 2013). Our methods were quite robust against over-fitting. With increasing number of bands (>4 bands), the fitted models were slightly improved. In agreement with the findings of THENKABAIL et al. (2000), the over-fitting problem was avoided using the M/N evaluation criteria (M=number of bands, N=number of samples), with a ratio not exceeding 0.15–0.20. In this study, the ratio was always smaller (M/N<0.02) using 1–6 bands. Most of the studies using MLR indicate that ten or fewer wavelengths are required to obtain the best crop information (e.g., AGB or nitrogen) (THENKABAIL et al., 2000; HANSEN and SCHJOERRING, 2003; WANG et al., 2008; YU et al., 2013).

7.4.3 Derivative analysis

A major objective of this study was to determine if derivative spectra could further improve the performance of optimized VIs and OMNBR models using raw reflectance for estimating rice AGB at different growth stages. The results of this study indicate that the optimized VIs using FDR were worse at the tillering and stem elongation stages, similar or slightly better at the booting, heading, and across growth stages. On the other hand, the optimized VIs using either raw reflectance or FDR was consistently better than SDR-based VIs.

However, with OMNBR models, FDR made improvements over raw reflectance, with largest improvements for 1–2 band models. ZHANG et al. (2011) also found better model accuracy in estimating rice neck blasts by using 1 band FDR (R^2=0.58) than raw reflectance (R^2=0.47). SDR further improved performance of FDR-based OMNBR models with 1–5 bands at the tillering or 4–6 bands at the stem elongation stage. These results suggest that the derivative analysis can reduce the influence of soil and water background as well as illumination variability at early stages (tillering and stem elongation stages). At later growth stages (booting and heading stages), soil and water background may not be a main issue, but illumination variability could still be a problem, which could be partially addressed by incorporating FDR without the need of SDR. Across growth stages, FDR-based OMNBR models performed better than raw reflectance-based OMNBR models, which were better than SDR-based models in this study. HUANG et al. (2012) developed SMLR models using VIs as independent variables for estimating rice leaf folder damage at the booting stage. They also found that the FDR-based regression was better than using SDR, but none were better than models using raw reflectance at canopy level. In our study, we found no improvements with derivative analysis for optimized VIs either, possibly because the bands were less reactive to noise, and VIs may also be able to decrease influence of external factors (PALACIOS-ORUETA et al., 2012). Regression models using

individual bands would need derivative analysis, but the benefits of derivative analysis were reduced with more bands.

7.4.4 Importance of including data from farmers' fields for model calibration

For the optimized VIs and OMNBR models to be useful for practical management, they must be able to perform well in farmers' fields. It is important to include data that fully represents real farm conditions when developing prediction models if they are to be used to guide on-farm crop management. However, many studies have not validated their results using data from farmers' fields. For those who did, some have achieved good results (LI et al., 2012; CAO et al., 2013), and others did not (LI et al., 2008, 2010b; GNYP et al., 2013). In this study, we included data from farmers' fields in the calibration dataset, and we achieved consistent results for both calibration and validation, with validation results being only slightly worse than calibration for most cases.

7.5 Conclusions

This study evaluated the ability to improve estimating rice AGB at different growth stages relative to simulated fixed band GreenSeeker RVI and NDVI through the use of: (a) soil adjusted VIs, (b) optimized narrow band RVI, NDVI, and (c) OMNBR models. Raw reflectance, FDR and SDR comprised our primary data. We applied these techniques to controlled experimental field plots and to actual rice paddies managed by individual farmers. Some of the main findings are summarized below:

- Fixed band RVI performed best at the tillering stage while fixed band NDVI became saturated at the stem elongation stage when biomass was less than 3 t ha^{-1}.
- The selected soil adjusted VIs only performed slightly better than the fixed band RVI or NDVI at the stem elongation and booting stages.
- Optimized RVI and NDVI explained 17–27% more variation in AGB than the best performing fixed band RVI or NDVI for all four stages.
- The FDR- and SDR-based optimized VIs made no substantial improvements over raw reflectance-based optimized VIs.
- Raw reflectance-based 6-band OMNBR models explained 21–35% more AGB variation over the best performing fixed band RVI or NDVI.
- The FDR-based 6-band OMNBR models explained 4–8% more variability of AGB from stem elongation to heading stage than raw reflectance-based 6-band OMNBR models.
- The SDR-based 6-band OMNBR models performed slightly better than the FDR-based 6-band OMNBR model only at the stem elongation stage.

We conclude that with suitable band combinations, optimized RVI or NDVI can considerably improve estimation of rice AGB at different growth stages, without the need of derivative analysis.

Six-band OMNBR models can further improve the estimation of AGB over optimized 2-band VIs by incorporating SDR at stem elongation stage and FDR at other growth stages.

Acknowledgments

The authors would like to express their gratitude to many graduate students from China Agricultural University and University of Cologne for their field assistance. This research was financially supported by the Natural Science Foundation of China (31071859), the German Federal Ministry of Education and Research BMBF (CHN 08/051), National Basic Research Program (973-2009CB118606), Innovative Group Grant of Natural Science Foundation of China (31121062). The supports from the Qixing Modern Agriculture Development Center and Jiansanjiang Institute of Agricultural Science are highly appreciated. The authors also acknowledge the funding support of the CROP.SENSe.net project in the context of Ziel 2-Programms NRW 2007-2013 "Regionale Wettbewerbsfähigkeit und Beschäftigung (EFRE)" by the Ministry for Innovation, Science and Research (MIWF) of the state North Rhine Westphalia (NRW) and European Union Funds for regional development (EFRE) (005-1103-0018).

References * (*for chapter 7)

BECKER, B.L., LUSCH, D.P., QI, J., 2005. Identifying optimal spectral bands from in situ measurements of Great Lakes coastal wetlands using second-derivative analysis. Remote Sensing Environment, 97 (2), 238-248.

CAO, Q., CUI, Z., CHEN, X., KHOSLA, R., DAO, T.H., MIAO Y., 2012. Quantifying spatial variability of indigenous nitrogen management in small scale farming. Precision Agriculture, 13 (1), 45-61.

CAO, Q., MIAO, Y., WANG, H., HUANG, S., CHENG, S., KHOSLA, R., JIANG, R., 2013. Non-destructive estimation of rice plant nitrogen status with crop circle multispectral active canopy sensor. Field Crops Research, 154, 133-144.

CANTRELL, R.P., REEVES, T.G., 2002. The cereal of the world's poor takes center stage. Science, 296 (5565), 53-53.

CASANOVA, D., EPEMA, G.F., GOUDRIAAN, J., 1998. Monitoring rice reflectance at field level for estimating biomass and LAI. Field Crops Research, 55, 83-92.

DIACONO, M., RUBINO, P., MONTEMURRO, F., 2013. Precision nitrogen management of wheat. A review. Agronomy for Sustainable Development, 33 (1), 219-241.

DEMETRIADES-SHAH, T.H., STEVEN, M.D., CLARK, J.A., 1990. High resolution derivative spectra in remote sensing. Remote Sensing of Environment, 33 (1), 55-64.

GAUSMAN, H.W., 1974. Leaf reflectance of near-infrared. Photogrammetric Engineering and Remote Sensing, 40 (2), 183-191.

GNYP, M.L., YU, K., AASEN, H., YAO, Y., HUANG, S., MIAO, Y., BARETH, G., 2013. Analysis of crop reflectance for estimating biomass in rice canopies at different phenological stages. Photogrammetrie Fernerkundung Geoinformation, 2013 (4), 351-365.

HABOUDANE, D., MILLER, J.R., PATTEY, E., ZARCO-TEJADA, P.J., STRACHAN, I.B., 2004. Hyperspectral vegetation indices and novel algorithms for predicting green LAI of crop canopies: Modeling and validation in the context of precision agriculture. Remote Sensing of Environment, 90 (3), 337-352.

HANSEN, P.M., SCHJOERRING, J.K., 2003. Reflectance measurements of canopy biomass and nitrogen status in wheat crop using normalized difference vegetation indices and partial least squares regression. Remote Sensing of Environment, 86 (4), 542-553.

HARRELL, D.L., TUBAÑA, B.S., WALKER, T.W., PHILIPS, S.B., 2011. Estimating rice grain yield potential using normalized difference vegetation index. Agronomy Journal, 103 (6), 1717-1723.

HATFIELD, J.L., PRUEGER, J.H., 2010. Value of using different vegetative indices to quantify agricultural crop characteristics at different growth stages under varying management practices. Remote Sensing, 2, 562-578.

HEEGE, H.J., REUSCH, S., THIESSEN, E., 2008. Prospects and results for optical systems for site-specific on-the-go control of nitrogen-top-dressing in Germany. Precision Agriculture, 9 (3), 115-131.

HUANG, J., LIAO, H., ZHU, Y., SUN, J., SUN, Q., LIU, X., 2012. Hyperspectral detection of rice damaged by rice leaf folder. Computers and Electronics in Agriculture, 82, 100-107.

HUETE, A.R., 1988. A soil vegetation adjusted index (SAVI). Remote Sensing of Environment, 25 (3), 295-309.

IMANISHI, J., SUGIMOTO, K., MORIMOTO, Y., 2004. Detecting drought status and LAI of two Quercus species canopies using derivative spectra. Computers and Electronics in Agriculture, 43 (2), 109-129.

JORDAN, C.F., 1969. Derivation of leaf area index from quality of light on the forest floor. Ecology, 50, 663-666.

KNIPLING, E.B., 1970. Physical and physiological basis for the reflectance of visible and near-infrared radiation from vegetation. Remote Sensing of Environment, 1, 155-159.

KOBAYASHI, T., KANDA, E., KITADA, K., ISHIGURO, K., TORIGOE, Y., 2001. Detection of rice blast with multispectral radiometer and the potential of using airborne multispectral scanners. Epidemiology, 91 (3), 316-323.

LAWRENCE, R.C., RIPPLE, W.J., 1998. Comparisons among vegetation indices and bandwise regression in a highly disturbed, heterogeneous landscape: Mount St. Helens, Washington. Remote Sensing of Environment, 64 (1), 91-102.

LEMAIRE, G., JEUFFROY, M.H., GASTAL, F., 2008. Diagnosis tool for plant and crop N status in vegetative stage. Theory and practices for crop N management. European Journal of Agronomy, 28 (4), 614-624.

LI, F., GNYP, M.L., JIA, L. MIAO, Y., YU, Z., KOPPE, W., BARETH, G., CHEN, X., ZHANG, F., 2008. Estimating N status of winter wheat using a handheld spectrometer in the North China Plain. Field Crops Research, 106 (1), 77-85.

LI, F., MIAO, Y., CHEN, X., ZHANG, H., JIA, L., BARETH, G., 2010a. Estimating winter wheat biomass and nitrogen status using an active crop sensor. Intelligent Automation and Soft Computing, 16 (6), 1219-1228.

LI, F., MIAO, Y., HENNIG, S.D., GNYP, M.L., CHEN, X., JIA, L., BARETH, G., 2010b. Evaluating hyperspectral vegetation indices for estimating nitrogen concentration of winter wheat at different growth stages. Precision Agriculture, 11 (4), 335-357.

LI, F., MISTELE, B., HU, Y., YUE, X., MIAO, Y., CHEN, X., CUI, Z., MENG, Q., SCHMIDTHALTER, U., 2012. Remotely estimating aerial N status of phenologically differing winter wheat cultivars grown in contrasting climatic and geographic zones in China and Germany. Field Crops Research, 138, 21-32.

LI., F., MISTELE, B., HU, Y., CHEN, X., SCHMIDHALTER, U., 2013. Comparing hyperspectral index optimization algorithms to estimate aerial N uptake using multi-temporal winter wheat datasets from contrasting climatic and geographic zones in China and Germany. Agriculture and Forest Meteorology, 180, 44-57.

LIU, Z., WU, H., HUANG, J., 2010. Application of neural networks to discriminate fungal infection levels in rice panicles using hyperspectral reflectance and principal components analysis. Computers and Electronics of Agriculture, 72 (2), 99-106.

MARTIN, R.D., HEILMAN, J.L., 1986. Spectral reflectance patterns of flooded rice. Photogrammetric Engineering and Remote Sensing, 52 (2), 1885-1890.

MIAO, Y., MULLA, D.J., RANDALL, G.W. VETSCH, J.A., VINTILA, R., 2009. Combining chlorophyll meter reading and high spatial resolution remote sensing images for in-season site-specific nitrogen management of corn. Precision Agriculture, 10, 45-62.

NORMILE, D., 2008. Reinventing rice to feed the world. Science, 321 (5887), 330-333.

PALACIOS-ORUETA, A., HUESCA, M., WHITING, M.L., LITAGO, J., KHANNA, S., GARCIA, M., USTIN, S.L., 2012. Derivation of phonological metrics by function fitting to time-series of Spectral Shape Indexes AS1 and AS2: Mapping cotton phonological stages using MODIS time series. Remote Sensing of Environment, 126, 148-159.

PATEL, N.K., SINGH, T.P., SAHAI, B., PATEL, M.S., 1985. Spectral response of rice crop and its relation to yield and yield attributes. International Journal of Remote Sensing, 6 (5), 657-664.

PENG, Y., GITELSON, A.A., 2011. Application of chlorophyll-related vegetation indices for remote estimation of maize productivity. Agricultral and Forest Meteorology, 151(9), 1267-1276.

QI, J., CHEHBOUNI, A., HUETE, A.R., KERR, Y.H., SOROOSHIAN, S., 1994. A modified soil adjusted vegetation index. Remote Sensing of Environment, 48 (2), 119-126.

RONDEAUX, G., STEVEN, M., BARET, F., 1996. Optimization of soil-adjusted vegetation indices. Remote Sensing of Environment, 55 (2), 95-107.

ROUSE, J.W., HAS, R.H., SCHELL, J.A., DEERING, D.W., 1974. Monitoring vegetation systems in the Great Plains with ERTS. -Third ERTS Symposium, NASA Sp-351, Vol. 1, NASA, pp 309-317.

SAMBORSKI, S.M., TREMLAY, N., FALLON, E., 2009. Strategies to make use of plant sensors-based diagnostic information for nitrogen recommendations. Agronomy Journal, 101 (4), 800-816.

SAVITZKY, A., GOLAY, M.J.E., 1964. Smoothing and differentiation of data by simplified least squares procedures. Analytical Chemistry, 36 (8), 1627-1639.

SHIBAYAMA, M., MUNAKATA, K., 1986. A spectroradiometer for field use. III. A comparison of some vegetation indices for predicting luxuriant paddy rice biomass. Japanese Journal of Crop Science, 55 (1), 47-52.

SHIBAYAMA, M., AKIYAMA, T., 1989. Seasonal visible, near-infrared and mid-infrared spectra of rice canopies in relation to LAI and above-ground dry phytomass. Remote Sensing of Environment, 27 (2), 119-127.

SHIKADA, K., MIYAKITA, K., 1992. Effects of solar and view angles on reflectance for paddy field canopies. Geocarto International, 7 (3), 9-17.

TANG, Y., HUANG, J., WANG, R., 2004. Change law of hyperspectral data in related with chlorophyll and carotenoid in rice at different developmental stages. Rice Science, 11, 274-282.

THENKABAIL, P.S., SMITH, R.B., PAUW, E.D., 2000. Hyperspectral vegetation indices and their relationship with agricultural crop characteristics. Remote Sensing of Environment, 71 (2), 152-182.

THENKABAIL, P.S., ENCLONA, E.A., ASHTON, M.S., VAN DER MEER, B., 2004. Accuracy assessements of hyperspectral waveband performance for vegetation analysis applications. Remote Sensing of Environment, 91 (3-4), 354-376.

TSAI, F., PHILPOT, W., 1998. Derivative analysis of hyperspectral data. Remote Sensing Environment, 66 (1), 41-51.

TUBAÑA, B., HARRELL, D., WALKER, T., TEBOH, J., LOFTON, J., KANKE, Y., PHILIPS, S., 2011. Relationships of spectral vegetation indices with rice biomass and grain yield at different sensor view angles. Agronomy Journal, 103 (5), 1405-1413.

VAN NIEL, T.G., MCVICAR, T.R., 2004. Current and potential uses of optical remote sensing in rice-based irrigation systems: a review. Australian Journal of Agricultural Research, 55 (2), 155-185.

WANG, Y., YANG, Y., 2001. Effects of agriculture reclamation on hydrologic characteristics in the Sanjiang Plain. Chinese Geographical Science, 11 (2), 163-167.

WANG, F., HUANG, J., WANG, X., 2008. Identification of optimal hyperspectral bands for estimation of rice biophysical parameters. Journal of Integrative Plant Biology, 50 (3), 291-299.

WANG, W., YAO, X., YAO., X.F., TIAN, Y.C., LIU, X. J., NI, J., CAO, W.X., ZHU., Y., 2012. Estimating leaf nitrogen concentration with three-band vegetation indices in rice and wheat. Field Crops Research, 129, 90-98.

XAVIER, A.C., RUDORFF, B.F.T., MOREIRA, M.A., ALVARENGA, B.S.A., DE FREITAS, J.G., SALOMON, M.V., 2006. Hyperspectral field reflectance measurements to estimate wheat grain yield and plant height. Scientia Agricola, 63 (2), 130-138.

XING, B., DUDAS, M.J., ZHANG, Z., QI, X., 1994. Pedogenetic characteristics of albic soils in the three river plain, Heilongjiang Province (In Chinese with English abstract). Acta Pedologica Sinica, 31(1), 95-104.

YANG, C.M., CHEN, R.K., 2004. Modeling rice growth with hyperspectral reflectance data. Crop Science, 44 (4), 1283-1290.

YAO, Y., MIAO, Y., HUANG, S., GAO, L., MA, X., ZHAO, G., JIANG, R., CHEN, X., ZHANG, F., YU, K., GNYP, M.L., BARETH, G., LIU, C., ZHAO, L., YANG, W., ZHU, H., 2012. Active canopy sensor-based precision N management strategy for rice. Agronomy for Sustainable Development, 32 (4), 925-933.

YU, K., LI, F., GNYP, M.L., MIAO, Y., BARETH, G., CHEN, X., 2013. Remotely detecting canopy nitrogen concentration and uptake of paddy rice in the Northeast China Plain. ISPRS Journal of Photogrammetry and Remote Sensing, 78, 102-115.

YUAN, Z., LU, X., ZHOU, J., 2006. Cumulative effects of different cultivating patterns on properties of albic soil in Sanjiang Plain. Chinese Geographical Science, 16, 133-140.

ZHANG, H., HU, H., ZHANG, X., ZHU, L., ZHENG, K., JIN, Q., ZENG, F., 2011. Estimation of rice neck blasts severity using spectral reflectance based on BP-neural network. Acta Physiologiae Plantarum, 33, 2461-2466.

ZHAO, G., MIAO, Y., WANG, H., SU, M., FAN, M., ZHANG, F., JIANG, R., ZHANG, Z., LIU, C., LIU, P., MA, D., 2013. A preliminary precision rice management system for increasing both grain yield and nitrogen use efficiency. Field Crops Research, 154, 23-30.

8. Discussion

In the context of food security and environment protection, the monitoring and estimating of biomass and plant nitrogen using hyperspectral remote sensing and proximal sensing play a central role. This dissertation includes four qualitative methods for model development based on hyperspectral data. The methods are explained in four published papers and one accteped paper for publication that show the model improvements step by step. Because at least two methods were used in most of the published papers and the one accepted paper, this chapter follows the diverse methods stepwise: vegetation indices and their limits, the potential of two-band combinations and, furthermore, the potential of three and four-band combinations, OMNBR and MLR, and the potential of derivatives of reflectance. The results in chapters 3–7 highlight the stepwise improvements of these methods and their advantages and disadvantages. Thus, this chapter focuses on indicating the improvements of the methods and comparing the improvements with published studies. In addition, several problems occurred and caused the diverse methods and their models to be prone to unexplained variances, which are uncertainties induced by model up-scaling, the importance of single growth stages and growing season, effects of sample size, and by diverse calibration/validation methods. Furthermore, topics such as potential errors in hyperspectral data collection and unexplained biomass and plant nitrogen variability indicated in hyperspectral reflectance are discussed. Of note, models are simplified representations of reality based on observations.

8.1 Limits of published vegetation indices

Estimating biophysical and biochemical parameters by vegetation indices (VIs) was solely a powerful tool for analyses of hyperspectral and multispectral data 20–30 years ago. VIs gained widespread popularity because of the benefit of remote sensing. However, VIs are dependent on green plant quantity, such as green biomass or leaf area index, for extracting a signal from the canopy reflectance (PINTER et al., 2003). Once the peak quantity is reached, the VIs tend to saturate (SELLERS, 1985; GAO et al., 2000; HABOUDANE et al., 2004; MUTANGA and SKIDMORE, 2004). More recently, increasingly powerful computers and new techniques of hyperspectral analysis have offered new opportunities and a better explanation of the predicted parameters while avoiding saturation effects. A few of the techniques are discussed in the following chapters of 8.2–8.4. However, many studies remain focused on the published broad band VIs and their comparison or on new broad or narrow band VIs developments (e.g., HATFIELD and PRUEGER, 2010; INOUE et al., 2012; YAO et al., 2013; LI et al., 2014). These VIs often utilize a simple equation and may be quickly calculated by end-users. Current remote sensing software (e.g., ENVI, ERDAS) has implemented tools for broad band VIs calculation, such as NDVI or SR, particularly for selected bands from satellite images, to facilitate analysis. Some of these VIs were selected and were used for comparison in chapters 3–7.

All chapters confirm the well-known saturation problem of fixed broad band VIs that normally occurs before the heading stage. Based on broad band VIs, LI et al. (2008) found that RVI performed

best for estimating plant nitrogen across a two year growing season. However, KOPPE et al. (2010) could not reproduce those results using RVI for plant nitrogen from Hyperion data across the 2006 growing season. In the case of biomass estimation, the broad band VIs, such as NDVI and RVI, saturated when the observed biomass was less than 5 t/ha (see GNYP et al., 2014b). Therefore, broad band VIs were less suitable for estimating biomass in rice. Once the rice plant cover became more dense at the stem elongation stage and the biomass reached 3 t/ha, the broad band VIs responded weaker than for wheat. This finding is in agreement with VAN NIEL and MCVICAR (2004), who observed decreasing NDVI values in a rice canopy shortly after panicle initiation. GNYP et al. (2014a) concluded in chapter 7 that VI calculations based on a simple combination of VIS and NIR bands are sensitive to biomass but are susceptible to environmental and soil background effects. In particular, when measurements are obtained with low variability in backgrounds, VIs are more appropriate for assessing LAI than for estimating biomass (SERRANO et al., 2000; ROYO and VILLEGAS, 2011). In addition, rice reflectance was affected by leaf chlorophyll and water absorption. In particular, the reflectance response in the region of 750–1350 nm indicated decreased water absorption at the observed growth stages. At later stages (booting and heading), the use of broad band VIs was impractical. Both the rice and the wheat studies confirmed the recommendation of different VIs at different growth stages, as noted by HATFIELD and PRUEGER (2010).

To avoid saturation across a growing season, in chapter 5 (see GNYP et al., 2014b), a newly developed VI, GnyLi, was introduced for biomass estimation. This VI had a pronounced performance but was only fitted by one year's field dataset of winter wheat. The developed estimation model was successfully applied to Hyperion satellite data for two growing seasons in 2006 and in 2007. The GnyLi's relation to biomass was tested against fourteen VIs and against five VIs in detail. Generally, newly introduced VIs should be compared with many published and related VIs. To test their transferability to other sites, crops, and scales, additional analyses are needed. In the past, several new VIs (e.g., MSAVI, NDWI) were introduced, followed by comprehensive applications on diverse crops and study sites.

8.2 Potential of two- to four-band combinations

As mentioned in the method description and in the chapter above, the best band combinations significantly outperformed the broad band VIs and avoided an early saturation. The band combinations are useful for developing new VIs, and their bands are mostly suitable for the investigated sites, crops, cultivars, and growth stages. Since THENKABAIL et al. (2000)'s successful outcome of all possible band combinations of a half range spectrum, many studies have followed this approach and have made an easy practice of simple broad band VIs (NDVI, RVI, DVI) for many remote sensing applications. Scanning the best band combinations has become a standard and widely applied approach for the discrimination of hyperspectral data. This method is required by researchers for studies focusing on VIs.

KOPPE et al. (2010) and GNYP et al. (2013, 2014a) studied band combinations (see chapters 4, 6, 7) and compared these combinations using simple broad band or narrow band VIs. Invariably, the explained variability in biomass, plant nitrogen, or plant height was 25–50% higher when optimized band combinations were used (see KOPPE et al., 2010; GNYP et al., 2014a). The differences are most distinctive when the band combinations were derived from Hyperion imagery across a growing season (see KOPPE et al., 2010; GNYP et al., 2014b) or from a field spectrometer at single growth stages, particularly at the booting and heading stages (see GNYP et al., 2014a). Each combination was only efficient for the selected stage or season. Thus, the band combination of NRI introduced by KOPPE et al. (2010) was similar to the proposed bands (±15 nm) for the Normalized Difference Water Index (NDWI) by GAO (1996). NRI bands were found to be sensitive to dry matter, whereas NDWI is sensitive to liquid water. In addition, the band combination derived from 2006 Hyperion imageries was valid for 2007 Hyperion imageries (KOPPE et al., 2012) and was recalibrated using field reflectance data (see chapter 6, GNYP et al., 2014b). Critically, using single dates across one season leads to a linear regression model. However, the standard deviation indicated precise predictability. The band combination derived from Hyperion was not tested on single growth stages.

Moreover, the band combination for wheat and rice studies indicated the importance of the NIR and SWIR domains for biomass estimation. This finding is in agreement with many other studies related to the biomass of diverse plants (DARVISHZADEH et al., 2008; PSOMAS et al., 2011; MARIOTTO et al., 2013, FU et al., 2014). Thus, the biophysical and biochemical changes during crop growth affected the results of band selection. For winter wheat, the detected SWIR bands were sensitive to lignin and starch (KUMAR et al., 2006), whereas for rice, the bands were mainly ingenious to plant moisture and biomass (THENKABAIL et al., 2011). In contrast, the best correlated bands to rice biomass at the heading are in the green and NIR regions. This finding might be caused by the flowering of some plants. Because the flowering proceeds from the top of the panicle downwards (ZADOCKS et al., 1974), the light yellow or white color of the flowers and dark green color of the panicle axis may falsify the canopy reflectance. In the case of estimating plant nitrogen of rice, the SWIR domain was less important in the band combinations than the VIS and NIR domains (YU et al., 2013). However, band combinations for winter wheat and rice are not comparable, as shown in both studies. To improve the biomass and plant nitrogen estimation, three or four-band combinations may be helpful.

TIAN et al. (2011) indicated the potential of a three-band combination, although these authors did not systematically calculate all possible combinations. In addition, the GnyLi index, which was introduced by GNYP et al. (2014b), demonstrated a further development of four-band combinations. Its investigation highlighted the time-consuming process of band selections and the impossible visualization of the fourth dimension. Hence, currently, most available studies still focus on two-band combinations.

8.3 Performance of OMNBR and MLR

OMNBR and MLR follow a linear regression, which involves several bands (THENKABAIL et al., 2000; XAVIER et al., 2006). OMNBR and MLR outperformed the best two-band combinations in estimating biomass when at least four bands were used. Moreover, two or more feature wavebands by MLR improve the sensitivity to biomass than broad band VIs. This finding was consistent at each single stage and across all stages. The rice study highlighted and confirmed known problems, such as over-fitting and collinearity of redundant bands (see chapters 6–7). Hence, the effective band number for multiple regressions was limited to six. Six bands explained 2–10% more biomass variability in model fitting at the tillering, stem elongation, and booting stages but 2–3% less at the heading and across all stages (see chapter 7, GNYP et al., 2014a) than two bands based combinations. Compared with band combinations, the validated OMNBR models performed more accurately with lower RMSE and RE. This result conforms to the findings by XAVIER et al. (2006), who compared OMNBR-based and models based on the best band combination for estimating the yield and plant height of winter wheat. A comparison of two different calibration and validation approaches indicated that the MLR models were more robust with randomly pooled and then divided subsets, including observations from experiments and farmers in calibration and validation. In comparison, MLR models fitted by experimental data and tested by farmers' data were more inaccurate (GNYP et al., 2013).

YU et al. (2013) tested OMNBR models for rice nitrogen estimation at the same study site and found that these models improved the explained variability of approximately 18% before the heading and 3% after the heading compared with the best two-band combination models. RYU et al. (2011) explained 93% of plant nitrogen variability using an 8-band MLR model, highlighting annual changes and the importance of multiyear observations. Their single year-based MLR models showed a significantly weaker performance (R^2<0.70) and varied greatly in selected bands. In aforementioned studies, the detected bands in the OMNBR and MLR models were mostly in the VIS, red-edge, and SWIR for plant nitrogen detection and in the red-edge, NIR, and SWIR domains for biomass estimation. This finding is comparable to the results of WANG et al. (2008), who tested fresh and dry biomass for rice with 1–4 bands based on MLR but is different from YANG and CHEN (2004), who identified green bands in their MLR models for biomass estimation. Additionally, PSOMAS et al. (2011) also compared diverse methods for estimating grass biomass. These authors noted similar results that indicated a gradually increasing accuracy of fitted models based on broad band VIs (R^2<0.30), band combinations (R^2=0.65), and a four band MLR (R^2=0.86).

Some researchers reported that Principle Component Analysis (PCA) may improve the MLR models. PCA was additionally tested for the study by GNYP et al. (2014a) but is not included in the published paper because the PCA result was not promising. The PCA did not explain more biomass variability. TAKAHASHI et al. (2000) and YI et al. (2007) tested a MLR model against PCA for estimating biomass and plant nitrogen in rice. These authors found that PCA was less useful and required more components than MLR to achieve higher predictability. More detailed analysis is

required to test whether PCA may improve MLR models based on the same or a higher number of components. MLR and PCA are often compared with PLSR. YU et al. (2014) indicated some improvements by PLSR in biomass estimation across stages in a single year dataset. Several studies demonstrated that PLSR performed at least similarly (WANG et al., 2011) or clearly outperformed MLR (TAKAHASHI et al., 2000; ZHANG et al., 2012b). Although a method comparison was not performed, it might be assumed that such a comparison will confirm the published outcomes.

OMNBR or MLR was solely tested for rice data and not for wheat. The preliminary MLR analysis for wheat, which is not presented in the result chapters, indicated a high potential of estimating biomass with a highly explained variability (86%) using 2 bands and 4 bands (>93%) mainly in the NIR domain. This finding is in agreement with MARIOTTO et al. (2013), who used a 6-band SMLR model to explain biomass variability of wheat (96%); however, their study based on a small sample size (n=24). The results of this dissertation implied that hyperspectral remote sensing and proximal sensing are more efficient for wheat than for rice crops. The reason for this efficiency is because of the different morphologies of the two crops, which will be discussed later in chapter 8.9. Thus, further analysis must compare the 4-band MLR with the proposed GnyLi for winter wheat.

Generally, end-users and data availability (satellite data) influence the decision as to whether two or more bands may be used. The wheat and rice studies showed that OMNBR or MLR models require more than two bands to achieve similar or better performance than the method based on band combinations.

8.4 Potential of derivatives of reflectance

Derivative spectra analysis is an established technique for eliminating background signals and for reducing spectral variations due to skylight (DEMETRIADES-SHAH et al., 1990; TSAI and PHILPOT, 1998; BECKER et al., 2005). Derivatives of reflectance were tested as independent variables in band combinations following the NDVI and RVI equations and in OMNBR models. In chapter 7 (see GNYP et al., 2014a), the first derivative of reflectance (FDR) models performed similar to those models based on the raw reflectance, whereas the second derivative of reflectance (SDR) was not beneficial in band combination calculations. Nevertheless, the derivatives of reflectance were more suitable to estimate biomass than the tested VIs based on broad and narrow bands. Positive outcomes of biomass estimation were observed in SDR-based OMNBR models with 2–6 bands at the stem elongation and in FDR-based OMNBR models with 1–6 bands at other and across all stages, with some exceptions at the tillering. The validation results indicated that FDR-based OMNBR models generally yielded higher accuracy with lower RMSE and RE than the investigated models based on other methods. FDR is beneficial in detecting reflectance peaks in red-edge, NIR, and SWIR regions.

FENG et al. (2008) achieved comparable results for estimating plant nitrogen of wheat leaves, with a model accuracy of 87% by FDR-based VIs, compared with accuracies of less than 86% by reflectance-based VIs. MIPHOKASAP et al. (2011) showed a better estimation of plant nitrogen in

sugarcane using FDR-based MLR models than band combinations. In addition, this study is in conformity with GROSSMANN et al. (1996) and FENG et al. (2008), who revealed a better performance of FDR in OMNBR or MLR than raw reflectance or SDR. GROSSMANN et al. (1996) investigated several biochemical parameters based on dried leaves of diverse vegetation types. These authors reported the highest benefit of FDR for estimating cellulose or lignin and of SDR for estimating biomass and water content. In addition to using derivatives in band combinations, OMNBR, and MLR models, derivatives have become popular in new VIs development (e.g., FENG et al., 2008).

In contrast to many published studies that reported effective bands in the range of 400-900 nm (LIU et al., 2010; HUANG et al., 2012), the NIR and SWIR did not appear noisy in the rice spectra. Similar to GNYP et al. (2014a)'s study, ASNER (1998) showed clear derivative spectra in the SWIR domains of 1000–1350 nm and 1500–1850 nm. This finding and the positive outcomes in biomass estimation support the hypothesis that derivatives may decrease background signals, although spectra of water, soil, and plant were not separately investigated. However, KOKALY and CLARK (1999) applied a normalized band depth method to diminish background signals, and their MLR models based on this method outperformed FDR and SDR-based MLR models. The derivatives could reduce the impact of light variation, as reported by YAO et al. (2012) in their soybean study. Additional analysis is required to improve the impact of light variation in this study.

Despite their advantages, derivatives of reflectance have to be critically regarded because the spectra are manipulated by diverse pre-processing steps, such as averaging, smoothing, and calculation of derivatives (see chapter 7). GROSSMANN et al. (1996) criticized these pre-processing steps of hyperspectral data as statistical manipulations. In particular, the smoothing process clearly changes the spectra. Depending on the frame size of data points and on polynomial degree of the spline function, some peaks in the reflectance may lose their impact or change their position in the spectrum. With a higher frame size, the amplitude becomes smaller, and the spectra appear over-smoothed. RUFFIN et al. (2008) proposed additional smoothing filters to minimize this peak distortion. An objective justification of the needed smoothing technique is required to minimize damage to the original data in terms of significant difference. As such, a comparative t-test may help to choose the best smoothing filter (VAIPHASA, 2006). The positive effect of derivatives, such as the elimination of background signals from detector instabilities (OWEN, 1995), seemed to be counteracted by other background signals in the rice canopy. Hence, the affected bands in the sensor offsets were excluded from the calculation of derivatives. However, the rice study clearly confirmed the advantage of derivatives in detecting subtle peaks in reflectance.

8.5 Uncertainties by model up-scaling

Up-scaling or bottom-up is a prosperous tool for decision making that is dependent on scale and related data availability (VAN DELDEN et al., 2011). Up-scaling from an experimental to a regional scale is rarely practiced in proximal sensing but is frequently applied in airborne and satellite remote

sensing due to unprecedented spatial and temporal coverage (LOBELL, 2013). Up-scaling is a typical remote sensing approach that transfers knowledge to a larger observational scale without taking time-consuming destructive samples in the fields. This method is advantageous particularly for large and inaccessible areas (JI et al., 2012). Commonly, medium resolution imagery (>100 m) is used. However, up-scaling has its scale-specific uncertainties, and hence, a potentially small user community. A mismatch between the scale of measurements and the scale of comparison leads to potential errors (JONES and VAUGHAN, 2010). Resampling is required when optical satellite or airborne imagery is from two scales of different resolutions. This situation causes some information losses. Moreover, different views of science and statistical methods may not support transferring knowledge from one site or scale to another.

Chapters 3 and 6 denote a model transfer from an experimental scale to a farmers' scale by LI et al. (2008) and by GNYP et al. (2013). Both studies achieved robust calibrated models for estimating plant nitrogen or biomass; however, moderate validation results were noted when using farmers' data. Only at the early tillering stage, calibration and validation performed similarly, with highly explained variability. At the later stages, crop management practices had a significant impact on the models. Different management practices might cause high variability in plant nitrogen and in biomass. The descriptive statistics of model validation revealed high coefficients of variation, particularly at the stem elongation stage, when internodes develop and the plants height greatly increases (50% increase in height compared with the tillering stage). In addition, diverse cultivars of the farmers' fields were not represented in the fitted models. Apart from this observation, nitrogen rates of the experimental sites caused high variability in biomass and in plant nitrogen, whereas farmers managed their fields with higher nitrogen rates. Previous studies generally focused on self-designed controlled fields for validation due to limited number of satellite bands (JARMER, 2013). Hence, these studies had robust models but are useless for real farm conditions. Both studies (LI et al., 2008; GNYP et al., 2013) indicated problems associated with up-scaling and the importance of growth stages.

Chapter 4 refers to a model transfer from a farm scale to a regional level. KOPPE et al. (2010) derived their model from hyperspectral Hyperion data for regional applications. Their approach utilized the observed biomass from farmers' fields and explained a high variability in biomass, plant height, and biomass. That study solely indicated the potential of model transfer. However, there was no independent data available to improve their findings. Despite the advantages of satellite remote sensing, drawbacks such as weather conditions, image availability, and high cost for imagery acquisition and its pre-processing (HERRMANN et al., 2011; MUÑOZ-HUERTA et al., 2013) may limit the up-scaling of biomass or plant nitrogen estimation to large areas, particularly for cereals. It is expected that future hyperspectral satellite sensors will not solve the quick data availability problem but will improve the spatial and spectral resolutions of the remote sensing data.

In chapter 5 (GNYP et al., 2014b), a bottom-up approach was proposed, which included stepwise data from four scales. The research may encourage researchers to develop models on a plot

or local scale and then transfer the models to a regional scale. However, independent data were not available for that region, and hence, the conceptual validity of the link from experimental-farmer scale may be insufficient. Further analysis is required to test the transferability of the multiscale approach to other sites and crops. Because the VIs derived from spectrometers and Hyperion imagery yielded similar predictability in comparison to the results of KOPPE et al. (2010) and GNYP et al. (2014b), it might be assumed that different resolutions had an insignificant impact on the results in this study. PSOMAS et al. (2011) resampled the spectrometer reflectance and matched the spatial resolution to Hyperion, and hence, these authors reduced the variance of the estimated biomass. However, VAN DELDEN et al. (2011) concluded that scaling aspects are always a balancing act between the user, the science, and the data.

LAUSCH et al. (2012) established a scale-specific approach with three scales (plot, local, and regional). LE MAIRE et al., (2008) found that up-scaling from small forest canopy (FieldSpec) to forest canopy (Hyperion) increased errors and radiometric noises. LAUDIEN and BARETH (2006) developed a knowledge-based approach to up-scale sugar beet diseases from plot to regional scale. Aforementioned studies used different non-imaging and imaging sensors, which varied from a small level (ASD spectrometer) to a large or regional level (satellite or airborne imagery). Sensor-specific behaviors may cause some troubles, which result in partly different reflectance responses (e.g., KOPPE et al., 2010; TIAN et al., 2011) or different spatial resolutions (BAO et al., 2009). Proximal and remote sensing sensors take different footprints of the surface and have different center wavelengths and bandwidths. The spectrometer acquires an area of several cm^2, whereas Hyperion has a 30 m pixel size. The question is whether the reflectance taken by a spectrometer sufficiently represents an area that Hyperion has covered. Canopy reflectance measurements are collected by both sensors.

8.6 Importance of single growth stages and growing season

Phenology largely governs the temporal changes observed from remotely sensed plant or canopy reflectance. The remote sensing of vegetation enables plant growth monitoring at a specific growth stage and across a growing season. Although precision agriculture applications are focused on specific growth stages, remote sensing or proximal sensor applications are commonly based on a growing season. Substantial differences between these applications frequently appear in models.

Models or scatterplots derived from data collected from observed growing season produce typical point clouds with clusters. From a mathematical view, these data lead to a regression model that shows less scattering along the regression line but more scattering around the clusters. To obtain a high coefficient of determination, it is sufficient to take one point cloud from an early growth stage and one point cloud from a later stage and to build a regression from those two groups of points. In that case, additional statistical parameters, such as RMSE and RE, are required to assess the actual precision of that regression. This problem is usually noted from scientists. However, an estimation across growth stages might be useful for efficient biomass estimation without considering

management practices, whereas models based on a single growth stage might be more efficient for precise management.

Observations on single growth stages require a scale because growth stages may vary from area to area (ZADOCKS et al., 1974). Hence, phenology provides a useful scale to compare plants within the same "life cycle" wherever the plants are growing (ZADOCKS et al., 1974). Phenology is based on and considers cause-effect relations between biophysical processes in the plant and driving external forces, such as temperature (RUML and VULIC, 2005). Agricultural production follows strong seasonal patterns related to the biological lifecycle of crops (ATZBERGER, 2013). Management decisions, e.g., the input of fertilizer or pesticides and irrigation, are often based on crop development stages (JOHANNSEN and DAUGHTRY, 2009). RUML and VULIC (2005) indicated that phenology may contribute to pest species control and to species protection. An understanding of phenology and their patterns is beneficial for maximizing crop yield and profit (BOWDEN et al., 2008) by optimized management practices during the growth cycle (FAGIERA and DOS SANTOS, 2013). The determination of phenology using satellite data (e.g., MODIS) is important due to increasing food insecurity (YOU et al., 2013). In the context of the remote sensing of vegetation, the growth stages affect the optical and thermal properties of plant canopies (PINTER et al., 2003), and hence, the performance of different VIs and the selection of sensitive wavelengths (LI et al., 2010). Links between crop phenology and remote sensing are potentially most important for influencing on-farm management practices (VAN NIEL and MCVICAR, 2004).

Nevertheless, the determination of the right growth stage is often time-consuming and complex and has its disadvantage for practical use. End-users must have the corresponding knowledge regarding crop phenology, its process, and its impacts on plants. The dynamics of phenology are mainly driven by temperature (RUML and VULIC, 2005), and some growth stages may be reached earlier or later than on previous years. Higher temperatures might cause skipping of some secondary growth stages (e.g., the development of 11 leaves instead of 12 leaves) and initiating the next principle growth stage. Lower temperatures extend the duration of growth stages, and crops may not reach grain filling before harvest time in the worst case. Moreover, the classification of precise secondary growth stages is always impossible for a plant population, which results in recording several overlapping growth stages in a population per area. This observation may support some researchers' remote sensing or proximal sensing studies using data from the entire growing season rather than from individual growth stages.

The investigations in Huimin and Jiansanjiang sites at single growth stages showed that biomass and plant nitrogen estimations were greatly affected by growth stages (LI et al., 2008; GNYP et al., 2013; YU et al., 2013; GNYP et al., 2014b). Furthermore, the findings confirmed that growth stages and plant development (e.g., biomass) were greatly influenced by annual weather variations. Variations in a single growth stage and interannual variations resulted in different patterns in observed and predicted biomass. The findings in a recent rice crop study showed that models developed based

on three years' data may perform weaker than those models based on independent years at the same growth stage (AASEN et al., 2014); however, those models are better than models based on a single year's data (RYU et al., 2011). Climate graph of the Jiansanjiang test site (Fig. 2.9) indicated the effects of lower temperature on plant growth caused by higher monsoon precipitations and lower insolation compared with the same month in a previous year. Similar seasonal variability attributed to annual differences in biomass and plant nitrogen (RYU et al., 2011) or in the yield (VAN NIEL and MCVICAR, 2004) of rice crops. Yield was not studied in chapters 6–7; however, the observed yield data indicated interannual variations in response to temperature and insolation changes during the growth stages. Particularly for rice, a sufficient temperature is required for plant growth after transplanting (see 2.1.2.2). In 2009, an extremely low temperature in End-May and Early-June resulted in the earlier maturity of several pre-germinated plants per hills and later affected the reflectance and destructive biomass measurements at the tillering stage. Hence, the canopy was less dense, and the rice plants produced less biomass than in previous years at the same growth stage.

8.7 Effect of sample size and diverse calibration/validation methods

Statistical tests generally assume a random sample size of data or measurements. It is challenging to decide which sample strategy is most optimal. Plants grow in populations having a clustered or uneven distribution. Moreover, management practices, such as drilling, transplanting strategy, and seed rates, lead to biased plant distributions in the fields. Hence, the sampling strategy must fit the distribution of plants, including clusters, rows, and plot edges. In the studies of remote sensing of vegetation, researchers must critically weigh the advantages and disadvantages of a selected sample strategy. JONES and VAUGHAN (2010) discussed five strategies: random, stratified random, regular, clustered, and transects. These authors assumed that researchers often use a subjective or judgmental strategy.

In the case of winter wheat, a random sampling strategy was conducted in the experimental fields, whereas a regular strategy was used to fit the spatial resolution of Hyperion image covering the farmers' fields. In the case of rice, plants were clustered in hills and rows. However, in the experimental fields, the plants were manually transplanted, which resulted in uneven rows. In farmers' fields, the rows were mostly even. As for the Huimin test site, samples in farmers' fields followed the spatial resolution of satellite images with a regular grid cell size. In the experimental fields, samples were randomly taken based on average tillers per plot. Random sampling is statistically optimal; however, smaller categories may be underestimated. Regular sampling is easy to practice but lacks true statistical randomness. Hence, the sampling strategy may result in an underestimation or overestimation of parameters. This observation partially explains the weak results of model transfer from the experimental to farmers' fields (see chapters 3 and 6; LI et al., 2008; GNYP et al., 2013).

Additionally, the sampling size has extra impacts on the model performance. First, a statistical minimum sample size (>30) is mandatory for calculating the standard deviation of confidence interval.

A larger sample size better explained the accuracy of standard deviation. Compared with published studies, the Huimin and Jiansanjiang test sites offer a large sample size, with n=901 for a single year's winter wheat growing season and n=1,685 for three years' rice growing season, respectively. Published studies for winter wheat or rice are content with less than 400 observations for a single year (HANSEN and SCHOERRING, 2003; WANG et al., 2011), two years (STROPPIANA et al., 2009; FU et al., 2014; JIN et al., 2013; LI et al., 2014), three years (FENG et al., 2008; ZHU et al., 2008), or six years (WANG et al., 2012). Furthermore, the standard deviation parameters (RMSE, RE) are more important for comparing the proposed methods in the published studies.

In practice, the samples are divided into two datasets for model calibration and validation. Particularly for larger data sets, analytical techniques are required to handle and to preserve the original information (DASZYKOWSKI et al., 2002). In this context, random sampling is a popular technique because of its simplicity and because a group of data randomly extracted from a larger set follows the statistical distribution (GALVAO et al., 2005). Alternatives to random sampling are the Kennard-Stone algorithm and cluster-based algorithm, which select a representative subset from a pool dataset and are time-consuming (DASZYKOWSKI et al., 2002). Choosing a reasonable subset division and a suitable validation method is critical. These steps may be considered data processing. In chapters 3–6, experimental and farmers' fields were used as two independent datasets. Some studies used two experimental fields or sites (LIU et al., 2010; WANG et al., 2012) as independent datasets, others used two years as independent dataset (FENG et al., 2008; FU et al., 2014). In that case, statistical inference from independent data is often disadvantageous when the two datasets are too different. Plant growth, biomass, reflectance, fertilizer input, and other uneven management variables affect prognostic models. VIGNEAU et al. (2011) pooled two different datasets (one from greenhouse and another one from field), and hence, they received relevant models to estimate plant nitrogen in wheat. In chapter 7, data were pooled and then randomly divided into a calibration (75%) and a validation (25%) datasets to minimize the variations caused by diverse management strategies and unequal distribution of two datasets. Similar dataset arrangement was used for two rice experiments by NGUYEN and LEE (2006). Commonly, a higher portion of samples (>60%) are used for calibration, whereas a lower portion for validation (<40%) purpose (WANG et al., 2011, MIPHOKASAP et al., 2012). Methods, such as "leave one out", share a pooled dataset and even take one observation into account twice. Bootstrapping considers many statistical parameters, such as the mean, median, or correlation coefficient, which provides a robust alternative method based on parametric assumptions. In the case that the data are not pooled but are divided into subsets for calibration and validation, a cross-validation approach may be an alternative. However, TAKAHASHI et al. (2000)'s finding indicated the weakness of that approach, despite their procedure being repeated ten times, which resulted in high R^2; however, the model's predictability was inadequate.

8.8 Potential errors and disadvantages in statistics and in hyperspectral data collection

Non-destructive methods have their specific accuracies and uncertainties in biomass and plant nitrogen estimation. Saturation, over-fitting, collinearity, diverse calibration and validation issues may be caused by different estimation methods selected and may reduce the uses of a model. However, in addition to these drawbacks, some other effects from the destructive methods, such as statistics, human errors, and scaling of observed agronomics, also increase model uncertainties. Potential errors and disadvantages in hyperspectral data collection include field spectrometer-specific or optical sensor-specific problems, atmospheric conditions, and other technical particularities. Both the uncertainties embedded in destructive methods and errors caused by hyperspectral remote sensing reduce the potential predictability of biomass and plant nitrogen.

Statistical analysis indirectly influences the hyperspectral and agronomic data and the corresponding results. General descriptive statistics can identify outliers that may be excluded from further processing. Nevertheless, outliers such as in plant growth are normal in nature and have to be clearly defined. Their exclusion in model development is primarily depending on scientists' decisions. A model's performance is explained by statistics as well. Their accuracies cannot solely be explained by correlation coefficient (R) or coefficient of determination (R^2). Additional parameters, such as RMSE and RE, have a better predictive value of the models. When RMSE and RE are low, the observed and measured values distribute close to the regression line. In that case, the R^2 might be a second choice to decide whether a model is accurate. A simple explanation based on coefficient of determination requires at least a graphic visualization of the distribution in the regression. However, model accuracy should be explained by R^2, RMSE, and RE along with a regression line. A validation has to use a regression format of $y=ax+b$, where the coefficient a close to 1 and coefficient b close to 0 indicating an accurate model. If the result of a validation regression is not sufficiently accurate, then the original regression has no practical value as a model, and a new model specification is required (MONTGOMERY et al., 2012). The validity and manipulation effects of statistics are well known and are based on human-driven interpretation.

Human errors are common and must be taken into consideration. These errors include mistakes in destructive ground sampling and incorrect sample processing in the laboratory. Hence, a large sampling size is important to minimize human errors by statistics. In the case of destructive samplings, human-effected biomass losses or errors in plant nitrogen calculation by chemical digestion method are typical. It may be assumed that the measured biomass has a potential loss of 5–10% due to biomass processing (washing or cutting of samples) and determination (balancing and scaling). Typical errors include losses of some parts of the samples during the balance process and misplaced or mismatched sample labels. Because plant nitrogen is derived from dry matter, its determination process is directly influenced by human errors. Additionally, the biomass is scaled from "m^2" to a larger scale of "ha" by assuming that the plant growth is similar at the larger scale. Although up-scaling biomass samples is a common mathematical procedure, nature and crops have no standards;

thus, no linear relation between biomass and scale may be assumed. There are always variations in plant growth, soil, and micro-climate. Plants of the same cultivar have growth variability. Scaling from small scale to larger scale assumes the same management and growth at both scales, which normally is not the case. Hence, up-scaling is often connected with inaccurate models.

Additionally, the acquisition geometry of field spectrometers and atmospheric conditions distort the reflectance measurements. Shadows occur when the sensor was not exactly vertical to the acquisition area (off-nadir acquisition). Because a plant canopy is never built on a flat and homogenous acquisition area, such as a calibration target, the reflectance is mostly measured nadir-off. PERBANDT et al. (2011) showed that the spectral response significantly depends on the height and sensor view angle adjustment. However, the off-nadir effect should be small in both studies considering the observed canopy scale. In addition to the acquisition geometry, environmental factors, such as light intensity or wind, cause potential errors in non-destructive measurements using passive proximal sensors. Green biomass may be overestimated by measurements taken on cloudy days because the increased diffuse radiation improves the penetration of light into the canopy (ROYO and VILLEGAS, 2011). Wind leads to unstable reflectance signals due to the moving of a canopy's structure. A canopy's structure increases the unexplained variance (see chapter 8.9). Because only stable reflectance signals were captured in both study sites, effects by wind may be excluded.

Optical satellite data are extremely sensitive to atmospheric conditions. Additional atmospheric correction is required for field spectral measurements to be useful. Hazy conditions cannot be removed from optical data, which falsify the real ground conditions. In some cases, researchers reported regarding reduced or lost information from satellite images in some wavelengths due to atmospheric effects (e.g., TIAN et al., 2011). It remains doubtful as to how the technology of future satellite sensors overcomes that obstacle of optical data. Available hyperspectral satellite systems still have many disadvantages: fixed spectral bands, low spatial resolution, inadequate repeat intervals, and long delivery times for many applications (MORAN et al., 1997). These systems cause some mismatching problems in potential bands or at critical growth stages. UAV-based systems have a fine resolution and are independent from large delivery companies; however, many have troubles with radiometric and geometric corrections and are unsuitable for large areas monitoring in a short time. Hence, the hyperspectral proximal sensors, such as field spectrometers, are undisputable in terms of their advantages, particularly their flexibility. However, these instruments will lose those advantages to UAV-based sensors soon.

In the SWIR domain, additional issues, such as temperature changes of a sensor detector, can cause insecurities in reflectance taken by field spectrometers. BROWN et al. (2001) investigated the performance of two spectrometers (GER 3700 and FieldSpec FR) in the VIS, NIR, and SWIR domains and showed that the reflectance between one and another detector may differ as much as 5%. These authors concluded that detectors change their sensitivity after several-hour's warm-up. As the instrument warms up, the sensitivity of the VNIR detector will increase, whereas that of the SWIR2

(1830–2500 nm) will decrease, leading to discontinuities (FIELDSPEC USER MANUAL, 2007). Moreover, BROWN et al. (2001) showed that the variation in the SWIR detector was even 9% and 17% higher at 1243 nm and 2403 nm, respectively. Because the SWIR domain was used in the range of 350 to 1800 nm, it can be assumed a potential reflectance uncertainty of 5% in the VNIR and 9% in the SWIR range driven by technical particularities.

8.9 Unexplained biomass and plant nitrogen in hyperspectral reflectance

Common non-destructive methods based on canopy reflectance explain 60–85% variability in biomass or in plant nitrogen, and the performance is better for winter wheat than for rice crops. The presented hyperspectral pre-processed data and applied methods usually used two to six best band combinations to estimate biomass or plant nitrogen. Even the derivatives of reflectance could not significantly improve the explained variability to more than 80% for rice. Several studies have demonstrated that the PLS models using six bands also have their limits. It seems that the selection of a few bands of the 1,451 possible bands is not sufficient to explain higher variability. However, the proposed hyperspectral data processing is a common method in remote sensing and is widely adapted and end-user friendly. The execution indicated that, depending on which method is used, approximately 15–40% of the variability in biomass or plant nitrogen is unexplained by reflectance. Hence, hyperspectral data alone cannot explain the total variability of biomass or plant nitrogen. Both studies indicated the highly temporal influence on variability. Even within two or three years, the variability in biomass or plant nitrogen has high variance. A fusion of hyperspectral data with ancillary information, including weather impact or with-in field soil variability, may improve the estimates. The remained insecurity in estimates might be resulted from with-in field variability, e.g., in soils, temporal influence on plant growth, canopy structure, and morphology.

Although winter wheat and rice belong to the same family of Poaceae, they differ in their morphology. Winter wheat canopy had a dark green color in the field, and its leaf width was bigger than that one of rice. In addition, the wheat canopy appeared very dense. Rice had light green colored leaves and a shorter leaf width. Hence, the spectral reflectance of wheat was much higher, particularly in the VIS and NIR domains. The measured plant reflectance represents a canopy or volume of a canopy, including mixed information from different plant organs. A plant structure includes parameters, such as leaf angle, leaf length, leaf density or distribution and drives variation in canopy reflectance characteristics, e.g. scattering (ASNER, 1998; KUMAR et al., 2006; JONES and VAUGHAN, 2010). Scattering effects of leaf, stem, and canopy become most apparent in the NIR domain and explain the importance of that domain for remote sensing of vegetation (OLLINGER, 2011). Investigating the source of variability in canopy reflectance, OLLINGER (2011) reported that solar irradiance reached its peak at approximately 600 nm and decreased from that peak. Sources of variability in vegetation reflectance are extremely complex because of diversity in the size, shape, composition, arrangement of cells, and plant organs. The effect of whole-canopy structure on

reflectance may be portioned into factors that describe the plant structure and those factors that describe the outer canopy structure (OLLINGER, 2011). Outer canopy surfaces without vegetation cover have the effect of reducing whole-canopy reflectance.

Typical outer canopy surfaces in the fields are from soil or water, which are completely different from vegetation in their reflectance. However, these reflectance signals also appear within the canopy when the vegetation cover is less than 100%. Canopy reflectance is always remotely sensed in sensor's field of view and contains signals from soil or water (KOKALY and CLARK, 1999). These background signals contribute to canopy spectral reflectance and increase the unexplained variability at early growth stages with low canopy density. These signals lose their effect when canopy cover is closed. It was shown in chapter 7 (see GNYP et al., 2014a) that high variability in biomass (55%) was observed at the early tillering stage and decreased (33%) at the heading stage with dense canopy cover. These observations assumed that background signals contributed to unexplained variability. Partial portion of background signals reduced canopy reflectance. However, hyperspectral reflectance explained 80% biomass variability at the early stage using derivatives of reflectance in OMNBR models at the stem elongation stage when the variance in biomass was high (52%). In contrast, low biomass variance (30%) at the heading stage explained less variability (55%). Thus, other parameters, such as with-in field variability in soil and nutrition might further increase the unexplained variability in biomass and in plant nitrogen when a canopy reaches its highest density. In the case of winter wheat, soil dominates the background signal, whereas for rice, the major background noises are caused by water and wet soils in the paddies. Particularly for rice, water may change from clear water to turbid or loamy when the water is moved. However, the reflectance of clear water and turbid water has different spectral reflectance, and hence, may have dissimilar influence on rice reflectance. Due to these facts, the two crops are incomparable, and different sensitive bands are identified for biomass or plant nitrogen estimation. The results conform to ZHU et al. (2008)'s finding that higher reflectance and better VIs performance were observed for winter wheat than rice.

9. Conclusions and future challenges

9.1 Conclusions

Non-destructive estimation of biomass and plant nitrogen by hyperspectral remote sensing may contribute to food security and sustainable agriculture. Although the proposed estimation methods have their disadvantages, monitoring plant growth without direct contact is a major advantage of these methods. It has been demonstrated that three to six band combinations are often optimal, and when more bands are used in the estimation models, the known problems of overfitting and collinearity occur. Models based on broad bands are prone to saturation, whereas models based on optimized narrow bands delay that effect. The results of this dissertation suggest that it is feasible to use narrow bands and diverse regression models for biomass and plant nitrogen estimation. The developed models and the proposed GnyLi index must be tested on different study sites, scales, and crops. In particular, the GnyLi must be tested at a large observation scale. The findings may be easily applied to UAV-based sensors or satellite sensors. Because UAVs have the advantage to collect data below the cloud cover (HONKAVAARA et al., 2013) they may offer the opportunity for regionalization approaches. Hence, the transfer from experimental and farmers' fields may enable the knowledge of crop sensing at a large scale. However, further analysis is required for using this method with airborne or satellite data because there are challenges in the up-scaling method.

Both studies highlighted the importance of the SWIR domain. Although the SWIR domain is not regularly used to estimate biophysical or biochemical parameters due to their masked absorption features by water content in leaves (KUMAR et al., 2006), the studies of both winter wheat and rice crops indicated the need of that domain. This finding is in agreement with studies focusing on biomass estimation (MARIOTTO et al., 2013). SWIR seems to be useful at single growth stages and across stages in different methods. Derivatives of reflectance, which are known to reduce background signals, were calculated as well, and the results also showed the importance of SWIR domain at early growth stages, such as tillering and stem elongation.

To date, the non-destructive estimation of biomass and plant nitrogen is solely based on methods of vegetation indices, best bands combinations, MLR, OMNBR, PLSR, Artificial Neural Network, or Support Vector Machines. However, no well-established rules exist on how to test and train the diverse approaches. Some of these methods are excessively time-consuming and user-unfriendly for farmers. In addition, these methods cannot explain all of the variability of biophysical or biochemical parameters. However, a plant's reflectance in multiyear dataset is influenced significantly by multitemporal conditions. A combination of hyperspectral data and weather data, such as temperature and insolation, might be of high value. In both study sites, climographs and the discussed results in chapters 3–7 indicated that reflectance must be somehow related to multitemporal interannual variations across diverse years. One single year's dataset is useless and may not represent the previous or future years' dataset. The question is whether temperature and insolation, as additional

independent parameter, could improve the variability in biomass or plant nitrogen, and how this measurement could be performed or implemented in the proposed models described in chapters 3–7?

A possibility would be to establish a temporal constant, which might be added to predictive equations of the models. First, an empirical analysis of the relation between reflectance and multiyear influence must be performed to distinguish how to set the constant. The temporal constant might be variable similar to the constant L in SAVI developed by HUETE (1988). The constant may be calculated based on the measured temperature and insolation when the reflectance measurements were taken. Then, the variable constant "called T for temporal influence" might be implemented to the proposed model. In addition, a new vegetation index, such as "Temporal Adjusted Vegetation Index", might be developed to reduce signals from annual variation in hyperspectral data. Another way might be to implement hyperspectral data in an ecosystem model. Because this type of models requires more detailed input from climate and soils and additional growth parameters, the available data from both studies might be insufficient.

Currently, hyperspectral research requires many processing steps for a precise estimation dependent on the selected non-destructive estimation method. Simple processing methods or implemented models in new sensors would be a user-friendly end-product for farmers. Farmers need a quick and efficient spatial decision support information system without time-consuming arithmetic technique and highly skilled professionals. However, science will never be satisfied with inaccurate models while farmers depend on fast decisions during the critical growth stages and may be satisfied with lower model accuracy. High accuracy means explanation of a high variability with very low probability of error. However, this is impractical under real farm conditions.

9.2 Future challenges and outlook

The challenges of non-destructive methods for agronomics parameters estimation using hyperspectral data are manifold in term of their implementation and relevant sensor technology. They need to provide a quick information system to assess the potential biomass and nitrogen input in advance. This information system has site-specific management information from all farms at large observation scale with high spatial resolution that depends on new technologies. Sensor technology based on the integration of hyperspectral and lidar data is promising. This combined hyperspectral-lidar system would be independent of acquisition time and offer high-resolution data. The data would have image and non-image information and would be able to visualize the canopy in 3D.

The technology might be of more efficient and economic use first on tractor-mounted sensors than on airborne or satellite sensors due to the expensive costs. An automated analysis of the provided data would offer a quick decision information system to the end-users regarding the mandatory field inputs, such as fertilizer or pesticides, for achieving economic-efficient high yield and a sustainable and environmental-friendly use of the arable land. Currently, tractors and other large agricultural

machines in developed countries are equipped with one or more personal computers for monitoring some of the processing in the field, such as sowing or harvest.

However, the machines are still expansive and only large agricultural companies have access to such technologies. Funding is the big issue for these systems to become available in all countries including developing countries. Moreover, it appears that this technology will not be adopted very fast in developing countries. The problems or challenges are: how those people from rural areas can find new jobs in the cities and where the people have to go. Rice farming in Asia is labor-intensive and cannot be performed with large machines. New technologies must provide crop-specific machines. However, it may be assumed that China will be able to improve its agriculture to current development level as South Korea or Japan. The question is when China will reach this level? In 10, 20 or 30 years?

Satellite or airborne based system with medium resolution and less expensive might be the best choice for developing countries, whereas UAV systems with high resolution might be financially bearable for developed countries. The spatial and spectral resolution of those systems, as well as their agricultural applications, may increase in the future. Unprompted and emergency acquisitions for plant growth monitoring will have an important role in the world to ensure food security for an increasing world population. Thus, monitoring areas of high population density with high agricultural outputs will be most important.

References* (chapters 1, 2, 8, 9)

AASEN, H., GNYP, M.L., MIAO, Y., BARETH, G., 2014 (accepted). Automated hyperspectral vegetation index retrieval from multiple correlation matrices with HyperCor. PE & RS Special Issue.

ACEVEDO, E., SILVA, P., SILVA, H., 2002. Wheat growth and physiology. In: B.C., CURTIS, RAJAMAN, S., MACPHERSON, H.G. (Eds.), Bread wheat - Improvements and production, Food and Agriculture Organization of the United Nations, Rome, Italy, 603 pages.

ALVARO, F., DEL MORAL, L.F.G., ROYO, C., 2007. Usefulness of remote sensing for the assessment of growth traits in individual plant grown in the field. International Journal of Remote Sensing, 28 (11), 2497-2512.

ASD TECHNICAL GUIDE, 1999. 136 pages.

ASNER, G.P., 1998. Biophysical and biochemical sources of variability in canopy reflectance. Remote Sensing of Environment, 64, 234-253.

ATZBERGER, C., 2013. Advances in remote sensing of agriculture: Context of description, existing operational monitoring systems and major information needs. Remote Sensing, 5, 949-981.

BAJWA, S.G., KULKARNI, S.S., 2011. Hyperspectral data mining. In: P.S., THENKABAIL, J.G., LYON, A., HUETE (Eds.), Hyperspectral remote sensing of vegetation, CRC Press, Boca Raton, FL, USA, pp. 93-120.

BAO, Y., GAO, W., GAO, Z., 2009. Estimation of winter wheat biomass based on remote sensing data at various spatial and spectral resolutions. Frontier of Earth Science in China, 3 (1), 118-128.

BARETH, G., 2003. Möglichkeiten und Grenzen der regionalen agrarumweltrelevanten Modellierung unter Nutzung von GIS in China am Beispiel der Nordchinesischen Tiefebene. Habilitation dissertation, University of Hohenheim, Germany. 320 pages.

BARKER, A.V., BRYSON, G.M., 2007. Nitrogen. In: A.V., Barker, D.J., Pilbeam (Eds.), Handbook of plant nutrition, CRC Press, Boca Raton, London, New York, pp. 21-50.

BEADLE, C.L., LONG, S.P., 1985. Photosynthesis-it limiting to biomass production. Biomass, 8, 119-168.

BECKER, B.L., LUSCH, D.P., QI, J., 2005. Identifying optimal spectral bands from in situ measurements of Great Lakes coastal wetlands using second-derivative analysis. Remote Sensing of Environment, 97 (2), 238-248.

BONGIOVANNI, R., LOWEBERG-DEBOER, 2004. Precision Agriculture and Sustainability. Precision Agriculture, 5, 359-387.

BOWDEN, P., EDWARDS, J., FERGUSON, N., M'NEE, T., ROBERTS, K., SCHIPP, A., SCHULZE, A., WILKINS, J., 2008. Wheat growth and development. NSW DPI, Australia, 91 pages.

BROWN, S.W., JOHNSEN, B.C., YOON, H.W., BUTLER, J.J., BARNES, R.A., BIGGAR, S., SPYAK, P., THOME, K., ZALEWSKI, E., HELMLINGER, M., BRUEGGE, C., SCHILLER, S., FEDOSEJEVS, G., GAUTHIER, R., TSUCHIDA, S., MACHIDA, S., 2001. Radiometric characterization of field

radiometers in support of the 1997 Luna Lake, Nevada, experiment to determine surface and top-of-atmosphere radiance. Remote Sensing of Environment, 77, 367-376.

BUDDE, M., ROWLAND, J., FUNK, C., 2010. Agriculture and food availability - Remote sensing of agriculture for food security monitoring in the developing world. Agriculture, Articles, Climate Earth Observation, Health, Technology.

BÜNEMANN, E.K., SCHWENKE, G.D., VAN ZWIETEN, L., 2006. Impact of agricultural inputs on soil organisms - a review. Australian Journal of Soil Research, 44, 379-406.

CAI, H., YANG, X., XU, X., 2013. Spatiotemporal patterns of urban encroachement on cropland and its impacts on potential agricultural procuctivity in China. Remote Sensing, 5, 6443-6460.

CASANOVA, D. EPEMA, G.F., GOUDRIAAN, J., 1998. Monitoring rice reflectance at field level for estimating biomass and LAI. Field Crops Research, 55, 83-92.

CHAUHAN, H.J., MOHAN, B.K., 2013. Development of agricultural crops spectral library and classification of crops using Hyperion hyperspectral data. Journal of Remote Sensing Technology, 1 (1), 9-12.

CHEN, X., CUI, L., VIOUSEK, P.M., CASSMANN, K.G., MATSON, P.A., BAI, J., MENG, Q., HOU, P., YUE, S., RÖMHELD, V., ZHANG, F., 2011. Integrated soil-crop system management for food security. PNAS, 108 (16), 6399-6404.

CHEN, C., QIAN, C., DENG, A., ZHANG, W., 2012. Progressive and active adaptations of cropping system to climate change in Northeast China. European Journal of Agronomy, 38, 94-103.

CLEVERS, J.G.P.W., 1999. The use of imaging spectrometry for agricultural application. ISPRS Journal of Photogrammetrie & Remote Sensing, 54, 299-304.

CUI, Z., ZHANG, F., CHEN, X., DOU, Z., LI, J., 2010. In-season nitrogen management strategy for winter wheat: Maximizing yields, minimizing environmental impact in an over-fertilization context. Field Crops Research, 116, 140-146.

CUI, Z., CHEN, X., ZHANG, F., 2013. Development of regional nitrogen rate guidelines for intensive cropping systems in China. Agronomy Journal, 105 (5), 1411-1416.

DARVISHZADEH, R., SKIDMORE, A., ATZBERGER, C., VAN WIEREN, S., 2008. Estimation of vegetation LAI from hyperspectral reflectance data: Effects of soil type and plant architecture. International Journal of Applied Earth Observation and Geoinformation, 10, 358-373.

DASZYKOWSKI, M., WALCZAK, B., MASSART, D.L., 2002. Representative subset selection. Analytics Chimica Acta, 468, 91-103.

DEMETRIADES-SHAH, T.H., STEVEN, M.D., CLARK, J.A., 1990. High resolution derivative spectra in remote sensing. Remote Sensing of Environment, 33 (1), 55-64.

DEMIRCAN, A., 1995. Die Nutzung fernerkundlich bestimmter Pflanzenparameter zur flächenhaften Modellierung von Ertragsbildung und Verdunstung. PhD thesis, University of Munich, Munich, Germany, 160 pages.

DIE LANDWIRTSCHAFT, 2006. Pflanzliche Erzeugung. BLV Buchverlag, München, Germany.

DU, G., LEI, W., ZHOU, M., ZHANG, J., 1990. Fluvo-aquic soils and calcic concretation black soils. In: C., LI, O., SUN (Eds.), Soils of China, Science Press, Beijing, China, pp. 196-211.

DUVEILLER, G., BARET, F., DEFOURNY, P., 2012. Remotely sensed green area index for winter wheat crop monitoring: 10-year assessment at regional scale over a fragmented landscape. Agricultural and Forest Meteorology, 166-167, 156-168.

FAGIERA, N.K., DOS SANTOS, A.B., 2013. Lowland rice growth and development and nutrient uptake during growth cycle. Journal of Plant Nutrition, 36 (12), 1841-1852.

FANG, Q.F., MA, L., GREEN, T., YU, Q., WANG, T., AHUJA, L., 2010. Water resource and water use efficiency in the North China Plain: Current status and agronomic management options. Agricultural Water Management, 97 (8), 1102-116.

FAOSTAT, 2011. Food and Agricultural commodities production.

FAOSTAT, 2012. Food and Agricultural commodities production.

FAO, 2013. The state of food insecurity in the world.

FENG, W., YAO, X., ZHU, Y., TIAN, Y.C., CAO, W.X., 2008. Monitoring leaf nitrogen status with hyperspectral reflectance in wheat. European Journal of Agronomy, 28, 394-404.

FIELDSPEC USER MANUAL, 2007. ASD Document 600540 Rev. G, 104 pages.

FRANKE, W. (1997). Nutzpflanzenkude. Georg Thieme Verlag, Stuttgart, Germany. 490 pages.

FU, Y., YANG, G., WANG, J., SONG, X., FENG, H., 2014. Winter wheat biomass estimation based on spectral indices, band depth analysis and partial least squares regression using hyperspectral measurements. Computers and Electronics in Agriculture, 100, 51-59.

FUKAI, S., COOPER, M., 1995. Development of drought-resistant cultivars using physio-morphological traits in rice. Field Crops Research, 40, 67-86.

GALVAO, R.K.H., ARAUJO, M.C.U., JOSÉ, G.E., PONTES, M.J.C., SILVA, E.C., SALDANHA, T.C.B., 2005. A method for calibration and validation subset partitioning. Talanta, 67, 736-740.

GAO, B.-C., 1996. NDWI-A normalized difference water index for remote sensing of vegetation liquid water from space. Remote Sensing of Environment, 58, 257-266.

GAO, X., HUETE, A.R., NI, W., MIURA, T., 2000. Optical biophysical relationships of vegetation spectra without background contamination. Remote Sensing of Environment, 74 (3), 609-620.

GAO, C., SUN, B., ZHANG, T., 2006. Sustainable nutrient management in Chinese Agriculture: Challenges and Perspective. Pedosphere, 16 (2), 253-263.

GAO, J., LIU, Y., 2011. Climate warming and land use change in Heilongjiang Province, Northeast China. Applied Geography, 31, 476-482.

GAO, J., LIU, Y., 2012. Deforestation in Heilongjiang Province of China, 1896-2000: Severity, spatiotemporal patterns and causes. Applied Geography, 35, 345-352.

GEBBERS, R., ADAMCHUK, V.I., 2010. Precision agriculture and food security. Science, 327, 828-830.

GNYP, M.L., YU, K., AASEN, H., YAO, Y., HUANG, S., MIAO, Y., BARETH, G., 2013. Analysis of crop reflectance for estimating biomass in rice canopies at different phonological stages. Photogrammetrie Fernerkundung Geoinformation, 2013(4), 351-365.

GNYP, M.L., MIAO, Y., YUAN, F., USTIN, S.L., YU, K., YAO, Y., HUANG, S., BARETH, G., 2014a. Hyperspectral canopy sensing of paddy rice aboveground biomass at different growth stages. Field Crops Research, 155, 42-55.

GNYP, M.L., BARETH, G., LI, F., LENZ-WIEDEMANN, V.I.S., KOPPE, W., MIAO, Y., HENNIG, S.D., JIA, L., LAUDIEN, R., CHEN, X., ZHANG, F., 2014b (accepted). Development and implementation of a multiscale biomass model using hyperspectral vegetation indices for winter wheat in the North China Plain. Internatioanl Journal of Applied Earth Observation and Geoinformation.

GONG, Z., XU, Q., 1990. Paddy soils. In: C., LI, O., SUN (Eds.), Soils of China, Science Press, Beijing, China, pp. 233-260.

GROSSMANN, Y.L., USTIN, S.L., JACQUEMOUD, S., SANDERSON, E.W., SCHMUCK, G., VERDEBOUT, J., 1996. Critique of stepwise multiple linear regression for the extraction of leaf biochemistry information from leaf reflectance data. Remote Sensing of Environment, 56, 182-193.

GUYOT, G., BARET, F., 1988. Utilisation de la haute resolution spectrale pour suivre l'etat des couverts vegetaux, Proceedings 4th International Colloquium on Spectral Signatures of Objects in Remote Sensing, Aussios, France, 18-22 January 1988, pp. 279-286.

HABOUDANE, D., MILLER, J.R., PATTEY, E., ZARCO-TEJADA, P.J., STRACHAN, I.B., 2004. Hyperspectral vegetation indices and novel algorithms for predicting green LAI of crop canopies: Modeling and validation in the context of precision agriculture. Remote Sensing of Environment, 90 (3), 337-352.

HANSEN, P.M., SCHJOERRING, J.K., 2003. Reflectance measurement of canopy biomass and nitrogen status in wheat crops using normalized difference vegetation indices and partial least squares regression. Remote Sensing of Environment, 86 (4), 542–553.

HATFIELD, J.L., PRUEGER, J.H., 2010. Value of using different vegetative indices to quantify agricultural crop characteristics at different growth stages under varying management practices. Remote Sensing, 2, 562–578.

HERRMANN, I., PIMSTEIN, A., KARNIELI, A., COHEN, Y., ALCHANATIS, V., BONFIL, D.J., 2011. LAI assessment of wheat and potato crops by VENμS and Sentimel-2 bands. Remote Sensing of Environment, 115, 2141-2151.

HOERING, U., 2010. Landwirtschaft in China: Zwischen Selbstversorgung und Weltmarktintegration. Asienstiftung und Netzwerk EU-China, Essen, Germany, 44 pages.

HONNKAVAARA, E., SAARI, H., KAIVOSOJA, J., PÖLÖNEN, I., HAKALA, T., LITKEY, P., MÄKYNEN, J., PESONEN, L., 2013. Processing and assessment of spectrometric, stereoscopis imagery collected using a lightweight UAV spectral camera for precision agriculture. Remote Sensing, 5, 5006-5039.

HUANG, J., 1998. Agricultural policy, development, and food security in China. In: T.C., TSO, F., TUAN, M., FAUST (Eds.), Agriculture in China 1949-2030. IDEALS Inc., Beltsville, MD, USA, pp. 209-257.

HUANG, J., LIAO, H., ZHU, Y., SUN, J., SUN, Q., LIU, X., 2012. Hyperspectral detection of rice damaged by rice leaf folder (Cnaphalocrosis medinalis). Computers and Electronics in Agriculture, 82, 100-107.

HUETE, A.R., 1988. A soil-adjusted vegetation index (SAVI). Remote Sensing of Environment, 25 (3), 295-309.

INGRAM, K.T., 2005. Drought-related characteristics of important cereal crops. In: V.K., Boken, A.O. Cracknell, R.L., Heathcote (Eds.), Monitoring and predicting agricultural drought. Oxford University Press, pp. 11-27.

INOUE, Y., SAKAIYA, E., ZHU, Y., TAKAHASHI, W., 2012. Diagnostic mapping of canopy nitrogen content in rice based on hyperspectral measurements. Remote Sensing of Environment, 126, 210-221.

INSTITUTE OF SOIL SCIENCE, 1986. The soil atlas of China. Cartographic Publishing House, Beijing, China.

JARMER, R., 2013. Spectroscopy and hyperspectral imagery for monitoring summer barley. International Journal of Remote Sensing, 34, 6067-6078.

JI, L., WYLIE, B.K., NOSSOV, D.R., PETERSON, B., WALDROP, M.P., MCFARLAND, J.W., ROVER, J., HOLLINGSWORTH, T.N., 2012. Estimating aboveground biomass in interior Alaska with Landsat data and field measurements. International Journal of Applied Earth Observation and Geoiformation, 18, 451-461.

JIN, X., DIAO, W., XIAO, C., WANG, F., CHEN, B., WANG, K., LI, S., 2013. Estimation of wheat agronomic parameters using new spectral indices. PLOS ONE, 8 (8), 1-8.

JOHANNSEN, C.J., DAUGHTRY, C.S.T., 2009. Surface reference data collection. In: T.A., WARNER, M. D., NELLIS, G.W., FOODY (Eds.), The Sage Handbook of Remote Sensing, SAGE Publications, London, UK, pp. 244-256.

JONES, H.G., VAUGHAN, R.A., 2010. Remote sensing of vegetation -Principle, techniques, and applications. Oxford University Press, Oxford, UK, 353 pages.

KATO, Y., KAMOSHITA, A., ABE, J., YAMAGISHI, J., 2007. Improvement or rice (Oryza sativa L.) growth in upland conditions with deep tillage and mulch. Soil & Tillage Research, 92, 30-44.

KOKALY, R.F., CLARK, R.N., 1999. Spectroscopic determination of leaf biochemistry using band-depth analysis of absorption features and stepwise multiple linear regression. Remote Sensing of Environment, 67 (3), 267-287.

KOPPE, W., LI, F., GNYP, M.L., MIAO, Y., JIA, L., CHEN, X., ZHANG, F., BARETH, G., 2010. Evaluating multispectral and hyperspectral satellite remote sensing data for estimating winter wheat

growth parameters at regional scale in the North China Plain. Photogrammetrie Fernerkundung Geoinformation, 2010 (3), 167-178.

KOPPE, W., GNYP, M.L., HENNIG, S.D., LI, F., MIAO, Y., CHEN, X., JIA, L., BARETH, G., 2012. Multi-temporal hyperspectral and radar remote sensing of estimating winter wheat biomass in the North China Plain. Photogrammetrie Fernerkundung Geoinformation, 2012 (3), 281-298.

KUMAR, L., SCHMIDT, K., DURY, S., SKIDMORE, A., 2006. Imaging spectrometry and vegetation science. In: F.D., VAN DER MEER, S.M., DE JONG (Eds.), Imaging spectrometry - Basic principle and prospective applications, Kluwer Academic Publishers, Dordrecht, Boston, London, pp. 111-156.

KUENZER, C., KNAUER, K., 2013. Remote sensing of rice crop areas. International Journal of Remote Sensing, 34 (6), 2101-2139.

LANG, G., MIAO, B., 2013. Food security for China's cities. International Planning Studies, 18 (1), 5-20.

LAUDIEN, R., BARETH, G., 2006. Multitemporal hyperspectral data analysis for regional detection of plant diseases by using a tractor- and an airborne-based spectrometer. Photogrammetrie Fernerkundung Geoinformation, 2006 (3), 217-227.

LAUDIEN, R., BÜRCKY, K., DOLUSCHITZ, R., BARETH, G., 2006. Establishment of a Web-based spectral database for the analysis of hyperspectral data from Rhizoctonia solani-inoculated sugarbeets. Zuckerindustrie, 131 (3), 164-170, (in German).

LAUSCH, A., PAUSE, M., MERBACH, I., GWILLYM-MARGIANTO, S., SCHULZ, K., ZACHARIAS, S., SEPPELT, R., 2012. Scale-specific hyperspectral remote sensing approach in environmental research. Photogrammetrie Fernerkundung Geoinformation, 2012 (5), 589-602.

LELE, U., NYBERG, A., GOLDBERG, J., 1998. Multilateral institutions in China's agricultural production and trade. In: T.C., TSO, F., TUAN, M., FAUST (Eds.), Agriculture in China 1949-2030. IDEALS Inc., Beltsville, MD, USA, pp. 54-76.

LE MAIRE, G., FRANÇOIS, C., SOUDANI, K., BERVEILLER, D., PONTAILLER, J.-Y., BREDA, N., GENET, H., DAVI, H., DUFRENE, E., 2008. Calibration and validation of hyperspectral indices for the estimation of broadleaved forest leaf chlorophyll content, leaf mass per area, leaf area index and leaf canopy biomass. Remote Sensing of Environment, 112, 3846-3864.

LEUNG, G.Y., 1996. Reclamation and sediment control in the middle yellow river valley. Water International, 21 (1), 12-19.

LI, F., GNYP, M.L., JIA, L., MIAO, Y., YU, Z., KOPPE, W., BARETH, G., CHEN, X., ZHANG, F., 2008. Estimating N status of winter wheat using a handheld spectrometer in the North China Plain. Field Crops Research, 106, 77-85.

LI, F., MIAO, Y., HENNIG, S.D., GNYP, M.L., CHEN, X., JIA, L., BARETH, G., 2010. Evaluating hyperspectral vegetation indices for estimating nitrogen concentration of winter wheat at different growth stages. Precision Agriculture, 11, 335-357.

LI, F., MISTELE, B., HU, Y., CHEN, X., SCHMIDTHALTER, U., 2014. Reflectance estimation of canopy nitrogen content in winter wheat using optimised hyperspectral spectral indices and partial least squares regression. European Journal of Agronomy, 52, 198-209.

LIANG, L., LI, L., LIU, Q., 2011. Precipitation variability in Northeast China from 1961 to 2008. Journal of Hydrology, 404, 62-76.

LILLESAND, T.M., KIEFER, R.W., CHIPMAN, J.W., 2008. Remote sensing and image interpretation. Wiley, New York, USA, 756 pages.

LIU, W., HSEUNG, Y., 1990. The comprehensive improvement of the soils in the Huang-Hua-Hai plain. In: C., LI, Q., SUN (Eds.), Soils of China, Science Press, Beijing, pp. 724-733.

LIU, C.M., YU, J.J., KENDY, E., 2001. Groundwater exploitation and its impact on the environment in the North China Plain. Water International, 26, 265-272.

LIU, Y., WANG, D., GAO, J., DENG, W., 2005. Land use/cover changes, the environment and water resources in the Northeast China. Environmental Management, 36 (5), 691-701.

LIU, Z.-Y., WU, H.-F., HUANG, J.-F., 2010. Application of neural networks to discriminate fungal infection levels in rice panicles using hyperspectral reflectance and principal components analysis. Computers and Electronics, 72, 99-106.

LIU, X., GUIHUA, D., WANG, X., XUE, Z., JIANG, M., JIANG, M., LU, X., ZHANG, Y., 2013. Characterizing the spatial pattern of marshlands in the Sanjiang Plain, Northeast China. Ecological Engineering, 53, 335-342.

LIU, F., ZHANG, H., 2013. Novel methods to assess environmental, economic, and social sustainability of main agricultural regions in China. Agronomy of Sustainable Development, 33, 621-633.

LOBELL, D.B., 2013. The use of satellite sata for crop yield gap analysis. Field Crops Research, 143, 56-64.

MCDERMOTT, J., GRACE, D., 2011. Agricultural-associated diseases: Adapting agriculture to improve human health. International Food Policy Research Institute, pp. 103-111.

MARIOTTO, I., THENKABAIL, P.S., HUETE, A., SLONECKER, E.T., PLATONOV, A., 2013. Hyperspectral versus multispectral crop-productivity modeling and type discrimination for the HyspIRI mission. Remote Sensing of Environment, 139, 291-305.

MARTIN, R.D., HEILMAN, J.L., 1986. Spectral reflectance patterns of flooded rice. American Society for Photogrammetry and Remote Sensing, 52 (12), 1885-1890.

MEIER, U., 2001. Growth stages of mono- and dicotyledonous plants. – BBCH monograph. Federal Biological Research Centre for Agriculture and Forestry. Berlin, Braunschweig, Germany.

MEYERS CHINA ATLAS, 2010. On the road to world power. Meyers, Mannheim, Germany, 221 pages (in German).

MIAO, Y., STEWART, B.A., ZHANG, F., 2011. Long-term experiments for sustainable nutrient management in China. A review. Agronomy for Sustainable Development, 31 (2), 397-414.

MIGDALL, S., BACH, H., BOBERT, WEHRHAN, M., MAUSER, W., 2009. Inversion of canopy reflectance model using hyperspectral imagery for monitoring wheat growth and estimating yield. Precision Agriculture, 10, 508-524.

MILTON, E.J., SCHAEPMAN, M.E., ANDERSON, K., KNEUBÜHLER, M., FOX, N., 2009. Progress in field spectroscopy. Remote Sensing of Environment, 113, S92-S109.

MIPHOKASAP, P., HONDA, K., VAIPHASA, C., SOURIS, M., NAGAI, M., 2012. Estimating canopy nitrogen concentration in sugarcane using field imaging spectroscopy. Remote Sensing, 4, 1651-1670.

MISTELE, B., SCHMIDTHALTER, U., 2008. Estimating the nitrogen nutrition index using spectral canopy reflectance measurements. European Journal of Agronomy, 29, 184-190.

MONFREDA, C., RAMANKUTTY, N., FOLEY, J.A., 2008. Farming in the planet: 2. Geograpic distribution of crop areas, yields, physiological types, and net primary production in the year 2000. Global Biogeochemical Cycles, 22 (1), 19 pages.

MONTGOMERY, D.C., PECK, E.A., VINING, G.G., 2012. Introduction to linear regression analysis. Wiley Series, Hoboken, New Jersey, USA, 662 pages.

MORAN, M.S., INOUE, Y., BARNES, E.M., 1997. Opportunities and limitations for image-based remote sensing in precision crop management. Remote Sensing of Environment, 61, 319-346.

MOORMANN, F.R., VAN BREEMEN, N., 1978. Rice: Soil, water, land. The International Rice Research Institute, Los Banos, Laguna, Philippines, 185 pages.

MULLA, D.J., 2013: Twenty five years of remote sensing in precision agriculture: Key advances and remaining knowledge gaps. Biosystems Engineering, 114, 358-371.

MÜLLER, J., 1997. Kulturlandschaft China. Justus Perthes Press, Gotha, Germany, 343 pages.

MUÑOZ-HUERTA, R.F., GUEVARA-GONZALEZ, R.G., CANTRERAS-MEDINA, L.M., TORRES-PACHECO, I., PRADO-OLIVAREZ, J., OCAMPO-VELAZQUEZ, R.V., 2013. A review of methods for sensing the nitrogen status in plants: Advantages, disadvantages and recent advances. Sensors, 13, 10823-10843.

MUTANGA, M., Skidmore, A.K., 2004. Hyperspectral band depth analysis for a better estimation of grass biomass (Cenchrus ciliaris) measured under controlled laboratory conditions. International Journal of Applied Earth Observation and Geoinformation, 5, 87-96.

NELLIS, M.D., PRICE, K.P., RUNDQUIST, D., 2009. Remote sensing of cropland agriculture. In: T.A., WARNER, M.D., NELLIS, G.M., FOODY, The sage handbook of remote sensing, Sage Publications Ltd, London, UK, pp. 368-380.

NGUYEN, H.T., LEE, B.-W., 2006. Assessment of rice leaf growth and nitrogen status by hyperspectral canopy reflectance and partial least square regression. European Journal of Agronomy, 24, 349-356.

NYBERG, A.J., 1998. Food security strategy for the early twenty-first century. In: T.C., TSO, F., TUAN, M., FAUST (Eds.), Agriculture in China 1949-2030. IDEALS Inc., Beltsville, MD, USA, pp.

159-208.

OLLINGER, S.V., 2011. Source of variability in canopy reflectance and the convergent properties of plants. New Phytologist, 189, 375-394.

ORTENBERG, F., 2011. Hyperspectral sensor characteristics - Airborne, spaceborne, hand-held, and truck-mounted; integration of hyperspectral data with LIDAR. In: P.S., THENKABAIL, J.G., LYON, A., HUETE (Eds.), Hyperspectral remote sensing of vegetation, CRC Press, Boca Raton, FL, USA, pp. 39-68.

OSBORNE, S.L., SCHEPERS, FRANCIS, D.D., SCHLEMMER, M.R., 2002. Use of spectral radiance to estimate in-season biomass and grain yield in nitrogen- and water-stressed corn. Crop Science, 42, 165-171.

OWEN, A.J. (1995). Uses of derivative spectroscopy.-Application note. Agilent Technologies. 8 pages.

PERBANDT, D., FRICKE, T., WACHENDORF, M., 2011. Off-nadir hyperspectral measurements in maize to predict dry matter yield, protein content and metabolisable energy in total biomass. Precision Agriculture, 12 (2), 249-265.

PIMSTEIN, A., EITEL, J.U.H., LONG, D.S., MUFRADI, I., KARNIELI, A., BONFIL, D.J., 2009. A spectral index to monitor the head-emergence of wheat in semi-arid conditions. Field Crops Research, 111, 218-225.

PINTER, P.J.L, HATFIELD, J.S., SCHEPERS, E.M., BARNES, E.M., MORAN, M.S., DAUGHTRY, C.S.T., UPCHURCH, D.R., 2003. Remote sensing for crop management. Photogrammetric Engineering and Remote Sensing, 69, 647-644.

PSOMAS, A., KNEUBÜHLER, M., HUBER, S., ITTEN, K., ZIMMERMANN, N.E., 2011. Hyperspectral remote sensing for estimating aboveground biomass and for exploring species richness patterns of grassland habitats. International Journal of Remote Sensing, 32 (24), 9007-9031.

QUYANG, W., XU, Y., HAO, F., WANG, X., CHEN, S., LIN, C., 2013. Effect of long-term agricultural cultivation and land use conversion and soil nutrient contents in the Sanjiang Plain. Catena, 104, 243-250.

RAUN, W.R., SOLIE, J.B., JOHNSEN, G.V., STONE, M.L., MULLEN, R.W., FREEMAN, K.W., THOMASON, W.E., LUKINA, E.V., 2002. Improving nitrogen use efficiency in cereal grain production with optical sensing and variable rate application. Agronomy Journal, 94, 815-820.

ROBERTS, D.A., ROTH, K.L., PERROY, R.L., 2011. Hyperspectral vegetation indices. In: P.S., THENKABAIL, J.G., LYON, A., HUETE (Eds.), Hyperspectral remote sensing of vegetation, CRC Press, Boca Raton, FL, USA, pp. 309-327.

ROYO, C., VILLEGAS, D., 2011. Field measurements of canopy spectra for biomass assessment of small-grain cereals. In: D., MATOVIC (Ed.). Biomass-Detection, Production and Usage, InTech, pp. 27-52.

ROZENSTEIN, O., DEVIR, A., KARNIELI, A., 2014. In-field absolute calibration of ground and airborne VIS-NIR-SWIR hyperspectral point spectrometers. Remote Sensing, 6, 1158-1170.

RUFFIN, C., KING, R.L., YOUNAN, N.H., 2008. A combined derivative spectroscopy and Savitzy-Golay filtering method for the analysis of hyperspectral data. GIScience & Remote Sensing, 45 (1), 1-15.

RUML, M., VULIC, T., 2005. Importance of phenological observations and predictions in agriculture. Journal of Agricultural Science, 50 (2), 217-225.

RYU, C., SUGURI, M., UMEDA, M., 2011. Multivariate analysis of nitrogen content for rice at heading stage using reflectance of airborne hyperspectral remote sensing. Field Crops Research, 122, 214-224.

SAVITSKY, A., GOLAY, M.J.E., 1964. Smoothing and differentiation of data by simplified least squares procedures. Analytical Chemistry, 36, 1627-1639.

SCHAEPMAN, M.E., 2009. Imaging spectrometers. In: T.A., WARNER, M.D., NELLIS, G.W., FOODY (Eds.), The Sage Handbook of Remote Sensing, SAGE Publications, London, UK, pp. 166-178.

SCHELLEBERG, J., HILL, M., GERHARDS, R., ROTHMUND, M., BRAUN, M., 2008. Precision agriculture on grassland: Applications, perspectives and constraints. European Journal of Agronomy, 29, 59-71.

SEELAN, S.K., LAGUETTE, S., CASADY, G.M., 2003. Remote sensing applications for precision agriculture: A learning community approach. Remote Sensing of Environment, 88, 157-169.

SELF, J.R., WASKOM, R.M., 2013. Nitrates in drinking water. Colorado State University, Fact Sheet No. 0.517, 3 pages.

SELLERS, P.J., 1985. Canopy reflectance, photosynthesis and transpiration. International Journal of Remote Sensing, 6 (8), 1335-1372.

SERRANO, L., FILLELA, I., PENUELAS, J., 2000. Remote sensing of biomass and yield of winter wheat under different nitrogen supplies. Crop Science, 40, 723-731.

SONG, D., XU, Q., 1990. Forest soils. In: C., LI, O., SUN (Eds.), Soils of China, Science Press, Beijing, China, pp. 115-130.

STROPPIANA, D., BOSCHETTI, M., BRIVIO, P.A., BOCCHI, S., 2009. Plant nitrogen concentration in paddy rice from field canopy hyperspectral radiometry. Field Crops Research, 111, 119-129.

SUN, S.M., KUNG, S.D., 1998. From the green revolution to gene revolution. In: T.C., TSO, F., TUAN, M., FAUST (Eds.), Agriculture in China 1949-2030. IDEALS Inc., Beltsville, MD, USA, pp. 446-467.

TAKAHASHI, W., NGUYEN-CONG, V., KAWAGUCHI, S., MINAMIYAMA, M., NONOMIYA, S., 2000. Statistical models for prediction of dry weight and nitrogen accumulation based on visible and near-infrared hyper-spectral reflectance of rice canopies. Plant Production Science, 3 (4), 377-386.

TFZ (2013). www.tfz.bayern.de/rohstoffpflanzen/index.php

THENKABAIL, P.S., SMITH, R.B., DE PAUW, E., 2000. Hyperspectral vegetation indices and their relationship with agricultural crop characteristics. Remote Sensing of Environment, 71 (2), 158-182.

THENKABAIL, P.S., LYON, J.G., HUETE, A., 2011. Advances in hyperspectral remote sensing of vegetation and agricultural croplands. In: P.S., THENKABAIL, J.G., LYON, A., HUETE (Eds.), Hyperspectral remote sensing of vegetation, CRC Press, Boca Raton, FL, USA, pp. 3-38.

THENKABAIL, P.S., MARIOTTO, I., GUMMA, M.K., MIDDLETON, E.M., LANDIS, D.R., HUEMMRICH, K.F., 2013. Selection of hyperspectral narrowbands (HNBs) and composition of hyperspectral twoband vegetation indices (HVIs) for biophysical characterization and discrimination of crops types using field reflectance and Hyperion/EO-1 data. IEEE Journal of Selected Topics in Applied Earth Observations and Remote Sensing, 6 (2), 427-439.

TIAN, Y.C., YAO, X., CAO, W.X., HANNAWAY, D.B., ZHU, Y., 2011. Assessing newly developed and published vegetation indices for estimating rice leaf nitrogen concentration with ground- and space-based hyperspectral reflectance. Field Crops Research, 120, 299-310.

TIVY, J., 1993. Agriculture and Environment - Agricultural ecosystems in the biosphere. Spektrum, Heidelberg, Berlin, Oxford, 344 pages (in German).

TSAI, F., PHILPOT, W., 1998. Derivative analysis of hyperspectral data. Remote Sensing of Environment, 66 (1), 41-51.

UN, 2012. United Nations, Department of Economic and Social Affairs: Population division, population estimates and projections section.

VAIPHASA, C., 2006. Consideration of smoothing techniques for hyperspectral remote sensing. ISPRS Journal of Photogrammetry and Remote Sensing, 60, 91-99.

VAN DELDEN, H., VAN VLIET, J., RUTLEDGE, D.T., KIRKBY, M.J., 2011. Comparison of scale and scaling issues in integrated land-use models for policy support. Agriculture, Ecosystem and Environment, 142, 18-28.

VAN DER MEER, F., 2006. Basic physics of spectrometry. In: F.D., VAN DER MEER, S.M., DE JONG (Eds.), Imaging spectrometry - Basic principle and prospective applications, Kluwer Academic Publishers, Dordrecht, Boston, London, pp. 3-16.

VAN LEEUWEN, W.J.D., 2009. Visible, Near-IR, and Shortwave IR spectral characteristics of terrestrial surfaces. In: T.A., WARNER, M.D., NELLIS, G.W., FOODY (Eds.), The Sage Handbook of Remote Sensing, SAGE Publications, London, UK, pp. 33-50.

VAN NIEL, T.G., MCVICAR, T.R., 2004. Current and potential uses of optical remote sensing in rice-based irrigation systems: a review. Australian Journal of Agricultural Research, 55, 155-185.

VIGNEAU, N., ECARNOT, M., RABATEL, G., ROUMET, P., 2011. Potential of field hyperspectral imaging as a non destructive method to assess leaf nitrogen content in wheat. Field Crops Research, 122, 25-31.

WANG, E., ENGEL, T., 1998. Simulation of phenological development of wheat crops. Agricultural

Systems, 58 (1), 1-24.

WANG, Y., YANG, Y., 2001. Effects of agriculture reclamation on hydrologic characteristics in the Sanjiang Plain, China. Chinese Geographical Science, 11 (2), 163-167.

WANG, Z., ZHANG, B., ZHANG, S., LI, X., LIU, D., SONG, K., LI, J., LI, F., DUAN, H., 2006. Changes of land use and of ecosystem service values in the Sanjiang Plain, Northeast China. Environmental Monitoring and Assessment, 112, 69-91.

WANG, F., HUANG, J., WANG, X., 2008. Identification of optimal hyperspectral bands for estimation of rice biophysical parameters. Journal of Integrative Plant Biology, 50 (3), 291-299.

WANG, F., HUANG, J., LOU, Z., 2011. A comparison of three methods for estimating leaf area index of paddy rice from optimal hyperspectral bands. Precision Agriculture, 12 (3), 439-447.

WANG, W., YAO, X., YAO, X., TIAN, Y., LIU, X., NI, J., CAO, W., ZHU, Y., 2012. Estimating leaf nitrogen concentration with three-band vegetation indices in rice and wheat. Field Crops Research, 129, 90-98.

WATANABE, T., HANAN, J.S., ROOM, P.M., HASEGAWA, T., NAKAGAWA, H., TAKAHASHI, W., 2005. Rice morphogenesis and plant architecture: measurements, specifications and the reconstruction of structural development by 3D architectural modelling. Annals of Botany, 95, 1131-1143.

WILSON, J.H., ZHANG, C., KOVACS, J.M., 2014. Separating crop species in Northeastern Ontario using hyperspectral data. Remote Sensing, 6, 925-945.

XAVIER, A.C., RUDORFF, B.F.T., MOREIRA, M.A., ALVARENGA, B.S., DE FREITAS, J G., SALOMON, M.V., 2006. Hyperspectral field reflectance measurements to estimate wheat grain yield and plant height. Scientia Agricola, 63 (2), 130-138.

YANG, C.-M., CHEN, R.-K., 2004. Modeling rice growth with hyperspectral reflectance data. Crop Science, 44 (4), 1283-1290.

YAO, H., TANG, L., TIAN, L., BROWN, R.L., BHATMAGAR, D., CLEVELAND, T.E., 2011. Using hyperspectral data in precision applications. In: P.S., THENKABAIL, J.G., LYON, A., HUETE (Eds.), Hyperspectral remote sensing of vegetation, CRC Press, Boca Raton, FL, USA, pp. 591-607.

YAO, H., HUANG, Y., HRUSKA, Z., THOMSON, S.J., REDDY, K.N., 2012. Using vegetation index and modified derivative for early detection of soybean plant injury from glyphosate. Computers and Electronics in Agriculture, 89, 145-157.

YAO, X., YAO, X., JIA, W., TIAN, Y., NI, J., CAO, W., ZHU, Y., 2013. Comparison and intercalibration of vegetation indices from different sensors for monitoring above-ground plant nitrogen uptake in winter wheat. Sensors, 13, 3109-3130.

YI, Q.-X., HUANG, J.-F., WANG, F.-M., WANG, X.-Z., LIU, Z.-Y., 2007. Monitoring rice nitrogen status using hyperspectral reflectance and artificial neural network. Environmental Science & Technology, 41 (19), 6770-6775.

YOU, X., MENG, J., ZHANG, M., DONG, T., 2013. Remote sensing based detection of crop phenology for agricultural zones in China using a new threshold method. Remote Sensing, 5, 3190-3211.

YOSHIDA, S., 1981. Fundamentals of rice crop science. The International Rice Research Institute, Los Banos, Laguna, Philippines, 269 pages.

YU, K., LI, F., GNYP, M. L., MIAO, Y., BARETH, G., CHEN, X., 2013. Remotely detecting canopy nitrogen concentration and uptake of paddy rice in the Northeast China Plain. ISPRS Journal of Photogrammetry and Remote Sensing, 78, 102-115.

YU, K., GNYP, M.L., CHEN, X., MIAO, Y., BARETH, G., 2014 (in print). Using partial least squares (PLS) to estimate canopy nitrogen and biomass of paddy rice in China's Sanjiang Plain. In: J. BENDIG, G. BARETH (Eds.), Proceedings of the Workshop on UAV-based remote sensing methods for monitoring vegetation, 9-10 September 2013, University of Cologne, Germany. Kölner Geographische Arbeiten.

ZADOCKS, J.C., CHANG, T.T., KONZAK, C.F., 1974. A decimal code for the growth stages of cereals. Weed Research, 14, 415-421.

ZENG, Z., QIAO, Q., ZHUANG, J., 1990. Black soils, Chernozems and Albic soils. In: C., LI, O., SUN (Eds.), Soils of China, Science Press, Beijing, China, pp. 131-153.

ZENG, Z., CHENG, B., 1990. Meadow soils and bog soils. In: C., LI, O., SUN (Eds.), Soils of China, Science Press, Beijing, China, pp. 220-232.

ZHANG, W.L., TIAN, Z.X., ZHANG, N., LI, X.Q., 1996. Nitrate pollution of groundwater in northern China. Agriculture, Ecosystems and Environment, 59, 223-231.

ZHANG, N., WANG, M., WANG, N., 2002. Precision agriculture - a worldwide overview. Computers and Electronics in Agriculture, 36, 113-132.

ZHANG, MA, K., FU, B., 2010. Wetland loss under the impact of agricultural development in the Sanjiang, NE China. Environmental Monitoring Assessment, 166 (1-4), 139-148.

ZHANG, F., CUI, Z., CHEN, X., JU, J., SHEN, Q., LIU, X., ZHANG, W., MI, G., FAN, M., JIANG, R., 2012a. Integrated nutrient management for food security and environemental quality in China. Advances in Agronomy, 116, 1-40.

ZHANG, J.-C., PU, R.-L., WANG, J.-H., HUANG, W.-J., YUAN, L., LUO, J.-H., 2012b. Detecting powdery mildew of winter wheat using leaf level hyperspectral measurements. Computers and Electronics in Agriculture, 85, 13-23.

ZHOU, Z., LIU, T., 2005. The current status, threats and protection way of the Sanjiang Plain wetland, Northeast China. Journal of Forestry Research, 16(2), 148-152.

ZHU, Y., YAO, X., TIAN, Y.C., LIU, X.J., CAO, W.X., 2008. Analysis of common canopy vegetation indices for indicating leaf nitrogen accumulation in wheat and rice. International Journal of Applied Earth Observations and Geoinformation, 10, 1-10.

Appendix A: Erklärung

Ich versichere, dass ich die von mir vorgelegte Dissertation selbständig angefertigt, die benutzten Quellen und Hilfsmittel vollständig angegeben und die Stellen der Arbeit - einschließlich Tabellen, Karten, und Abbildungen - , die anderen Werken im Wortlaut oder dem Sinn nach entnommen sind, in jedem Einzelfall als Entlehnung kenntlich gemacht habe; dass diese Dissertation noch keiner anderen Fakultät oder Universität zur Prüfung vorgelegt hat; dass sie - abgesehen von unten angegebenen Teilpublikationen - noch nicht veröffentlicht worden ist, sowie, dass ich eine solche Veröffentlichung vor Abschluss des Promotionsverfahrens nicht vornehmen werde. Die Bestimmungen der Promotionsordnung sind mir bekannt. Die von mir vorgelegte Dissertation ist von Prof. Dr. Georg Bareth betreut worden.

Köln, den (Unterschrift)

Folgende Teilpublikationen liegen vor:

LI, F., GNYP, M.L., JIA, L., MIAO, Y., YU, Z., KOPPE, W., BARETH, G., CHEN, X., ZHANG, G., 2008. Estimating N status of winter wheat using a handheld spectrometer in the North China Plain. Field Crops Research, 106 (1), 77-85. DOI: 10.1016/j.fcr.2007.11.00

KOPPE, W., LI, F., GNYP, M.L., MIAO, Y., JIA, L., CHEN, X., ZHANG, F., BARETH, G., 2010. Evaluating Multispectral and Hyperspectral Satellite Remote Sensing Data for Estimating Winter Wheat Growth Parameters at Regional Scale in the North China Plain. Photogrammetrie Fernerkundung Geoinformation, 2010 (3), 167-178. DOI: 10.1127/1432-8364/2010/0047

GNYP, M.L., BARETH, G., LI, F., LENZ-WIEDEMANN, V.I.S., KOPPE, W., MIAO, Y., HENNIG, S.D., JIA, L., LAUDIEN, R., CHEN, X., ZHANG, F., (2014, accepted 9 May 2014). Development and implementation of a multiscale biomass model using hyperspectral vegetation indices for winter wheat in the North China Plain. International Journal of Earth Observation and Geoinformation

GNYP, M.L., YU, K., AASEN, H., YAO, Y., HUANG, S., MIAO, Y., BARETH, G., 2013. Analysis of crop reflectance for estimating biomass in rice canopies at different phenological stages. Photogrammetrie Fernerkundung Geoinformation, 2013 (4), 0351-0365. DOI: 10.1127/1432-8364/2013/0182

GNYP, M.L., MIAO, Y., YUAN, F., USTIN, S.L., YU, K., YAO, Y., HUANG, S., BARETH, G. (2014). Hyperspectral canopy sensing of paddy rice aboveground biomass at different growth stages. Field Crops Research, 155, 42-55. DOI: 10.1016/j.fcr.2013.09.023

Appendix B: Curriculum vitae

Martin Leon Gnyp

Date of birth: July 23 1979

Place of birth: Oppeln

Nationality: German

Adress: Mönchengladbach

Email: mgnyp1@uni-koeln.de

Education

1986-1989	Elementary school No. 26, Oppeln
1989-1990	Elementary school Burbongert in Mönchengladbach (MG)
1990-2000	Gymnasium Odenkichen in MG Graduation: Abitur, grade: 2.0
2000-2001	Alternative civialian service in MG
2001-2008	Studies of Geography (main subject), Geology, and Cartography, Universitiy of Cologne and University of Bonn, Germany Graduation: Diplom, grade: 2.0 Diploma thesis: Establishment of a spectral and data library for analysis of reflectance spectra of winter wheat- case study Huimin-County, China.

Internships

2004	City of MG, Division of survey, cadaster, GIS; 2 months
2005	Plansystem Köln, Geodata management; 2 months

Academic Carrier

2004-2008	University of Cologne, Institute of Geography, GIS & RS group Student assistent
2008-2011	China Agricultural University, Beijing, PR China Enrolled as foreign PhD student
April 2008-present	University of Cologne, Institute of Geography, GIS & RS group Research assistant and PhD student

Field trips to China

2006	Huimin project (4 months)
2007	Huimin project+Jiansanjiang project (4 months)
2008	Jiansanjiang project (4 months)
2009	Jiansanjiang project (5 months)
2010	Jiansanjiang project (2 months)
2011	Jiansanjiang project (3 months)
2012	Jiansanjiang project (1 month)

Appendix C: Publicationlist

Peer-reviewed journal publications (in chronological order; bold=part of dissertation)

AASEN, H., GNYP, M.L., MIAO, Y., BARETH, G., 2014 (accepted). Automated hyperspectral vegetation index retrieval from multiple correlation matrices with HyperCor. Photogrammetric Engineering & Remote Sensing.

GNYP, M.L., MIAO, Y., YUAN, F., USTIN, S.L., YU, K., YAO, Y., HUANG, S. BARETH, G., 2014a. Hyperspectral canopy sensing of paddy rice aboveground biomass at different growth stages. Field Crops Research, 155, 42-55.

GNYP, M.L., BARETH, G., FEI, L., LENZ-WIEDEMANN, V.I.S., KOPPE, W., MIAO, Y., HENNIG, S.D., JIA, L., LAUDIEN, R., CHEN, X., ZHANG, F., 2014b (accepted). Development and implementation of a multiscale biomass model using hyperspectral vegetation indices for winter wheat in the North China Plain. International Journal of Applied Earth Observation and Geoinformation.

YAO, Y., MIAO, Y., CAO, Q., WANG, H., GNYP, M.L., BARETH, G., KHOSLA, R., YANG, W., LIU, C., 2014 (accepted). In-season estimation of rice nitrogen status with an active canopy sensor. IEEE Journal of Selected Topics in Applied Earth Observations and Remote Sensing.

YU, K., GNYP, M.L., LEI, GAO., MIAO, X., CHEN, X., BARETH, G., (in review). Estimate leaf chlorophyll of rice using reflectance indices and partial least squares.

GNYP, M.L., YU, K., AASEN, H., YAO, Y., HUANG, S., MIAO, Y., BARETH, G., 2013. Analysis of crop reflectance for estimating biomass in rice canopy at different phenological stages. Photogrammetrie Fernerkundung Geoinformation, 2013 (4), 351-365.

KOPPE, W., GNYP, M.L., HÜTT, C., YAO, Y., MIAO, Y., CHEN, X., BARETH, G., 2013. Rice monitoring with multi-temporal and dual-polarimetric TerraSAR-X data. International Journal of Applied Earth Observation and Geoinformation, 21, 568-576.

YU, K., LI, F., GNYP, M.L., MIAO, Y., BARETH, G., 2013. Remotely detecting canopy nitrogen status of paddy rice in the Northeast China Plain. ISPRS Journal of Photogrammetry and Remote Sensing, 78, 102-115.

KOPPE, W., GNYP, M.L., HENNIG, S.D., LI, F., MIAO, Y., CHEN, X., JIA, L., BARETH, G., 2012. Multitemporal hyperspectral and radar remote sensing for estimating winter wheat biomass in the North China Plain. Photogrammetrie Fernerkundung Geoinformation, 2012 (3), 0281-0298.

YAO, Y., MIAO, Y., HUANG, S., GAO, L., MA, X., ZHAO, G., JIANG, R., CHEN, X., ZHANG, F., YU, K., GNYP, M.L., BARETH, G., LIU, C., ZHAO, L., YANG, W., ZHU, H., 2012. Active canopy sensor-based precision N management strategy for rice. Agronomy for Sustainable Development, 32 (4), 925-933.

KOPPE, W., LI, F., GNYP, M.L., MIAO, Y., JIA, L., CHEN, X., ZHANG, F., BARETH, G., 2010. Evaluating multispectral and hyperspectral satellite remote sensing data for estimating winter wheat growth parameters at regional scale in the North China Plain. Photogrammetrie Fernerkundung Geoinformation, 2010 (3), 167-178.

LI, F., MIAO, Y., HENNIG, S.D., GNYP, M.L., CHEN, X., JIA, L., BARETH, G., 2010. Evaluating hyperspectral vegetation indices for estimating nitrogen concentration of winter wheat at different growth stages. Precision Agriculture, 11 (4), 335-357.

LI, F., GNYP, M.L., JIA, L., MIAO, Y., YU, Z., KOPPE, W., BARETH, G., CHEN, X., ZHANG, F., 2008. Estimating N status of winter wheat using a handheld spectrometer in the North China Plain. Field Crops Research, 106 (1), 77-85.

Peer-reviewed conference proceedings (in chronological order)

BENDIG, J., WILLKOMM, M., GNYP, M.L., BENNERTZ, S., QIANG, C., MIAO, Y., LENZ-WIEDEMANN, V.I.S., BARETH, G., 2013. Very high resolution crop surface models (CSMs) from UAV-based stereo images for rice growth monitoring in Northeast China. International Archives of the Photogrammetry, Remote Sensing and Spatial Information Sciences, Vol. XL-1/W2, 2013, UAV-g2013, 4-6 September 2013, Rostock, Germany.

GNYP, M.L., YAO, Y., YU, K., HUANG, S., LENZ-WIEDEMANN, V.I.S., MIAO, Y., BARETH, G., 2012. Hyperspectral analysis of rice phenological stages in Northeast China. ISPRS Annals of the Photogrammetry, Remote Sensing and Spatial Information Science, I-7, pp. 77-82. DOI: 10.5194/isprsannals-I-7-77-2012, 2012.

JIA, L., YU, Z., LI, F., GNYP, M.L., KOPPE, W., BARETH, G., MIAO, Y., CHEN, X., 2012. Nitrogen status estimation of winter wheat using an Ikonos satellite image in the North China Plain. Computers and Computing Technologies in Agriculture. V, PT II, 369, pp. 174-184.

YAO, Y.K., MIAO, Y., HUANG, S.Y., JIANG, R., GNYP, M.L., BARETH, G., KHOSLA, R., 2012. In-season diagnosis of rice nitrogen status using an active canopy sensor. In: R., KHOSLA (Ed.): Proceedings of the 11th International Conference on Precision Agriculture, 15-18 July 2012, Indianapolis, IN, USA [CD-ROM].

YAO, Y., MIAO, Y., HUANG, S., GAO, L., YU, L., JIANG, R., CHEN, X., GNYP, M.L., BARETH, G., ZHAO, L., LIU, C., 2010. Developing an active crop sensor-based in-season nitrogen management strategy for rice in Northeast China. In: KHOSLA, R. (Ed.): Proceedings of the 10th International Conference on Precision Agriculture, 18-21 July 2010, Denver, Colorado, USA [CD-ROM].

GNYP, M.L., LI, F., MIAO, X., KOPPE, W., JIA, L., CHEN, X., ZHANG, F., BARETH, G., 2009. Hyperspectral data analysis of N fertilization effects on winter wheat using spectrometer in North China Plain. 1rd. Workshop on Hyperspectral Image and Signal Processing - Evolution in Remote Sensing, 26-29 August 2009, Grenoble, France, pp. 255-258.

JIA, L., YU, Z., LI, F., GNYP, M.L., KOPPE, W., BARETH, G., MIAO, Y., CHEN, X., ZHANG, F., 2009. Nitrogen status estimation of winter wheat by using a Ikonos satellite image in the North China Plain. Joint International Agricultural Conference, 7-8 June 2009, Wageningen, The Netherlands.

LI, F., MIAO, Y., HENNIG, S.D., GNYP, M.L., CHEN, X., JIA, L., BARETH, G., 2009. Comparing hyperspectral vegetation indices for estimating nitrogen concentration of winter wheat. In: E.J., VAN HENTEN, D., GOENSE, C., LOKHORST, (Eds.): Precision Agriculture'09, Wageningen Academic Publishers, Wageningen, Netherlands, pp. 141-149.

LI, F., MIAO, Y, GNYP, M.L., HENNIG, S.D., CHEN, X., JIA, L., BARETH, G., 2009. Evaluating red edge vegetation indices for estimating winter wheat under high canopy coverage condition. The Proceedings of the International Plant Nutrition Colloquium XVI, Paper 1301.

BAASER, U., HENNIG, S., AASEN, H., DORNAUF, E., GNYP, M.L., HOFFMEISTER, D., KÖHN, N., LOUWEN, B., LAUDIEN, R., BARETH, G., 2008. AJAX-based for location -based-services: The Online-CampusGIS of the University of Cologne.-Proceedings of XXI ISPRS Congress, 3-11 July 2008, Beijing, China.

GNYP, M.L., LI, F., HENNIG, S.D., KOPPE, W., JIA, L., CHEN, X., ZHANG, F., LAUDIEN, R., BARETH, G., 2008. Hyperspectral data analysis of N-fertilization effects on winter wheat: a case study of Huimin County, North China Plain. Proceedings of VII/3 ISPRS Congress, 3-11 July 2008, Beijing, China, pp. 309-314.

JIA, L., YU, Z., LI, F., GNYP, M.L., KOPPE, W., BARETH, G., MIAO, Y., CHEN, X., ZHANG, F., 2007. Nitrogen status estimation of winter wheat by using Ikonos satellite image in the North China Plain. In: S.O., CHUNG, (Ed.) Proceedings of the Second Asian Conference on Precision Agriculture, August 2-4. 2007, Pyeongtak, Korea. [CD-ROM]

BAASER, I., GNYP, M.L., HENNIG, S., HOFFMEISTER, D., KÖHN, N., LAUDIEN, R., BARETH, G., 2006. Online CampusGIS for the University of Cologne: a tool for the orientation, navigation, and management. - SPIE Proceedings Geoinformatics'2006, Vol. 6421, Wuhan, China, pp. L4211-L4211.

KOPPE, W., GNYP, M.L., LAUDIEN, R., JIA, L., LI, F., CHEN, X., BARETH, G., 2006. Deriving of winter wheat characteristics from combined radar and hyperspectral data analysis. - SPIE Proceedings Geoinformatics'2006, Vol. 6419, Wuhan, China, pp. R4190-R4190.

Non-reviewed conference proceedings (in chronological order)

GNYP, M.L., MIAO, Y., YUAN, F., YU, K., YAO, Y., HUANG, S. BARETH, G., 2014 (in print): Derivative analysis to improve rice biomass estimation at early growth stages. In: J., BENDIG, G., BARETH (Eds.), Proceedings of the Workshop on UAV-based remote sensing methods for monitoring vegetation, 9-10 September 2013, University of Cologne, Germany. Kölner Geographische Arbeiten.

YU, K., GNYP, M. L., CHEN, X., MIAO, Y., BARETH, G., 2014 (in print). Using partial least squares (PLS) to estimate canopy nitrogen and biomass of paddy rice in China's Sanjiang Plain. In: J., BENDIG, G., BARETH (Eds.), Proceedings of the Workshop on UAV-based remote sensing methods for monitoring vegetation, 9-10 September 2013, University of Cologne, Germany. Kölner Geographische Arbeiten.

KOPPE, W., GNYP, M.L., YAO, Y., MIAO, Y., BARETH, G., 2011. Agricultural monitoring with spaceborne X-band SAR data. In: V.I.S., LENZ-WIEDEMANN, G., BARETH, (Eds.), Proceedings of the Workshop on Remote Sensing Methods for Change Detection and Process Modeling, 18-19 November 2010, University of Cologne, Germany. Kölner Geographische Arbeiten, 192, 55-61.

GNYP, M.L., YAO, Y., MIAO, Y., YU, K., HUANG, S., DORNAUF, E., HÜTT, C., LENZ-WIEDEMANN, V.I.S., LAUDIEN, R., JIANG, R., CHEN, X., BARETH, G., 2010. Evaluating within-field rice growth variability using Quickbird and Ikonos images in Northeast China. The 3rd ISDE Digital Earth Summit, 12-14 June 2010, Nessebar, Bulgaria, CD Proceedings, ISBN 978-954-724-039-1, 9 pages.

CHEN, G., MIAO, Y., POILVÉ, H., MATHIAN, C., GNYP, M.L., YAO, Y., 2009. Overland: an image processing software to retrieve biophysical parameters from satellite images in Northeast China. Proceedings of the 6th International Symposium of Digital Earth, 9-12 September 2009, Beijing, China.

BAASER, U., GNYP, M.L., HENNIG, S., HOFFMEISTER, D., KÖHN, N., BARETH, G., 2006. Online CampusGIS for the University of Cologne (in German). -Angewandte Geoinformatik 2006. Beiträge zum 18. AGIT-Symposium, Salzburg, Austria, Wichmann, Heidelberg, pp. 24-31.

KOPPE, W., GNYP, M.L., LAUDIEN, R., JIA, L., CHEN, X., BARETH, G., 2006. Spektrale Charakterisierung von Winterweizen für hyperspektrale Fernerkundungsanalysen. DGPF annual conference, 2006, Berlin.

Appendix D: List of figures and tables